

Chromium Poisoning: The Needle in the SOFC Stack

THÈSE N° 5428 (2012)

PRÉSENTÉE LE 16 AOÛT 2012

À LA FACULTÉ DES SCIENCES ET TECHNIQUES DE L'INGÉNIEUR
LABORATOIRE D'ÉNERGÉTIQUE INDUSTRIELLE
PROGRAMME DOCTORAL EN SCIENCE ET GÉNIE DES MATÉRIAUX

ÉCOLE POLYTECHNIQUE FÉDÉRALE DE LAUSANNE

POUR L'OBTENTION DU GRADE DE DOCTEUR ÈS SCIENCES

PAR

Josef Andreas SCHULER

acceptée sur proposition du jury:

Dr S. Mischler, président du jury
Dr J. Van Herle, Dr A. Hessler-Wyser, directeurs de thèse
Dr K. Föger, rapporteur
Prof. C. Ludwig, rapporteur
Prof. R. Steinberger-Wilckens, rapporteur



ÉCOLE POLYTECHNIQUE
FÉDÉRALE DE LAUSANNE

Suisse
2012

Acknowledgements

funding Swiss Federal Energy Office (AccelenT / SOF-CH-ase)

supervision Dr. Jan Van herle and Dr. Aïcha Hessler-Wyser

thesis jury Prof. Christian Ludwig, Prof. Steinberger-Wilckens and Dr. Karl Föger

hosting Prof. Daniel Favrat (LENI) and Prof. Cécile Hébert (CIME)

collaborators EPFL - LENI and - CIME

in particular Dr. Henning Lübbe, Dr. Pietro Tanasini and Dr. Zacharie Wuilemin

academic partners EMPA, PSI, ZHAW and VTT

industry HEXIS and HTceramix-SOFCpower

personal Eva M. Kissling, Dr. med. Josef J. Schuler, Moira M. Schuler, Anja R. Schuler, Timo E.V. Schuler and Iris Odermatt.

Lausanne, 2012

J. Andreas Schuler

Preface

This PhD thesis was conducted at the Ecole Polytechnique Fédérale de Lausanne (EPFL), Switzerland, between October 2008 and May 2012 under the co-supervision of two Laboratories: the Center for Electron Microscopy (CIME) headed by Prof Dr Cécile Hébert and the Industrial Energy Systems Laboratory (LENI) headed by Prof Dr Daniel Favrat, both of whom are here warmly thanked and sincerely acknowledged for full, continuous, financial and technical support and providing a great research work environment throughout. The work was cosupervised by Dr Aïcha Hessler-Wyser from CIME and MER Dr Jan Van herle from LENI. Funding has been provided from different sources: the Swiss Federal Energy Office (BfE/OFEN, Dr Stefan Oberholzer) with the projects AccelenT and SOF-CH-ASE, swisselectric research (Dr Michael Paulus, Dr Martin Kauert) with the project SOF-CH-ASE, as well as SOFC-Life, a project coordinated by the Jülich Research Centre (FZJ) - Prof Dr Robert Steinberger, Dr Josef Mertens, Dr Bert de Haart) within the European Joint Technology Initiative on Fuel Cells and Hydrogen funded by the European Commission. All these funding sources and the people associated with it are gratefully acknowledged for their confidence and collaboration. Many sincere thanks also go to all EPFL colleagues too numerous to mention, other ETH Domain colleagues (PSI - Prof. Christian Ludwig, Albert Schuler, Empa - Prof. Thomas Graule and his team), industry partners (HTceramix/SOFCpower, HEXIS, EU partners) for technical support and guidance, samples and collaboration.

Andreas Schuler has delivered a remarkable contribution. Contaminant poisoning, foremost by Cr species at the cathode, is one of the major nuts to crack towards commercialisation of SOFC technology, the most efficient energy conversion device for small scale combined heat and power generation poised to fulfill an important part of our future energy provision landscape worldwide, from both fossil and renewable sources. The contaminant poisoning occurs on different levels and scales (electrode catalyst, current collectors, metallic interconnection plates, balance-of-plant alloy components) at medium to long term operation, causing performance loss on the order of 1%/1000h and less. Everyone knows it's there but it's hard to detect, quantify and nail down. Indeed a needle in a SOFC stack which causes it to gently bleed down if left uncontrolled. It required a thoroughly systematic and pluridisciplinary approach to search for the needle, its various sources, its deposition and poisoning mechanisms, its separation from other superimposing influences, its quantification down to nanometric scale, and finally its mitigation. Andreas Schuler has managed to do so, employing a wide variety of techniques, methods and analyses, to answer many of the raised questions and to propose, implement and validate solution strategies. His enormous efficiency and

Preface

productivity is testified, among others, by 20 publications, the large majority of which he compiled as first author, by the variety of student projects he coached and by the number of collaborations he started and brought to fruition.

Above all, his unabatable good humour, autonomy, maturity, ideas and practicality made this work to a passionately entertaining and superbly pleasant experience. No doubt he will continue to deliver excellent contributions to materials science. Our most sincere thanks, wishes, respect and friendship accompany him on his further journey.

Lausanne, 2012

Jan Van herle & Aïcha Hessler-Wyser

Abstract

This thesis focuses on Cr-poisoning in solid oxide fuel cells (SOFC), which currently presents a key challenge for the development of this technology. By the implementation of dedicated experimental tools, this work offers a new access to, and comprehension of, electrochemical performance degradation caused by Cr contamination accumulation.

An experimental setup for the *in situ* assessment of Cr vapor concentrations within the hot air flux of an SOFC system inlet gives direct proof, and a measure of severity, of the Cr contamination issue. An energy-dispersive X-ray spectroscopy (EDX) based Cr quantification methodology leads this work to objective and therefore comparable data from *post-test* observations performed by scanning electron microscopy (SEM). Moreover, the developed methods are time-efficient.

To understand Cr-poisoning, in particular the deposition mechanisms of Cr_g^{VI} to Cr_s^{III} , electronic conducting cathode materials such as $(\text{La,Sr})\text{MnO}_3$ as well as mixed ionic electronic conductors (MIEC) such as $(\text{La,Sr})\text{CoO}_3$, $(\text{La,Sr})(\text{Co,Fe})\text{O}_3$, $(\text{La,Sr})\text{MnO}_3-(\text{Y,Zr})\text{O}_2$ and $\text{Nd}_{1.95}\text{NiO}_{4+\delta}$ are investigated during and after medium- to long-term electrochemical testing involving deliberate exposure to Cr contamination in button cell and stack test arrangements. The deposition rate of both chemically-driven and electrochemically-driven cathode mechanisms related to Cr-poisoning depends on the material, its operating conditions as well as on superimposed degradation phenomena, such as sulfur-poisoning.

Investigation and subsequent results at the SOFC stack level combine the different aspects of Cr contamination encountered within this work. The severity of Cr-poisoning of a cathode, depending on the electrode overpotential, guides the development of less-sensitive materials towards high performing cathodes, in particular MIEC electrode materials at lower temperature. The crucial role of electrode proximal layers within the cathodic half-cell, such as current collectors and protective coatings of metallic interconnects (MIC) is found to be adequately dispatched by present SOFC technology. Their role is to lower the concentration of Cr vapor species reaching electrochemically active cathode regions both by diffusion resistance and reactive trapping. In contrary, sealing materials do not achieve satisfactory tightness to hydrogen diffusion into the cathode compartment, causing aggravated Cr-poisoning by local steam generation and hence increased Cr-evaporation. As the protection against Cr evaporation of the entire balance-of-plant (BoP) of a real SOFC system, or its construction with non-emitting components regarding Cr evaporation, is not practicable, a Cr-getter-based air filter, developed within this work and validated *in situ*, offers a suitable solution for BoP-caused Cr pollution.

Preface

Keywords: Solid Oxide Fuel Cell (SOFC), Cathode, Metallic Interconnect (MIC), Balance-of-plant (BoP), Oxidation, Contamination, Degradation, Cr-Poisoning, Solid-State Chemistry, Rare-Earth Compounds, Scanning Electron Microscopy (SEM), Energy-Dispersive X-ray Spectroscopy (EDX), *In Situ* Gas Sampling.

Résumé

Cette thèse porte sur l’empoisonnement au Cr des piles à combustibles à oxyde solide (SOFC), qui représente actuellement un défi majeur pour le développement de cette technologie. Par la réalisation d’outils expérimentaux dédiés, cet ouvrage offre un nouvel accès à la dégradation des performances électrochimiques causée par l’accumulation de Cr, ainsi qu’une meilleure compréhension des mécanismes liés à cette contamination.

Un dispositif expérimental pour l’évaluation *in situ* de concentrations de vapeurs de Cr dans un flux d’air chaud à l’entrée d’un système SOFC donne ici une preuve directe du problème de contamination au Cr et une mesure de sa gravité. Une méthodologie de quantification du Cr basée sur la spectroscopie de rayons X à dispersion d’énergie (EDX) facilite dans ce travail l’obtention de données objectives, et donc comparables, provenant d’observations *post-test* effectuées par microscopie électronique à balayage (SEM), ceci de façon rapide.

Pour comprendre l’empoisonnement au Cr, en particulier les mécanismes de déposition de Cr_g^{VI} en Cr_s^{III} , des matériaux de cathode conducteurs électroniques tels que le $(\text{La,Sr})\text{MnO}_3$, ainsi que des conducteurs mixtes ioniques et électroniques (MIEC) tels que le $(\text{La,Sr})\text{CoO}_3$, $(\text{La,Sr})(\text{Co,Fe})\text{O}_3$, $(\text{La,Sr})\text{MnO}_3-(\text{Y,Zr})\text{O}_2$ et $\text{Nd}_{1.95}\text{NiO}_{4+\delta}$, sont étudiés pendant et après des tests électrochimiques. Ces expériences de moyenne à longue durée impliquent une exposition délibérée à la contamination au Cr, effectuées sur des cellules "bouton" ou empilées. Le taux de déposition lié au mécanisme d’empoisonnement au chrome est entraîné à la fois chimiquement et par l’activité électrochimique de la cathode. Il dépend du matériau, de ses conditions d’exploitation ainsi que de phénomènes de dégradation superposés, tels que l’empoisonnement au soufre.

L’examen et les résultats subséquents au niveau de l’empilement SOFC combinent les différents aspects de la contamination au Cr rencontrés dans ce travail. L’intensité de l’empoisonnement au Cr d’une cathode dépend du surpotentiel de l’électrode ce qui guide le développement de matériaux moins sensibles vers des cathodes à haute performance, en particulier vers les électrodes MIEC à plus basse température. Le rôle crucial des couches à proximité de l’électrode dans la demi-cellule cathodique, telles que les collecteurs de courant et les revêtements protecteurs des interconnecteurs métalliques (MIC), consiste à abaisser la concentration des vapeurs de Cr atteignant les régions de cathode électrochimiquement actives à la fois par une barrière de diffusion et par le piégeage réactif. Ceci est adéquatement accompli par l’actuelle technologie SOFC. Les matériaux de jointures au contraire ne donnent pas une étanchéité satisfaisante contre la diffusion d’hydrogène dans le compartiment cathode qui peut y générer de la vapeur d’eau et ainsi aggraver l’empoisonnement par une évaporation accrue.

Preface

Comme la protection de l'ensemble de la périphérie (BoP) d'un véritable système SOFC, ou sa construction avec des composants non-émetteurs de chrome, n'est pas envisageable, un filtre d'air basé sur le piégeage de Cr, est mis au point dans ce travail avec une preuve *in situ* de la réduction de contamination de Cr, et offre ainsi une solution adaptée à la pollution au Cr causée par le BoP.

Mots-clé: Pile à Combustible (SOFC), Cathode, Interconnecteur Métallique (MIC), Système Périphérique (BoP), Oxidation, Contamination, Dégradation, Empoisonnement au Cr, Chimie du Solide, Composés de Terres Rares, Microscope Électronique à Balayage (MEB/SEM), Spectroscopie Dispersive en Énergie (EDX), *In Situ* Échantillonnage de gas.

Zusammenfassung

Diese Dissertation befasst sich mit der Cr-Vergiftung in Festoxidbrennstoffzellen (SOFC), die gegenwärtig eine zentrale Herausforderung für die Entwicklung der SOFC Technologie darstellt. Mit der Realisierung von adaptierten experimentellen Methoden bietet diese Arbeit einen neuen Zugang und ein Verständnis vom elektrochemischen Leistungsabbau, welcher durch akkumulierte Cr-Verunreinigung verursacht ist.

Ein Versuchsaufbau für die direkte Bewertung von Cr-Dampfkonzentrationen *in situ* im heißen Luftstrom eines SOFC-Systems beweist und misst die Stärke des Cr-Verunreinigungsproblems. Eine auf energiedispersive Röntgenspektroskopie (EDX) basierte Methodik zur Cr-Quantifizierung erleichtert einerseits die Beschaffung von objektiven und daher auch vergleichbaren Daten aus *post*-Versuch-Beobachtungen durchgeführt mit Rasterelektronenmikroskopie (REM), andererseits wird durch diese Methodik der Zeitaufwand gering gehalten.

Um die Cr-Vergiftung und insbesondere die Mechanismen der Ablagerung von Cr_g^{VI} in Cr_s^{III} , zu verstehen, werden hier elektronisch leitende Kathodenmaterialien wie $(\text{La,Sr})\text{MnO}_3$, sowie gemischte ionische und elektronische Leiter (MIEC) wie $(\text{La,Sr})\text{CoO}_3$, $(\text{La,Sr})(\text{Co,Fe})\text{O}_3$, $(\text{La,Sr})\text{MnO}_3$ - $(\text{Y,Zr})\text{O}_2$ und $\text{Nd}_{1,95}\text{NiO}_{4+\delta}$ erforscht. Diese Untersuchungen werden während und nach mittel- bis langzeitigen elektronischen Experimenten vorgenommen, wobei absichtlich die Auslagerung von Knopfzellen oder Zellenstapel gegenüber Cr-Verunreinigung involviert wird. Die Ablagerungsrate von Cr, welche sowohl durch chemische als auch durch elektrochemische Kathodenaktivität angetrieben wird, hängt einerseits vom Material, andererseits von den Betriebsbedingungen der Zelle, sowie von zusätzlichen Degradationsphänomenen (wie Schwefel-Vergiftung) ab.

Die Untersuchungen und anschließenden Ergebnisse auf der SOFC-Stapel-Ebene verbinden die verschiedenen Aspekte der im Rahmen dieser Arbeit angetroffenen Cr-Verunreinigung. Da die Heftigkeit der Cr-Vergiftung einer Kathode von der Elektrodenüberspannung abhängt, führt die Entwicklung von weniger empfindlichen Werkstoffen zu hochleistungsfähigen Kathoden, insbesondere MIEC-Elektroden bei niedrigeren Temperaturen. Eine entscheidende Rolle von elektrodenproximalen Schichten innerhalb der kathodischen Halbzelle spielen Stromabnehmer und Schutzschichten metallischer Interkonnektoren (MIC). Letztere bewirken die Senkung der Konzentration des zu den elektrochemisch aktiven Kathodenbereiche vordringenden Cr, was wiederum durch Diffusionswiderstand und reaktives Abfangen verursacht wird. Die gegenwärtige SOFC Technologie erfüllt diese Rolle ausreichend. Die Versiegelungsmaterialien liefern hingegen keine zufriedenstellende Dichtigkeit zur Verhinderung von Wasserstoffdiffusion und der folgenden Cr-Vergiftungsverschlimmerung durch Wasserdampferzeugung. Da

Preface

der Schutz der gesamten Systemperipherie (BoP) eines realen SOFC-Systems oder dessen Konstruktion mit nicht-emittierenden Komponenten in Bezug auf Cr-Verdampfung nicht durchführbar ist, bietet ein Cr-abfangender Luftfilter, der im Rahmen dieser Arbeit entwickelt und *in situ* zur Senkung von Cr-Verunreinigung nachgewiesen worden ist, eine passende Lösung für BoP-verursachte Cr-Verschmutzung.

Stichwörter: Festoxidbrennstoffzelle (SOFC), Kathode, Metallischer Interkonnektor (MIC), Anlagenperipherie (BoP), Oxidation, Kontamination, Degradierung, Cr-Vergiftung, Festkörperchemie, Seltene-Erden-Verbindung, Rasterelektronenmikroskop (REM/SEM), Energiedispersive Röntgenspektroskopie (EDX), *In Situ* Gasentnahme.

Contents

Acknowledgements	iii
Preface	v
Abstract (English/Français/Deutsch)	vii
Introduction	1
0.1 Context	1
0.2 Objectives	1
0.3 State-of-the-art	2
0.4 Structure of the present work	3
1 The solid oxide fuel cell	9
1.1 SOFC operating principle	9
1.2 SOFC materials	10
1.3 Material Degradation	11
1.4 Cr-poisoning: a needle in a haystack	12
2 Experimental: Cr contamination generation	15
3 Cr detection and quantification	17
3.1 Rapid chromium quantification in solid oxide fuel cell cathodes	17
4 Overpotential-driven Cr-poisoning	25
4.1 Cathode thickness-dependent tolerance to Cr-poisoning in solid oxide fuel cells	25
5 Electrochemical Cr_g^(VI) reduction	33
5.1 Nd-nickelate SOFC cathode sensitivity to Cr/Si contamination	33
6 Cr contamination sources	45
6.1 Multi-scale assessment of Cr contamination levels in SOFC cathode environment	45
6.2 Air side contamination in solid oxide fuel cell stack testing	54
7 Superimposed degradation effects	71
7.1 Glass-forming exogenous silicon contamination in solid oxide fuel cell cathodes	71
7.2 Sulfur as pollutant species on the cathode side of a SOFC system	78

Contents

7.3 Combined Cr and S poisoning in solid oxide fuel cell cathodes	87
8 Long-term stack performance	105
8.1 Cr-poisoning in (La,Sr)(Co,Fe)O ₃ cathodes after 10'000 h SOFC stack testing . . .	105
9 Counteracting strategies	119
9.1 Mitigating Cr contamination by hot air filtering in solid oxide fuel cells	119
10 Synthesis	125
10.1 Cathode material level	125
10.2 Cell and repeat-unit level	128
10.3 SOFC system level	130
11 Conclusion	133
11.1 Own contributions and achievements	133
11.2 Future work	134
Bibliography	146
A Appendix	147
A.1 Locally-resolved study of degradation in a SOFC repeat-element	147
A.2 Segmented cell testing for cathode parameter investigation	149
A.3 Coached student projects	152
A.4 Publications	153
Curriculum vitae	157

Introduction

0.1 Context

The Swiss Federal Council recently set guidelines for the Swiss energy strategy by 2050¹, which implies a gradual phasing out of nuclear power by the non-replacement of existing plants at the end of their technically safe operating period. In order to ensure electricity supply, emphasis is placed on increased energy savings (efficiency), the expansion of hydropower and new renewables, as well as temporarily on imports and natural gas-based electricity production (cf. Fig. 1).

In particular, decentralized combined heat and power (CHP) plants are expected to generate by 2035 up to 7 TWh of electricity. CHP plants can especially in the winter, when the electricity production from solar and wind is reduced, deliver band energy to contribute to grid stability, while providing valuable heat. Only facilities, which fulfill certain requirements for electrical efficiency, heat recovery and allowable CO₂ emissions per kWh should be promoted.

Solid oxide fuel cell (SOFC) technology application as stationary energy conversion devices that produce electricity and heat with a high total efficiency via electrochemical reactions of air with a fuel such as natural gas, meet these requirements and should enter the Swiss market as household electricity-generating heating equipment by 2013.

In this context, SOFC lifetime achievement of over 40'000 h is a prerequisite, where the constituent components have to withstand different degradation phenomena. In particular, the so-called Cr-poisoning degradation effect reduces the SOFC device lifetime. It involves Cr emanation from cell-proximal Cr containing alloys, with subsequent Cr accumulation in electrochemically active cathode regions. This blocks gaseous and electric paths, necessary for the oxygen reduction reaction, and therefore causes electrode performance losses.

Consequently, methods have to be developed to understand this degradation phenomenon and to protect SOFCs from Cr-poisoning. This thesis aims to contribute to these aspects.

0.2 Objectives

The main objectives of this thesis fit into the context of energy supply, more precisely the electricity generation using solid oxide fuel cells with low lifetime degradation. They are: i) Cr-poisoning detection ii) Cr-poisoning understanding iii) Cr-poisoning alleviation.

¹Several documents from the Swiss Federal Office of Energy at : <http://www.bfe.admin.ch/energie>

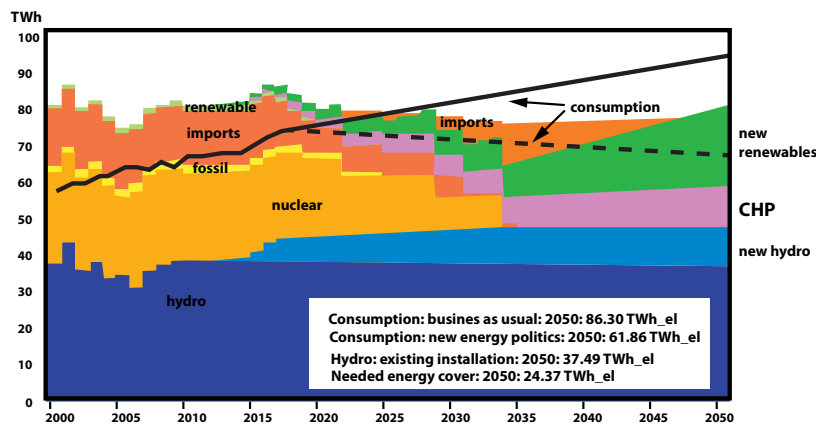


Figure 1: The Swiss energy strategy 2050 implies the non-replacement of existing nuclear power plants at the end of their technically safe operating time. The shortfall to be covered by an optimized mixture of hydroelectric power, new renewables, fossil fuel-based electricity production (including CHP) and electricity imports, is foreseen to reach ca. 25 TWh_{el} under the new energy politics, which are underpinned by the concept of the 2'000 W society or 1 tonne/year of CO₂ emissions per capita (adapted from [1]).

Thesis main objectives

- i Develop Cr detection techniques to quantify Cr-poisoning in SOFC during (*in situ*) and after (*post-test*) operation. Such detection methods can then be transferred, if required in a simplified form, to industrial partners as a quality control solution regarding Cr-poisoning.
- ii Apply advanced investigations techniques to understand and predict the Cr-poisoning phenomenon and its correlation to degradation. Such academic key competences can then by extension also be used for SOFC degradation phenomena other than Cr-poisoning.
- iii Mitigate this degradation phenomenon with guidance from the industrial's needs, where Cr alleviating solutions can be delivered to industrial partners.

0.3 State-of-the-art

Although the Cr-poisoning phenomenon is well known in SOFC technology [2, 3, 4, 5], quantification issues remain generally open in studies facing this degradation effect. State of the art researches on Cr-poisoning on the three levels, i) cathode, ii) cell and iii) system, generally involve the following techniques:

- i For Cr investigations on the materials level, scanning electron microscopy (SEM) combined to energy-dispersive X-ray spectroscopy (EDX) is the prevalent technique [3, 6, 7, 8, 9, 10, 11]. The related wavelength-dispersive X-ray spectroscopy (WDS) technique

is less widespread [12, 13] as this method does not imply a quantification without calibrated standards. Transmission electron microscopy (TEM) techniques are as prevailing [12, 14, 15, 16] as X-ray diffraction (XRD) [9, 17, 18, 19]. Detection issues at extremely low elemental concentrations are generally solved using secondary ion mass spectrometry (SIMS) [20, 21, 22, 23] or X-ray photoelectron spectroscopy (XPS) [24, 25]. Whereas some studies apply rather exotic characterization techniques such as scanning photoelectron microscopy (SPEM) [14], nanoprobe Auger electron spectroscopy (NAES) [15] or synchrotron-based micro-focused X-ray probe [26], only few researches make use of fairly simple, but probably under-exploited, techniques such as Raman spectroscopy [15].

- ii For the assessment of the Cr poisoning impact on electrochemical cell behavior, nearly all researches rely, besides voltammetry, on electrochemical impedance spectroscopy (EIS) [2, 3, 7, 15, 27, 28, 29].
- iii *In situ* gas sampling techniques have so far only been implemented on the anode side [30, 31]. To judge on the contamination severity brought about by SOFC component corrosion, *ex situ* methods include the transpiration technique [32, 33, 34], combined with conductivity measurement of the condensed vapors in solution [35, 36] or with a denuder technique [37] (Cr-trapping with Na_2CO_3), or with Rutherford backscattering spectroscopy (RBS) after thermophoresis (Cr vapors condensed on a cold plate) [38].

This thesis intends to shortcut complicated quantification issues: i) on the one hand by the development of a fast and objective EDX methodology for *post-test* analysis, close to what is achievable with image analysis [39], despite the challenge [40] caused by the strong X-ray emission line overlaps [41, 42]; ii) on the other hand, by the application of this methodology on samples from SOFCs that have been tested in controlled and therefore comparable operating conditions, in combination with electrochemical performance data acquired during operation; iii) finally, by the development of an *in situ* gas sampling technique for the assessment of volatile Cr vapor concentrations under SOFC operating conditions.

0.4 Structure of the present work

The thesis comprises 10 chapters where the content of chapters 3-9 has been published in the form, as presented here², of 10 scientific journal articles. The synthetic chapter at the end of this document summarizes the thesis results in a holistic manner: from nano to macro and from powder to power.

Chapter 1: context and motivation for Cr-poisoning investigations in SOFC. The operating principle of an SOFC is given in this chapter, while highlighting the efficiency of its direct energy conversion as key advantage. To meet lifetime requirements for stationary application,

²Footnotes refer to precisions requested by the thesis jury.

SOFC material stability over long time-scale at elevated temperatures is a main issue. Electrolyte, electrode and stacking materials are introduced in chapter 1. Degradation issues focus on the cathode compartment, in particular on Cr-poisoning; its investigation is described as searching for a "needle in a SOFC hay-stack". Three main questions arise, which this thesis aims to answer: i) what is the effect of this Cr-"needle", ii) where is it localized and iii) how can we dislodge it?

Chapter 2: experimental SOFC endurance testing at different scales. Experimental arrangements for button cell, multicathode cell, single repeat-unit and stack testing are briefly exposed in chapter 2. Focus is given on the different main Cr sources, including tubing, flanges and (un)protected metallic interconnects (MIC).

Chapter 3: fast and objective Cr detection in *post-test* studies. Chapter 3 solves the initial question whether Cr can be, quantitatively and not only qualitatively, detected, despite its low concentration and the multi-element cathode composition. The identified tool is the use of peak height ratios in energy-dispersive X-ray spectra. The outcome of this chapter is a Cr quantification methodology [43], coming along with an emerging question: are Cr distribution and amounts predictable?

Chapter 4: Cr-poisoning deposition mechanisms assessment by Cr profiling. The question how and which amounts of Cr accumulations distribute in SOFC cathodes is addressed in this chapter by Cr profiling, i.e. the application of the aforementioned Cr quantification technique on EDX spectra extracted from thin cathode slices. The feasibility of direct comparison of Cr data from identical cathodes with different thicknesses, allowed the detected Cr amounts to be linked to the electrochemical cathode activity (overpotential) [44]. This however raises the question whether Cr deposition involves direct electrochemical reduction or chemical interaction with polarization-induced Mn-nuclei in the case of (La,Sr)MnO₃-based cathodes, an issue of some controversy in literature.

Chapter 5: Cr-poisoning alleviating by the suppression of Cr_g^{VI} nucleation sites? This chapter investigates the feasibility of Mn-free and Sr-free cathode material as a first proposed solution against Cr-poisoning. If Cr deposition was purely chemically-driven, the absence of Mn and Sr, which form spinel or chromate phases upon reaction with Cr, would make a material such as Nd-nickelate intrinsically tolerant to Cr-poisoning. This chapter however shows Cr-poisoning not to be avoidable by only changing the cathode material [45]. Indeed also Nd₂NiO₄ is electrochemically Cr-poisoned. Solutions at the system level have therefore to be found. Cr profiling through the complete airflow is suggested to pragmatically localize places for appropriate solutions to be implemented.

Chapter 6: unavoidable degradation upon Cr contamination; Cr source localization. Chapter 6 evidences how Cr profiling through the entire cathode compartment of a single repeat-unit, to assess the main Cr sources, was approached. This was done by the application of the herein developed EDX Cr quantification technique on numerous samples; the intrinsically fast characteristic of the methodology was here very helpful. A crucial finding from this work

was the major contamination source to be located upstream of the cell, polluting the air fed to the cathode. Such notice triggered the inquiry if the contamination level can be assessed directly within the hot air feed. A gas sampling technique was therefore developed, which proved Cr vapor detection to be possible [46]. The quantification of trace Cr amounts within the hot air flux moreover enabled correlations to be established between the oxidation of Cr containing alloys with subsequent Cr species evaporation, transport of Cr vapors and their deposition within the cathode compartment [47]. The supplementary identification of other contaminants, mainly S and Si, raises the question of the influence of such additional pollutants, in particular regarding their effect on Cr-poisoning.

Chapter 7: additional pollutant species contributing to overlaying degradation effects.

The application of space averaging EDX in combination with chemical tricks enabled additional Si and S contamination-caused degradation effects to be exposed within this chapter [48, 49]. Thermodynamic considerations of multicomponent systems, involving combined Cr and S contamination, pointed out new degradation/mitigation mechanisms related to Cr-poisoning [50]. Are correlations between the poisoning extent and the performance degradation feasible, with this extended comprehension of Cr-poisoning and the awareness of additional air side contaminants?

Chapter 8: correlation between contamination and long-term degradation. This chapter examines the severity of Cr-poisoning after long-term testing of an SOFC stack. Substantial Cr profiling across and along the airflow enabled to depict the distribution of Cr accumulations, which were found affected by the proximity to sealing locations [51]. Although a direct quantitative correlation between Cr amounts and performance degradation could not be established, an encouraging low-level Cr contamination was found to be induced by metallic interconnects. This chapter therefore suggests that counteracting strategies, currently applied in SOFC technology, seem well adapted to alleviate MIC-induced Cr-poisoning. The invariable presence of extensive Cr pollution originated from system components located upstream of the stack inquires additional solutions.

Chapter 9: counteracting by air filtering. By the implementation of the most pragmatic choice, which is to use the Cr trapping properties of reactive cathode materials as an air filter, Cr-poisoning reduction is shown in this chapter to be possible already at its source [52]. To the final query, if the Cr "needle" has been completely removed from the SOFC "hay-stack", the following chapter tries to answer.

Chapter 10: general synthesis. The main outcomes of this thesis are described on the cathode material level, the cell/repeat-unit level and the SOFC system level while focusing on i) measurement solutions, ii) knowledge of Cr-poisoning mechanisms and iii) counteracting solutions. An impatient reader, or one who already encountered the publications from chapters 3-9 in the open literature, can readily be directed towards this general synthesis of the entire work.

Chapter 11: conclusions and outlook. This work concludes on the achievement of the main objectives as well as on future work. The Cr-poisoning issue is encouragingly depicted regarding the commercial application of SOFC.

Appendix: experimental details. The addition of the experimental sections of two publications [53, 54], with J.A. Schuler as coauthor, has been requested by the thesis jury. Appendix 1 describes the segmented repeat-unit assembly [53]; *post-test* analysis are given in chapters 6.1, 6.2, 7.1, 7.2 and 7.3. Appendix 2 presents experimental precisions for electrode preparations [54], which find application in chapters 3.1, 4.1 and 5.1, as well as the description of multicathode test arrangements (chapter 4.1 and 7.3).

Collaborations

This thesis has been performed within the framework of the Swiss Federal Office of Energy (SFOE) funded projects *AccelenT* and *SOF-CH-ASE* co-funded by *Swisselectric* research, as well as the project SOFC-life funded by the European Commission.

EPFL Internal: within LENI and CIME

- Zacharie Wuillemin: his advice and guidance for *post-test* analysis fostered the identifications of additional and superimposed degradation effects. He provided access to a stack test bench for the evaluation of air sampling and filtering; access was also possible to the BoP components as well as the electrochemical data from the cells tested on this bench (appendix 1).
- Pietro Tanasini: his contributions are visible in the description of the overpotential-driven Cr-poisoning mechanisms in LSM-YSZ-based cathodes. Electrochemical performance and degradation data, in addition to *post-test* samples, were gathered from his multicathode button cell tests (appendix 2).
- Henning Lübke: his contribution to the implementation of nickelate-based button cell tests was very valuable in the scope of Cr-poisoning description of Sr-free and Mn-free cathode materials.
- Arata Nakajo: this collaboration will be intensified for the valorization of quantitative Cr data to validate a Cr-poisoning model.
- CIME - Marco Cantoni, Pierre Burdet and Guillaume Lucas: electron microscopy, especially EDX, related results were audited by CIME's collaborators, who also largely contributed to the implementation of PCA (see section 11.2) for EDX data treatment with fast Cr imaging in scope.

Swiss level: industry and research

- HTceramix - Zacharie Wuillemin: enabled the access to post mortem analysis of a long-term test as well as the evaluation of materials interactions for new stack designs. An adapted version of a Cr getter was also collaboratively developed.
- Hexis - Andreas Mai: shared knowledge on LSM/YSZ behavior lead to the description of Cr-poisoning mechanisms; insights into the ageing behavior of YSZ were brought by available long-term exposed samples. Advices from his side also encouraged the Cr getter development.
- PSI - Albert Schuler and Christian Ludwig: the hot air sampling technique they designed and developed could be readily transfered into an application for SOFC.
- ZHAW - Dirk Penner: his advices enabled the realization of a macroporous ceramic support for the LSC-based Cr getter functionalization.
- Empa - Thomas Graule and Andre Heel: the EDX methodologies developed within this work found application on Ni/alternative fuel electrodes.

International: academic level

- VTT, Finland - Olivier Thomann: the shared knowledge on BoP alloys motivated the development of the hot gas sampling device as well as the complementary *in situ* Cr quantification methodology based on a denuder technique.
- AIST, Japan - Harumi Yokokawa: his thermodynamic analysis of multicomponent systems corroborated the possible appearance of S-rich Sr-chromate compounds in LSM under combined Cr/S contamination.
- IHTE, Russia - Maxim Ananyev: the completion of this collaborative work on Cr-poisoned microstructure quantification should be achieved within the EU project *SOFC-life*.

1 The solid oxide fuel cell

1.1 SOFC operating principle

A solid oxide fuel cell (SOFC) is a direct energy conversion device, generating electrical power and heat via the electrochemical reaction of a fuel and air. A gas-tight, electronically insulating, ceramic ionic conductor (electrolyte) in contact with two electrically conductive electrodes (anode and cathode) constitute the core of an SOFC. Figure 1.1 illustrates the oxygen reduction reaction at the cathode and the fuel oxidation on the anode side, by the oxygen ions selectively conducted through the electrolyte. The key advantage of this technology is the high achievable electrical efficiency, hence reduced CO₂ emission per kWh of generated electricity.

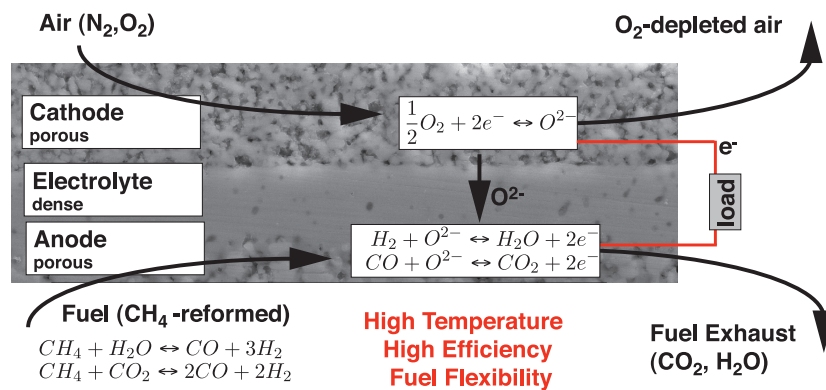
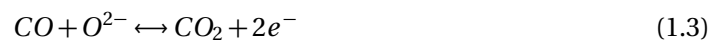
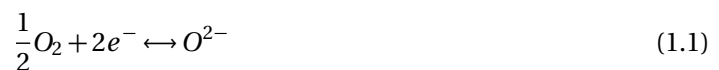


Figure 1.1: Schematic description of the working principle of a solid oxide fuel cell (SOFC).

The overall electrochemical reaction can be written as two half reactions occurring at the cathode (1.1) and the anode (1.2)/ (1.3).



Other fuels than hydrogen and carbon monoxide, such as methane from natural or bio-gas via an additional fuel processing step (reforming eqn. (1.4)), can be converted in an SOFC, representing another key advantage of this technology. The equilibrium of the water-gas shift reaction, equation (1.5), is translated to the right side at SOFC operating conditions, hence CO is indirectly consumed through the predominant conversion of hydrogen.



Stacked cells To increase the power output SOFC single cells are piled into a cell stack. In particular, planar SOFC stacks, which are the focus in this thesis, achieve high power density. A typical assembly includes a gas-tight interconnect plate electronically connecting anodes and cathodes. In addition, current collecting and gas diffusion layers enable adequate contacting and gas delivery between cell and interconnect within both electrode compartments. The two atmospheres are partitioned with sealing materials. A planar stack illustration is given in figure 1.2.

1.2 SOFC materials

Electrolyte The requisite gas-impervious, electronic insulating and ionic conducting properties are obtained by oxide ceramic materials, from which the solid oxide fuel cells obtained their naming [55]. Ytria-stabilized zirconia (YSZ) is frequently used as electrolyte, with a certain amount of dopant to stabilize the fluorite phase and obtain maximal ionic conductivity, i.e. 8 mol% Y_2O_3 - 92 % ZrO_2 . Higher conductivities can be achieved, with drawbacks on other properties, by scandia doped zirconia (ScSZ) or gadolinia-doped ceria (GDC).

Anode The fuel electrode is usually constituted of a Ni-based cermet offering electrochemical activity for H_2 and CO oxidation as well as chemical activity for the reforming of hydrocarbons [56]. The ceramic phase, which is generally YSZ or GDC, enables oxygen ion diffusion towards the electrochemically active anode sites located at metal-ceramic-pore triple-phase-boundaries (TPB). The metallic phase, besides catalytic properties, implements electronic conduction towards the interconnect.

Cathode The air electrode is generally composed of a perovskite material like strontium-doped lanthanum manganite $(La,Sr)MnO_3$ (LSM), which is an electronic conductor. The extent of electrochemically active cathode sites, limited in this case to the electrolyte/electrode interface, is amplified by mixing LSM to a electrolyte phase hence increasing the number of TPB [57], or by the use of a mixed ionic electronic conductive (MIEC) compound, such as

(La,Sr)(Co,Fe)O₃ [58]. Contacting the electrode to the interconnect is facilitated by the use of highly conductive perovskite compositions that are typically cobaltites.

Interconnect and sealings Gas impermeability and high electronic conductivity can be obtained from dense perovskite based ceramics, such as lanthanum chromite [56, 59, 60, 61] or metallic alloys that can withstand the corrosive SOFC environment [62]. In particular, chromia formers [63], i.e. Cr₂O₃-covered alloys in oxidizing conditions [64, 65], exhibit suitable electronic conductivity [66] for their application as metallic interconnect (MIC) [67, 68, 69, 70]. Ferritic stainless steel is predominantly used in planar SOFC technology, as it offers a pondered balance between performance, degradation and cost; such compromise is essentially required for all SOFC components.

Different types of sealing solutions exist, spanning from rigid to compressive or hybrid types. Compressive gaskets, typically based on mica-silicates [71] offer high compliance and therefore reduced efforts on proximal cell components, whereas metal brazes or glass-ceramic hybrid materials present increased hermetic properties [72, 73].

1.3 Material Degradation

As the market entry for SOFC stationary application is promised for systems reaching reliably a lifespan of 40'000 h and more, the above listed components have to withstand degradation issues caused by the harsh SOFC operating conditions of high temperature and corrosive atmospheres. Focus is given here on the cathode compartment only.

Numerous reactions between SOFC materials are listed in the literature [74, 75, 76]. For instance, cathode and electrolyte materials react at high temperature, with resulting insulating zirconate formation in the case of zirconia-based electrolytes [77, 78, 79]. This issue is suppressed by the use of a GDC buffer layer, which is a prerequisite in the presence of reactive cobaltite perovskite cathodes.

Impurities generally involve deleterious degradation by their interaction with the cathode and cathode-proximal components. Impurity contamination generally originates from stacking components such as interconnects or sealing materials [75], balance-of-plant system compounds [80] or from the environmental air [81, 82, 83]. Adequate material compatibility within the cell as well as the system components is therefore essential.

Intrinsic cathode material degradation implies particle coarsening [84, 85, 86] and elemental demixing [87, 86], both strongly affected by the operating conditions (temperature, current density, i_{dots}).

The decrease of ionic conductivity with time, known as electrolyte ageing [88, 89, 90, 91], involves continuous increase of ohmic resistance [70, 92]. The same applies for MIC oxidation and scale thickening [93, 94, 95] with operating time. Only the reduction of operating temperature slows down these effects.

1.4 Cr-poisoning: a needle in a haystack

MIC oxidation via Cr_2O_3 scale formation also relates to Cr evaporation [95, 96, 97, 98], which is additionally influenced by water vapor [96, 97, 99] and the presence of alkali elements [100]. Cr-poisoning, i.e. the accumulation of Cr contamination within the cathode, blocking gaseous and electronic paths necessary for the oxygen reduction reaction [2, 3, 4] and hence leading to performance degradation, is a major degradation effect in high temperature electrochemical devices (also relevant to solid oxide electrolyzer cells, SOEC [15]) and is the focus of this thesis. Decreasing the Cr evaporation rate from MICs [101] by the application of an adequate protective coating is the most common mitigation strategy. The barrier coating layers are generally perovskite compounds [102, 103, 104], ceramics with spinel structure [33, 105, 106] or metallic coatings [33, 107]. Such protective layers react with the chromia scale to form a spinel phase with reduced Cr evaporation rate, presenting moreover a lower contact resistance and a lower increase of this resistance with time [106]. In addition, the MIC alloy composition is adjusted to form intrinsically a spinel-type oxide scale upon oxidation [68, 108, 109], to limit the amount and thickness of coating needed for an effective protection.

The cathode has to withstand $> 40'000$ h in proximity of Cr evaporating MIC, even when low-emitting through protective coatings. As such time a span precludes repetitive testing within a 4-year doctoral thesis, electrochemical SOFC tests over 1'000 h with subsequent Cr analysis meet first assessments.

Accumulated Cr amounts are on the order of $18 \mu\text{g}\cdot\text{cm}^{-2}$ Cr and responsible for ca. 1 % voltage decay at time-scales of 1'000 h (chapter 6.2). Figure 1.2 evidences such a quantity of Cr to correspond to a sewing needle finely distributed within a 200-cell SOFC stack with a cathode surface of 50 cm^2 per cell. The thesis objectives could be summarized by this question: " how to dislodge a Cr needle from an SOFC haystack?".

1.4. Cr-poisoning: a needle in a haystack

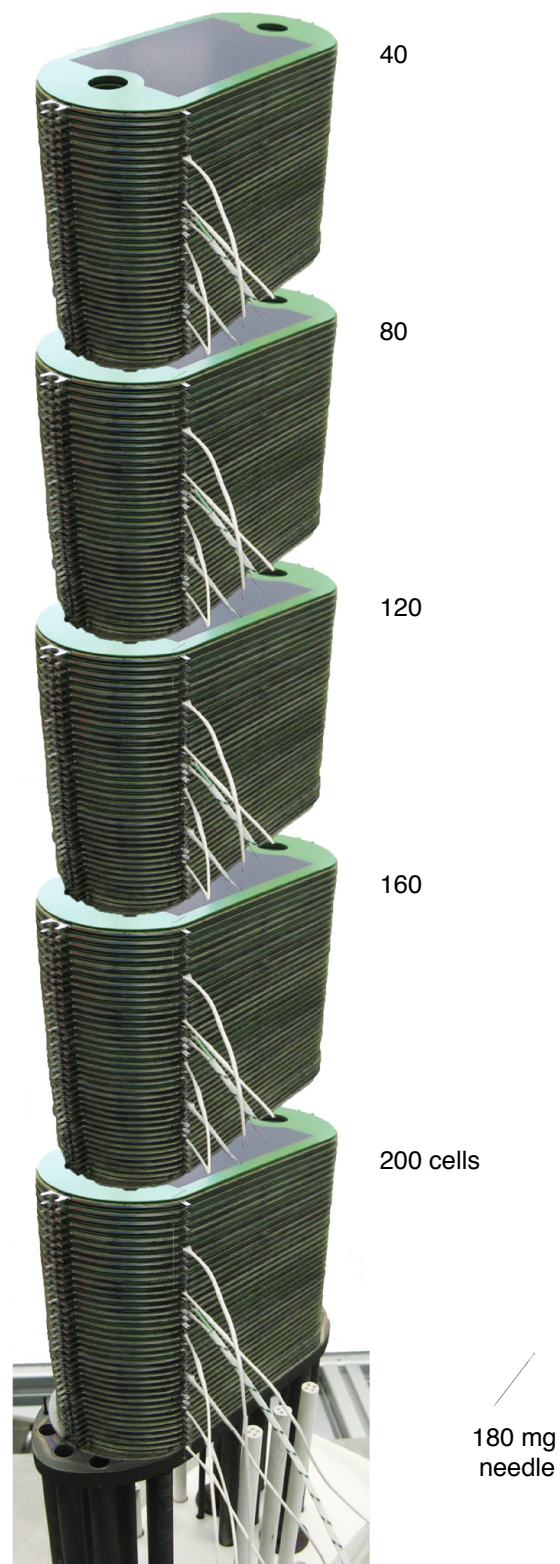


Figure 1.2: Representation of $18 \mu\text{g}\cdot\text{cm}^{-2}$ Cr accumulation typically responsible for $1\% \cdot \text{h}^{-1}$ degradation (chapter 6.2) with a 180 mg needle which would be distributed within the cathode area ($50 \text{ cm}^2/\text{cell}$) of this fictive 200-cell stack ($10'000 \text{ cm}^2$).

2 Experimental: Cr contamination generation

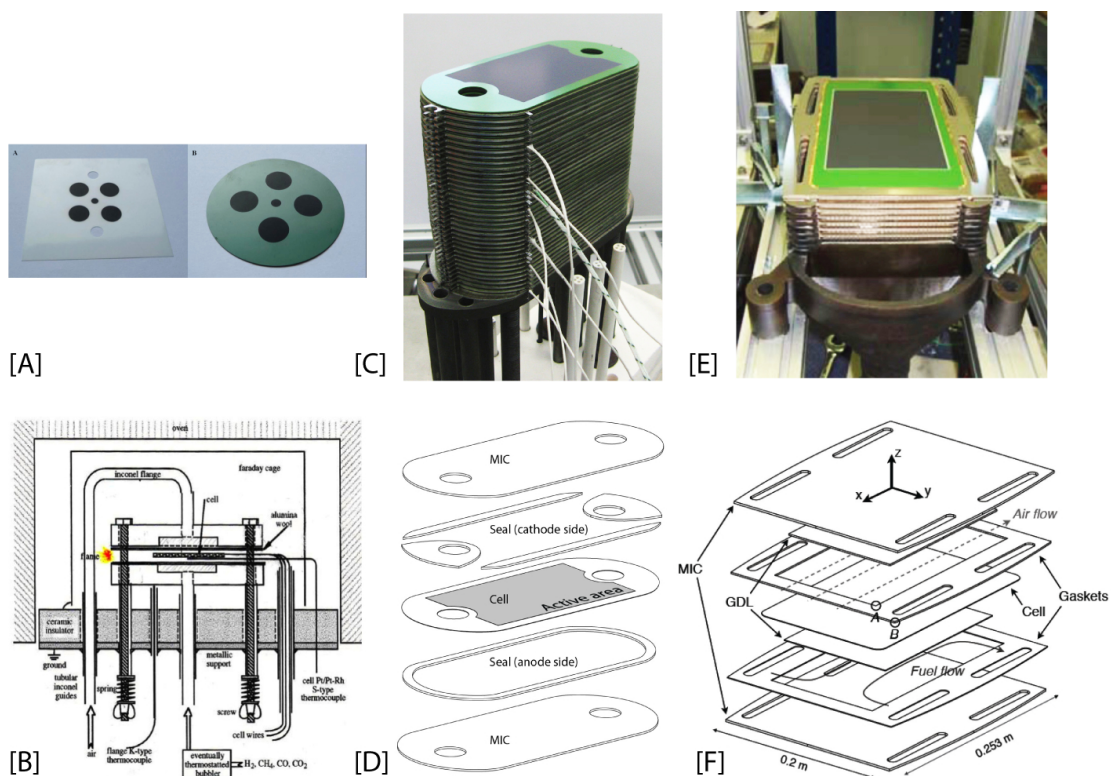


Figure 2.1: [A] Electrolyte-supported (left) and anode-supported (right) multicathode cells as well as button cells (not shown here) have been tested in open-flange-based experimental arrangements. [B] Such setups comprises Inconel flanges and tubing used for deliberate Cr contaminating conditions encountered in chapters 3-5. [C] This anode-supported cell with 50 cm² active area (black cathode region) was used for stack testing in chapter 8 where MIC and BoP compounds contributed to Cr-poisoning. [D] Compressive gaskets are used as sealing between cell and MIC. [E] The anode-supported cell dealt with in chapter 6 and 7 comprises a larger active area of 200 cm². [F] The repeat-unit assembly of this larger cell is similarly obtained, with Cr contamination originating also here from both MIC and BoP components.

Chapter 2. Experimental: Cr contamination generation

Figure 2.1 illustrates cell sizes and designs, with corresponding test arrangements¹, encountered within this thesis. Endurance testing with subsequent *post-test* analysis is the starting point of this work, which comes along with an initial query: is Cr detection, quantitatively and not only qualitatively, possible with *post-test* analysis? This question is addressed in chapter 3. The cell assemblies shown in Figure 2.1 comprise (ordered by cell size):

- Symmetrical button cells in chapter 5: $\text{Nd}_{1.95}\text{NiO}_{4+\delta}$ electrodes on thick $\text{Gd}_{0.10}\text{Ce}_{0.90}\text{O}_{1.95}$ pellets, including gold/ $\text{La}_{0.7}\text{Sr}_{0.3}\text{CoO}_3$ current collectors. Cr contamination sources are Inconel 600 tubing and flange components of an open-flange testing arrangement (appendix 2).
- Electrolyte-supported multicathode cell in chapter 3: $(\text{La}_{0.70}\text{Sr}_{0.30})_{0.90}\text{MnO}_{3\pm\delta}$ -8YSZ composite cathodes on 3YSZ electrolyte, where $(\text{Y}_2\text{O}_3)_{0.08}(\text{ZrO}_2)_{0.92}$ and $(\text{Y}_2\text{O}_3)_{0.03}(\text{ZrO}_2)_{0.97}$ are abbreviated 8YSZ and 3YSZ, respectively. Cr contamination was obtained by chromium nitrate impregnation prior to sintering.
- Anode-supported multicathode cell in chapters 3 and 4: $(\text{La}_{0.70}\text{Sr}_{0.30})_{0.90}\text{MnO}_{3\pm\delta}$ -8YSZ composite cathodes on Ni-YSZ anode-supported thin 8YSZ, including $(\text{La}_{0.65}\text{Sr}_{0.35})_{0.95}\text{MnO}_{3\pm\delta}$ cathode current collectors. Multicathode cell preparation and operation was described in P. Tanasini's thesis [110, 54] (appendix 2). Cr contamination originated from Inconel 602 tubing and flange components.
- Anode-supported cell stack in chapter 8: $(\text{La}_{0.6}\text{Sr}_{0.4})(\text{Co}_{0.8}\text{Fe}_{0.2})\text{-Gd}_{0.10}\text{Ce}_{0.90}\text{O}_{1.95}$ composite cathode (abbreviated LSCF-CGO) with LSCF current collector on Ni-YSZ supported thin YSZ, including a CGO cathode/electrolyte buffer layer. In depth description of stack assembly and testing is given in ref. [111]. Cr contamination was stemming from Crofer22APU interconnect covered with a $(\text{Mn}_1\text{Co}_{1.9}\text{Fe}_{0.1})\text{O}_4$ protective coating as well as from different high temperature BoP alloys.
- Anode-supported cell repeat-unit in chapters 6 and 7: $(\text{La}_{0.75}\text{Sr}_{0.25})_{0.95}\text{MnO}_{3\pm\delta}$ -8YSZ composite cathodes on Ni-YSZ supported thin 8YSZ including $(\text{La}_{0.8}\text{Sr}_{0.2})\text{CoO}_3$ current collector. In depth description of cell testing can be found in the thesis work of Z. Wullemin [53, 112] (appendix 1). Cr contamination originated nearly exclusively from 1.4828, 1.4849 and Incoloy 800 BoP alloys.

¹enlarged fig. 2.1B is given in appendix 2

3 Cr detection and quantification

Scripta Materialia **63** (2010) 895

3.1 Rapid chromium quantification in solid oxide fuel cell cathodes

J. Andreas Schuler^{a,b}, Pietro Tanasini^c, Aïcha Hessler-Wyser^b and Jan Van herle^a

^a *Laboratoire d'Énergie Industrielle (LENI), École Polytechnique Fédérale de Lausanne (EPFL), 1015 Lausanne, Switzerland*

^b *Centre Interdisciplinaire de Microscopie Electronique (CIME), École Polytechnique Fédérale de Lausanne (EPFL), 1015 Lausanne, Switzerland*

^c *Groupe de Génie Electrochimique (GGEC), École Polytechnique Fédérale de Lausanne (EPFL), 1015 Lausanne, Switzerland*

The detection and quantification of small quantities of Cr in (La,Sr)MnO₃/Y-ZrO₂ solid oxide fuel cell (SOFC) cathodes by energy-dispersive X-ray spectroscopy (EDXS) is not straightforward as Cr X-ray emission lines overlap with La/Mn and O lines. This work proposes an empirical law correlating the La peak height ratio $L_{\beta 2.15}/L_{\alpha 1}$ to Cr concentrations determined on Cr-doped LSM-YSZ samples characterized by EDXS. Calibration for the law was obtained by chemical analysis of dissolved cathodes. Quantification was confirmed by wavelength-dispersive X-ray spectroscopy.

1 Introduction

In state-of-the-art planar solid oxide fuel cell (SOFC) technology, a metallic interconnect material (MIC) ensures current collection and gas separation between cells stacked in series [1]. MICs are generally made of ferritic heat-resistant steels which are chromia formers, i.e. a Cr-rich oxide scale forms on their surface upon oxidation. In addition, balance-of-plant (BoP) components made of similar materials, like housing, tubing and heating elements, are also mostly covered by Cr oxide layers under oxidizing conditions.

Under SOFC operation conditions, volatile Cr species evaporate from MIC and BoP alloy surfaces in the form of oxide (CrO₃) and oxyhydroxide (CrO₂(OH)₂) species, in dry and humid

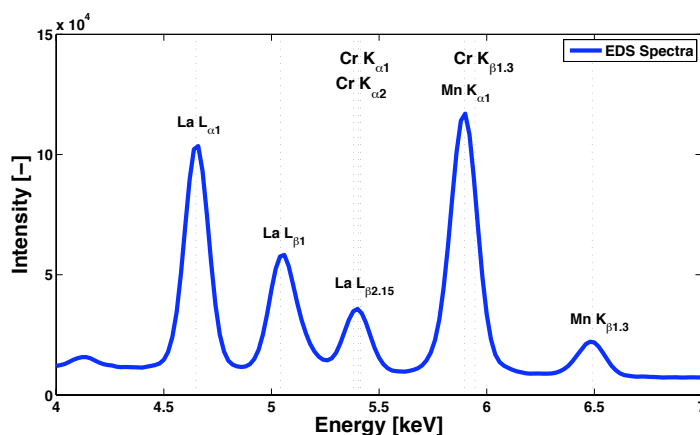


Figure 3.1: Cr X-ray emission lines overlap with those of La, Mn and O in the EDXS spectrum of LSM-YSZ SOFC cathodes.

air, respectively [2]. Tanigushi *et al.* [3] reported that these Cr^{6+} vapor species are reduced and accumulated at the cathode/electrolyte/air triple phase boundary (TPB), blocking oxygen access and reduction; the cathode polarization increase was shown to correlate with the presence of Cr at TPBs and to SOFC performance degradation. This is known as Cr poisoning [3,4]. In order to understand the Cr poisoning mechanism and its impact on SOFC operation, cathode degradation has to be linked to detection and quantification of Cr accumulations. For this purpose, an adequate characterization technique is needed, which ideally should be relatively simple and fast to implement.

Although the detection sensitivity of energy-dispersive X-ray spectroscopy (EDXS), of the order of 0.1%, is rather low [5,6], this technique provides localized information on large length scales (from micrometers to millimeters). This is essential, as shown by Wuillemin *et al.* [7-10, (ch. 6.2, 7.2, A.1)], who revealed the intrinsically local character of SOFC degradation by relating spatial distribution of degradation to spatial distribution of pollutant species.

SOFC cathodes are usually made of a porous strontium-doped lanthanum manganite (LSM) yttria-stabilized zirconia (YSZ) composite material. The $(\text{La,Sr})\text{MnO}_3$ perovskite phase, as catalyst and electronic conductor, promotes oxygen reduction at its TPB interfaces with air and YSZ; the latter conducts oxygen ions, O_2 , to the electrolyte. Detection of Cr accumulations by EDXS in this material faces an intrinsic difficulty due to the overlap of Cr X-ray emission lines with those from La, Mn and O.

Indeed, overlaps of Cr K with La L and Mn K lines, as well as Cr L with O K emission lines, are observed in EDXS spectra. Figure 3.1 illustrates an EDXS spectrum zoomed in the region of interest, where the principal Cr K-shell ($K_{\alpha 1}$ 5414 eV, $K_{\alpha 2}$ 5405 eV and $K_{\beta 1,3}$ 5946 eV) emission lines overlap with La L-shell ($L_{\alpha 1}$ 4650 eV, $L_{\alpha 2}$ 5042 eV and $L_{\beta 2,15}$ 5383 eV) and Mn K-shell ($K_{\alpha 1}$ 5898 eV and $K_{\beta 1,3}$ 6490 eV) emission lines [11,12]. Therefore, detection and quantification of small Cr amounts in SOFC cathodes is not straightforward.

Chen *et al.* [13] suggested using the L_{α}/L_{β} peak height ratio as an indicator of the presence of Cr. In their Cr-poisoning study of LSBCF $(\text{La,Sr,Ba})(\text{Co,Fe})\text{O}_3$ cathodes, the L_{α}/L_{β} atomic

3.1. Rapid chromium quantification in solid oxide fuel cell cathodes

ratio was found to be 5.21 for LBCF ((La,Ba)(Co,Fe)O₃), 5.25 for LSCF ((La,Sr) (Co,Fe)O₃) and 5.23 as an average value for LSBCF. Lower values of the peak ratio in the tested cathodes indicated the presence of Cr, due to the increase in L_β peak height stemming from the overlap with K_α emission lines (Fig. 3.1).

2 Experimental

The present study investigates peak height ratios of La L and Mn K emission lines in LSM-YSZ cathodes doped or impregnated with low concentrations of Cr (the presence of Cr was verified by X-ray fluorescence (XRF)), correlated to Cr contents, which were quantified by chemical analysis after acidic dissolution of the cathode materials. Moreover, the influence of the acceleration voltage in EDXS analysis is studied.

Porous LSM-YSZ layers, 5 μm thick and with a volume ratio of 33/33/33 LSM-YSZ-pores, were produced by screen-printing a powder-terpineol (3.2% ethylcellulose) ink on a YSZ support from Kerafol (Germany), according to an experimental method described in a recent work [14 (A.2)]. LSM powder (La_{0.70},Sr_{0.30})_{0.90}MnO_{3±δ} from Praxair (USA), YSZ powder ((Y₂O₃)_{0.08}(ZrO₂)_{0.92}) from Tosoh (Japan) and chromium nitrate nonahydrate solution from Alfa Aesar (Germany) were the raw materials. Cr-doped samples were obtained by adding a chromium nitrate-ethanol solution to the ink. The samples were sintered at 1050°C for 1 h. In one case, the LSM-YSZ layer was sintered without Cr, but followed by impregnation with a chromium nitrate/ethanol solution and a second heat treatment at 600°C for 1 h; this temperature was chosen high enough to decompose Cr nitrate in the cathode and low enough to avoid subsequent Cr evaporation.

Characterization was performed by (i) EDXS with a FEI scanning electron microscope (USA) coupled to an EDS analyzer, plus a Si-drift detector from Oxford Instruments (UK) combined with Inca software; (ii) by wavelength-dispersive X-ray spectroscopy (WDXS) with a Wave 700 detector, a LiF diffraction crystal and Inca software on a Zeiss 1525 scanning electron microscope (Germany); and (iii) by XRF with a Fischer Xan system (UK) equipped with WinFam32 software. The samples were immersed in hot concentrated nitric acid to dissolve perovskite cathode layers (complete dissolution was verified by EDXS on zirconia remnants). The obtained solutions were analyzed for Cr and Sr content by inductively coupled plasma optical emission spectrometry (ICP-OES) with a Perkin-Elmer Optima 3300DV (USA) calibrated with standards. Sr was used for comparative quantitative analysis as appropriate Sr standards were available.

Peak heights (counts) were extracted from raw spectra, from EDXS data-cubes obtained by mapping Cr containing LSM-YSZ layer surfaces (circular geometry; 4 mm diameter), of different regions of homogeneous composition (~9 mm²). The presence/absence of Cr was verified by XRF for 12 doped, 2 impregnated and 1 blank sample prior to EDXS analyses. The spot intensity and the aperture size for the electron beam, as well as the process time of the EDXS software, were kept constant, for a given acceleration voltage, to ensure high and constant X-ray count rates with a high spectral resolution.

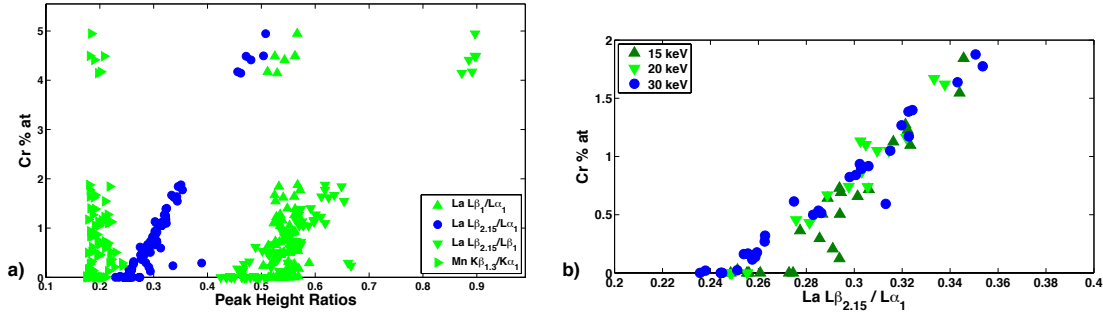


Figure 3.2: (a) Cr quantification (normalized to LSM content) given by EDXS measurements related to peak height ratios of principal La L- and Mn K-shell X-ray emission lines. (b) Increasing acceleration voltage reduces the deviation from a linear ratio/concentration correlation, especially at low Cr concentration.

3 Results and discussion

Cr quantification (normalized to LSM, using the Sr amount obtained by ICP-OES for normalization) by EDXS related to peak height ratios is given in Figure 3.2a. The lanthanum $L_{\beta 2.15}/L_{\alpha 1}$ ratio results to be the most reliable indicator for Cr presence as its variation is sensitive to Cr concentrations. Figure 3.2b illustrates the effect of acceleration voltage on EDXS quantification measurements: higher acceleration voltages reduce the deviation from a linear¹ correlation of peak ratio to concentration, especially at low Cr concentrations. Total Cr concentrations were obtained from ICPOES measurements after dissolving Cr-containing samples. To ensure Cr amounts were within ICP-OES detection limits, several samples with similar Cr contents were dissolved simultaneously. The measurement results for four solutions are plotted in Figure 3.3. The normalization to LSM was enabled by the simultaneous measurement of Cr and Sr ions². Mn ions were not quantified as their concentration after dissolution is changed, compared to their initial value, by Mn diffusion into YSZ during sintering. Quantification of La ions was not done due to the absence of available standards. The Cr concentrations were related to a La peak height ratio $L_{\beta 2.15}/L_{\alpha 1}$, obtained by averaging ratios from several samples before dissolution. Weighted least-square (WLS) regression was performed on ICP-OES data; in order to take into account the difference in precision, the reciprocal of the measurement variance was used as a weighting parameter. The WLS regression generated an empirical relation for Cr quantification as follows:

$$Cr [\%] = 16.24 \frac{L_{\beta 2.15}}{L_{\alpha 1}} - 4 \quad (3.1)$$

¹The linear dependence between the amount of Cr and the $L_{\beta 2.15}/L_{\alpha 1}$ peak height ratio was questioned; such a correlation should strictly speaking be described with higher exponentiation; as the Cr amounts in question, which add to the $L_{\beta 2.15}$ peak, are very low in this application (1-2%), the linear approximation is believed to be sufficient.

²The deviation of the amounts of Sr measured by ICP-OES from the quantity given by geometrical considerations (1.12 cm² electrode area, 5 μ m thickness, 33 % porosity, 50/50 LSM/YSZ ratio, (La_{0.7},Sr_{0.3})_{0.9}MnO_{3± δ} LSM composition) was chosen as precision indicator for the Cr quantification (cf error-bars in Fig. 3.3).

3.1. Rapid chromium quantification in solid oxide fuel cell cathodes

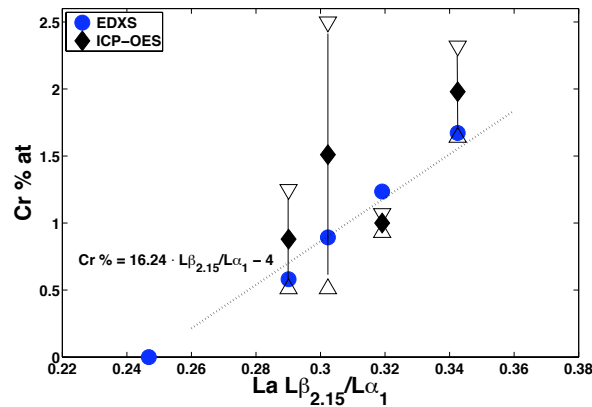


Figure 3.3: An empirical relation (dashed line) for Cr quantification in LSM-YSZ cathode material using the EDXS La $L_{\beta 2.15}/L_{\alpha 1}$ peak height ratio is obtained from Cr quantification results by ICP-OES after acidic dissolution (diamonds); this result is compared with Cr quantification by EDXS (circles).

The comparison between ICP-OES and EDXS quantification results indicates that this technique accurately quantifies Cr concentrations in LSM-YSZ cathode materials.

During SOFC operation, volatile Cr^{6+} species tend to deposit at the TPBs, forming resistive Cr_2O_3 , $(\text{Mn,Cr})_3\text{O}_4$ or Cr-doped LSM phases [3,4,15], blocking oxygen access and reduction. The present work does not aim to investigate the reaction of Cr within the porous LSM-YSZ cathode material, but simply to quantify the Cr content. Therefore, SEM EDXS observations were done at the lowest magnification (over several mm^2), using a defocalized electron probe, to analyze homogeneous zones.

Peak heights were extracted from EDXS spectra, instead of the probably more accurate peak areas, as the former information is easier to access from the measurement results, and one motivation for this study was rapid quantification.

A linear correlation was found between the La $L_{\beta 2.15}/L_{\alpha 1}$ peak height ratio and the concentration of Cr within the cathode material determined by EDXS. Cr quantification by the latter technique is close to the results from chemical analyses. This indicates that the EDXS software deconvolution algorithm allows proper quantification of Cr despite the strong overlap with La, Mn and O peaks.

The use of a high acceleration voltage allows a more accurate correlation between Cr concentration and the La $L_{\beta 2.15}/L_{\alpha 1}$ peak height ratio. Higher voltage generates higher fractions of more energetic X-rays, i.e. increased fraction of Cr K-shell to Cr L-shell emission. On the other hand, large interaction volumes of the electron beam within the cathode material, delocalizing the information, reduce imaging/mapping possibilities, and may overestimate the contributions of LSM or YSZ for instance.

However, once the presence of Cr is established, related techniques such as WDXS enable elemental mapping to be performed. Figure 3.4 illustrates a cathode where the electrochemical characterization of cathode performance degradation suggested the presence of Cr [14].

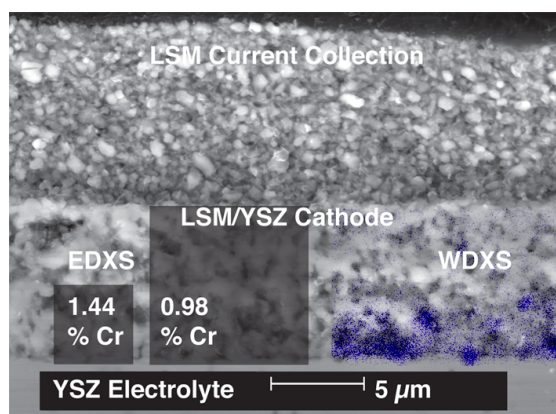


Figure 3.4: SEM image of a polished SOFC cathode cross-section. Peak height ratios from EDXS spectra of a defined region quantify the extent of Cr poisoning. WDXS Cr mapping localizes the pollutant near the cathode-electrolyte interface.

The here-proposed method (cf. Eq. 3.1) enabled the Cr content within the cathode to be quantified. Moreover, this approach allowed us to rapidly obtain concentration profiles over the cathode thickness. Cr contents in 25 and 100 μm^2 regions, reported in Figure 3.4, suggest Cr is preferentially accumulated at the active TPBs (near the electrolyte). Cr localization at active TPBs and its quantification was confirmed by the WDXS measurement.

4 Conclusion

The present study has highlighted the use of the lanthanum $L_{\beta 2.15}/L_{\alpha 1}$ peak height ratio as an adequate indicator for Cr presence. Moreover, using the hereproposed empirical relation, rapid Cr quantification by EDXS is possible.

This method reveals itself to be a valuable tool for the optimization of *post-test* analysis in SOFC research. Indeed, as cell sizes are increased for enhanced power output, rapid *post-test* methods are needed to scan for pollutant species over large cathode areas with degraded performance. Cr detection in SOFC cathodes should no longer be like searching for a needle in a haystack.

Acknowledgements

The Swiss Federal Energy Office (Contract 153569 AccelenT) is gratefully acknowledged for financial support. Christian Gehrig is thanked for sample preparation. Stéphane Thonney and Christophe Roussel (Chemical Engineering, Institute of Chemical Sciences and Engineering, EPFL), Jean-David Teuscher (Central Environmental Laboratory, EPFL), François Bussy (Institute of Mineralogy and Geochemistry, Faculty of Geosciences and Environment, UNIL), Daniel Zufferey (Design & Materials Unit, HES-SO Valais) are thanked for XRF, ICP-OES and WDS measurements, respectively. Many thanks to Marco Cantoni (CIME, EPFL) for his introduction to EDXS analysis.

References

- 1 T. Kadowaki, T. Shiomitsu, E. Matsuda, H. Nakagawa, H. Tsuneizumi, *Solid State Ionics* 67 (1993) 65-69.
- 2 B.B. Ebbinghaus, *Combust. Flame* 93 (1993) 119-137.
- 3 S. Tanigushi, M. Kadowaki, H. Kawamura, T. Yasuo, Y. Akiyama, Y. Miyake, T. Saitoh, J. *Power Sources* 55 (1995) 73-79.
- 4 S.P.S. Badwal, R. Deller, K. Foger, Y. Ramprakash, J.P. Zhang, *Solid State Ionics* 99 (1997) 297-310.
- 5 T. Horita, Y.P. Xiong, M. Yoshinaga, H. Kishimoto, K. Yamaji, M.E. Brito, H. Yokokawa, *ECS Trans.* 25 (2009) 2881-2888.
- 6 T. Horita, Y.P. Xiong, M. Yoshinaga, H. Kishimoto, K. Yamaji, M.E. Brito, H. Yokokawa, *Electrochem. Solid- State Lett.* 12 (2009) B146-B149.
- 7 Z. Wuillemin, A. Nakajo, A. Müller, J.A. Schuler, S. Diethelm, J. Van Herle, D. Favrat, *ECS Trans.* 25 (2009) 457-471. (appendix 1)
- 8 J.A. Schuler, Z. Wuillemin, A. Hessler-Wyser, J. Van Herle, *ECS Trans.* 25 (2009) 2845-2852. (ch. 7.2)
- 9 Z. Wuillemin, EPFL Ph.D. Thesis No. 4525, Lausanne, Switzerland, 2009.
- 10 J.A. Schuler, C. Gehrig, Z. Wuillemin, A.J. Schuler, J. Wochele, A. Hessler-Wyser, C. Ludwig, J. Van herle, *EFCF Proceeding* (2010) 0715. (ch. 6.2)
- 11 J.A. Bearden, *Rev. Mod. Phys.* 39 (1967) 78-124.
- 12 M.O. Krause, J.H. Oliver, *J. Phys. Chem. Ref. Data* 8 (1979) 329-339.
- 13 X. Chen, L. Zhang, S.P. Jiang, *J. Electrochem. Soc.* 155 (2008) B1093-B1101.
- 14 P. Tanasini, J.A. Schuler, M.L. Ben Ameer, C. Comninellis, J. Van herle, *Proc. Eur. Fuel cell Forum* 1504 (2010). (ch. 2)
- 15 E. Konyshova, J. Mertens, H. Penkalla, L. Singheiser, K. Hilpert, *J. Electrochem. Soc.* 154 (2007) B1252-B1264.

4 Overpotential-driven Cr-poisoning

Electrochemistry Communications **12** (2010) 1682

4.1 Cathode thickness-dependent tolerance to Cr-poisoning in solid oxide fuel cells

J. Andreas Schuler^{a,b}, Pietro Tanasini^c, Aïcha Hessler-Wyser^b,
Christos Comninellis^c, Jan Van herle^a

^a *Laboratoire d'Énergie Industrielle (LENI), École Polytechnique Fédérale de Lausanne (EPFL), 1015 Lausanne, Switzerland*

^b *Centre Interdisciplinaire de Microscopie Electronique (CIME), École Polytechnique Fédérale de Lausanne (EPFL), 1015 Lausanne, Switzerland*

^c *Groupe de Génie Electrochimique (GGEC), École Polytechnique Fédérale de Lausanne (EPFL), 1015 Lausanne, Switzerland*

This work aimed to set new guidelines for the quantification of Cr accumulation in solid oxide fuel cell cathodes after operation, and enabled to pinpoint a diffusion-controlled tolerance to Cr-poisoning for increased cathode thickness; the additional cathode material decreases the deposition rate from Cr vapor species in the active layer. These experimentally based findings were obtained by direct comparison of cathode performances measured on a segmented test arrangement enabling the independent control of four cathodes, with different thicknesses, on an anode-support. The cathode thickness-dependent performance degradation was correlated to deliberate poisoning by volatile Cr species stemming from the test arrangement.

1 Introduction

Under solid oxide fuel cell (SOFC) operating conditions, volatile Cr species emanate from Cr-containing materials and accumulate at the air/cathode/electrolyte triple phase boundaries (TPB), blocking oxygen access and reduction, and causing cathode performance losses. Although this phenomenon - so-called Cr-poisoning [1] - is well-known in SOFC technology, the lack of adapted tools for accurate quantification of Cr accumulation hindered so far the

implementation of a correlation between deposited Cr amounts and operating parameters to predict SOFC lifetime [2,3]. The present work aims to more closely investigate Cr-poisoning considering in particular this issue.

As Cr accumulations in cathodes are typically small and the detection of low Cr concentrations in SOFC cathode materials is not straightforward [2,3], we developed a new efficient Cr quantification methodology [4, (ch. 3.1)] to correlate the outcome to performance degradation.

This methodology is here applied to the *post-test* analysis of a segmented cell with four cathodes of different thicknesses, where air electrode poisoning by Cr, stemming from Cr-containing test rig material, is at the origin of cathode performance degradation [5, (A.2)].

To correlate Cr-poisoning to cathode performance, comparable cathode behavior measurements are needed, which are challenging to obtain in a series of consecutively run button cell tests. In repetitive testing, daily/seasonal and experimental variations are difficult to avoid; this is illustrated by the laboratory- or test-specific nature of SOFC component behavior [6], which can be due to e.g. impurity intakes in the preparation of reactants, samples or the test assembly itself. Moreover, longer equipment time and/or an increased number of test rigs are needed for repetitive experiments, that slow down the research progress.

The segmented test arrangement [5, (A.2)], including multiple (n) cathodes on a single anode-supported cell, enables to overcome both time and reproducibility issues, decreasing n-fold the testing time and ensuring the same test conditions for all cathodes operated in parallel, while varying only a single parameter - here the cathode thickness - per electrode.

2 Experimental

Four $(\text{La}_{0.70}\text{Sr}_{0.30})_{0.90}\text{MnO}_{3\pm\delta}$ (LSM)- $(\text{Y}_2\text{O}_3)_{0.08}(\text{ZrO}_2)_{0.92}$ (YSZ) composite cathodes were screen printed on a YSZ electrolyte-covered Ni-YSZ anode-support, by depositing successively a different number of layers ($5\ \mu\text{m}$ per layer: $1\ \text{cm}^2$ area) to obtain cathodes with thicknesses of 5, 10, 15, and $20\ \mu\text{m}$. A $10\ \mu\text{m}$ thick LSM current collection layer (CCL) covered the electrodes. A detailed experimental description can be found elsewhere [5, (A.2)].

The cathodes were fed with a $450\ \text{ml}\ \text{min}^{-1}$ air flux at 298 K with 5% relative humidity. The air was heated to 1123 K within a feed tube ($6\ \text{mm}$ int. diam./ $4.7\cdot 10^{-3}\ \text{m}^2$ area) of Inconel 602 alloy, which had been used under oxidizing conditions for many kilo-hours (kh) prior to this experiment.

Post-test analyses were done by energy-/wavelength-dispersive X-ray spectroscopy (EDS/-WDS), using the relation correlating the lanthanum $L_{\beta 2.15}/L_{\alpha 1}$ EDS peak height ratio to Cr concentrations, proposed in [4, (ch. 3.1)], and using the Cr quantification methodology described therein.

Cr detection by EDS in LSM-YSZ cathodes is challenged [2,3] by the overlap of Cr, La, Mn, and O emission lines. We recently established a methodology for rapid Cr quantification [4, (ch. 3.1)], which uses the La L_{β}/L_{α} peak height ratio, proposed elsewhere [7,8] as Cr presence indicator.

We aimed in particular to propose an objective procedure to quantify Cr in tested cathodes, as opposed to the subjective, only qualitative, interpretation of Cr-distribution mappings.

4.1. Cathode thickness-dependent tolerance to Cr-poisoning in solid oxide fuel cells

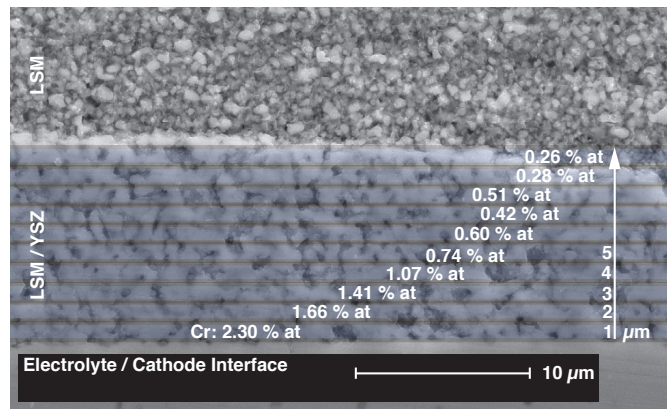


Figure 4.1: Cr concentrations from 1 μm cathode slices, near the cathode/electrolyte interface, are directly extracted from EDS spectra, using the $\text{La } L_{\beta 2.15}/L_{\alpha 1}$ peak height ratio for rapid quantification [4, (ch. 3.1)].

Therefore, cathode cross-sections were mapped over a given time (here 30 min), and Cr was quantified in geometrically defined regions ($40 \cdot 1 \mu\text{m}^2$ slices, cf. Fig. 4.1). The use of high acceleration voltage (30 keV) enables to detect even small Cr concentrations, in the order of 0.1 at.%; on the downside, the precise spatial imaging possibilities are lost by the high delocalization of generated X-rays. However, locally resolved Cr distribution can be accessed using a related technique, like WDS [4, (ch. 3.1)].

3 Results

3.1 Thickness-dependent degradation While the thinnest, 5 μm , cathode showed the worst relative performance, the three other cathodes showed initially similar performances; overall there was a clear trend of increasing degradation rate with decreasing thickness: voltage decay rates (at a constant current density for all cathodes) were estimated to 0.9, 1.5, 2.2 and 6 $\% \cdot \text{kh}^{-1}$, for the 20 μm down to 5 μm thick cathodes, respectively [5, (A.2)], and are reported in Fig. 4.3. The here observed thickness-dependent electrochemical behavior, as well as short-term re-activation caused by transients in operation, also reported by others [9-11], suggest the presence of Cr contamination [12,13], originating here deliberately from the Cr-containing test rig components (discussed in more detail also for a SOFC stack arrangement in [14, (ch. 7.2)]), in the active cathode layer.

3.2. Cr contamination In the pioneering study of Cr-poisoning by Taniguchi *et al.* [3], Cr transport towards the cathode was due to the presence of Inconel 600 alloy. Even in Al-containing Ni/Cr/Fe alloys, such as Inconel 602 used in this study, where a continuous outer alumina layer can under certain circumstances suppress Cr evaporation from underneath, the presence at the alloy surface of Cr-containing oxide is usual in oxidizing conditions. Cr evaporation from this alloy is estimated to $1 \cdot 10^{-11} \text{ kg m}^{-2} \text{ s}^{-1}$ under equilibrium evapo-

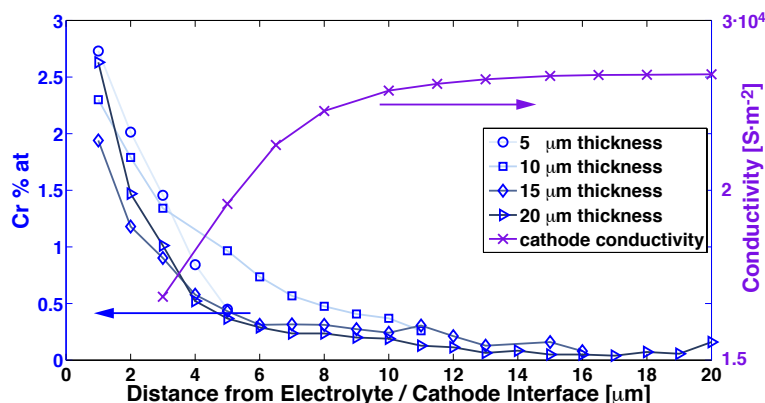


Figure 4.2: Cr concentration profiles in cathodes with 5, 10, 15 and 20 μm thickness indicate Cr to be preferentially located in the active cathode region near the electrolyte. Predicted value for electrode conductivity under operation indicates the active cathode area to extend ca. 10 μm from the interface.

ration conditions (imposed by the experimental conditions) [15], corresponding to a partial pressure for volatile Cr species of $3 \cdot 10^{-9}$ atm. This is below the saturation pressures, which are $4 \cdot 10^{-9}$ and $1.3 \cdot 10^{-8}$ atm for CrO_3 and $\text{CrO}_2(\text{OH})_2$, respectively [16, (ch. 6.2),17], at 1123 K and $1.8 \cdot 10^{-3}$ atm $p(\text{H}_2\text{O})$.

A total quantity of 0.17 mg Cr can then be estimated to evaporate from the test rig for 1 kh of testing time. Several authors reported that only a fraction of the supplied Cr is actually deposited in the cathode [2,3,18,19], which corresponds, on average, to 1/10. Given this consideration, together with the fact that 13% of the air feed is supplied to each electrode (due to the test geometry), roughly 2 μg of Cr is expected to deposit per cathode.

3.3 Cr-poisoning The distribution of Cr accumulations in cathodes can be related to the electrochemical activity either through direct reduction of Cr^{VI} volatile species to Cr^{III} at the active sites for oxygen reduction [1] or through the reaction of the Cr^{VI} species with Mn^{II} nucleation sites generated during polarization [13].

Either way, a preferential deposition is expected in the electrochemically active layer, the extent of which is estimated from percolation theory [20] by calculating the performance of LSM/YSZ cathode while varying the electrode thickness, as illustrated in Fig. 4.2. A 5 μm cathode has its performance limited by the insufficient extension of the cathode material, while 10-20 μm thick electrodes show better performances, in agreement with the experimental results [5, (A.2)].

Cr concentration profiles, by Cr quantification over 1 μm cathodes slices (cf. Fig. 4.1) taken across the cathode thicknesses are illustrated in Fig. 4.2 and clearly indicate a preferential accumulation near the cathode/electrolyte interface in the region with active sites for oxygen reduction, that extends to ca. 10 μm thickness, with a very good correspondence to model predictions.

The measured Cr quantities in the active cathode area, by extracting the Cr quantity from

4.1. Cathode thickness-dependent tolerance to Cr-poisoning in solid oxide fuel cells

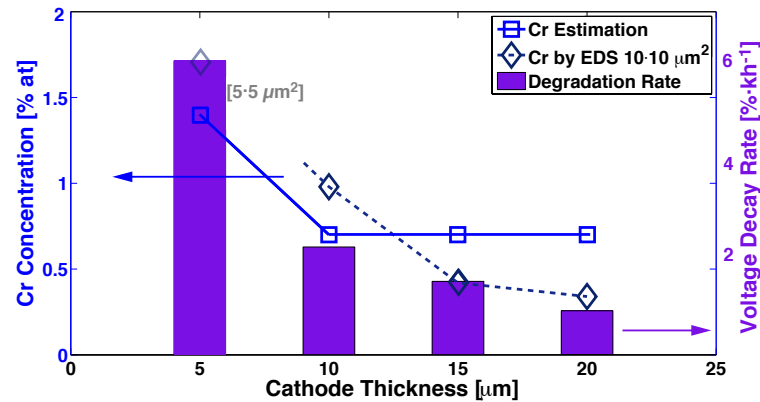


Figure 4.3: Cr concentrations in the active cathode region (by EDS from ca. $10 \cdot 10 \mu\text{m}^2$ adjacent to the electrolyte) are below the estimated values (evaporation-transport-deposition) for the thicker electrodes and are well correlating with cathode performance degradation.

EDS spectra taken over $10 \cdot 10 \mu\text{m}^2$ regions ($5 \cdot 5 \mu\text{m}^2$ for the thinnest cathode), are reported in Fig. 4.3. These values are below Cr accumulations calculated earlier (evaporation-transport-deposition) and normalized to the LSM content within the active layer.

Decreasing Cr amounts - related to decreasing degradation as shown in Fig. 4.3 - are found with increasing cathode thickness whereas the remaining cathode thickness and the LSM CCL are not liable to Cr deposition (negligible Cr quantities were found in these layers).

4 Discussion

These findings are in opposition to related studies reporting: i) that the presence of extended cathode material beyond the active layer protects the active area while acting as a chemical trap for poisoning species [9], ii) that 50% of accumulated Cr is located outside the active TPB region for LSM cathodes [2] and iii) that no clear correlation between Cr amounts and cathode performance is evident [3,18].

The total cathodic overpotential and its distribution along the active thickness are similar in the three thicker electrodes, and cannot explain the decreasing Cr amount for cathodes with increased thickness. Our conclusion, based on the observations and measurements presented here, is that the additional cathode thickness acts as a diffusion barrier, decreasing the effective concentration of Cr species in the underlying active area and therefore slowing down its accumulation there, as illustrated in Fig. 4.4.

5 Conclusions

The present study illustrates the possibility of space-resolved quantification of Cr accumulations in SOFC cathodes after operation, even at low concentrations (<0.5 at.%). We believe that the lack of objective quantification tools to study Cr-poisoning has complicated the search for correlations between Cr accumulations and SOFC operating parameters (e.g. electrode thick-

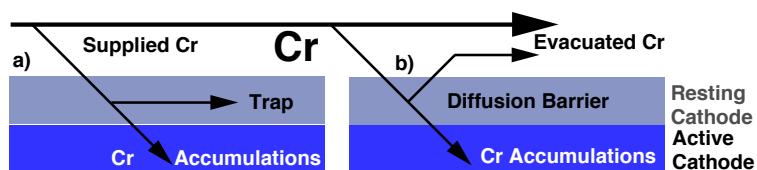


Figure 4.4: Cathode thickness-dependent tolerance to Cr-poisoning by a) trapping Cr species in extended cathode material beyond the active layer [9] or b) the here proposed diffusion-controlling barrier protecting the active cathode.

ness or current load) until into recent literature. Direct comparison of cathode performance was only enabled here by the experimental segmented cathode design, ensuring identical operating conditions for the four tested electrodes, with the added benefit of decreasing the total experimental time compared to repetitive button cell tests. Based on the experimental observations and the objective quantification method, preferential Cr accumulation in the active cathode region is confirmed. Additional cathode material on top of this active zone is suggested to act not as a chemical trap but as a diffusion barrier.

Acknowledgements

The Swiss Federal Energy Office - Contracts 153569, 152901 - is gratefully acknowledged for the financial support. M. L. Ben Ameer is thanked for her keen involvement in this work during her diploma thesis at EPFL and G. Foti for reviewing the manuscript. It is also a pleasure to acknowledge M. Cantoni for his encouraging interest in this work.

References

- 1 S. Taniguchi, M. Kadowaki, H. Kawamura, T. Yasuo, Y. Akiyama, Y. Miyake, T. Saitoh. *J. Power Sources* 55 (1997) 73.
- 2 T. Horita, Y. Xiong, M. Yoshinaga, H. Kishimoto, K. Yamaji, M.E. Brito, H. Yokokawa, *Electrochem. Solid-State Lett.* 12 (2009) B146.
- 3 T. Horita, Y. Xiong, H. Kishimoto, K. Yamaji, M.E. Brito, H. Yokokawa, *J. Electrochem. Soc.* 157 (2010) B614.
- 4 J.A. Schuler, P. Tanasini, A. Hessler-Wyser, J. Van herle, *Scr. Mater.* 63 (2010) 895. (ch. 3.1)
- 5 P. Tanasini, J.A. Schuler, Z. Wullemin, M.L. Ben Ameer, C. Comninellis, J. Van herle, *J. Power Sources* 196 (2011) 7079. (appendix 2)
- 6 M. Mogensen, K.V. Jensen, M.J. Joergensen, S. Primdahl, *Solid State Ionics* 150 (2002) 123.
- 7 M.C. Tucker, H. Kurokawa, C.P. Jacobson, L.C. De Jonghe, S.J. Visco, *J. Power Sources* 160 (2006) 130.

4.1. Cathode thickness-dependent tolerance to Cr-poisoning in solid oxide fuel cells

- 8 X. Chen, B. Hua, J. Pu, J. Li, L. Zhang, S.P. Jiang, *Int. J. Hydrogen Energy* 34 (2009) 5737.
- 9 E. Konyshева, J. Mertens, H. Penkalla, L. Singheiser, K. Hilpert, *J. Electrochem. Soc.* 145 (2007) B1252.
- 10 S.P.S. Badwal, R. Deller, K. Foger, Y. Ramprakash, J.P. Zhang, *Solid State Ionics* (1997) 297.
- 11 M.J. Joergensen, M. Mogensen, *J. Electrochem. Soc.* 148 (2001) A433.
- 12 Y. Matsuzaki, I. Yasuda, *Solid State Ionics* 132 (2000) 271.
- 13 S.P. Jiang, J.P. Zhang, K. Foger, *J. Electrochem. Soc.* 147 (2000) 3195.
- 14 J.A. Schuler, Z. Wuillemin, A. Hessler-Wyser, J. Van herle, *ECS Trans* 25 (2009) 2845. (ch. 7.2)
- 15 M. Stanislawski, E. Wessel, K. Hilpert, T. Markus, S. Singheiser, *J. Electrochem. Soc.* 154 (2007) A295.
- 16 J.A. Schuler, C. Gehrig, Z. Wuillemin, A.J. Schuler, J. Wochele, C. Ludwig, A. Hessler-Wyser, J. Van herle, *J. Power Sources* 196 (2011) 7225. (ch. 6.2)
- 17 Z. Wuillemin, EPFL PhD thesis no. 4525, Lausanne Switzerland (2009).
- 18 N.H. Menzler, I. Vinke, H. Lippert, *ECS Trans.* 25 (2009) 2899.
- 19 H. Yokokawa, H. Kishimoto, K. Yamaji, T. Horita, *ECS Trans.* 25 (2009) 401.
- 20 P. Costamagna, P. Costa, E. Arato, *Electrochim. Acta* 43 (1998) 967.

Electrochemical $\text{Cr}_g^{(VI)}$ reduction

Journal of Power Sources **213** (2012) 223

5.1 Nd-nickelate SOFC cathode sensitivity to Cr/Si contamination

J. Andreas Schuler^{a,b}, Henning Lübke^c, Aïcha Hessler-Wyser^b, Jan Van herle^a

^a *Laboratoire d'Énergie Industrielle (LENI), École Polytechnique Fédérale de Lausanne (EPFL), 1015 Lausanne, Switzerland*

^b *Centre Interdisciplinaire de Microscopie Electronique (CIME), École Polytechnique Fédérale de Lausanne (EPFL), 1015 Lausanne, Switzerland*

^c *Laboratoire de Technologie des Poudres (LTP), École Polytechnique Fédérale de Lausanne (EPFL), 1015 Lausanne, Switzerland*

The stability of Nd-nickelate, considered as an alternative solid oxide fuel cell (SOFC) cathode material, was evaluated in this work on its tolerance towards contaminants. Symmetrical cells with $\text{Nd}_{1.95}\text{NiO}_{4\pm\delta}$ electrodes sintered on gadolinia-doped ceria electrolyte supports were monitored over time-spans of 1000 h at 700°C under polarisation in an air-flux with deliberate chromium contamination. Impedance spectroscopy pointed out a polarization increase with time by the growth of the low frequency arc describing the electrode's oxygen reduction and incorporation processes. *Post-test* observations revealed polluted cathode regions with increasing amounts of Cr accumulations towards the electrolyte/cathode interface. Cr deposits were evidenced to surround active nickelate grain surfaces forming Nd-containing Cr oxides. In addition to exogenous Cr contamination, endogenous contamination was revealed. Silicon, present as impurity material in the raw NNO powder (introduced by milling during powder processing), reacts during sintering steps to form Nd-silicate phases, which decreases the active cathode surface. Nd-depletion of the nickelate, as a result of secondary phase formation with the contaminants Cr and Si (NdCrO_4 and $\text{Nd}_4\text{Si}_3\text{O}_{12}$), then triggers the thermally induced decomposition of NNO into stoichiometric $\text{Nd}_2\text{NiO}_{4\pm\delta}$ and NiO. Summarized, the alternative Nd-nickelate cathode also suffers from degradation caused by pollutant species, like standard perovskites.

0 Introduction

The oxygen-overstoichiometric Nd-nickelate $\text{Nd}_2\text{NiO}_{4\pm\delta}$ structure is described as alternately stacked perovskite- and rock-salt-like layers, as the first member of the Ruddlesden-Popper series $\text{A}_{n+1}\text{B}_n\text{O}_{3n+1}$. Contrarily to perovskite-based cathode materials, which generally need A-site doping (usually by Sr) to generate oxygen nonstoichiometry under certain conditions of temperature and oxygen partial pressure, oxygen can incorporate into the nickelate structure allowing for mixed electronic and ionic conductivity already at low temperature in air. Nd-nickelate is thus seen as an intermediate-temperature solid oxide fuel cell (IT-SOFC) electrode material alternative to perovskites [1].

Under SOFC operating conditions, volatile chromium species emanate from cell-proximal Cr-containing materials and accumulate at the active cathode sites for oxygen reduction, leading to polarization losses and performance decrease. An alternative composition free of strontium and manganese, is suggested to mitigate the extent of this degradation [2] - so-called Cr-poisoning [3]. Nickelate cathodes are supposedly more tolerant to Cr-poisoning, as indicated by a recent study [4], where only a negligible chemical oxygen surface exchange coefficient decrease was measured for Nd-nickelate material after exposure to Cr (10 nm thick Cr-layer on NNO). Investigations of Cr-poisoning in such cathodes are, however, scarce; the present work aims to contribute to this topic by testing $\text{Nd}_{1.95}\text{NiO}_{4\pm\delta}$ electrodes under deliberate Cr contamination conditions.

Cr-poisoning conditions are created here by humidifying the air fed to the cathode, preheated in a Cr-containing alloy tube, as the partial pressure of Cr-oxyhydroxide $\text{CrO}_2(\text{OH})_2$ species is proportional to the water vapour pressure [1,5, (ch. 6.2)]. To isolate the effects due to Cr, the tested cathode material should be tolerant to water vapour at operating temperature to avoid superimposed effects of humidity on the cathode performance. Recently, Nd-nickelates were reported to show high stability in H_2O -containing atmospheres [6,7] even if a decrease of 1 order of magnitude (low compared to standard perovskites) of the chemical surface exchange coefficient of oxygen was found after long-term (1000 h) testing [8]. Therefore, the use of Nd-nickelate cathodes in Cr-poisoning conditions with humid air is assumed to be possible here for reasonable time-spans.

1 Scientific approach

In ongoing parallel work, the authors aim to develop cathode supported microtubular SOFC using porous Nd-nickelate as the support tube, co-fired with thin dense gadolinia-doped ceria/scandia-stabilized zirconia double electrolyte layers [9]. To achieve densification of the electrolytes, the present target sintering temperature is 1573 K. In this work, examining at the outset the Cr-tolerance of the nickelate material, simpler samples were fabricated, that mimic the cathode side of the future microtubular fuel cells: symmetrical Nd-nickelate layers were deposited on sintered thick ceria-gadolinia pellets at the same firing temperature (1573 K), with one side subsequently exposed to Cr-containing air under polarization for ca. 1000 h, and finally post-analyzed. The analysis revealed several side reactions, originating from the starting powder and the high temperature step, which explain poor electrode performance.

5.1. Nd-nickelate SOFC cathode sensitivity to Cr/Si contamination

The emphasis in this article is therefore not the nickelate performance as cathode, but the results obtained from post analysis, which indicate the improvement steps required for further development of this system. The electrochemical testing should therefore be seen as a means to obtain cathode overpotential-driven C-poisoning, i.e. Cr deposition in the electrochemically active cathode, and not focusing on absolute performance.

2 Experiments

The studied samples are symmetrical cells of Nd-nickelate electrodes on thick (1 mm, 94 % dense) electrolyte supports. The latter were fabricated by axial compression of $\text{Ce}_{0.9}\text{Gd}_{0.1}\text{O}_{1.95}$ (GDC, Nextech, USA) powder within a 24 mm diameter mould by applying a pressure of 44 MPa prior to a sintering step of 120 min at 1573 K in air. Circular $\text{Nd}_{1.95}\text{NiO}_{4\pm\delta}$ (NNO, Marion Technologies, France) electrodes of 8 mm diameter were screen-printed on the GDC support, according to an experimental protocol described elsewhere [10, (A.2)], followed by a sintering step of 60 minutes at 1573 K, leading to an electrode thickness of ca. 15 μm . Subsequently, a gold grid was sintered on the NNO cathode at 1313 K while applying a load of ca. 250 g. Unfortunately, the NNO powder presented a silicon (Si) impurity content up to 1.5 at % in the as-received state, introduced before the final milling and detected only later. An NNO-based reference electrode was likewise deposited onto the support; the positioning on the solid electrolyte followed proposals by Nagata *et al.* [11] for accurate electrochemical impedance spectroscopy measurements (EIS). The gold grids were connected to a galvanostatic device using gold wires; the counter and reference electrodes were additionally covered with an unsintered $\text{La}_{0.7}\text{Sr}_{0.3}\text{CoO}_3$ (LSC, Praxair, USA) contacting layer for better current collection; this was avoided for the Cr-exposed NNO working electrode so as not to influence its reaction by the presence of another material. The absence of such a better current collection layer, which in addition may participate in the electrochemical reaction, contributed to higher losses overall, which was confirmed from parallel tests including LSC current collection, not reported here.

The symmetrical cells were kept in a furnace at 973 K, polarized for 1000 h with a constant current load of $0.5 \text{ A}\cdot\text{cm}^{-2}$, while monitoring the potential between the electrodes. Polarization was occasionally switched off for EIS measurements, performed on an IM6 impedance analyzer (Zahner, DE) with Thales 2.15 software. The cathode was fed with a $0.4 \text{ l}\cdot\text{min}^{-1}$ air flux, heated within a tubing element made of Inconel 600 (NiCrFe) alloy for deliberate emission of volatile Cr species. This experimental arrangement does not allow for comparison with a baseline test without Cr contamination; despite this drawback, the setup allows homogeneously distributed delivery of gaseous Cr species to the button cell cathode and therefore to study this particular effect, especially from *post-test* analysis. Fig. 5.1 provides a schematic illustration of the test setup. The water vapour pressure was $1.8\cdot 10^2 \text{ Pa}$ when using dry (compressed) air, and $3.0\cdot 10^3 \text{ Pa}$ in humidified conditions (bubbled through a water bottle). The partial pressures of volatile Cr are estimated from comparison with a similar experiment using Inconel 602 alloy [12, (ch. 4.1)], where they are close saturation pressures, which are $5.5\cdot 10^{-5}$ and $9.2\cdot 10^{-4} \text{ Pa}$, in dry and humidified air respectively.

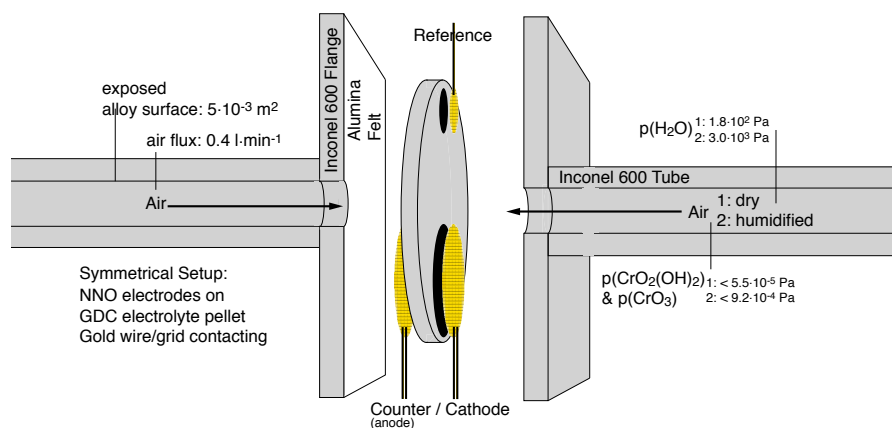


Figure 5.1: Schematic illustration of the testing arrangement, where symmetrical cells are placed between two metallic flanges covered with alumina felts. The flange-ending pipes ensure air feed, heat exchange, contacting (compressed by calibrated springs) and deliberate Cr-poisoning conditions. Switching the air feed from dry to humidified air changes the Cr contamination levels as indicated on the figure.

Analyses of *post-test* and fresh samples included X-ray diffraction (XRD), which were performed on a D8 diffractometer (Bruker, DE) and energy-dispersive X-ray spectroscopy (EDS) on both scanning and transmission electron microscopes (SEM/STEM). *Post-test* analyses and sample preparation protocols, like embedding, cross-section cutting, polishing and focused ion beam (FIB) TEM-lamellae preparation steps are described elsewhere [13, (ch. 7.1)].

3 Results and discussion

Two symmetrical cells were successively monitored under current load at operating temperature. Apparently stable performance, even slightly improving, was observed by voltammetry, during testing in dry air (see Fig. 5.2, first cell) as well as in both dry and humidified air (see Fig. 5.3, second cell) over time spans of 1000 h. An ohmic resistance of ca. 3.6 Ω can be attributed to the electrolyte, supposing 0.055 S·cm⁻¹ for the conductivity of GDC at 973 K [14] and taking into account the electrolyte's porosity [15]. As mentioned before, the absolute performance being poor, we focus here on the relative performance evolution with respect to the presence of Cr contamination, in combination with *post-test* analysis.

3.1 Electrochemical behaviour To focus on the relative electrode response with time, EIS measurements are reported under zero current bias in Figs. 5.2-5.3 for both cells. EIS recording under bias was noisy and the variations small; one notices in fact that overall dc performance at 0.5 A/cm² is rather stable (Fig. 5.2A, 5.3A). Initial spectra for NNO cathodes Fig. 5.2C, taken before ageing, reveal two major contributions: a medium frequency arc around 10⁴ Hz and a low frequency arc around ca. 10² Hz, representing processes at the cathode/electrolyte interface and oxygen reduction at the cathode/air interface, respectively, according to Mauvy *et al.* [16].

5.1. Nd-nickelate SOFC cathode sensitivity to Cr/Si contamination

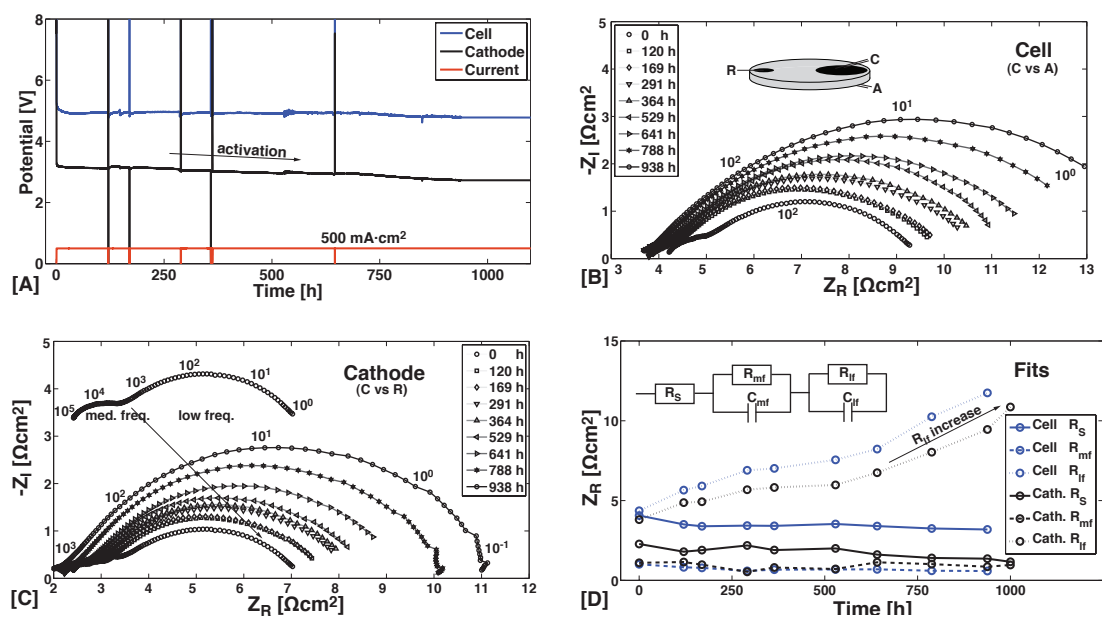


Figure 5.2: [A] Cell and cathode potential (vs reference) evolution with time in dc conditions at 0.5 A/cm² show an apparent degradation-free behaviour. Impedance spectra (at zero bias current) evidence an increase of polarization resistance with time. For both the symmetrical cell [B] and the cathode [C] the evolution of resistive contributions, obtained by fitting a simple equivalent circuit on EIS spectra [D], underline an increase of the low frequency arc (R_{lf}), which describes oxygen reduction on the electrodes, whereas small decreases of the ohmic and the medium frequency cathode/electrolyte interface contributions are observed.

Equivalent circuit fitting on EIS spectra evidenced an increase of the low frequency contribution with polarization time, likely indicating the effect of Cr-contaminating conditions besides other possible electrode altering phenomena on the catalytic properties of NNO for oxygen reduction discussed further below. The relatively stable performance at 0.5 A/cm² bias indicated by voltammetry (see Fig. 5.2A and 5.3A) could be explained by the intrinsic mixed conductivity of NNO delocalisable throughout the cathode thickness. Cr deposits observed close to the interface (shown further below) likely constrict total current but do not block it. Furthermore, the ohmic contribution decreases with time, visible from the high frequency intercept, in part balancing the polarization resistance increase. This ohmic decrease is probably due to contact improvement, i.e. sintering of the gold mesh and increasing contact points.

Spectra at 500 h and 530 h in Fig. 5.3B indicate no significant change in impedance behaviour under higher water vapour pressure, which would confirm the supposed relative tolerance of NNO cathode material towards H₂O [6-7]. Also, no change in slope during polarization is observed when switching from dry to humidified gas (see Fig. 5.3a). Thus, although higher amounts of Cr are fed to the cathode with humidified gas, the rate of Cr accumulation at active cathode sites appears to be constant, underlining a Cr deposition process driven by the electrochemical reduction of volatile Cr^(VI) species [3].

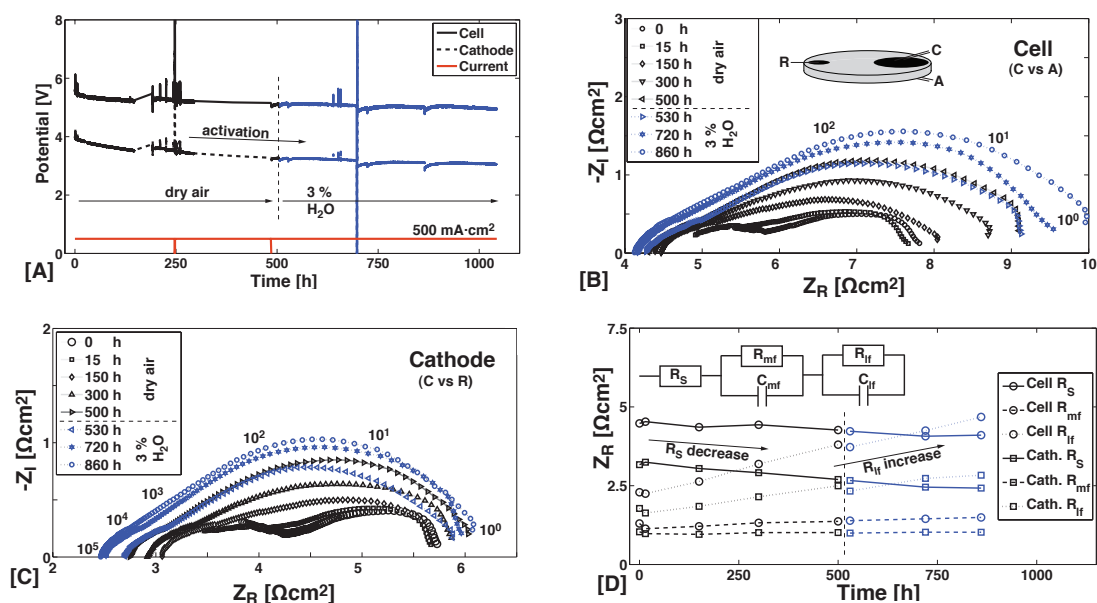


Figure 5.3: [A] Evolution of Cell (C vs A) and cathode (C vs R) potentials under polarization at a current load of $500 \text{ mA}\cdot\text{cm}^{-2}$ under dry and humidified air. [B] Impedance spectra of the symmetrical cell and [C] the cathode; the last three acquisitions were performed under higher water vapor conditions to the cathode (second part, $\geq 500 \text{ h}$, of the test). The cathode contribution to resistivity is marked by an increase of polarization resistance partly counterbalanced by contact improvement. [D] EIS fitting with a simple equivalent circuit-based model underlines this observation.

3.2 Cr contamination For the interpretation of cathode behaviour under deliberate Cr contaminating conditions, and likely affecting the cathode performance with time, *post-test* analyses were conducted on cathodes. Distributions of Cr accumulations through the cathode thickness were obtained by extracting Cr concentrations from EDS spectra of $1 \mu\text{m}$ thick cathode slices, similarly to the Cr quantification methodology described elsewhere [12,17, (ch. 3.1, 4.1)]. Fig. 5.4 shows the Cr-profile superimposed to the SEM-FIB image on the left. The Cr distribution shows a rather slowly decaying profile over $7 \mu\text{m}$, as opposed to a much steeper profile observed for $(\text{La,Sr})\text{MnO}_3/\text{Y-ZrO}_2$ cathodes, with Cr accumulating towards the electrolyte interface [12, (ch. 4.1)]. This observation corroborates the spreading of the reaction zone into the nickelate cathode thickness, as expected for materials with mixed ionic and electronic conductivity.

To identify the nature of Cr accumulations more closely, a TEM lamella (cf. Fig. 5.4, right) was prepared by FIB extraction from the electrolyte/cathode interface. At higher magnification, STEM-EDS results, given on the right of Fig. 5.4 together with elemental maps, revealed Cr in combination with Nd, in the form of Nd-chromate, NdCrO_4 . The latter is the thermodynamically favored phase of the Nd-Cr-O system under cathode operating conditions [18]. The Cr-rich phases decorate the active NNO particle surfaces, indicating again the mixed conductivity of NNO. This result is in clear opposition with a supposed Cr-tolerance of NNO,

5.1. Nd-nickelate SOFC cathode sensitivity to Cr/Si contamination

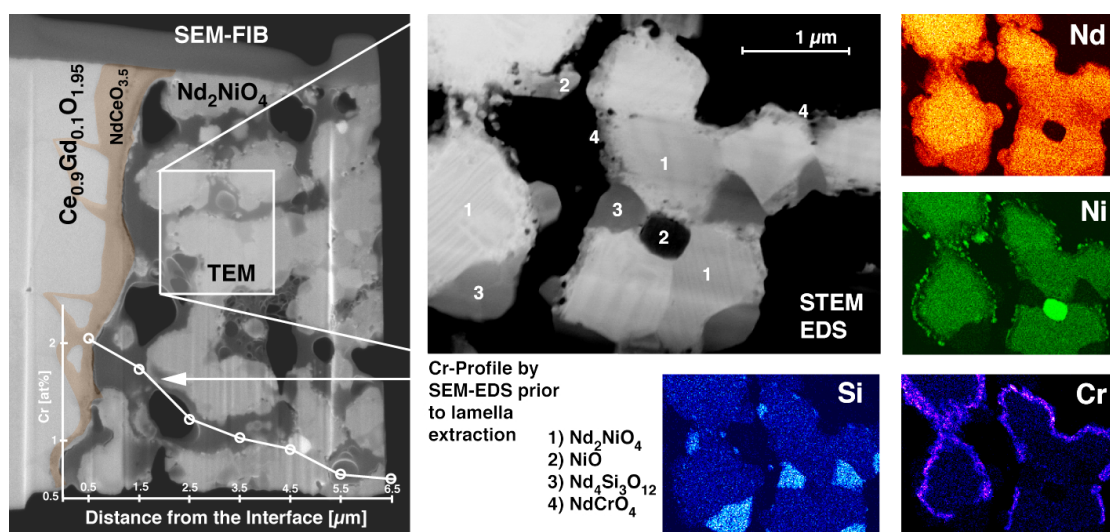


Figure 5.4: Left: the SEM imaging of a TEM-lamella, extracted by FIB from the cell described in Fig. 5.2, shows an NNO cathode region on a GDC support with an intermediate $\text{NdCeO}_{3.5}$ reaction layer. A Cr profile through the cathode thickness is superimposed to the bottom of the SEM-FIB picture; the profile was obtained by extracting Cr concentrations from $1 \mu\text{m}$ cathode slices from EDS spectra. Right: the dark STEM image and corresponding EDS elemental maps, from the central part of the FIB-lamella from the left side of the picture, reveal Cr deposits on active NNO grain surfaces as well as secondary Ni- and Si-rich phases.

free of Sr and Mn. Considering that a decrease (40 %) in chemical oxygen surface exchange coefficient was reported for 20 nm Cr deposits on the NNO surface and 2000 h testing time [4], the ca. 100 nm thick Cr phases observed here are therefore believed to be at least in part responsible for the cathode performance decrease seen in the EIS measurements.

3.3 Additional contamination Besides Cr, silicon contamination was revealed to a significant extent in *post-test* samples. Although XRD measurements on raw powder had not revealed patterns corresponding to Si-phases (cf Fig. 5.5[A]), Si was identified by EDS in the delivered powder. Silicon therefore seems to be present as amorphous material and had been introduced by milling during powder processing for particle size reduction. The XRD measurements (Fig. 5.5[A]), as well as STEM-EDS (Fig. 5.4 right) and SEM-BSE (Fig. 5.5[B]) images taken on sintered and *post-test* cathodes allowed to identify Nd-silicate as thermally-induced reaction phase. The deleterious effect of Si-poisoning is obvious, as the $\text{Nd}_4\text{Si}_3\text{O}_{12}$ phase decreases the number of active cathode sites. The absence of Cr around the silicate phase surfaces, clearly visible from Cr and Si EDS maps in Fig. 5.4 strengthens these findings; if the $\text{Nd}_4\text{Si}_3\text{O}_{12}$ phase were active for oxygen reduction, the Cr deposits would have been expected here as well.

Finally, sulfur-rich phases were identified by SEM-EDS (not presented here) as reaction products of NNO cathode material with SO_2 present to 10 ppb in urban air [5, (ch. 6.2)], which accumulate in long-term tests. Nickelate seems therefore not tolerant to sulphur contamination either, similar to reactive perovskites, that form sulfates [19, (ch. 7.2)].

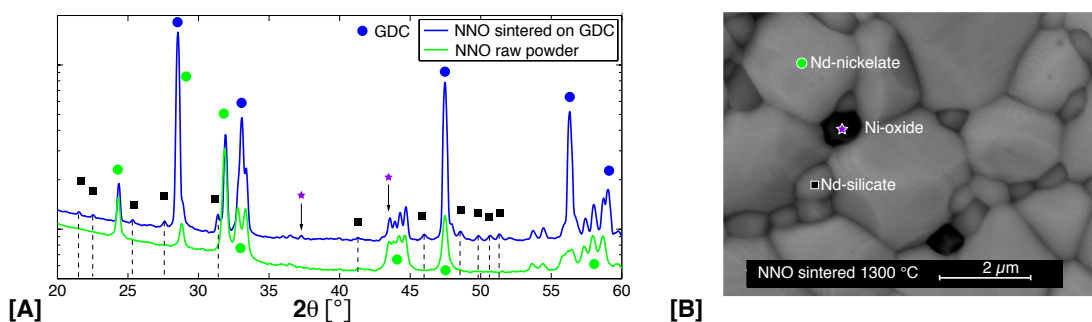


Figure 5.5: [A] The changes in XRD spectra between raw and sintered NNO (Nd_2NiO_4 00-021-1274, green circle symbol) powder indicates Nd-silicate $\text{Nd}_4\text{Si}_3\text{O}_{12}$ (00-042-0171, black square symbol) to originate from amorphous Si impurity. NiO (00-078-0429, purple star symbol) phase appears also after the high-temperature step. The pattern corresponding to GDC ($\text{Ce}_{0.8}\text{Gd}_{0.2}\text{O}_2$ 00-050-0201, blue circle symbol) stems from the electrolyte support. The numbers in brackets are ICDD references. [B] The BSE-SEM image of sintered NNO powder clearly reveals the thermally-induced NNO (large grains) decomposition into NiO (small black grains) triggered by the Si contamination-caused Nd-silicate (small grey grains) formation.

3.4 Synergistic degradation effects NiO precipitates illustrated in Fig. 5.4[right] and Fig. 5.5[B] suggest a contamination-induced decomposition of the nickelate structure. As Nd-deficient nickelate tends to transform into $\text{Nd}_2\text{NiO}_{4\pm\delta}$ and NiO, the initial Si contamination of the raw powder leads to additional Nd-deficiency (by Nd-silicate formation) and so to enhanced NiO precipitation during high temperature cathode sintering. A degradation mechanism of Si-contaminated NNO powder, suggested from the findings in this work, in addition to observations from a previous study [20], is illustrated in Fig. 5.6. Bulky NiO grains are suggested to have their origin in electrode preparation and not in high overpotential at the cathode under polarization.

During Cr-poisoning, the reductive deposition of volatile Cr species in form of Cr_2O_3 and its subsequent reaction with nickelate to form NdCrO_4 compounds induces additional Nd-depletion of NNO and leads to precipitation of NiO as suggested in Fig. 5.6 and evidenced in the Ni mapping of Fig. 5.4[right].

Figure 5.4[left] moreover shows a reaction layer between NNO and GDC materials. The GDC electrolyte is meant to act as a reaction buffer layer between NNO and zirconia-based electrolyte materials, which would react severely, to produce full microtubular cells based on porous nickelate support tubes. In order to simulate the co-sintering process of nickelate tubes and the electrolyte layers, the electrodes were sintered at 1300°C, believed to be the limiting fabrication temperature for the tubular SOFC. This study shows a marked interfacial Nd-cerate $\text{NdCeO}_{3.5}$ reaction phase [21]; additional reactivity studies showed this phase to appear during high temperature treatments (sintering) of the combination of NNO and CGO materials and not to evolve under IT-SOFC operating temperatures. Essentially corresponding to ceria doped with ca. 25 % Nd_2O_3 , and therefore an ionic conductor just like other rare earth

5.1. Nd-nickelate SOFC cathode sensitivity to Cr/Si contamination

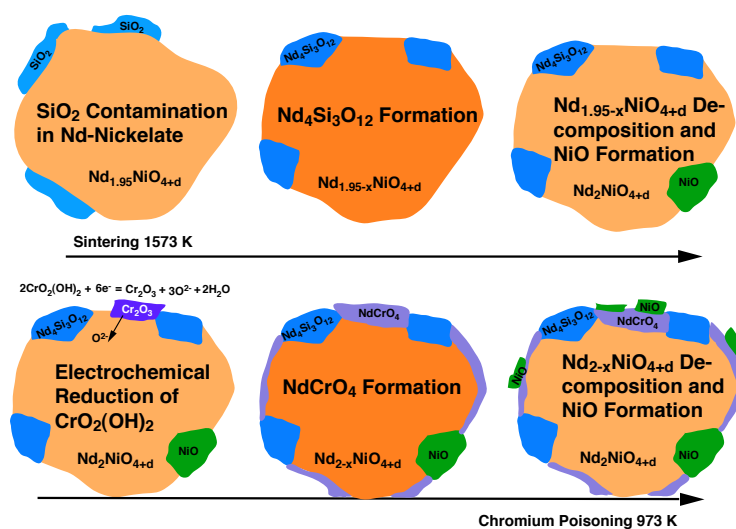


Figure 5.6: Decomposition of Nd-deficient nickelate into the more stable stoichiometric phase and Ni oxide are triggered by a Si contamination-induced Nd-depletion during the high temperature sintering step; Cr-poisoning during electrochemical polarisation, i.e Cr deposition on active NNO surfaces and involving Nd-chromate formation, leads to further Nd-depletion and decomposition of the NNO phase.

doped cerias, it does not affect the overall resistive drop in our testing conditions; even if its conductivity could be one order of magnitude below that of 10-GDC, its thickness of only half a micron makes any additional ohmic drop to that of the 1 mm 10-GDC pellet negligible.

4 Conclusion

Sensitivity to contamination effects, in particular towards chromium and silicon, was revealed for Nd-nickelate based cathode material in the present study. The hypothesis that Cr-poisoning should be limited or even suppressed using alternative cathode materials free of Sr and Mn [2] has been invalidated here, and the electrochemical reduction of Cr-vapor species [3] appears independent of the cathode material. The findings indicating Cr-intolerance of Nd-nickelate will probably delay its use in SOFC, in contrast to electrolyzer cells [22], as long as the Cr-poisoning issue is not resolved by other means [23] than changing electrode materials. Our results evidence additional degradation effects, in particular a synergistic decomposition of Nd-nickelate induced by raw powder contamination. Introduction of silicon has to be clearly avoided in early stages of SOFC processing to prevent Nd-nickelate decomposition into nickel oxide due to Nd-silicate formation. Finally, the material combination and high fabrication temperature of the nickelate-ceria interface does lead to an interfacial reaction layer before electrochemical testing; this layer, however, still a doped ceria ionic conductor, did not add here significant resistive effects due to its marginal thickness.

Acknowledgements

The Swiss Federal Office of Energy (contracts 153569,154156) is acknowledged for financial support. Many thanks to Fabienne Bobard for manipulating the FIB.

References

- 1 E. Boehm, J.M. Bassat, P. Dordor, F. Mauvy, J.C. Grenier, Ph. Stevens, *Solid State Ionics* 176 (2005) 2717.
- 2 T. Komatsu, H. Arai, R. Chiba, K. Nozawa, M. Arakawa, K. Sato, *Electrochem. Solid-State Lett.* 9 (2006) A9.
- 3 K. Hilpert, D. Das, M. Miller, D.H. Peck, R. Weiss, *J. Electrochem Soc.* 143 (1996) 3642.
- 4 Y. Yang, E. Bucher, W. Sitte, *J. Power Sources* 196 (2011) 7313.
- 5 J.A. Schuler, C. Gehrig, Z. Wuillemin, A.J. Schuler, J. Wochele, C. Ludwig, A. Hessler-Wyser, J. Van herle, *J. Power Sources* 196 (2011) 7225. (ch. 6.2)
- 6 A. Egger, E. Bucher, W. Sitte, C. Lalanne, J.M. Bassat, *ECS Trans.* 25 (2009) 2547.
- 7 E. Bucher, A. Egger, M. Yang, W. Sitte, *Proceedings of the 9th EFCF* 7 (2010) 14.
- 8 A. Egger, W. Sitte, F. Klauser, E. Bertel, *J. Electrochem. Soc.* 157 (2010) B1537.
- 9 H. Luebbe, J. Van herle, H. Hofmann, P. Bowen, U. Aschauer, A. Schuler, F. Snijkers, H-J. Schindler, U.Vogt, C. Lalanne, *Solid State Ionics*, 180 (2009) 805.
- 10 P. Tanasini, J.A. Schuler, Z. Wuillemin, M.L. Ben Ameer, C. Comninellis, J. Van herle, *J. Power Sources* 196 (2011) 7097. (appendix 2)
- 11 N. Nagata, Y. Itoh, H. Iwahara, *Solid State Ionics*, 67 (1994) 215.
- 12 J.A. Schuler, P. Tanasini, A. Hessler-Wyser, C. Comninellis, J. Van herle, *Electrochem. Commun.* 12 (2011) 1682. (ch. 4.1)
- 13 J.A. Schuler, Z. Wuillemin, A. Hessler-Wyser, J. Van herle, *Electrochem. Solid-State Lett.* 14 (2011) B20. (ch. 7.1)
- 14 J. Van herle, T. Horita, T. Kawada, N. Sakai, H. Yokokawa, M. Dokiya, *Solid State Ionics* 86-88 (1996) 1255.
- 15 A. Holt, P. Kofstad, *Solid State Ionics* 69 (1994) 127.
- 16 F. Mauvy, C. Lalanne, J.B. Bassat, J.C. Grenier, H. Zhao, L. Huo, P. Stevens, *J. Electrochem. Soc.* 153 (2006) A1547.
- 17 J.A. Schuler, P. Tanasini, A. Hessler-Wyser, J. Van herle, *Scr. Mater.* 63 (2010) 895. (ch. 3.1)

5.1. Nd-nickelate SOFC cathode sensitivity to Cr/Si contamination

- 18 H. Schwarz, Z. allg. Chemie, 322 (1963) 9.
- 19 J.A. Schuler, Z. Wullemin, A. Hessler-Wyser, J. Van herle, ECS Trans. 25 (2009) 2845. (ch. 7.2)
- 20 J.A. Schuler, Master Thesis, EPFL (2008).
- 21 J. Hauck, K. Bickmann, K. Mika, Supercond. Sci. Technol. 11 (1998) 63.
- 22 V.I. Sharma, B. Yildiz, J. Electrochem. Soc. 157 (2010) B441.
- 23 Y. Matsuzaki, I. Yasuda, J. Electrochem. Soc. 148 (2001) A126.

6 Cr contamination sources

ECS Transactions **35** (2011) 2001

6.1 Multi-scale assessment of Cr contamination levels in SOFC cathode environment

J. Andreas Schuler^{a,b}, Albert J. Schuler^c, Zacharie Wullemin^a, Aïcha Hessler-Wyser^b,
Christian Ludwig^{c,d}, Jan Van herle^a

^a *Laboratoire d'Énergie Industrielle (LENI), École Polytechnique Fédérale de Lausanne (EPFL), 1015 Lausanne, Switzerland*

^b *Centre Interdisciplinaire de Microscopie Electronique (CIME), École Polytechnique Fédérale de Lausanne (EPFL), 1015 Lausanne, Switzerland*

^c *Labor für Bioenergie und Katalyse (LBK), Paul Scherrer Institut (PSI), 5232 Villigen, Switzerland*

^d *Institut d'Ingénierie de l'Environnement (ENAC-IIE), École Polytechnique Fédérale de Lausanne (EPFL), 1015 Lausanne, Switzerland*

This study aims to quantify in a holistic approach chromium (Cr) contamination in solid oxide fuel cell (SOFC) stack testing using adapted tools: i) a hot gas sampling method to analyze volatile Cr species in the air flux at the cathode inlet location; ii) a rapid quantification method for Cr as condensed matter in cathode material of *post-test* samples. The hot air sampling method reveals itself as a reproducible and time-resolved quantification technique for Cr trace amounts in a gas flow; this technique is seen as a promising evaluation tool for Cr contamination issues in SOFC systems. The quantification method reveals severe Cr-poisoning in a cell. The combined findings indicate that Cr contamination generated by system components located upstream the cell must be suppressed by hindering the access of Cr pollutants to the cathode compartment.

1 Introduction

Solid Oxide Fuel Cells (SOFC) experience performance degradation at long operating time spans that is caused by the pollution of the cathode by volatile chromium (Cr) species - so called Cr-poisoning [1]. To understand this degradation phenomenon, in particular to predict SOFC device lifetimes, correlations between performance degradation and Cr amounts in the air electrodes are needed; correlations that were so far rather difficult to establish [2]. Knowledge on Cr amounts fed to the cathode by cell- proximal metallic compounds, amounts depositing under operation within the cathode material and Cr being evacuated from the cathode compartment are challenging to access. The Cr-poisoning degradation phenomenon has to be studied with a holistic approach that concentrates on complete systems rather than on the analysis of discrete system parts; adapted diagnostic tools are therefore needed.

Cr concentrations in the cathode compartment are generally determined indirectly by measuring Cr evaporation rates from metal coupons. Researches were mainly driven by the transpiration method [3], which delivered extensive Cr evaporation rate data for high- temperature alloys and evaluation of protective solutions [4]. The main benefit of this technique is the detection possibility of trace elements accumulating in the sampling apparatus. However, the transpiration method generally (except for [5]) includes a condensation step of the volatile Cr species on a silicon (Si) containing support [6], limiting detection to Cr and therefore precluding of Si as additional pollutant species.

Cr concentration levels within an SOFC system, or during stack testing, might differ significantly from expectations predicted from experiences on metal coupons, as additionally to metallic interconnects (MIC), complex-shaped balance-of-plant (BoP) system components, such as heat-exchanger or tubing sections, also generate Cr contamination. Direct measurements of Cr concentrations within an SOFC system are therefore of high interest.

In situ and real-time measurements of gas compositions, including gas chromatography [7], laser spectroscopy [8] and Raman spectroscopy [9], were recently developed to access anode gas compositions. These methods do however not allow measuring trace amounts of pollutant species; nor does the free jet sampling method [5] allow easy quantification.

Just recently, Thomann *et al.* [10] elaborated a method to quantify Cr amounts in hot air, inspired from the denuder technique that was developed by Froitzheim *et al.* [11], which can be adapted for time-resolved measurements at different locations in an SOFC system, and does not need cooling down the system for sample extraction. Similarly, the present authors published recently a hot gas sampling technique [12, (ch. 6.2)], using the liquid quench concept developed by Koebel and Elsener [13]. The metallic sampling apparatus allows overcoming the use of fragile quartz-tubes and so enables measurements at previously inaccessible locations within an SOFC system. The present study aims in particular to elaborate this technique to determine reproducibly Cr contamination levels in the hot air flux entering the cathode compartment and to allow the detection of Cr trace amounts within a reasonable time lapse for evaluation purposes.

Besides degradation signatures observed under operation, generally done by electrochemical impedance spectroscopy, analysis for Cr amounts in *post-test* cathode samples indicates the Cr-poisoning extent. However, the quantification of Cr accumulations in cathode samples ob-

6.1. Multi-scale assessment of Cr contamination levels in SOFC cathode environment

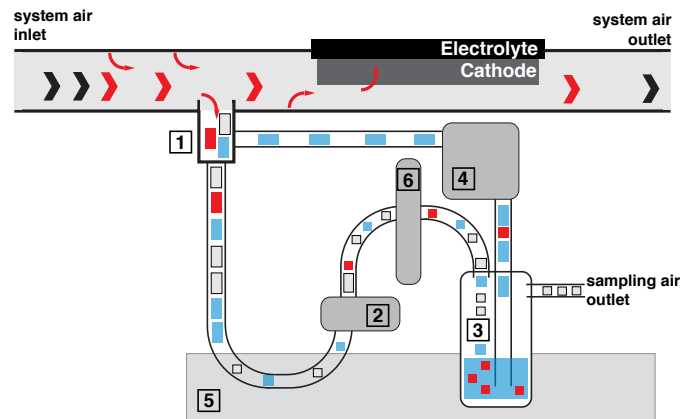


Figure 6.1: Gas sampling apparatus. 1 = Heated gas probe; 2 = membrane pump; 3 = bottle with absorption liquid (diluted HNO_3); 4 = dosing pump; 5 = cooling medium; 6 = gas meter.

tained by their dissolution followed by chemical analysis may introduce or neglect additional Cr amounts and lead to mistaken results [14], which is also the case in the subjective interpretation of Cr distribution maps generally obtained by X-ray spectroscopy related techniques. The authors recently proposed a method for rapid Cr quantification in *post-test* cathode samples [15, (ch. 3.1)] in the scope of objective and standardized quantification of Cr amounts [16, (ch. 4.1)]. The present study aims to highlight results obtained by applying this methodology for Cr quantification in a SOFC repeat-element tested in stack configuration under a known Cr contamination level at the cathode determined by the hot gas sampling technique.

2 Experimental

The hot gas sampling, taken at the air-inlet location of the cathode (temperature 1043 K; fed with $20 \text{ L}\cdot\text{min}^{-1}$ at room temperature), is performed using an adapted version of the liquid quench method described elsewhere [13] with the sampling apparatus shown in Fig. 6.1. The membrane pump 2 (KNF, model N814KTE) draws a constant fluid probe through the absorption unit 1. The gas volume is measured by the gas meter 6 and equals $3.5 \text{ L}\cdot\text{min}^{-1}$. The absorption liquid, diluted HNO_3 stored in the bottle 3, is added to the gas sample in the T-shaped heated gas probe (Ti grade 1) by means of the dosing pump 4 (KNF, model stepdos 03RC), which recycles the absorption liquid. Analysis of Cr dissolved in the absorption liquid for a known duration and sampling flow is finally done on an inductively-coupled plasma optical emission spectrometer (ICP-OES, PerkinElmer, model Optima3300DV) calibrated with standards. In order to reach the limit of detection, the absorption liquid is limited to 100 ml. System components located upstream the cell, including metallic heat-exchanger and tubing elements, were previously found to saturate the hot air with Cr vapor species and lead to severe Cr-poisoning of the cathode [12, (ch. 6.2)]. Contrary to Cr accumulation quantification in *post-test* cathode samples involving dissolution and chemical analysis, the present work uses

a rapid and localized quantification method that involves Cr quantification through the La $L_{\beta 2.15}/L_{\alpha 1}$ peak height ratio in energy-dispersive X-ray spectroscopy (EDS) spectra, described elsewhere [15,16, (ch. 3.1, 4.1)]. This technique is applied here on cathode *post-test* samples from the cell tested within the above-described system, where the air electrode is composed of yttria-doped zirconia (YSZ) and strontium-doped lanthanum manganite (LSM) composite cathode material and is covered with a strontium-doped lanthanum cobaltite (LSC) current collection layer (CCL).

3 Results and Discussion

3.1 Hot gas sampling: reliability: Type A sampling results given in Tab. 6.1 prove the reliability of the method for Cr concentration quantification in an air flux, as the 4 measurements taken under identical conditions lie within a concentration span of $5 \mu\text{g}\cdot\text{L}^{-1}$.

3.2 Time-resolution Type B results reported in Tab. 6.1 and graphically illustrated in Fig. 6.2 show a linear dependence of the measured Cr concentrations with time indicating that the sampling method allows time-resolution. As the Cr detection limit of the ICP-OES analyzer is around $10 \mu\text{g}\cdot\text{L}^{-1}$, a sampling time of around 10 hours is needed to reveal Cr within the hot air flux, for the conditions used here.

3.3 Acid concentration-dependence Type C results reported in Tab. 6.1 and illustrated in between the measured Cr amounts and the acid concentration of the absorption medium. Increasing Cr amounts were trapped within the diluted HNO_3 solution with increasing acid concentration reaching a plateau at higher values above 0.1 Mol. The measurement points show a logarithmic tendency. This result stresses the need to run further experiments at higher acid concentrations or to increase the residence time of the quenched volatile Cr species to enable their dilution in the diluted acidic absorption medium and avoid their evacuation with the air flux.

Both assumptions - min. sampling time of ca. 10 h and the logarithmic behavior of Cr measurement with increasing acid concentration - need further experimental verification. Nevertheless, an extrapolated value (for 1 Mol acid concentration) can be used to compare the sampling results to Cr vapor pressures, which are thermodynamically in equilibrium with their evaporation sources in this experiment [12, (ch. 6.2)], i.e. the air flux is saturated with volatile Cr species. On the one hand, 18.2 pg Cr is vehicled through the sampling apparatus per liter air (at room temperature) for Cr vapor partial pressures of $6\cdot 10^{-10}$ and $8\cdot 10^{-9}$ atm for CrO_3 and $\text{CrO}_2(\text{OH})_2$ respectively at cathode air entry location (at 1043 K) and with the non-condensation hypothesis of these species on the walls of the sampling tube. On the other hand, only 1.84 pg Cr is dissolved within the absorption medium for 1 liter sampled air.

EDS-analyses of the inner walls of the sampling capillary upstream the quench location reveal deposits of small Cr condensates on the oxidized Ti surface; their formation is caused by the thermodynamic instability of Cr vapor species with decreasing temperature. This deposition, combined with the evacuation of Cr species with the air flux before their dissolution into the

6.1. Multi-scale assessment of Cr contamination levels in SOFC cathode environment

Table 6.1: Sampling Runs for [A] reliability, [B] time-resolution and [C] acid-dependence demonstration. The acid concentration is set by dilution of concentrated HNO₃ in purified and deionized water. Raw Cr concentrations in the absorption liquid are given here.

Type	Time [hours]	HNO ₃	Cr conc. [$\mu\text{g per liter}$]
A	ca. 22 h	10 mMol	$30 \mu\text{g}\cdot\text{L}^{-1}$
A	ca. 22 h	10 mMol	$29 \mu\text{g}\cdot\text{L}^{-1}$
A	ca. 22h	10 mMol	$34 \mu\text{g}\cdot\text{L}^{-1}$
B	17.5 h	10 mMol	$22 \mu\text{g}\cdot\text{L}^{-1}$
B	26.5 h	10 mMol	$46 \mu\text{g}\cdot\text{L}^{-1}$
C	22 h	0.1 mMol	$13 \mu\text{g}\cdot\text{L}^{-1}$
A,B,C	11 h	10 mMol	$33 \mu\text{g}\cdot\text{L}^{-1}$
C	22 h	30 mMol	$50 \mu\text{g}\cdot\text{L}^{-1}$
C	22 h	100 mMol	$68 \mu\text{g}\cdot\text{L}^{-1}$

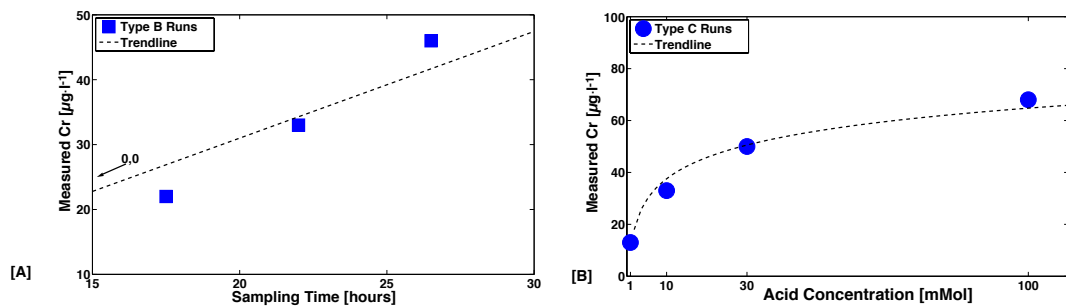


Figure 6.2: Gas sampling results: [A] time-resolution indicates a min. sampling time of 10 hours to reach Cr detection limits of ca. $10 \mu\text{g}\cdot\text{L}^{-1}$; [B] the acid concentration dependence of the Cr measurements suggests the use of higher HNO₃ concentrations for dissolution of quenched volatile Cr species into the absorption liquid.

absorption medium, limit the measured Cr to ca. 10 % of the actual Cr amounts. Besides Cr, Si deposits are found on the Ti capillary surfaces indicating the possibility of Si contamination quantification using such a gas sampling technique.

3.4 Cr-Profiling: precision and acid-dependence As suggested by our previous study [12, (ch. 6.2)], the Cr contamination of the cell from upstream system components has here been reconfirmed. The distribution of Cr accumulations within the cell is now analyzed to generate a comprehensive insight of Cr pollutant transport along their complete path in the cathode compartment.

3.5 Across the cathode thickness A number of 6 cathode samples (each ca. 4 mm length) were extracted along an airflow channel at ca. 3 cm intervals from the air inlet to the air outlet; the sample locations are indicated in Fig. 5.3. Cr concentrations from 1 μm cathode slices through the electrode thickness are reported in the same figure. For sample 1 located at the air inlet, which suffered from highest Cr-poisoning, the Cr profile through the cathode

thickness shows a preferential Cr distribution near the electrolyte/cathode interface. The Cr distribution is correlated with the number of active sites for oxygen reduction [16, (ch. 4.1)] that decreases with increasing distance from this interface. The Cr profile drops however to negligible amounts after only 5 μm , whereas the active sites should be distributed over the whole cathode thickness. The latter result was predicted by a percolation model for an LSM-YSZ composite cathode with 250 nm YSZ and 500 nm LSM grains, respectively. The reactive trapping of volatile Cr species within the LSC CCL, as previously reported in [17, (ch. 7.2)], is suggested to lower the Cr concentration on the cathode surface decreasing both the Cr amounts at the interface and their distribution in the cathode thickness. Regarding the nature of the Cr accumulations, analyses of composition and phase identification is already reported elsewhere [18] and beyond the scope of the present work.

3.6 Along the air channel Cr profiles of the remaining samples distributed along the airflow are very similar as illustrated in Fig. 6.3. Only a minor Cr amount is found in these samples and the Cr-poisoned cathode area is confined to the electrolyte/cathode interface. The small amount of Cr in samples 2-6 compared to sample 1 is due to the trapping of volatile Cr species by the reactive LSC at the air inlet regions of the cell; the preferential distribution of Cr on the LSC CCL surface was already reported in previous publications [17,19, (ch. 7.2, A.1)]. However, the results from Fig. 6.3 indicate a remaining Cr contamination despite the protective LSC CCL. The remaining Cr contamination may occur through the gas diffusion layer (GDL) that protects the cathode from the MIC; minor Cr leakage through this layer may also explain the slightly higher Cr contamination for sample 6 at the cathode air outlet.

Profiling Cr accumulation along the air channel reveals a preferential distribution of Cr-poisoned cathode areas at the air entry that can be linked to a preferential distribution of performance degradation as reported by Wullemin *et al.* [19, (A.1)], who showed in a locally-resolved degradation study that the air inlet area of the cell suffered from large performance drops whereas the remaining active area observed only low degradation. However, an additional contamination effect, silicon-poisoning, generated superimposed degradation effects [20, (ch. 7.1)] that complicate direct correlation of only Cr amounts and local degradation rates.

4 Conclusion

Two techniques were synergistically used in this study to profile Cr species along the air-flow into a SOFC stack element: i) a hot air sampling method confirms Cr evaporation from upstream BoP components; ii) the rapid Cr quantification in *post-test* samples locates Cr accumulations in active cathode regions. We believe that such insights on Cr amounts entering the cathode compartment, deposited within the cathode material and evacuated with the air flux, can provide charging rates of active cathode regions with Cr accumulations giving access to lifetime predictions. Such extrapolations are however only possible for models that take into account superimposed degradation effects, in particular those due to contaminant species other than Cr that are often neglected.

This stresses the need of a more general contamination assessment and supports the choice

6.1. Multi-scale assessment of Cr contamination levels in SOFC cathode environment

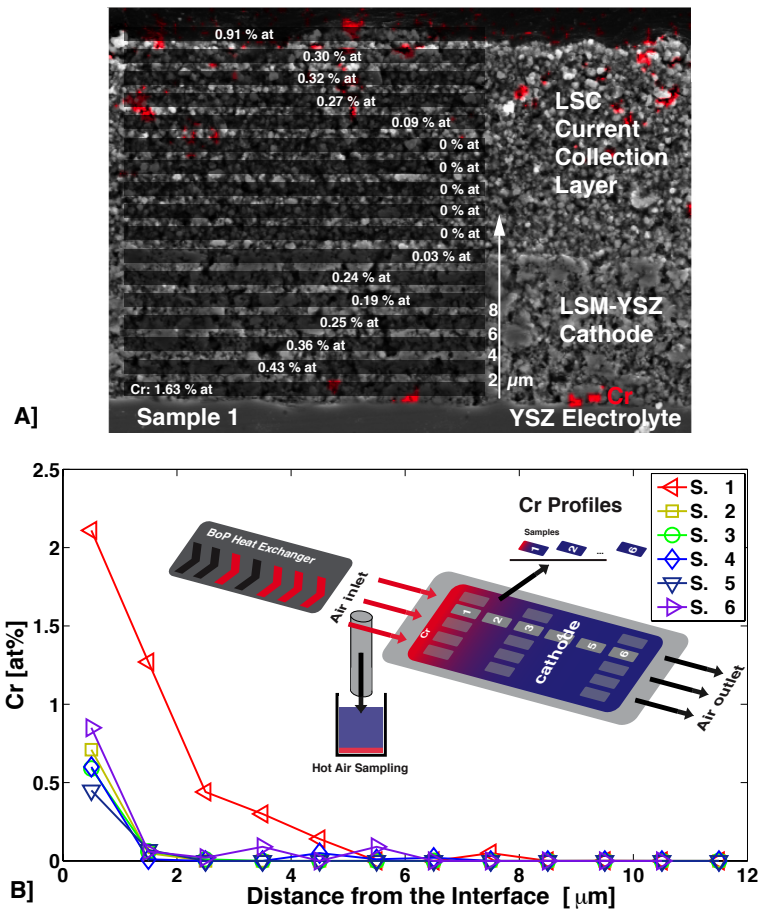


Figure 6.3: A]: the Cr profile (normalized to the perovskite content) across the cathode thickness indicates a preferential distribution of Cr accumulation near the electrolyte/cathode interface where most active sites for oxygen reduction reside and on the reactive LSC current collection layer surface. B]: Cr profiles for different analysis locations; sample 1 at the cathode air entry is highly polluted whereas the remaining samples show minor Cr amounts confined to the interface.

of a pure Ti sampling apparatus, which allows for analysis of additional contaminant species, such as Si besides Cr, in contrast to other sampling methods that are based on the use of quartz tubes. The identification of Cr contamination stemming from system parts stresses the need for adequate protective solutions. As BoP components represent, in volume, the larger part of SOFC systems, it is unreasonable to build them with expensive materials showing limited Cr evaporation or to protect cheaper materials over their complete surface (even if approaches for protecting complex-shaped system parts have been recently developed elsewhere [21]). More pragmatic is the implementation of an air-filtering material upstream the cathode entry, to act as a chemical trap for Cr vapor species.

Acknowledgements

The Swiss Federal Office for Energy (153569-AccelenT), the Competence Center Energy and Mobility (705028-WoodGas) and the Swisselectric Research (TREGAS) are acknowledged for financial support. Many thanks to Jean-David Teuscher (ENAC- IIE) for ICP-OES measurements.

References

- 1 K. Hilpert, D. Das, M. Miller, D.H. Peck, R. Weiss, J. Electrochem. Soc., 143, 3642 (1996).
- 2 A. Neumann, N.H. Menzler, I. Vinke, H. Lippert, ECS Trans., 25, 2889 (2009).
- 3 M. Stanislawski, U. Seeling, D.H. Peck, S.K. Woo, L. Singheiser, K. Hilpert, Solid State Ionics, 176, 2523 (2005).
- 4 J. Froitzheim, E. Larsson, L.G. Johansson, J.E. Svensson, ECS Trans., 25, 1423 (2009).
- 5 N.S. Jacobson, E.J. Opila, D.L. Myers, E.H. Copland, J. Chem. Thermodyn., 37, 1130 (2005).
- 6 S.H. Hong, P. Madakashira, D.I. Kim, Y.W. Cho, S.H. Han, H.N. Han, ECS Trans., 25, 1437 (2009).
- 7 P. Metzger, K.A. Friedrich, H. Mueller-Steinhagen, G. Schiller, Solid State Ionics, 177, 2045 (2006).
- 8 M. Lengden, W. Johnstone, R. Cunningham, Proceedings of the 9th European Fuel Cell Forum, 1503, (2010).
- 9 G. Schiller, W. Bessler, C. Willich, K.A. Friedrich, Proceedings of the 9th European Fuel Cell Forum, 1501, (2010).
- 10 O. Thomann, M. Pihlatie, J.A. Schuler, O. Himanen, J. Kiviaho, ECS Trans., 35, 2609 (2011).
- 11 J. Froitzheim, H. Ravash, L.G. Johansson, J.E. Svensson, Proceedings of the 9th European Fuel Cell Forum, 1205, (2010).
- 12 J.A. Schuler, C. Gehrig, Z. Wullemin, A.J. Schuler, J. Wochele, C. Ludwig, A. Hessler-Wyser, J. Van herle, J. Power Sources, 196, 7225 (2011). (ch. 6.2)
- 13 M. Koebel and M. Elsener, J. Chromatogr., A., 689, 164 (1995).
- 14 N.H. Menzler, I. Vinke, H. Lippert, ECS Trans., 25, 2899 (2009).
- 15 J.A. Schuler, P. Tanasini, A. Hessler-Wyser, J. Van herle, Scr. Mater., 63, 895 (2010). (ch. 3.1)

6.1. Multi-scale assessment of Cr contamination levels in SOFC cathode environment

- 16 J.A. Schuler, P. Tanasini, A. Hessler-Wyser, C. Comninellis, J. Van herle, *Electrochem. Commun.*, 12, 1682 (2010). (ch. 4.1)
- 17 J.A. Schuler, Z. Wuillemin, A. Hessler-Wyser, J. Van herle, *ECS Trans.*, 25, 2845 (2009). (ch. 7.2)
- 18 A. Hessler-Wyser, Z. Wuillemin, J.A. Schuler, A. Faes, J. Van herle, *J. Mater. Sci.*, 46, 4532 (2011).
- 19 Z. Wuillemin, A. Nakajo, A. Müller, J.A. Schuler, S. Diethelm, J. Van herle, D. Favrat, *ECS Trans.*, 25, 457 (2009). (appendix 1)
- 20 J.A. Schuler, Z. Wuillemin, A. Hessler-Wyser, J. Van herle, *Electrochem. Solid- State Lett.*, 14, B20 (2011). (ch. 7.1)
- 21 M. Stanislovski, K. Hilpert, U. Hilpert, Patent, 20090317679 (2010).

6.2 Air side contamination in solid oxide fuel cell stack testing

J. Andreas Schuler^{a,b}, Christian Gehrig^a, Zacharie Wuillemin^a Albert J. Schuler^c,
Joerg Wochele^c, Christian Ludwig^{c,d}, Aïcha Hessler-Wyser^b, Jan Van herle^a

^a *Laboratoire d'Énergie Industrielle (LENI), École Polytechnique Fédérale de Lausanne (EPFL), 1015 Lausanne, Switzerland*

^b *Centre Interdisciplinaire de Microscopie Electronique (CIME), École Polytechnique Fédérale de Lausanne (EPFL), 1015 Lausanne, Switzerland*

^c *Labor für Bioenergie und Katalyse (LBK), Paul Scherrer Institut (PSI), 5232 Villigen, Switzerland*

^d *Institut d'Ingénierie de l'Environnement (ENAC-IIE), École Polytechnique Fédérale de Lausanne (EPFL), 1015 Lausanne, Switzerland*

This work aimed to quantify air side contaminants during Solid Oxide Fuel Cell (SOFC) testing in stack configuration. Post-analyses of a long-term test have shown that performance degradation was mainly due to cathode pollutants originated upstream of the cell, therefore their source identification is crucial. The compressed air system, feeding the airflow to the cathode, was investigated by filtering and subsequent chemical analysis of the filters. Hot-air-sampling was redone *in situ* at the cathode air entry during a new test run to assess the contaminant concentrations in air in SOFC test conditions. In addition, the behavior of SOFC proximal system components, i.e. alloy oxidation, was characterized separately. Besides the investigation of silicon and sulfur contamination, the present work focused on chromium from high-temperature alloys used in Balance-of-Plant (BoP) components in direct contact with the airflow. Concentrations of volatile Cr-species under SOFC testing conditions were compared to Cr-accumulation on the tested cell as well as to Cr-evaporation rates from BoP alloys, which were individually characterized regarding oxidation behavior. Evaporated Cr quantities were found to saturate the air with Cr-vapors at the cathode air-inlet, as confirmed by the *in situ* measurement of volatile species in the hot airflow, and correlate well to accumulated Cr in the cell after long term testing. The results of this study suggest guidelines to reduce air side contamination from exogenous sources in SOFC stacks.

1 Introduction

In the present context of global warming and increased energy demand, efficiency in energy conversion with minimal environmental impact is a major issue. Direct conversion of chemical energy into electrical energy can be achieved using Fuel Cells. High system efficiency, especially when operated in combined heat and power generation (CHP), and manageable fuel flexibility are expected from Solid Oxide Fuel Cells (SOFCs).

6.2. Air side contamination in solid oxide fuel cell stack testing

Stationary SOFC-CHP-units have lifetime requirements exceeding 40'000 h. Device longevity over such a time-scale imposes on SOFC components to withstand endogenous degradation effects, and in particular contamination by pollutant species generated in stack and system components, as well as supplied from external sources.

In a previous study, a 200 cm² anode-supported cell was tested in repeat-element configuration over 1900 h at 800°C, showing a degradation rate of 1 %kh⁻¹, on a dedicated test bench, allowing locally-resolved studies of performance degradation. Localized X-ray fluorescence (XRF) and scanning/transmission electron microscopy - energy dispersive X-ray spectroscopy (SEM/TEM-EDS) *post-test* investigations, combined with impedance spectroscopy deconvolution, allowed to pinpoint the origin of local performance degradation, i.e. mainly pollution contamination of the cathode by chromium (Cr), silicon (Si) and sulfur (S). The distribution of impurities on the cathode surface indicated SOFC proximal system components, located upstream the airflow, to be at the origin of volatile contaminants [1,2, (ch. 7.2, A.1)].

Contamination effects on the durability of SOFC during stack testing were revealed by numerous authors [3-7]. Repeat-element compounds such as metallic interconnects (MICs) are known as possible cathode pollutant sources [8]. Balance-of-Plant (BoP) elements can generate additional contamination [9]. Finally the quality of laboratory air has been mentioned to act on cathode performance [6,10]. However, localization and quantification of air side contaminants is generally insufficient in SOFC testing to ensure controlled operating environments and thereby isolate the studied processes from overlapping effects complicating the interpretation of results.

In the present work, the behavior of SOFC proximal system components, especially the oxidation behavior of BoP alloys, is related to identification and quantification of major pollutant species in *post-test* studies, as well as to *in situ* measurements of contaminant concentrations on the air side of a SOFC stack.

2 Methods

This work presents a three-level analysis of air side contaminations in SOFC testing. Indeed, as illustrated in Fig. 6.4, contaminants vehicled by the airflow were sampled at different locations in the test bench, i.e. by filtering the compressed air at ambient temperature, sampling the hot air at stack temperature and by analyzing contaminant accumulation in the cathode from *post-test* experiments. Moreover, focus is given on Cr- containing heat-resistant alloys from the BoP part of the test bench, which are in contact with the hot air flow, and from which evaporation of contaminant species is expected.

3 Experimental

Samples for *post-test* analyses were taken from an anode-supported repeat-element, including a composite strontium doped lanthanum manganite (LSM) - yttria stabilized zirconia (YSZ) cathode, a strontium doped lanthanum cobaltite (LSC) current collection layer (CCL) and a gas diffusion layer (GDL) made of SOFCConnexTM, which has been tested over 1900 h at 800°C [2].

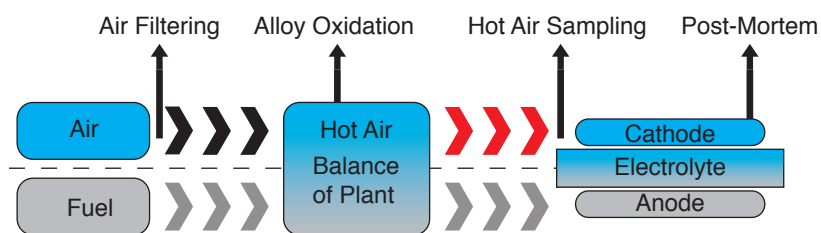


Figure 6.4: Schematic drawing of SOFC gas supply. Focus is here on the air-side: the laboratory air stems from a compressed air system; heat-exchangers and tubing elements from the BoP feed the cathode with hot air; hot air sampling is done at the cathode air- inlet; *post-test* analysis of these regions is mainly done by SEM/EDS observations.

The samples were immersed in hot nitric acid to dissolve perovskite cathode layers. The solution was analyzed for Cr-content with a PerkinElmer-AAnalyst400 (Winlab32 software) atomic absorption spectrometer (AAS), calibrated with standards. After dissolution, zirconia remnants were observed both by XRF, performed on a Fischer Xan system and equipped with WinFam software, and with a FEI-SEM coupled to an EDS- analyzer with a silicon-drift detector from Oxford Instruments combined to Inca software.

The hot gas sampling was performed using an adapted version of the liquid quench method described by Koebel and Elsener [11]. This was done by pumping the gas during 12 h through a capillary, placed at the air-inlet localization of the cathode, at a sampling flow rate of 1 l·min⁻¹ from a 20 l·min⁻¹ 770°C airflow. Volatile contaminants, present in the hot air, were condensated in an acidic solution, which was analyzed for Cr, Si and S contents on a PerkinElmer-Optima3300DV inductively coupled plasma optical emission spectrometer (ICP-OES), calibrated with standards.

The quality of laboratory air was analyzed by SEM-EDS observations of sub-micron syringe filters placed in the compressed air stream during several days at a flow rate of 15 l·min⁻¹. The air is dehumidified at 3°C under 10 bar pressure and its water content is confirmed as 5 % relative humidity (RH) at 25°C with a hygrometer, type MIK 3000 from Refco.

Oxidation behavior of BoP alloys, including austenitic steels, grades 1.4849, 1.4828 and Incoloy 800, was characterized by SEM-EDS measurements on surfaces and polished cross-sections after oxidizing alloy samples at 800°C for different durations.

4 Approach

Under oxidizing conditions, Cr-containing high temperature alloys form chromium rich oxide scales on their surface, i.e. mainly Cr₂O₃ chromia and (Cr,Mn)₃O₄ spinel phases [12,13]. When exposed to flowing gases, the oxide scale growth is dictated by the mass transfer in the gas boundary layer as well as by the oxidation behavior of the considered alloy [14,15]. In stagnant atmosphere, the oxide scale growth follows a parabolic law according to Wagner's theory of

6.2. Air side contamination in solid oxide fuel cell stack testing

oxidation: dominated by diffusion, it is given by [16-18]:

$$\frac{dX}{dt} = \frac{k_p}{X}; X = \sqrt{2 \cdot k_p \cdot t} \quad (6.1)$$

where X [cm] is the scale thickness, k_p [$\text{cm}^2 \cdot \text{s}^{-1}$] is the parabolic oxidation constant, evaluated from experiments in stagnant air, and t [s] the time.

When exposed to flowing gases, the Wagner's parabolic growth rate can be corrected [15,19] by an evaporation factor k_{ev} [$\text{cm} \cdot \text{s}^{-1}$] which depends locally on the mass transfer properties of the flow, on the difference between the partial pressure of the evaporated species at the oxide scale surface and the one in the gas stream, and consequently on the thermodynamic equilibrium of the vaporization reaction:

$$\frac{dX}{dt} = \frac{k_p}{X} - k_{ev} \quad (6.2)$$

When the oxide scale growth reaches a steady state, the above equation becomes

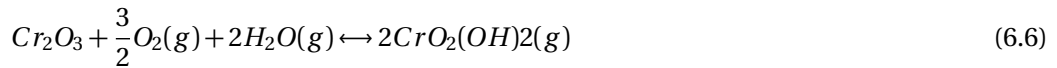
$$\frac{k_p}{X_{SS}} = k_{ev} \quad (6.3)$$

where X_{SS} [cm] is the steady state thickness, determined from samples exposed to flowing gases. The steady-state Cr evaporation rate J_{Cr} [$\text{g} \cdot \text{cm}^{-2} \cdot \text{s}^{-1}$] from an oxidized alloy in a non-saturated gas can thus be estimated from thickness measurements using the following equation:

$$J_{Cr} = \frac{3 \cdot \rho_{Cr_2O_3} \cdot k_p}{M_{Cr_2O_3} \cdot X_{SS}} \quad (6.4)$$

where $M_{Cr_2O_3}$ [$\text{g} \cdot \text{mol}^{-1}$] is the molar mass of chromia and M_O the one for oxygen; $\rho_{Cr_2O_3}$ [$\text{g} \cdot \text{cm}^{-3}$] is the density of chromia, which equals $5.2 \text{ g} \cdot \text{cm}^{-3}$.

Volatile Cr species - CrO_3 in dry air and both $\text{CrO}_3 / \text{CrO}_2(\text{OH})_2$ in humid air - evaporate from Cr-containing oxide scales at high temperature. By increasing the water vapor concentration in air, the oxyhydroxide $\text{CrO}_2(\text{OH})_2$ species becomes dominant and its concentration increases [20-22]. Cr^{6+} gaseous species are generated according to the following oxidation equations:



Along the flow through the different BoP components, the gas stream becomes progressively saturated by the evaporated species, reaching possibly the maximal saturation (i.e. the equilibrium partial pressure) for the conditions existing at the cathode air-inlet of the SOFC.

Considerable disagreement is found in literature for the estimation of equilibrium partial pressures [23]. The present work uses data from Wullemin [24], who extracted thermodynamic data for both Cr-vapor species from the literature.

For CrO_3 , the equilibrium partial pressure p_{CrO_3} can be calculated [24], using an equilibrium

constant, K_{CrO_3} , fitted on data from Ebbinghaus [20], which is consistent with results from Gindorf *et al.* [21]:

$$p_{CrO_3} = K_{CrO_3} \cdot p_{O_2}^{3/4} \quad (6.7)$$

$$\log K_{CrO_3} = -12235.38 \cdot T^{-1} + 3.01 \quad (6.8)$$

where p_{O_2} [atm] is the oxygen partial pressure and T [K] the temperature. For the oxyhydroxide species $CrO_2(OH)_2$ data from Stanislawski *et al.* [23], which is in relatively good agreement with those from Opila *et al.* [14], was used to determine the equilibrium constant [24]:

$$p_{CrO_2(OH)_2} = K_{CrO_2(OH)_2} \cdot p_{H_2O} \cdot p_{O_2}^{3/4} \quad (6.9)$$

$$\log K_{CrO_2(OH)_2} = -2978.43 \cdot T^{-1} - 1.96 \quad (6.10)$$

In the following analyses, the experimentally determined amount of Cr-vapors transported in the air stream is compared to the values that could be evaluated using the non-saturation hypothesis (Eq 6.4) and the ones given by thermodynamic equilibrium calculations (Eqs 6.7 and 6.9).

5 Results and discussion

5.1 Cr contamination Accumulations of Cr, on the air side of the cell tested over 1900 h, were determined using AAS by measuring Cr-concentrations from *post-test* samples of the cell taken at different positions along the air-flow. An average value of 35 μg Cr per cm^2 of active area was found in cathode and CCL layers of the repeat-element. This corresponded to a total Cr accumulation of 38 mg for the 200 cm^2 cell, including cathode, CCL and GDL, taking into account the total surface exposed to the airflow and assuming that all Cr entering the cathode compartment is trapped therein [1,2, (ch. 7.2, A.1)].

Cr-contamination stemming from the MIC was avoided in this test by an effective protective coating [2, (A.1)]. Accumulation of Cr was mainly observed in the air-inlet regions of the cathode, suggesting Cr-contamination from upstream system components. Knowing the surface area of BoP alloys exposed to the hot air-flux (784 cm^2), the total Cr accumulation would correspond to an average Cr evaporation rate from BoP alloys of $7 \cdot 10^{-11} \text{ kg} \cdot \text{m}^{-2} \cdot \text{s}^{-1}$. Volatile Cr quantification in the hot air flux was enabled by hot air *in situ* sampling followed by chemical analysis. A concentration of 12 ppb ($\mu\text{g} \cdot \text{m}^{-3}$) volatile Cr in the hot air flux was established, which would correspond to an accumulation of 28 mg Cr in the cell for 1900 h of operation. Knowing the air-flux rate and the exposed alloy surface, one obtains an evaporation rate of $5 \cdot 10^{-11} \text{ kg} \cdot \text{m}^{-2} \cdot \text{s}^{-1}$. Both Cr-accumulation and evaporation rate are therefore well within the same order of magnitude.

Cr evaporation from BoP alloys exposed to the hot air flux was further estimated from oxidation experiments performed on metal coupons. A SEM picture of a polished cross-section of an

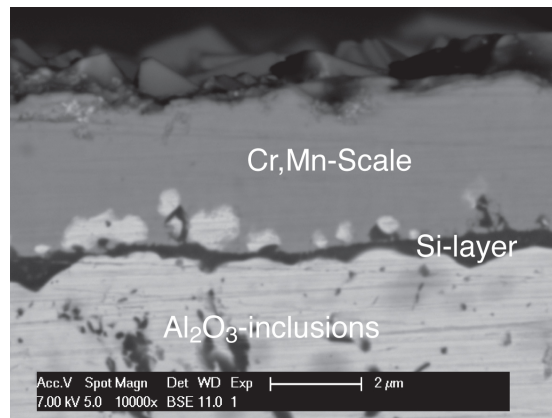


Figure 6.5: Cr,Mn-containing oxide scale (dark grey) formed on Incoloy 800 alloy (light grey) after 500 h oxidation at 800°C observed by SEM on a polished cross-section. A continuous Si-rich sub-scale layer appears for this oxidation time (dark phase).

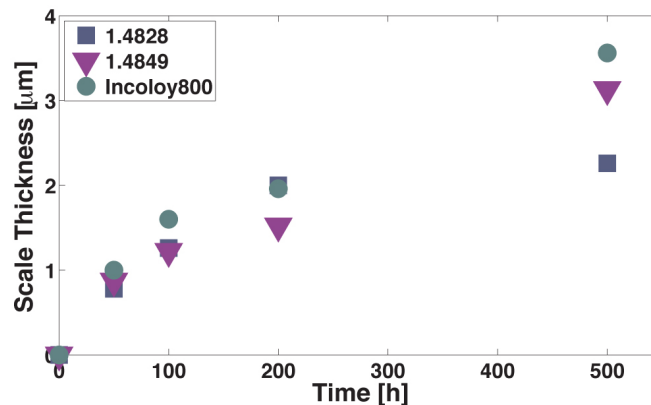


Figure 6.6: Oxide scale thickness evolution with time for 1.4828, 1.4849 and Incoloy 800 alloys. Steady-state thickness of 2.2, 5.1 and 4.2 μm , respectively for these alloys, result from scale thickness extrapolation at longer oxidation times.

Incoloy 800 sample oxidized at 800°C over 500 h is given in Fig. 6.5.

The layered structure includes, from bottom to top, the base alloy (light grey) with alumina Al_2O_3 inclusions (dark spots), a silicon-rich sub-scale layer (dark) and a Cr,Mn-containing oxide scale (dark grey). A scale thickness $X = 3.5 \mu\text{m}$ is measured; the thickness evolution with time, for all three alloys, is reported in Fig. 6.6.

As BoP alloys from the test bench had been operated for several kh before this work, steady-state thicknesses X_{SS} at longer oxidation times were extrapolated from these results, and are reported in Tab. 6.2. The growth rates k_p and the evaporation rates J_{Cr} were calculated, by making the hypothesis of non-saturation of the air by Cr-vapor species (Eq. 6.4), and are consistent with results from the literature [22,23].

From this data, a mean evaporation rate was calculated to $13 \cdot 10^{-11} \text{ kg} \cdot \text{m}^{-2} \cdot \text{s}^{-1}$ for the exposed alloy surfaces. However, this evaluation, using the non-saturation hypothesis, over-estimates

Chapter 6. Cr contamination sources

Table 6.2: Steady-state oxide scale thickness, parabolic growth rates and corresponding evaporation rates, calculated from the oxidation study of grades 1.4828, 1.4849 and Incoloy 800 alloys.

	1.4828	1.4849	Incoloy 800
Scale thickness, X_{SS} [μm]	2.2	5.1	4.2
Growth rate, k_p [cm^2s^{-1}] $\cdot 10^{-14}$	1.3	2.8	3.6
Evaporation rate, J_{Cr} [$\text{kg}\cdot\text{m}^{-2}\text{s}^{-1}$] $\cdot 10^{-10}$	1	0.9	1.4

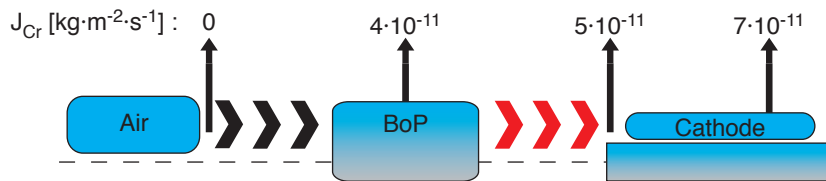


Figure 6.7: Hot air *in situ* sampling allowed direct access to the concentration of volatile Cr-species. The quantity of Cr in air can be related to Cr-evaporation from the source and to Cr-accumulation as cathode poison. Cr evaporation rates calculated from oxidation studies of BoP alloys, hot air sampling and *post-test* analyses all correlate well.

Cr-evaporation. Indeed, thermodynamic equilibrium calculations give saturation pressures of $6\cdot 10^{-10}$ and $8\cdot 10^{-9}$ (atm) for CrO_3 and $\text{CrO}_2(\text{OH})_2$, respectively, at the cathode air-inlet. This would correspond to a Cr-evaporation rate of $4.3\cdot 10^{-11} \text{ kg}\cdot\text{m}^{-2}\cdot\text{s}^{-1}$. In other words, Cr-containing BoP components saturate the hot air with volatile Cr-species.

As filtering the compressed air before the hot air zone (analyzing air-filters before the BoP) revealed no presence of Cr, Cr-evaporation from BoP alloys should equal Cr-concentrations in the hot air flux as well as Cr-accumulation in the cell. Indeed, the amount of Cr was found to be in the same order of magnitude for all three analysis-locations; this result is graphically summarized in Fig. 6.7.

A correlation between Cr content in the cathode ($18 \mu\text{g}\cdot\text{cm}^2$ for cathode and CCL for 1 kh) and degradation ($1 \%\cdot\text{kh}^{-1}$) can be done, neglecting other contamination effects similar to other studies. Indeed, Stanislawski *et al.* [25] report $4 \mu\text{g}\cdot\text{cm}^{-2}$ for degradation rates of $1 \%\cdot\text{kh}^{-1}$, considering that the evaporated Cr-content from a MIC, of equal surface compared to the cell, is totally trapped by the latter. The study of Menzler *et al.* [26], who correlated degradation rates to Cr-accumulation in cathodes for a dozen stack-tests, mentions $15 \mu\text{g}\cdot\text{cm}^{-2}$ for tests with less than $1.5 \%\cdot\text{kh}^{-1}$ degradation (averaged value). However, previous studies [2,24] pointed out the important difference between global and local degradation rates of a repeat-element. Local distribution of pollutant species [1, (ch. 7.2)] could be related to local degradation rates, whereas the low-degraded areas were mainly free of contamination.

5.2 Other contamination Scale composition is however not only limited to chromia. During oxidation, the scale composition evolves from a chromia-rich structure to a Cr/Mn-containing spinel type phase, reducing Cr-evaporation.

6.2. Air side contamination in solid oxide fuel cell stack testing

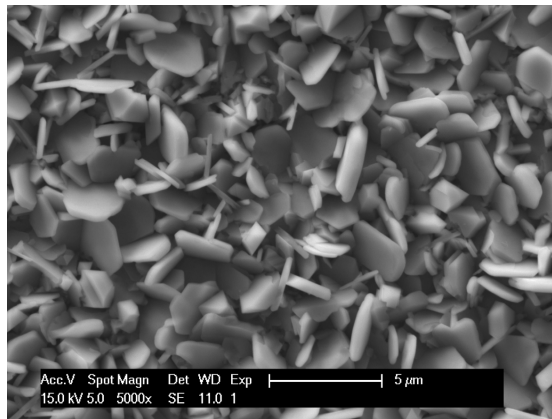


Figure 6.8: Hexagonal-shaped crystal plates, characteristic of a chromia scale, are observed on grade 1.4828 alloy surface after 50 h oxidation at 800°C.

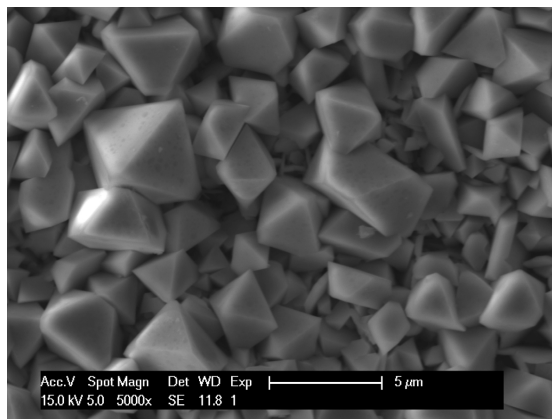


Figure 6.9: Surface view of grade 1.4828 alloy after 500 h oxidation at 800°C showing pyramidal-shaped crystals characteristic for Cr,Mn-spinels.

Fig. 6.8 shows the surface structure of a chromia oxide scale, with characteristic hexagonal-shaped plates, observed after 50 h oxidation on grade 1.4828 alloy. At longer oxidation times, as the Mn-content in the oxide scale increases, a structure transition from chromia plates into pyramidal spinel structures is observed. Fig. 6.9 illustrates a surface view of 1.4828 alloy after 500 h oxidation, with a coarsened structure.

Elemental analyses of oxide scales were performed by EDS surface scans adjusting acceleration potential to minimize signal contribution from the sub-scale bulk alloy. The evolution of the oxide scale composition for the studied alloys is reported in Fig 6.10. For all three alloys, the Mn-content increases with time and stabilizes. The oxide scales are tending towards the following compositions: $(\text{Cr}_{0.7}\text{Mn}_{0.3})_3\text{O}_4$, $(\text{Cr}_{0.8}\text{Mn}_{0.2})_3\text{O}_4$ and $(\text{Cr}_{0.75}\text{Mn}_{0.25})_3\text{O}_4$, for grade 1.4828, 1.4849 and Incoloy 800 alloys, respectively. In the case of Incoloy 800, contrary to the predicted formation of internal TiO_2 sub-scale precipitates, Ti was found in the scale, suggesting formation of $(\text{Cr,Mn})_2\text{Ti}_3\text{O}_4$ on the surface [22].

The oxide scales on all three alloys presented a tendency to delaminate; simple manipulations

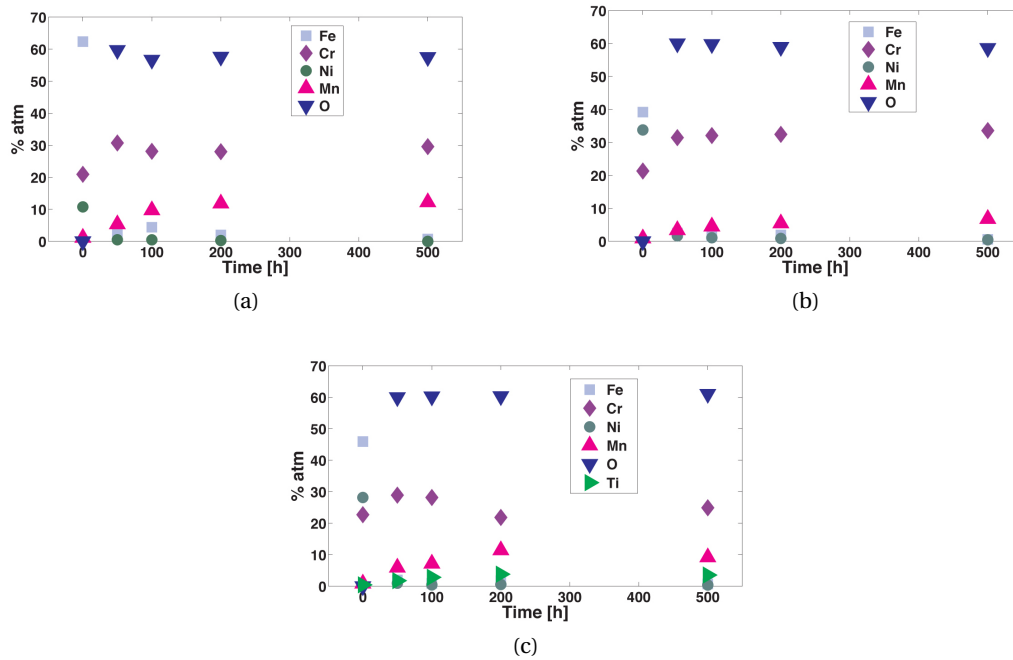


Figure 6.10: Evolution with time of oxide scale composition of grade (a) 1.4828, (b) 1.4849 and (c) Incoloy 800 alloys; the scale tends towards $(Cr_{0.7}Mn_{0.3})_3O_4$, $(Cr_{0.8}Mn_{0.2})_3O_4$ and $(Cr_{0.75}Mn_{0.25})_3O_4$, spinel-type compositions, respectively.

Table 6.3: Si concentration [% at] measured by EDS scans of sub-scale layers on alloy surface regions with delaminated oxide scales.

Time [h]	50	100	200	500
1.4828	3.99	3.96	3.91	4.15
1.4849	nd	nd	3.64	4.64
Incoloy 800	nd	nd	4.98	3.82

of oxidized alloy samples lead to spallation of the scale. Fig. 6.11 shows a low magnification view of an alloy surface with delaminated scale. Nevertheless, delaminated regions allowed EDS analyses on both scale remnants (dark regions) and sub-scale surfaces (light grey regions). In the latter, high concentrations of Si are observed, as shown in Tab. 6.3. Si-rich sub-scale phases are known to enhance scale delamination upon thermal variations, as the thermal expansion coefficient (TEC) is different for scale ($Cr_2O_3 \sim 8.5 \cdot 10^{-6} K^{-1}$) and sub-scale layers ($SiO_2 \sim 0.5 \cdot 10^{-6} K^{-1}$; alloy $\sim 15 \cdot 10^{-6} K^{-1}$) [27]. The sub-scale phase is expected to be amorphous SiO_2 , as reported by Bauer *et al.* [27]; the absence of grain-boundaries (fast diffusion) should lead to slow-growing chromia layers.

As scale delamination exposes Si-rich sub-scale alloy surfaces to the hot air flux in BoP components, high temperature alloys are supposed to be sources of Si-contamination in SOFC testing. Such observations were done before by Kaus *et al.* [28], where a 1.77 % Si- containing

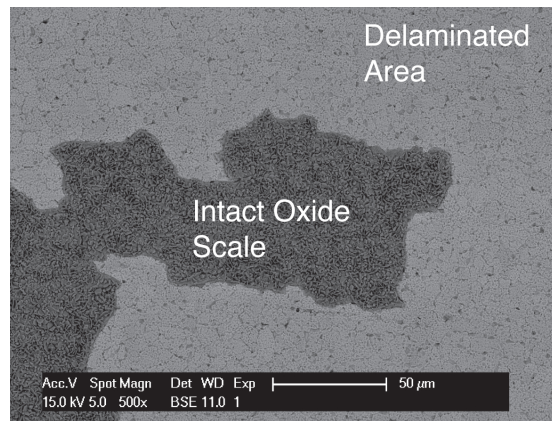
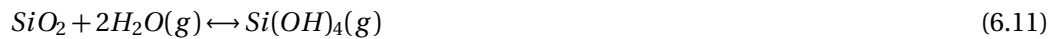


Figure 6.11: High Si-concentrations in sub-scale layers fragilize alloy/sub-scale and sub-scale/scale interfaces. This low magnification SEM image presents an oxide scale (dark grey) that partially delaminated exposing Si-rich sub-scale surface (light grey).

furnace tube material was a source of Si poisoning for oxygen membranes. Si-rich sub-scale phases result from internal oxidation of Si and segregation of Si-phases at the interface [22]. Si-containing volatile species evaporate from SiO_2 in the form of hydroxides and oxyhydroxides as described in the literature [14,29,30], according mainly to the following reaction, at temperature ranges of 800-1000°C.



Nevertheless, Kaus *et al.* reported the difficulty of Si identification by EDS in strontium (Sr) containing materials due to the overlap of Sr $L\alpha$ and Si $K\alpha$ X-ray emission lines, which are at 1.806 and 1.740 keV, respectively.

In this study, the *post-test* acidic dissolution of strontium allowed bypassing the difficulty of Si identification by EDS. Fig. 6.12 shows a characteristic pattern of Si-distribution within the zirconia remnants of the cathode, following the airflow, which allows to distinguish between Si as bulk impurity [31-34] and exogenous Si as pollutant; its source is located upstream of the airflow [1,2, (ch. 7.2, A.1)].

As expected after *post-test* observation, volatile Si species were also revealed by the analyses of hot air samples: $34 \mu\text{g}\cdot\text{m}^{-3}$ Si was measured. Such an amount of Si would correspond to a Si accumulation in the cell of 70 mg for 1900 h operation (Si was not yet quantified in *post-test* analyses), and to an evaporation rate of $J_{\text{Si}} 1.5\cdot 10^{-10} \text{ kg}\cdot\text{m}^{-2}\cdot\text{s}^{-1}$, when considering all Si stemming from the BoP alloys.

However, this result far exceeds the expected evaporation rates [14,28-30]. Indeed, considering evaporation of Si-tetraoxyhydroxide from SiO_2 , using thermodynamic data from Wullemin [24] who extracted an equilibrium constant (Eq. 6.13) from Jacobson and Opila's results [14,29,30], the equilibrium partial pressure of $\text{Si}(\text{OH})_4$ under the cathode air- inlet conditions,

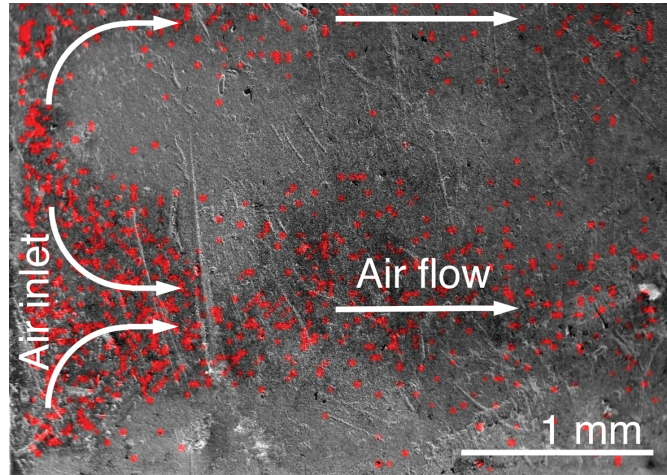


Figure 6.12: Spatial distribution of Si observed by EDS on zirconia remnants after cathode dissolution in acid. The low magnification surface view shows Si to follow the airflow pattern (air-entry on the left).

can be calculated according to the following equation:

$$p_{Si(OH)_4} = K_{Si(OH)_4} \cdot p_{H_2O}^2 \quad (6.12)$$

$$\log K_{Si(OH)_4} = -2857.84 \cdot T^{-1} - 3.53 \quad (6.13)$$

which equals $p_{Si(OH)_4} = 2 \cdot 10^{-12}$ atm. This would correspond to an evaporation rate of $7.3 \cdot 10^{-15}$ $\text{kg} \cdot \text{m}^{-2} \cdot \text{s}^{-1}$. Therefore, Si contamination from Si-species is expected in other forms than Si(OH)_4 .

Filtering the laboratory air did not reveal traces of Si that could stem from silicone oil and rubber or siloxane greases, as reported in literature [35,36]. On the other hand, atmospheric particular matter (PM) from environmental air, which is a complex mixture of elemental and organic carbon, ammonium, nitrates, sulphates, trace elements, water and mineral dust [37], might pass mechanical filtering. However, in this case, a maximum contribution of about $1 \mu\text{g} \cdot \text{m}^{-3}$ Si (calculated from mineral dust composition: $\text{Si} = 1.89\text{Al} + 1.66\text{Mg} + 1.21\text{K} + 1.40\text{Ca} + 1.43\text{Fe} + 2.14\text{Si}$) is expected [37].

Nevertheless, Si influences both electrolyte and electrode performance, limiting oxygen exchange reactions [6,32,35,36], as Si forms insulating amorphous low-melting eutectics with alkaline and alkaline rare-earth (RE) elements [14,28,34,38,39]. Rare-earth disilicates, in the form of RESi_2O_5 and RESi_2O_7 , are found in the literature [14,39], including La-silicate [34] and Sr-silicate Sr_2SiO_4 [27]; on the other hand, formation of ZrSiO_4 is reported to be unfavorable under SOFC operation conditions [32]. Delaminations in the cathode, upon silicate formation, are expected because of differences in TECs [38]. However, TEC values for RE-disilicates are not available in the open literature [39].

Backhaus-Ricoult [31] suggests that the bulk Si impurity level in ceramic powders is sufficient to produce full coverage of an electrolyte surface with a monolayer of silica; in the present

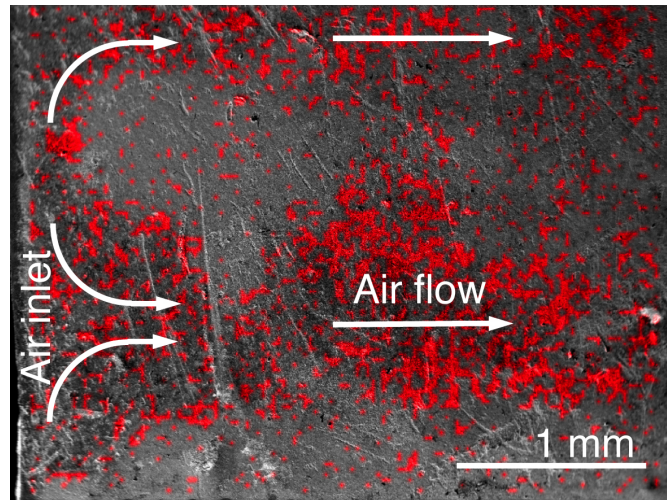
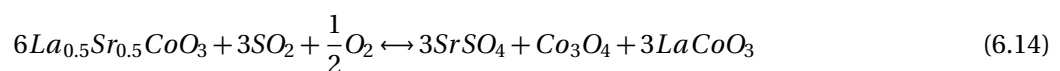


Figure 6.13: When sulfur reacts within the CCL, LSC decomposes (Eq 6.14) into Co_3O_4 . After dissolution of the cathode in acid, Co_3O_4 is observed in zirconia remnants and follows the pattern of the airflow, as shown by this EDS mapping, indicating the source of sulfur contamination to be located upstream of the cell.

study, severe Si-contamination from exogenous sources was shown. Already small coverage of Si can hinder oxygen exchange on electrolyte surfaces, as the oxygen-sticking factor on cathode materials is low at SOFC operation temperatures [31]. The influence of Si in SOFC testing has to be considered, as its presence is ubiquitous [40]; different Si-contamination levels may be responsible for the disagreement in the literature related to the behavior of air side components.

Similar to the observation of Si-pollution within the cathode, the effect of sulfur on the latter is shown in Fig. 6.13. Sulfur reacts with LSC from the CCL, according to the following equation [1, (ch. 7.2)]:



where LSC decomposes into strontium sulphate SrSO_4 , lanthanum-cobaltite LaCoO_3 (LC) and cobalt oxide Co_3O_4 . The latter is observed in Fig. 6.13 and follows the airflow pattern, whereas the perovskites LSM, LSC and LC have been dissolved. The source of sulfur pollution was thus located upstream of the cell.

Moreover, the *in situ* hot air sampling experiment enabled to determine an amount of $6 \mu\text{g}\cdot\text{m}^{-3}$ sulfur in the hot air flux; this would correspond to an accumulation of 14 mg sulfur in the cathode after 1900 h testing. Compressed air filtering revealed sulfur in combination with organic material, indicating the laboratory air to be the source of sulfur, conveying 12 ppb SO_2 . Amounts around 10 ppb of SO_2 are typical for Swiss urban air (daily measured by the Swiss Office for the Environment FOEN) and is close to the amount of sulfur measured in this work. Fig. 6.14 summarizes analysis-locations where Si and sulfur were revealed as air side contamination. Additional air contaminants were measured at different analysis-locations including

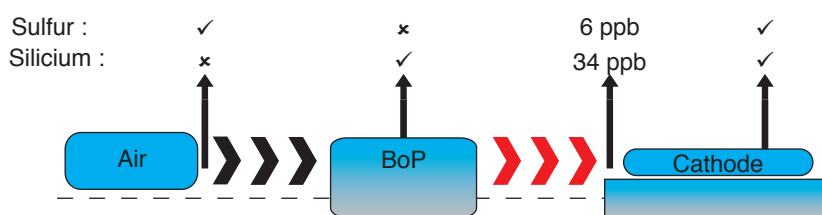


Figure 6.14: Silicon and sulfur were revealed as air side contaminants in SOFC testing. Quantitative data was so far only given by the in situ hot air sampling analysis. The symbols indicate whether a contamination source was identified upstream the contamination accumulations in the cathode or not.

sodium, potassium and chlorine; these foreign elements were reported, as air side contaminants, in other studies [10,26]. Alkaline species were shown to act in degradation chain mechanisms on the air side, as they promote the formation of eutectics [3,4]. The laboratory air can convey inorganic salts, in particular by its water content, as the salts are absorbed to form aqueous solutions when the humidity in air reaches the deliquescence point [37]. As analyses on the compressed air showed only 5 % RH, further studies are ongoing to access the sources of these pollutant species.

6 Conclusion

Severe air side contamination by pollutant species generated in system components, as well as supplied by external sources, was revealed in this study. Regarding Cr- contamination, it was shown that the BoP saturates the air with Cr-vapor species. Moreover, this concentration could be measured *in situ* in the hot air flux, and was well correlated to Cr accumulations in a cell tested within the system.

SOFC components and button cells are often tested in inert setups where Cr-poisoning is avoided by the absence of BoP system parts. Even in such an approach, unexpected contamination sources are introduced; for instance, a thermocouple in proximity of the cathode was shown to be a source of Cr-poisoning [41].

However, different behaviors are observed for cells, short stacks and stacks; the most important difference is their thermal environment. SOFC testing in stack configuration is necessary especially when testing durability issues and longevity. In such conditions, air- side contamination stemming from BoP components as well as from the air itself was confirmed in the present work, emphasizing the priority of Cr reduction from BoP when Cr protection from MICs is adequate, as already stated in a previous study [2, (A.1)].

Protection, filtering and trapping are hence necessary features that have to be integrated in the design of SOFC test benches. Testing in an inert setup with the possibility to change a single BoP component at a time is another interesting option [26]. Finally, the analyses on air-filters answered the requested need of analyzing the compressed air [10]; such strategies are suggested to reduce the laboratory specific nature of SOFC component behavior, which is mainly due to impurities [6].

Acknowledgements

Financial support from the Swiss Federal Energy Office (Contract 153569, AccelenT), the European Commission (FP6 contract SES6-019875, Flame-SOFC), the Competence Center Energy and Mobility (CCEM-CH) in the framework of WoodGas-SOFC (Project 705028) and the swisselectric research project TREGAS is gratefully acknowledged. Stéphane Thonney and Dr. Christophe Roussel (Section of Chemistry and Chemical Engineering / Institute of Chemical Sciences and Engineering / EPFL) are acknowledged for XRF and AAS measurements. Many thanks to Dr. Anca Haiduc (Environmental Engineering Institute / School of Architecture, Civil and Environmental Engineering / EPFL) for the ICP-OES measurements.

References

- 1 J.A. Schuler, Z. Wuillemin, A. Hessler-Wyser, ECS Trans. 25 (2009) 2845-2852. (ch. 7.2)
- 2 Z. Wuillemin, A. Nakajo, A. Mueller, J.A. Schuler, S. Diethelm, J. Van herle, D. Favrat, ECS Trans. 25 (2009) 457-471. (appendix 1)
- 3 H. Yokokawa, T. Horita, K. Yamaji, H. Kishimoto, Y.P. Yiong, M.E. Brito, EFCF Proceeding B1004 (2008) 1-12.
- 4 H. Yokokawa, H. Tu, B. Iwanschitz, A. Mai, J. Power Sources 182 (2008) 400-412.
- 5 H. Yokokawa, T. Watanabe, A. Ueno, K. Hoshino, ECS Trans. 7 (2007) 133-140.
- 6 M. Mogensen, K.V. Jensen, M.J. Jorgensen, S. Primdahl, Solid State Ionics 150 (2002) 123-129.
- 7 R.R. Liu, S.H. Kim, Y. Shiratori, T. Oshima, K. Ito, K. Sasaki, ECS Trans. 25 (2009) 2859-2866.
- 8 S. Tanagushi, M. Kadowaki, H. Kawamura, T. Yasuo, Y. Akiyama, Y. Miyake, T. Saitoh, J. Power Sources 55 (1995) 73-79.
- 9 K. Gerdes, C. Johnson, J. Fuel Cell Sci. and Technol. 6 (2009) 011018.
- 10 A. Hagen, Y.L. Liu, R. Barfod, P.V. Hendriksen, J. Electrochem. Soc. 155 (2008) B1047-B1052.
- 11 M. Koebel, M. Elsener, J. Chromatogr., A 689 (1995) 164-169.
- 12 P. Kofstad, R. Bredesen, Solid State Ionics 52 (1992) 69-75.
- 13 S.P.S. Badwal, R. Deller, K. Foger, Y. Ramprakash, J.P. Zhang, Solid State Ionics 99 (1997) 297-310.
- 14 E. J. Opila, N.S. Jacobson, D.L. Myers, E.H. Copland, J. Miner. Met. Mater. Soc. 58 (2006) 22-28.

- 15 D.J. Young, B.A. Pint, *Oxid. Met.* 66 (2006) 137-153.
- 16 C. Wagner, in *Atom Movements*. American Society of Metals, Cleveland OH, 1951.
- 17 K. Hauffe, *Oxidation of Metals*, Plenum Press, New York, 1965.
- 18 Z. Yang, K.S. Weil, D.M. Paxton, J.W. Stevenson, *J. Electrochem. Soc.* 150 (2003) A1188-A1201.
- 19 C.S. Tedmon, *J. Electrochem. Soc.* 113 (1966) 766-768
- 20 B.B. Ebbinghaus, *Combustion and Flame* 93 (1993) 119-137.
- 21 C. Gindorf, L. Singheiser, K. Hilpert, *J. Phys. Chem. Solids* 66 (2005) 384-387.
- 22 M. Stanislawski, E. Wessel, T. Markus, L. Singheiser, W.J. Quadackers, *Solid State Ionics* 179 (2008) 2406-2415.
- 23 M. Stanislawski, E. Wessel, K. Hilpert, T. Markus, L. Singheiser, *J. Electrochem. Soc.* 154 (2007) A295-A306.
- 24 Z. Wuillemin, EPFL Thesis 4525 (2009) 255-262.
- 25 M. Stanislawski, J. Froizheim, L. Niewolak, W.J. Quadackers, K. Hilpert, T. Markus, L. Singheiser, *J. Power Sources*, 164 (2007) 578-589.
- 26 N.H. Menzler, I. Vinke, H. Lippert, *ECS Trans.* 25 (2009) 2899-2908.
- 27 R. Bauer, M. Baccalaro, L.P.H. Jeurgens, M. Pohl, E.J. Mittemeijer, *Oxid. Met.* 69 (2008) 265-285.
- 28 I. Kaus, K. Wiik, M. Dahle, M. Brustad, S. Aasland, *J. Eur. Ceram. Soc.* 27 (2007) 4509-4514.
- 29 E.J. Opila, D.S. Fox, N.S. Jacobson, *J. Am. Ceram. Soc.* 80 (1997) 1009-1012.
- 30 N.S. Jacobson, E.J. Opila, D.L. Myers, E.H. Copland, *J. Chem. Thermodyn.* 37 (2005) 1130-1137.
- 31 M. Backhaus-Ricoult, *Solid State Sci.* 10 (2008) 670-688.
- 32 J-H. Lee, *Chem.* 140 (2009) 1081-1094.
- 33 B.C.H. Steele, *Solid State Ionics* 134 (2000) 3-20.
- 34 D. Kuscner, J. Holk, M. Hrovat, S. Bernik, Z. Samardzija, D. Kolar, *Solid State Ionics* 78 (1995) 79-85.
- 35 M. de Ridder, A.G.J. Vervoort, R.G. van Welzenis, H.H. Brongersma, *Solid State Ionics* 156 (2003) 255-262.

6.2. Air side contamination in solid oxide fuel cell stack testing

- 36 M.M. Viitanen, R.G. van Welzenis, H.H. Brongersma, F.P.F. van Berkel, *Solid State Ionics* 150 (2002) 223-228.
- 37 C. Hueglin, R. Gahrig, U. Baltensperger, M. Gysel, C. Monn and H. Vonmont, *Atmos. Environ.* 39 (2005) 637-651.
- 38 S.B. Adler, *Chem. Rev.* 104 (2004) 4791-4843.
- 39 E.J. Opila, R.C. Robinson, D.S. Fox, R.A. Wenglarz, M.K. Ferber, *J. Am. Ceram. Soc.* 86 (2003) 1262- 1273.
- 40 J-M. Bae, B.C.H Steele, *Solid State Ionics* 106 (1998) 247-253.
- 41 D. Oh, E. Armstrong, D. Jung, C. Kan, E. Wachsman, *ECS Trans.* 25 (2009) 2871-2879.

7 Superimposed degradation effects

Electrochemical and Solid-State Letters **14** (2011) B20

7.1 Glass-forming exogenous silicon contamination in solid oxide fuel cell cathodes

J. Andreas Schuler^{a,b}, Zacharie Wuillemin^a, Aïcha Hessler-Wyser^b, Jan Van herle^a

^a *Laboratoire d'Énergie Industrielle (LENI), École Polytechnique Fédérale de Lausanne (EPFL), 1015 Lausanne, Switzerland*

^b *Centre Interdisciplinaire de Microscopie Electronique (CIME), École Polytechnique Fédérale de Lausanne (EPFL), 1015 Lausanne, Switzerland*

Spatially resolved analyses, by energy-dispersive X-ray spectroscopy (EDS) and scanning electron microscopy, allowed the quantification of exogenous Si contamination in a solid oxide fuel cell (SOFC) cathode after operation. The Si quantification, taking into account the endogenous Si impurity level, correlated well with the expectation from the condensation of Si(OH)₄ vapor, originating from upstream alloy components and saturated in the hot inlet air. At higher resolution, EDS-transmission electron microscopy pointed out the deposition of Si vapor in the form of amorphous SiO₂, blocking oxygen incorporation into the electrolyte phase within a composite SOFC cathode.

1 Introduction

In solid oxide fuel cell (SOFC) technology, silicon (Si) is, by its insulating and glass-forming properties, a major limitation for electrochemical performance [1,2]. As endogenous impurity in SOFC ceramics, Si is present in raw materials and is introduced by costcutting exercises during powder preparation [3].

Besides bulk impurity, exogenous Si contamination is vehicled in SOFC operation by the reactants, stemming from oils and greases as well as mineral dust [2,4-6]. In particular, cell-proximal system components such as furnace materials [7-9] or the common use of quartz reactors can lead to Si contamination [10-12].

Although the presence of Si is ubiquitous and influences both the electrolyte and cathode resistivities [13], the understanding of its effect on electrochemical cathode processes, by a deleterious poisoning of the active catalytic sites for oxygen reduction, is lacking [14]. Moreover, it is suggested that different Si contamination levels are at least partially responsible for disagreements in the literature related to cathode performance and degradation [13], as well as for the laboratory specific behavior of SOFC electrodes [2,15].

To enable data correlation from different researches, quantification methods for Si contamination are needed [16]; an area where this study aims to contribute. Energy-dispersive X-ray spectroscopy (EDS) is employed here as an identification and quantification tool for both endogenous Si impurity levels and Si contamination stemming from exogenous sources.

2 Experimental

Samples for posttest analyses were taken from an anodesupported cell, including Sr-doped lanthanum manganite (LSM), yttria-stabilized zirconia (YSZ) composite cathode, a Sr-doped lanthanum cobaltite (LSC) current collection layer (CCL), and a gas diffusion layer made of SOFCConnex HTceramix, Switzerland, which had been tested over 1900 h at 1073 K [17,18, (A.1, ch. 7.2)].

The identification of Si in LSM-YSZ cathodes by EDS is challenged by the overlap of Si K-shell and Sr L-shell emission lines at 1.74 and 1.81 keV, respectively [8]. This difficulty was bypassed by the dissolution of Sr-containing perovskite layers. Dissolution was achieved by the immersion of the samples in hot concentrated nitric acid, to which a small amount of sulfuric acid was added [19, (ch. 6.2)]. The remnants were rinsed with distilled water, plasma cleaned, and carbon coated with instruments model 1020 Fischione (USA) and Edwards 306 Ceramisis (UK), respectively, prior to EDS measurements.

EDS analyses were conducted on XLF-30 FEI (USA) scanning and CM300 Philips (the Netherlands) transmission electron microscopes scanning electron microscopy (SEM) /transmission electron microscopy (TEM) equipped with Oxford Instruments (UK) detectors and INCA software. A focused ion beam (FIB) -SEM dual beam microscope NVision40 Zeiss (Germany) was used for the TEM lamella extraction at the cathode surface. Time of flight secondary ion mass spectroscopy (TOF-SIMS) was performed on an ION-TOF (Germany) apparatus using Bi_3^+ ions at 25 keV energy.

3 Results and discussion

The localization of Si accumulations along airflow channels, as illustrated in Fig. 7.1, indicated that Si originated from upstream components, i.e., Si-containing high temperature alloys. The presence of Si was further confirmed by measuring the volatile contaminants in the hot air flux at the cathode air inlet, as previously published [19, (ch. 6.2)].

Si phases are formed at the interface between the oxide scale and the metal in high temperature alloys, after internal oxidation and segregation of Si [20-23]. When exposed to a hot air flux, these phases generate volatile species. Si contamination from upstream alloys has been reported by other authors [8], but was not quantified in cells after operation in such studies.

7.1. Glass-forming exogenous silicon contamination in solid oxide fuel cell cathodes

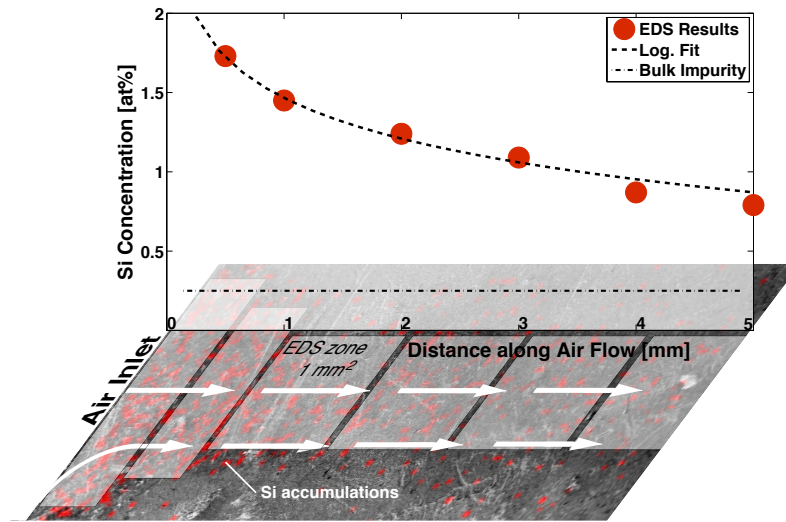


Figure 7.1: The quantification of Si contamination along an airflow channel was done by EDS analysis of defined regions of cathode remnants after the dissolution of perovskite phases, taking into account the endogenous Si impurity level, determined on nonexposed samples.

In the present work, Si quantification was done on geometrically defined regions, typically 1 mm x 1 mm areas along an air channel, from an EDS-measurement data cube obtained by mapping the cathode surface of a 25 mm² SEM sample, as illustrated in Fig. 7.1. The Si concentration is highest at the air entry and decreases along the airflow, reaching a constant level (ca. 0.25 atom % normalized to YSZ), after 25 mm (confirmed by additional EDS-measurement points).

The latter value corresponds to Si concentration as bulk impurity, also confirmed on various nonexposed as-sintered cathodes from a previous study [24, (ch. 3.1)]. The raw material used here was thus considerably contaminated compared to the typical impurity levels of 100-1000 ppm 0.1% [9], keeping in mind that levels below 10 ppm are needed to ensure that grain surfaces are not fully covered by Si [7,25].

By integrating the Si concentration along one air channel length of the repeat-element (17 cm), within the ca. 66 vol. % porous and 10 μm thick YSZ skeleton, and subtracting the endogenous impurity level, a quantity of 0.12 μg Si is found. This corresponds, taking into account the geometrical distribution of the air channels, to a value of 7.6 μg Si for the whole tested repeat-element 200 cm², which is related to the evaporation, transport, and accumulation of Si vapor species as follows.

Si(OH)₄ is the primary volatile species from the reaction of SiO₂ with steam in hot air [26]. The partial pressure of this species is highly dependent on the steam pressure but only little on temperature, as illustrated by thermodynamical equilibrium calculations [19, (ch. 6.2)], Eqs. 7.1 and 7.2, generated from [27] the thermodynamic data of Si-O-H species found in another study [28]

$$p_{\text{Si(OH)}_4} = K_{\text{Si(OH)}_4} \cdot p_{\text{H}_2\text{O}}^2 \quad (7.1)$$

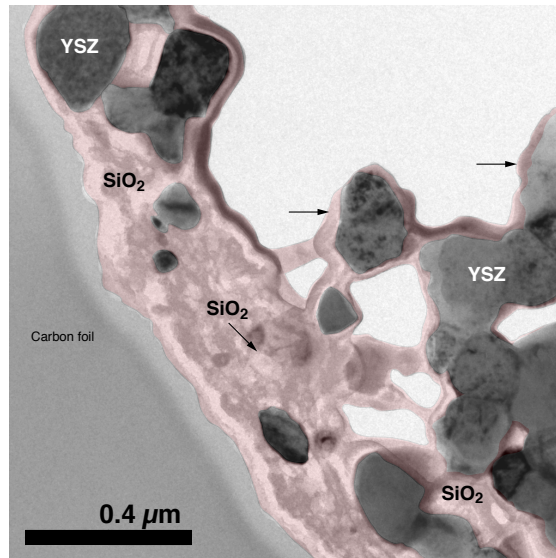


Figure 7.2: Exogenous Si contamination causes cathode pollution by the formation of amorphous SiO₂ phases surrounding zirconia grains, revealed by TEM investigations.

$$\log K_{\text{Si(OH)}_4} = -2857.84 \cdot T^{-1} - 3.53 \quad (7.2)$$

The cathode air entry during operation of the repeat-element at 1073 K was fed with an air flux of 20 l/min at room temperature and a water vapor pressure of $1.8 \cdot 10^2$ Pa. Under these conditions, a saturation pressure of $1.8 \cdot 10^{-7}$ Pa is found for Si(OH)₄ vapor, which would correspond to an accumulation of 4.8 μg of Si for 1900 h, close to the measured value of 7.6 μg.

The result confirms the preliminary findings of previous studies where Si contamination was revealed by EDS scans of the LSC- CCL surface [18, (ch. 7.2)] and cathode cross sections [17, (A.1)], but where a doubt on the quality of EDS analyses, due to a Sr/Si peak overlap, which persisted until the recent identification of Si by secondary ion mass spectroscopy (SIMS) within the cathode. However, up to now, endogenous and exogenous Si contamination could not be distinguished, in particular regarding their reaction with cathode materials.

Even if rare-earth-silicates are said to be formed in SOFC cathodes upon Si poisoning [7,29-31], phase identification is lacking in these studies. Taking into account that basic oxides, such as SrO, with a high chemical affinity for acidic SiO₂ are good scavenging materials, Sr-silicates are most likely to be formed [32]. Other compounds, such as Zr-silicate ZrSiO₄ or La-disilicates, are also reported to be possibly formed [32,33]. These phases, in particular La-silicates, are known as electrical insulators, as suggested by their use as electrolyte materials [34].

The present study evidenced Si poisoning in the form of amorphous SiO₂ surrounding YSZ grains of the composite cathode, as illustrated in Fig. 7.2, by scanning transmission electron microscopy- EDS and electron diffraction investigations. Our observations are in agreement with another study [35], where the energetically more favorable reaction of silica with zirconia than with LSM is explained by glasslike zirconia surface terminations, whereas LSM offers less favorable options for silicate formation.

7.1. Glass-forming exogenous silicon contamination in solid oxide fuel cell cathodes

In another study by the authors [36], Si was identified in TEM investigations at LSM/YSZ and zirconate/LSM interfaces, where Si was possibly combined with Zr and/or La as a silicate phase. As these phases were only sparsely observed within other TEM samples from this same repeat-element and as their formation is more likely linked to the reaction of endogenous Si with cathode material during sintering, the here-observed glass-forming exogenous Si contamination is suggested to have significantly contributed to cathode degradation. For oxygen exchange reactions, multivalent cations are needed: the glasslike surface terminations of Si, which have a single valence and are unlikely to change that valence [7], affect and inhibit the oxygen incorporation [35].

4 Conclusions

For the cell test dealt with in this study, a correlation was established between the local performance degradation of the cathode [17, (A.1)] and the distribution of Si contamination over this cathode [18, (ch. 7.2)]; the air entry regions with severe air pollution suffered from a performance decrease, whereas a stable performance was observed for the remaining cathode regions free of Si contamination. Model studies, which include detailed electrochemistry and the generation/ transport/redeposition of contaminants [27], confirmed a link between Si pollution and electrochemical degradation signatures. The present work, by revealing glassy cathode pollution from exogenous Si, contributes to access the cause of degradation. By the quantification of Si contamination and the identification of its origin, this work suggests means to protect SOFCs from Si pollution.

Acknowledgments

The Swiss Federal Energy Office Contract 153569 AccelenT is gratefully acknowledged for financial support. Many thanks to Vincent Laporte CIME for the SIMS measurements and Fabienne Bobard CIME for FIB operation. Stéphane Thonney and Christophe Roussel Chemical Engineering, Institute of Chemical Sciences and Engineering, EPFL are thanked for assisting in manipulations with acids.

References

- 1 C. C. Appel and N. Bonanos, *J. Eur. Ceram. Soc.*, 19, 847 1999 .
- 2 M. Mogensen, K. V. Jensen, M. J. Jorgensen, and S. Primdahl, *Solid State Ionics*, 150, 123 2002 .
- 3 C. Leach and C. E. Norman, *J. Mater. Sci.*, 27, 4219 1992 .
- 4 M. M. Viitanen, R. G. van Welzenis, H. H. Brongersma, and F. P. F. van Berkel, *Solid State Ionics*, 150, 223 2002 .
- 5 C. Hueglin, R. Gahrig, U. Baltensperger, M. Gysel, C. Monn, and H. Vonmont, *Atmos. Environ.*, 39, 637 2005 .

Chapter 7. Superimposed degradation effects

- 6 A. Hagen, Y. L. Liu, R. Barfod, and P. V. Hendriksen, *J. Electrochem. Soc.*, 155, B1047 2008.
- 7 M. de Ridder, A. G. J. Vervoort, R. G. van Welzenis, and H. H. Brongersma, *Solid State Ionics*, 156, 255 2003 .
- 8 I. Kaus, K. Wiik, M. Dahle, M. Brustad, and S. Aasland, *J. Eur. Ceram. Soc.*, 27, 4509 2007 .
- 9 J. L. Hertz, A. Rothschild, and H. L. Tuller, *J. Electroceram.*, 22, 428 2009 .
- 10 E. Bucher, A. Egger, M. Yang, and W. Sitte, in *Proceedings of the 9th European Fuel Cell Forum*, Vol. 2, European Fuel Cell Forum AG, p. 14 2010 .
- 11 E. Bucher and W. Sitte, *Solid State Ionics*, In press. DOI: 10.1016/ j.ssi.2010.01.006
- 12 M. Casteel, P. Wilson, T. Goron, P. O'Brien, and D. Lewis, *ECS Trans.*, 25 2 , 1411 2009 .
- 13 J.-M. Bae and B. C. H. Steele, *Solid State Ionics*, 106, 247 1998 .
- 14 S. B. Adler, *Chem. Rev.*, 104, 4791 2004 .
- 15 B. C. H. Steele, *Solid State Ionics*, 134, 3 2000 .
- 16 R. Steinberger-Wilckens, H.-P. Buchkremer, J. Malzbender, L. Blum, L. G. J. Bert de Haart, and M. Pap, in *Proceedings of the 9th European Fuel Cell Forum*, Vol. 2, European Fuel Cell Forum AG, p. 35 2010 .
- 17 Z. Wuillemin, A. Nakajo, A. Mueller, J. A. Schuler, S. Diethelm, J. Van herle, and D. Favrat, *ECS Trans.*, 25 2 , 457 2009 . (appendix 1)
- 18 J. A. Schuler, Z. Wuillemin, A. Hessler-Wyser, and J. Van herle, *ECS Trans.*, 25 2 , 2845 2009 . (ch. 7.2)
- 19 J. A. Schuler, C. Gehrig, Z. Wuillemin, A. J. Schuler, J. Wochele, C. Ludwig, A. Hessler-Wyser, and J. Van herle, *J. Power Sources*, 196 7225 2011 . (ch. 6.2)
- 20 M. Stanislowski, E. Wessel, K. Hilpert, T. Markus, and L. Singheiser, *J. Electrochem. Soc.*, 154, A295 2007 .
- 21 R. Bauer, M. Baccalaro, L. P. H. Jeurgens, M. Pohl, and E. J. Mittemeijer, *Oxid. Met.*, 69, 265 2008 .
- 22 Z. Yang, M. S. Walker, P. Singh, J. W. Stevenson, and T. Norby, *J. Electrochem. Soc.*, 151, B669 2004 .
- 23 Z. Yang, J. S. Hardy, M. S. Walker, G. Xia, S. P. Simmer, and J. W. Stevenson, *J. Electrochem. Soc.*, 151, A1825 2004 .
- 24 J. A. Schuler, P. Tanasini, A. Hessler-Wyser, and J. Van herle, *Scr. Mater.*, 63, 895 2010 . (ch. 3.1)

7.1. Glass-forming exogenous silicon contamination in solid oxide fuel cell cathodes

- 25 M. de Ridder, R. G. van Welzenis, A. W. Denier van der Gon, H. H. Brongersma, S. Wulff, W.-F. Chu, and W. Weppner, *J. Appl. Phys.*, 92, 3056 2002 .
- 26 E. J. Opila, D. S. Fox, and N. S. Jacobson, *J. Am. Ceram. Soc.*, 80, 1009 1997 .
- 27 Z. Wuillemin, EPFL Thesis no. 4525, 255 2009 .
- 28 N. S. Jacobson, E. J. Opila, D. L. Myers, and E. H. Copland, *J. Chem. Thermodyn.*, 37, 1130 2005 ..
- 29 D. Kuscner, J. Holk, M. Hrovat, S. Bernik, Z. Samardzija, and D. Kolar, *Solid State Ionics*, 78, 79 1995 .
- 30 E. J. Opila, R. C. Robinson, D. S. Fox, R. A. Wenglarz, and M. K. Ferber, *J. Am. Ceram. Soc.*, 86, 1262 2003 .
- 31 E. J. Opila, N. S. Jacobson, D. L. Myers, and E. H. Copland, *J. Miner. Met. Mater. Soc.*, 58, 22 2006 .
- 32 J.-H. Lee, *Monatsch. Chem.*, 140, 1081 2009 .
- 33 C. Yamagata, T. A. G. Restivo, N. B. Lima, S. R. H. M. Castanho, and J. R. Matos, in *Proceedings of the 9th European Fuel Cell Forum*, Vol. 5, European Fuel Cell Forum AG, p. 89 2010 .
- 34 S. Nakayama, H. Aono, and Y. Sadaoka, *Chem. Lett.*, 24, 431 1995 .
- 35 M. Backhaus-Ricoult, *Solid State Sci.*, 10, 670 2008 .
- 36 A. Hessler-Wyser, Z. Wuillemin, J. A. Schuler, A. Faes, and J. Van herle, *J. Mater. Sci.*, 46 4532 2011 .

7.2 Sulfur as pollutant species on the cathode side of a SOFC system

J. Andreas Schuler^{a,b}, Zacharie Wuillemin^a, Aïcha Hessler-Wyser^b, Jan Van herle^a

^a *Laboratoire d'Énergie Industrielle (LENI), École Polytechnique Fédérale de Lausanne (EPFL), 1015 Lausanne, Switzerland*

^b *Centre Interdisciplinaire de Microscopie Electronique (CIME), École Polytechnique Fédérale de Lausanne (EPFL), 1015 Lausanne, Switzerland*

In order to link electrochemical performance degradation of the cathode in a large solid oxide fuel cell (SOFC) to the presence of pollutant species, a spatially-resolved study of contaminants was performed. Distribution maps of pollutants over the cell allowed to identify their sources. Besides chromium and silicon, sulfur was found as a major pollutant species. Its preferential reaction with strontium doped lanthanum cobaltite (LSC), forming strontium sulfate SrSO_4 , compared to strontium doped lanthanum manganite (LSM) is revealed here. When sulfur poisoning arises in combination with chromium, a sulfur-containing strontium chromate compound is formed.

1 Introduction

Understanding degradation mechanisms is a major issue in the development of solid oxide fuel cells (SOFCs). In particular, in repeat-element and stack configuration, an important coupling of different degradation processes exists, with internal sources at the stack level and exogenous sources coming from system components. A specific diagnostic test station was developed to allow locally-resolved measurements of electrochemical performance and degradation in a repeat-element. Large differences in local degradation behavior were observed, affecting different electrochemical processes. A complete description of the experiment and of the analysis of degradation is given by Z. Wuillemin *et al.* in the same Proceedings [1, (A.1)]. This study points out the important difference between global and local distribution of pollutant species, and the resulting degradation rates in a repeat-element, showing the interest of a spatially-resolved experiment. Three major pollutants were identified and quantified on the cathode side: chromium, silicon and sulfur. While the effect of chromium [2-4] and silica [5-9] on the electrochemical behavior of SOFC cathodes is known, sulfur contamination of the cathode has received more attention just recently.

Yokokawa *et al.* identified sulfur as impurity after long-term operation of SOFC stacks in [10], and pointed out the effect of contamination on the durability of SOFC stacks and modules in [11]. Sulfur poisoning was reported in various related technologies using manganite, cobaltite and ferrite perovskite materials. A major limitation for the wide use of perovskite catalysts for treatment of car engine exhaust gas is the low temperature stable sulfite and sulfate formation

7.2. Sulfur as pollutant species on the cathode side of a SOFC system

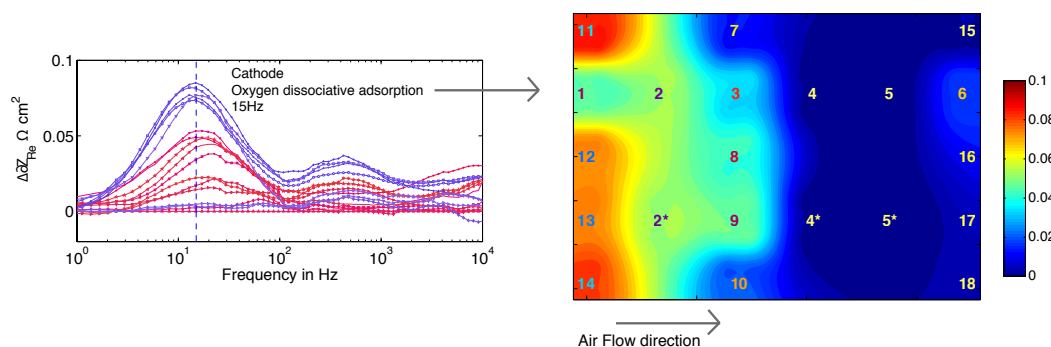


Figure 7.3: Local level of degradation after 1900 hours of operation. Left: difference plot of the $\delta Z'$ function between each segment and the reference segment n°5 (cf Ref. [16]) Right: corresponding spatial distribution (scale is in $\Omega \text{ cm}^2$) obtained for cathode (15 Hz) processes.

[12-13]. Sulfur pollution from trace SO_X in air and involving sulfate formation was reported by Xu *et al.*, where perovskite-type ceramics were used for oxygen permeation membranes [14]. Just recently, Xiong *et al.* reported a model study of accelerated sulfur poisoning, by exposing strontium doped samarium cobaltite (SSC) and strontium doped lanthanum manganite (LSM) cathode materials to SO_2 -concentrated air. Trace SO_X in air is supposed to affect long-term operation of SOFCs [15].

This study reveals severe sulfur contamination in a SOFC system, involving a large cell in stack configuration with balance of plant (BOP) components. The reaction of sulfur with a strontium doped lanthanum cobaltite (LSC) current collection layer and an active strontium doped lanthanum manganite (LSM) - yttria stabilized zirconia (YSZ) composite cathode is given here.

2 Experimental

2.1 Locally-resolved degradation study An anode-supported cell, with an active LSM-YSZ composite cathode and a LSC current collection layer, was tested over 1900 h around 1073 K. The evolution of electrochemical performance was measured *in situ* on 18 locations distributed within a cell [1, (A.1)]. Electrochemical impedance spectroscopy (EIS) measurements revealed that principally the cathode was affected by degradation, as indicated by large differences at the characteristic frequency attributed to dissociative adsorption of O_2 (cf Fig. 7.3). The highest loss in electrochemical performance was attained in the vicinity of the gas inlets, while the outlet region experienced low degradation. The contribution of the cathode to the area specific resistance (ASR), identified by impedance spectroscopy, followed the same trend.

2.3 Post-experiment analyses of current collection layer surfaces exposed to air- channels and polished cross-sections were performed on a FEI XL30 scanning electron microscope with an Oxford Instruments INCASynergy 350 system for energy-dispersive x-ray (EDX) microanalysis, incorporating a state-of-the-art INCAX-cat silicon drift detector for rapid and accurate EDX mapping. Spatial distribution of heavier elements was confirmed by X-ray fluorescence

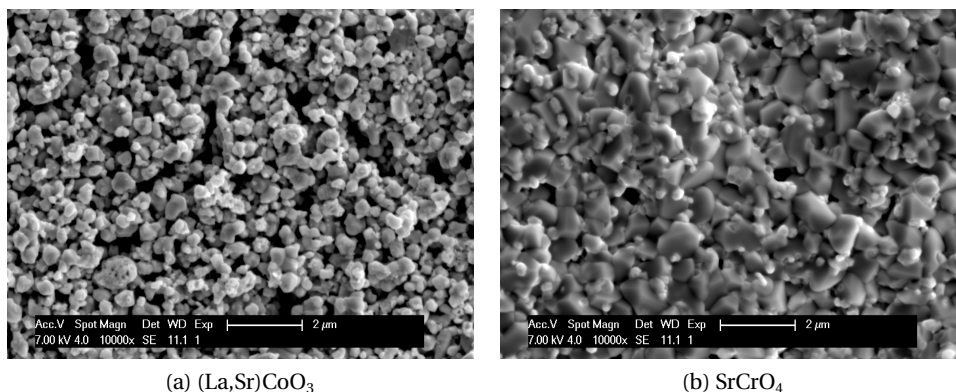


Figure 7.4: Strontium doped lanthanum cobaltite (LSC) current collector layer surface, before (left) and after (right) 1900 h exposure to sulfur-containing airflow, where strontium sulfate SrSO_4 is formed.

on a Fischer X-ray XAn system with WinFam software. Phase identification by X-ray diffraction was done on a Bruker D8 X-ray diffractometer.

3 Results

3.1 Sulfur poisoning in LSC Figure 7.4 shows the change on the LSC microstructure after exposure to sulfur-containing air. Formation and growth of new crystals on the porous LSC surface leads to a denser surface layer.

EDX analysis on several crystals indicated the formation of strontium sulfate SrSO_4 with a ratio of 23 % strontium, 19 % sulfur and 58 % oxygen (all atomic %). This phase was confirmed by XRD analysis on segment 16 (cf Fig. 7.5), which showed severe sulfur pollution at the air outlet of the repeat-element. The XRD pattern shows the characteristic peaks for SrSO_4 reported by Xiong *et al.* [15].

3.2 Sulfur in a cathode double layer The extent of sulfur poisoning was revealed by an EDX mapping (cf Fig. 7.6) on a polished cross-section of segment 16. Sulfur reacts preferentially with the LSC current collection layer. The active LSM-YSZ composite cathode is free from sulfur poisoning.

3.3 Sulfur in combination with chromium Chromium was found in the vicinity of the air inlet, with rapidly decreasing amounts in the direction of the airflow. The structure of the chromium-rich compounds is changing along the airflow direction, from a densified structure to isolated particles as shown in figure 7.7. While the microstructure is changing, EDX analysis on several crystals of each structure show a stable ratio of 17 % Sr 13 % Cr 2 % S and 68 % O (all in atomic %), indicating a sulfur-containing strontium chromate compound, of approximate composition $\text{Sr}(\text{Cr}_{0.85}\text{S}_{0.15})\text{O}_4$.

7.2. Sulfur as pollutant species on the cathode side of a SOFC system

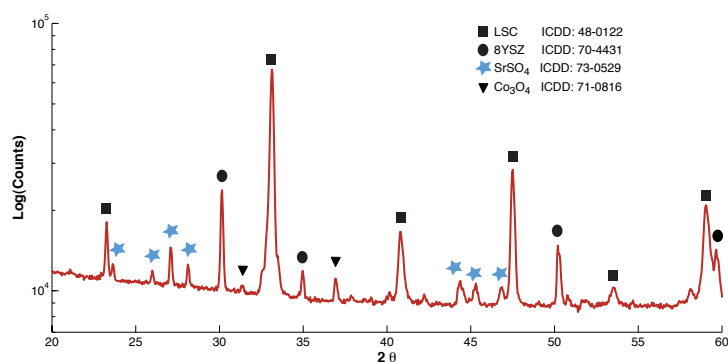


Figure 7.5: XRD pattern of segment 16, which presented severe sulfur poisoning, confirms the presence of strontium sulfate SrSO₄ among LSC, Co₃O₄ and YSZ (stemming from the electrolyte layer outside the cathode deposit).

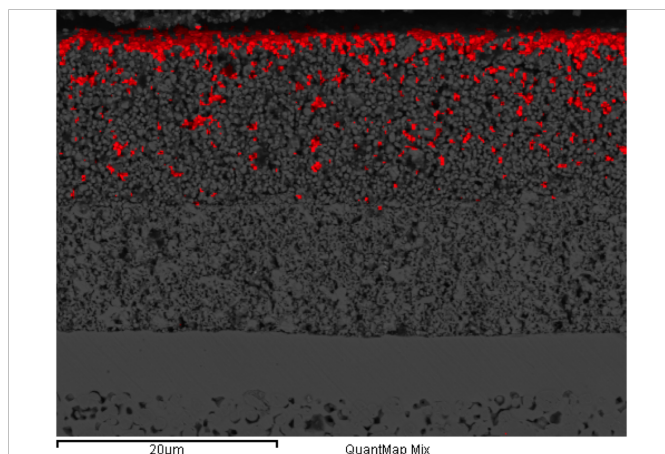


Figure 7.6: EDX mapping on a polished cathode cross-section reveals strontium sulfate (red spots) formation in the LSC layer, whereas LSM-YSZ composite cathode is free from sulfur poisoning.

A XRD pattern from an air-inlet region with severe Cr-S pollution is given in figure 7.8. This pattern is compared to a Cr-poisoned region from a repeat-element tested under similar conditions, but without segmentation. In the latter, where no sulfur was observed by EDX, strontium chromate SrSO₄ ICDD: 35-0743 is identified. On the other hand, the resulting pattern from the Sr-Cr-S-O compound could not be indexed.

4 Discussion

4.1 Strontium sulfate Grains formed at the interface between LSC and air channels (cf Fig. 7.4) are larger compared to observations done by Xiong *et al.* [15]. Coarsening from the latter, fine grained, structure observed after 8 h accelerated sulfur poisoning, is probable with longer test duration (here, 1900 h) at the same temperature (800 °C). The cobalt-rich phase Co₃O₄ was

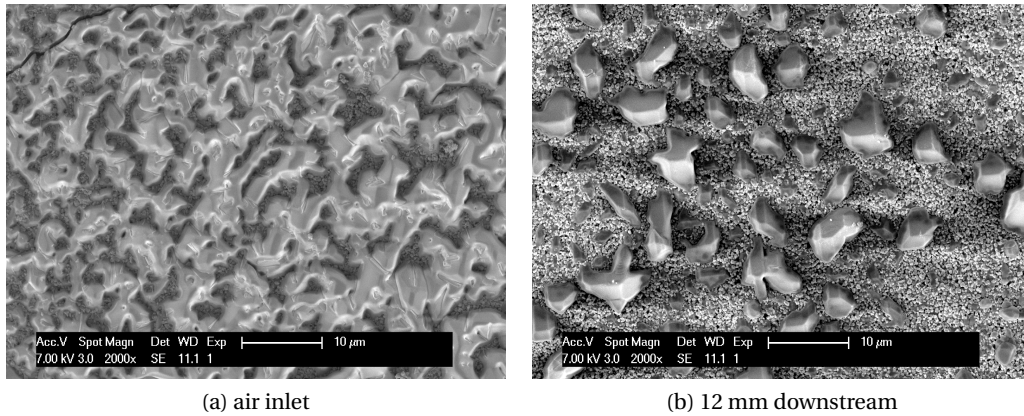


Figure 7.7: Chromium rich compounds, on LSC surface in an airflow channel, forming dense microstructure at the air inlet (left) and isolated grains 12 mm downstream (right). EDX analysis on the different structures revealed an identical composition, close to $\text{Sr}(\text{Cr}_{0.85}\text{S}_{0.15})\text{O}_4$.

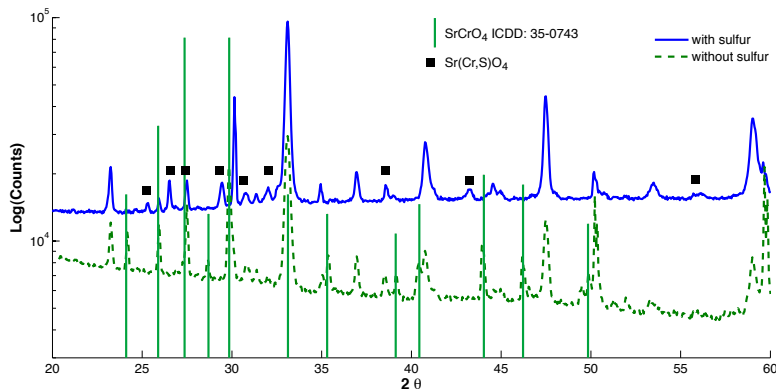
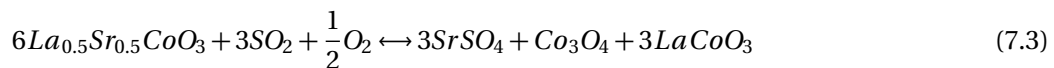


Figure 7.8: XRD pattern from an air-inlet region with Cr-S co-pollution (full line) compared to a Cr-polluted region from another test (dotted line) and main peaks of SrCrO_4 pattern ICDD: 35-0743.

identified from the XRD pattern. Even if this phase was not well localized on EDX mappings, the following reaction for the formation of strontium sulfate is proposed:



The perovskite lattice is probably maintained by the LaCoO_3 compound, which is not identified by XRD as LaCoO_3 peaks are hidden by LSC. It is thus difficult to estimate the performance degradation of a cathode with a sulfur-poisoned current collection layer; moreover, EIS results reported by Xiong *et al.* do not allow to identify the electrochemical mechanisms affected by sulfur poisoning.

7.2. Sulfur as pollutant species on the cathode side of a SOFC system

Preferential sulfur poisoning in LSC According to Yokokawa *et al.* [10], the behavior of perovskite cathodes should be examined in terms of the reactivity of strontium oxide SrO since Sr is one of its major components. A higher activity of SrO in LSC compared to LSM is reported [17] and differs by 4 orders of magnitude between $\text{La}_{0.8}\text{Sr}_{0.2}\text{CoO}_3$ and $\text{La}_{0.8}\text{Sr}_{0.2}\text{MnO}_3$ compounds [15]. Moreover, reactants of the basic SrO should be acidic. Acidic solids respectively gaseous species which can be found among others in this SOFC system are: SiO_2 , Cr_2O_3 and SO_2 .

SO_2 adsorption on a perovskite compound is reversible. The material is irreversibly poisoned by sulfur when adsorbed SO_2 forms sulfite and sulfate species [12]. Lower temperatures should lead to higher poisoning, as the adsorbate residence time is longer. Nevertheless, sulfur poisoning is not found to be enhanced in air-inlet regions where lower temperatures were found. Since the formation of strontium sulfate is an oxidative reaction, there is no reason for preferential sulfur poisoning at the triple phase boundaries (TPBs), like in the case of chromium poisoning, consistent with the observation why SrSO_4 is present on the LSC surface and not at the LSM/YSZ interface.

Observations in figure 7.6, showing sulfur poisoning in LSC, but a LSM-YSZ cathode free from contamination, agree with Ref. [15] where LSM was only slightly poisoned by SO_2 -concentrated air and restored when SO_2 feeding was interrupted. According to their thermodynamic considerations, LSM will not react with real SO_2 concentrations, corresponding to ppb in air. Moreover, sulfur-poisoned LSM can be restored by heating [12], and the regeneration rate is increased by the addition of water vapor [18].

Better SO_2 resistance of perovskite is obtained when Co is replaced by an element with lower heat of decomposition of the formed sulfate species. According to Ostroff *et al.* [19], strontium sulfate decomposes directly to the oxides at temperatures above 1647 K (others indicate [20-22] 1073, 1473 and 1873 K). Trivalent metal sulfates will decompose at lower temperatures than divalent metal sulfates. Moreover, the sulfate structure affects its stability: greater stability is given by lower electronegativity and larger crystal radius. The decomposition temperature is proportional to the square root of the radius-to-electronegativity ratio, which is almost double for Sr compared to Co, explaining the lower decomposition temperature of La/Co sulfates, which were not found in the sulfur-poisoned LSC.

4.3 Sr-Cr-S-O compound The main reaction product of chromium in the LSC system is SrCrO_4 [10,17,23], which transforms into SrCrO_3 when the oxygen partial pressure decreases [10]. Chromium oxide Cr_2O_3 and spinel phases $(\text{Cr,Mn})_3\text{O}_4$ are frequently reported when Cr pollution occurs in SOFC systems [3,24]. Finally, several other compound are found in the SrO- Cr_2O_3 - LaO_3 and Sr-Cr-O system [25-26] or LaCrO_3 -based perovskites [27]. None of these studies provides a diffraction pattern matching to the pattern of Sr-Cr-S-O compound found in this study. Lattice distortion, due to the incorporated sulfur, leading to a shift of XRD pattern, is possibly a reason for the impossibility to assign the peaks to any known phase. A shift of the XRD pattern in a Sr-Cr-S-O system was reported by Rendon-Angeles *et al.* [28], where the conversion of celestite SrSO_4 crystals to SrCrO_4 was studied.

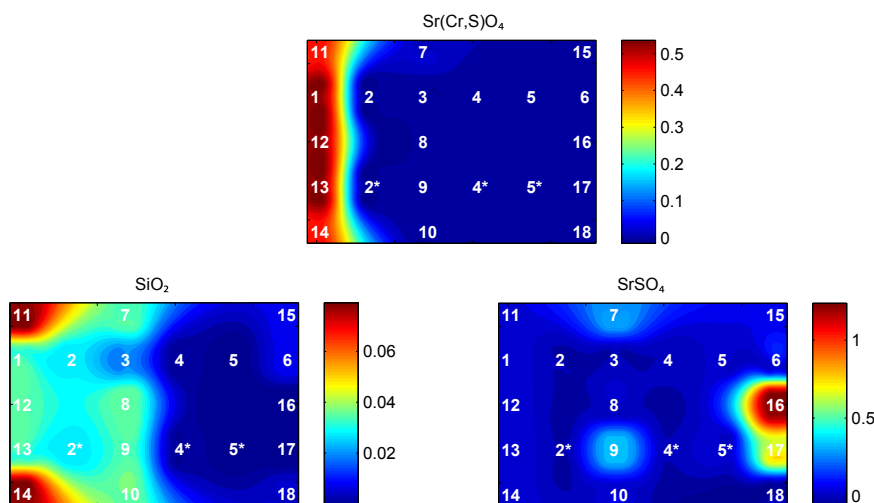


Figure 7.9: Relative amount of different pollutant species (molar %) in the LSC current collection layer, normalized to the amount of LSC.

4.4 Spatial distribution of the pollutants As shown above, chromium was found in a followed the same trend, with increasing values close to seal gaskets. Sulfur was detected at the air-inlet, and also on different spots over the active area. A representation of spatial distribution of these species, normalized to the amount of LSC, is given in figure 7.9. A good match was found between the presence of pollutants and the level of local degradation. A detailed comparison between pollutant species and the electrochemical performance is given by Z. Wullemmin *et al.* in these Proceedings [1, (A.1)].

While the chromium poisoning was mostly generated by upstream system components, seal gaskets were identified as sources of silica, in addition possibly exogenous sources such as traces of silicon in the compressed air system. An insulating high temperature sealing paste used for assembly of the segments (galvanic insulation) was identified as major sulfur source, besides a commercial vulcanized polymer air feed tubing; moreover, Ref. [11] mentions metal sulfate in water and metal parts in tubes as supplementary sulfur contamination sources other than trace SO_x in air.

5 Conclusion

This study took advantage of a spatially-resolved degradation study on a repeat- element for its post-mortem analysis. Chromium, silicon and sulfur were found as major pollutant species on the cathode side. The spatial distribution of these species allowed the identification of pollution sources. The interaction of sulfur with cathode materials is presented here: i) sulfur is easily captured by the LSC current collection layer, involving strontium sulfate formation ii) the more stable LSM-YSZ cathode is not affected by sulfur poisoning. The use of

7.2. Sulfur as pollutant species on the cathode side of a SOFC system

sulfur-containing insulating paste leads to accelerated sulfur contamination. Nevertheless, important conclusions can be derived from this study for the influence of sulfur in long-term operation of SOFCs. Finally, an unknown compound, sulfur-containing strontium chromate, was identified on regions simultaneously poisoned with chromium and sulfur. The structure of this compound will be investigated in more detail.

Acknowledgements

Financial support from the Swiss Federal Energy Office (Contract 153569, 'AccelenT'), as well as from the European Commission (FP6 contract SES6-019875, Flame-SOFC) is gratefully acknowledged.

References

- 1 Z. Wuillemin, A. Nakajo, A. Müller, A.J. Schuler, S. Diethelm, J. Van herle and D. Favrat, *ECS Trans.* 25 457 (2009). (appendix 1)
- 2 S. Tanagushi, M. Kadowaki, H. Kawamura, T. Yasuo, Y. Akiyama, Y. Miyake and T. Saitoh, *Journal of Power Sources*, 55, 73 (1995).
- 3 S.P.S. Badwal, R. Deller, K. Foger, Y. Ramprakash and J.P. Zhang, *Solid State Ionics*, 99, 297 (1997).
- 4 S.P. Jiang, J.P. Zhang, L. Apateanu and K. Foger, *Journal of the Electrochemical Society*, 147, 11 (2000).
- 5 S.B. Adler, *Chemical Reviews*, 104, 4791 (2004).
- 6 M. Backhaus-Ricoult, *Solid State Sciences*, 10, 670 (2008).
- 7 J-M. Bae and B.C.H. Steele, *Solid State Ionics*, 106, 247 (1998).
- 8 D. Kuscer, J. Holc, M. Hrovat, S. Bernik, Z. Samarzija and D. Kolar, *Solid State Ionics*, 78, 79 (1995).
- 9 M. de Ridder, A.G.J. Vervoort, R.G. van Welzenis and H.H. Brongersma, *Solid State Ionics*, 156, 255 (2003).
- 10 H. Yokokawa, T. Watanabe, A. Ueno and K. Hoshino, *ECS Trans.*, 7, 133 (2007).
- 11 H. Yokokawa, T. Horita, K. Yamaji, H. Kishimoto, Y.P. Xiong and M.E. Brito, *Proceedings of the 8th European SOFC Forum*, B1004, (2008).
- 12 L. Wan, in *Properties and Applications of Perovskite-Type Oxides*, L. G. Tejuca and J. L. G. Fierro, Editors, p. 145, Marcel Dekker Inc., New York (1993).
- 13 H. Wang, Y. Zhu, R. Tan and W. Yao, *Catalysis Letters*, 82, 199 (2002)

Chapter 7. Superimposed degradation effects

- 14 N. Xu, S. Li, W. Jin and J. Shi, *AiChE Journal*, 45, 2519 (1999).
- 15 Y. Xiong, K. Yamaji, T. Horita, H. Yokokawa, J. Akikusa, H. Eto and T. Inagaki, *Journal of the Electrochemical Society*, 156, B588 (2009).
- 16 S.H. Jensen, A. Hauch, P.V. Hendriksen, M. Mogensen, N. Bonanos and T. Jacobsen, *Journal of the Electrochemical Society*, 154, B1325 (2007)
- 17 H. Yokokawa, N. Sakai, T. Horita, K. Yamaji, M.E. Brito and H. Kisjimoto, *Journal of Alloys and Compounds*, 452, 41 (2008).
- 18 Y.F.Y. Yao, *Journal of Catalysis*, 39, 104 (1975)
- 19 A. G. Ostroff and R.T. Sanderson, *J. of Inorg. Nuclear Chemistry*, 9, 45 (1959)
- 20 P. S. Lowell, K. Schwitzgebel, T.B. Parsons and K.J. Sladek, *Industrial and Engineering Chemistry Process Design and Development*, 10, 384 (1971).
- 21 N. Unohara, *Journal of the Chemical Society of Japan*, 74, 998 (1953)
- 22 S.D. Shargorodskii, *Ukrain. Khim. Zh.*, 15, 332 (1949)
- 23 S. Miyoshi, S. Onuma, A. Kaimai, H. Matsumoto, K. Yashiro, T. Kawada, J. Mizusaki and H. Yokokawa, *Journal of Solid State Chemistry*, 177, 4112 (2004)
- 24 T. Komatsu, R. Chiba, H. Arai and K. Sato, *J. of Power Sources*, 176, 132 (2008)
- 25 D.H. Peck, M. Miller and K. Hilpert, *Solid State Ionics*, 123, 59 (1999)
- 26 K.T. Jacob and K.P. Abraham, *Journal of Phase Equilibria*, 21, 46 (2000)
- 27 H. Yokokawa, N. Sakai, T. Kawada and M. Dokiya, *Journal of the Electrochemical Society*, 138, 1018 (1991)
- 28 J.C. Rendon-Angeles, Y.M. Rangel-Hernandez, J. Lopez-Cuevas, M.I. PENCH- Canul, Z. Matamoros-Veloza and K. Yanagisawa, *Proceedings of the AIRAPT/EHPRG int. Conf. on High Press. Sci. and Tech.*, T13-O144, (2005).

7.3 Combined Cr and S poisoning in solid oxide fuel cell cathodes

J. Andreas Schuler^{a,b}, Harumi Yokokawa^c, Caroline F. Calderone^b, Quentin Jeangros^b,
Zacharie Wuillemin^a, Aïcha Hessler-Wyser^b, Jan Van herle^a

^a *Laboratoire d'Énergie Industrielle (LENI), École Polytechnique Fédérale de Lausanne (EPFL), 1015 Lausanne, Switzerland*

^b *Centre Interdisciplinaire de Microscopie Electronique (CIME), École Polytechnique Fédérale de Lausanne (EPFL), 1015 Lausanne, Switzerland*

^c *National Institute of Advanced Industrial Science and Technology (AIST), 305-8565 Ibaraki, Japan*

This work aims to compare the effect of combined chromium and sulfur contaminating conditions to the Cr contamination alone on the Cr poisoning mechanisms in (La,Sr)MnO₃-(Zr,Y)O₂ solid oxide fuel cell (SOFC) cathodes. Whereas Cr₂O₃ and (Cr,Mn)₃O₄ are found at active triple phase boundaries under the Cr-poisoning condition, the formation of SrCrO₄ is promoted under combined Cr and S contaminating conditions, where Cr accumulations act as getters incorporating sulfur, to form Sr(Cr,S)O₄ compounds. The identification of this phase is validated on synthesized and simulated species by scanning/transmission electron microscopy (SEM/TEM) techniques; its possible formation is predicted by thermodynamic analysis of the stability of perovskite compounds in presence of combined Cr and S polluting conditions. In contrast, sulfur alone is not found to poison active sites in these composite cathodes. These findings suggest that the Cr poisoning degradation mechanism is altered when (La,Sr)MnO₃ is exposed to Cr vapors in presence of sulfur contamination; the access to electrochemical active sites may be hindered by the formation of Sr(Cr,S)O₄ in a similar manner to a Cr-getter effect in (La,Sr)(Co,Fe)O₃ cathodes.

1 Introduction

Since the early seventies, Sr-doped perovskites have been suggested as substitutes to noble metals as lower cost electrode materials for fuel cells [1] and for the catalytic treatment of exhaust gas [2]. However, perovskites suffer from limitations in their applicability in some industrial processes, in particular from their susceptibility to poisoning by sulfur dioxide [3]. Originally proposed as potential automotive catalysts, the early perovskite compositions, mostly manganites and cobaltites, have failed to become practical because of their low resistance to sulfur; i.e. low temperature stable sulfate formation occurs [4,5].

In the field of solid oxide fuel cells (SOFC), where sulfur in the fuel is a known issue [6], less attention was brought so far to sulfur on the cathode side, as only a trace of SO₂, in the ppb range, is found in environmental air [7, (ch. 6.2)]. Recently, Yamaji *et al.* as well as Liu *et al.*

showed high tolerance of (La,Sr)MnO₃-based cathodes (LSM) towards deliberate S contamination [8-10], suggesting that S-poisoning is not a barrier in optimized manganite compositions [5]. In contrast to LSM cathodes, sulfur contamination significantly affects the cathode performance of (La,Sr)(Co,Fe)O₃ (LSCF) or related active cathodes [8-10]. In this sense, the chemical stability of the cathode is directly related to the degradation in presence of sulfur.

A contrasting situation is found in the so-called Cr-poisoning phenomenon; i.e. cathode degradation is caused by its accumulation of Cr vapor species generated by Cr-containing cell-proximal stack compounds. LSM, which is the most stable composition among the perovskite cathodes, undergoes the most severe Cr poisoning degradation as Cr vapors are preferentially deposited on electrochemical active sites. Contrarywise, in LSCF cathodes, where the major effect is recognized as SrCrO₄ formation near the cathode surface and remote from the active sites, Cr-poisoning is less severe [11].

The investigation of differences between these two contaminations Cr and S and plausible combined effects is therefore of interest. Nevertheless, testing of cathode poisoning by sulfur remains scarce, especially in stack configuration, where S contamination arises in combination with other pollutant species. This study addresses this specific point, by prospecting the effect of combined Cr and S poisoning in SOFC cathodes. It was based on the observation of having identified Sr/Cr/S-oxides in stack *post-test* samples, reported earlier [12-14, (A.1, ch. 7.2)].

In these previous studies, Cr₂O₃/MnCr₂O₄ phases in the LSM / (Y,Zr)O₂ composite cathode as well as SrCrO₄ and SrSO₄ phases in the (La,Sr)(Co)O₃ (LSC) current collection layer (CCL) were not found as expected under the combined Cr / S poisoning conditions, but an Sr(Cr,S)O₄ compound was identified in both cathode and CCL.

In the present investigation, the focus is placed on the identification of the important factors governing the Cr poisoning of LSM cathodes in presence of sulfur, by analyzing the chemical form of the Cr phases and their distribution within the cathode layers.

2 Materials and methods

This work compares *post-test* observations from stack testing under combined Cr and S contaminating conditions (hereafter named type A), to those from a button cell (type B) tested under controlled Cr poisoning conditions, without S, in a multicathode configuration.

Both A and B type cells were Ni-YSZ anode-supported with thin YSZ electrolyte and (La,Sr)MnO₃ / (Y₂O₃)_{0.08}(ZrO₂)_{0.92} (LSM/YSZ) composite cathodes, with slightly different perovskite compositions (La_{0.75}Sr_{0.25})_{0.95}MnO_{3±δ} for type A and (La_{0.70}Sr_{0.30})_{0.90}MnO_{3±δ} for type B, respectively, due to development reasons. The earlier used cathode stoichiometry, used for type A cell, was later found less stable towards zirconate formation than the more recent composition (due to a higher A-site deficiency), which became standard in our activities after cell test A. By the same token, different CCL were used in both test types: type A cathodes were covered with (La_{0.8}Sr_{0.2})CoO₃, type B with LSM (the same stoichiometry as for the active cathode composition). With respect to the contamination issue dealt with in this study, i.e. that in the active cathode region (not CCL), the A and B active cathode compositions can be regarded as close

7.3. Combined Cr and S poisoning in solid oxide fuel cell cathodes

enough for the purpose of comparison, and one can assume that the current collection layer does not significantly alter our conclusions, for the active cathode behavior under combined Cr and S contamination.

Type A cell (200 cm²) was tested for 1900 h at 1073 K on a highly instrumented, so-called segmented, 1-cell stack unit. Owing to the cathode segmentation, Fig. 7.10, it provided *in situ* local information with time of operation. The test was followed by post-mortem analysis (reported recently in [13 (ch. 7.2),14]) and coupled to model studies of detailed electrochemistry and the generation, transport and deposition of contaminants, which enabled to establish a strong correlation between local performance degradation and distribution of contaminant accumulations [15].

Combined contamination in the type A test was, for Cr, due to stack-upstream alloys (1.4828, 1.4849 and Incoloy800) used to feed hot air, and for S, due to an insulating high-temperature sealing paste (type1500 Coltogum, composition atomic %: 36 Si, 6 Na, 4 Ba, 3 S, 3 Al, 2 Mg, <1 Ca, K, Fe, balance O) used for the galvanic separation between cathode segments, besides SO₂ from compressed air.

During operation, Cr vapor species accumulated preferentially at air inlet regions locally causing higher degradation rates. Differences between global and local performance of the cell, polarized with a current density of 0.4 A·cm⁻² around 0.75 V, underlined these findings: air inlet regions showed a higher overpotential (mainly attributed to cathode losses) of ca. 0.35 V compared to the air outlet with only 0.25 V. Contrariwise, as S contamination from the insulating paste is generated within the complete airflow along the cell (due to its segmentation), S accumulations are found equally distributed on the cell; its impact on performance, however, is far less pronounced [15].

Type B cell was smaller (28 cm²) and carried 4 cathode segments of 1 cm² each (Fig. 7.10). In this test, NiCrFe alloy (Inconel 602) tubing was used for hot air feeding and deliberate generation of volatile Cr species [16, (ch. 4.1)]. This cell was operated at 1125 K over 700 h having as scope the evaluation of Mn-doping of the YSZ phase to prevent zirconate formations in the composite cathode but which are not addressed in the present study.

The investigation methods carried out on both A and B cells are summarized in Table 7.1, including references to the different result figures (Fig. 7.10 to 7.14) in this paper. For the large A type cell, samples from both the air inlet (A1) and air outlet (A2) regions were analyzed (Fig. 7.10).

In addition to *post-test* analysis including X-ray diffraction (XRD), energy-dispersive X-ray spectroscopy (EDS) in both scanning and transmission electron microscopes (SEM/TEM) and focused ion beam (FIB) also described in previous publications [13,14,17, (ch. 7.1, 7.2)], and selective area electron diffraction (SAED) were performed on a CM20 TEM (FEI-Philips), using JEMS software (P. Stadelmann [18]) for diffraction indexing), as well as energy-filtered TEM (EFTEM) with an in-column omega filter on a Jeol TEM (type 2200FS).

To profile contamination accumulations through the cathode thickness, a methodology based on the quantification of thin cathode slices, extracted from an EDS mapping is used according to our protocol described elsewhere [16, (ch. 4.1)] and that can be summarized as follows. To bypass the quantification issue for small Cr quantities within LSM-YSZ composite cathode,

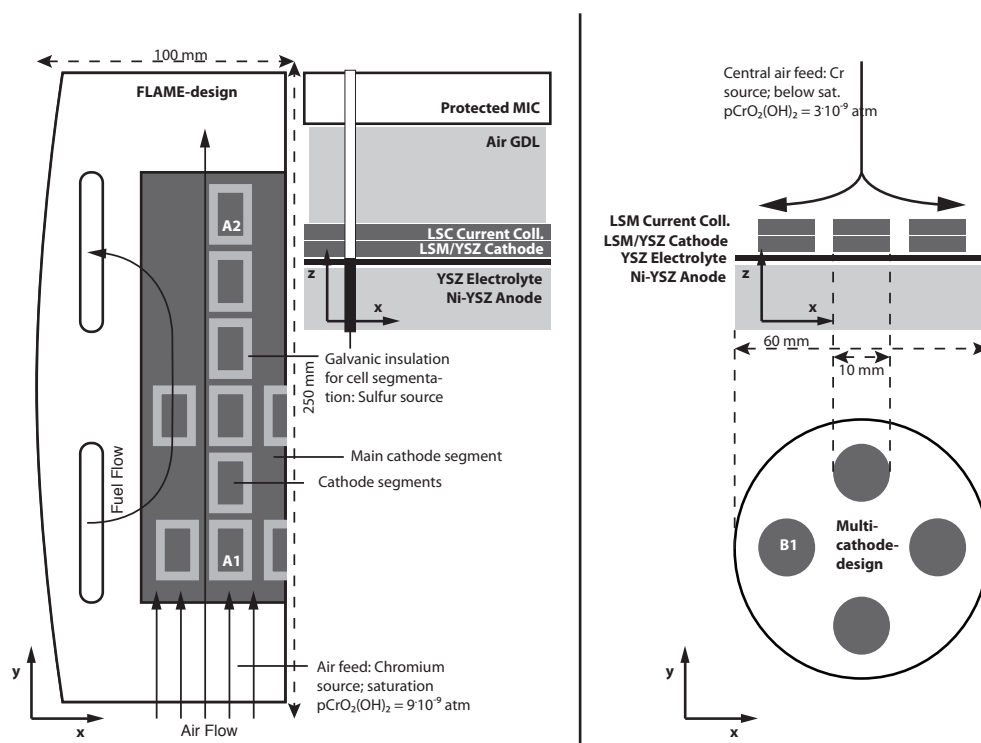


Figure 7.10: Schematic description of Cr contaminating conditions, in combination with S for type A cell (segmented 1-cell stack; left) or for Cr alone for type B cell (multicathode button cell; right), respectively. The S-containing insulating paste for segmentation of type A cell generated increasing S concentrations along the airflow in the cathode compartment. Preferential distribution of Cr accumulations at the cathode air inlet occurs from trapping of Cr species by reactive/protective LSC layers. Samples A1 and A2 were extracted at air inlet and air outlet regions, respectively, for post-analysis purposes.

due to the strong overlap of the Cr X-ray emission lines with the ones from La, Mn and O, Cr is quantified using an empirical law based on the $L_{\beta 2.15}/L_{\alpha 1}$ peak height ratio and calibrated on Cr-doped LSM-YSZ standards. Cr within the LSC CCL, as well as S in both cathode and CCL, were quantified using INCA (Oxford Instruments) software.

In addition, also included in table 1, a Sr/Cr/S-compound was synthesized in a separate experiment in this study, by blending chromium oxide Cr_2O_3 , strontium carbonate $SrCO_3$ and ammonium sulfate $(NH_4)_2SO_4$ powders (28, 63 and 9 % wt, ratio; all from Alfa Aesar) and pressing into pellets. A pellet was sintered at 1473 K for 10 h in stagnant air: these experimental conditions are known to favor the formation of $SrCrO_4$ [19-21]. Resulting reaction phases were crushed in an agate mortar and deposited onto an YSZ plate for analysis purpose.

The main data for thermodynamic analysis of perovskite stability is taken from the thermodynamic database MALT (Materials-oriented Little Thermodynamic database; kagaku.com/malt). Thermodynamic stability results, under Cr, SO_2 and simultaneous Cr and SO_2 contaminating conditions, are obtained for $(La_{0.8}Sr_{0.2})_1MnO_3$, $(La_{0.75}Sr_{0.2})_1MnO_3$ and $(La_{0.7}Sr_{0.25})_1MnO_3$ cath-

7.3. Combined Cr and S poisoning in solid oxide fuel cell cathodes

Table 7.1: Summary of *post-test* observations performed on different cathode samples to link sample type and location from Fig. 7.10 to electron microscopy results from Figs. 7.11-7.14. Numbers in brackets refer to previous *post-test* observations.

Type	Sample	Location	Observations in this study	Previously reported observations
A	A1	air inlet	SEM-EDS (Fig7.11) STEM-EDS (Fig7.12) TEM-SAED (Fig7.12) EFTEM (Fig7.12)	SEM-EDS (cathode) [12, (A.1)] SEM-EDS (CCL) [7,13, (ch. 6.2, 7.2)] TEM-EDS [14,15]
A	A2	air outlet	SEM-EDS(Fig7.11)	XRD (CCL) [13, (ch. 7.2)] SEM-EDS [13, (ch. 7.2)] XRD (CCL) [13, (ch. 7.2)]
Synthesized Pellet	Sr(Cr,S)O ₄	-	SEM-EDS (Fig7.13) XRD	
B	B1	(central air feed)	SEM-EDS (Fig7.11) STEM-EDS (Fig7.14)	

ode compositions. The latter composition is assumed closest to the $(La_{0.75}Sr_{0.25})_{0.95}MnO_{3\pm\delta}$ composition, as this cathode with A-site deficiency has a Sr content around 0.2-0.25. In this analysis, the effect of Cr contamination is evaluated by reaction of 1 mole LSM with 0.1 mole CrO₃, although the major gaseous species is CrO₂(OH)₂. The effect of S contamination on perovskite compounds is investigated for various SO₂ amounts. A prior reading of previous studies from Yokokawa *et al.* using the MALT database [11] should facilitate the interpretation of the resulting thermodynamic stability graphs.

3 Results: compound identification

This section aims to investigate the effect of sulfur presence on the Cr-poisoning mechanism in LSM/YSZ cathodes, by identifying the phase and composition of the Cr deposits. For this purpose, three different cell locations, with differences in the nature and the severity of contamination were investigated; i.e. high Cr and some S for sample A1, high S with minor Cr for sample A2 and Cr without S for sample B1. Figure 7.11 compares contamination profiles for samples A1, A2 and B. These cross-section profiles are obtained by an EDS space-averaging technique that is described elsewhere [16, (ch. 4.1)] and summarized above.

3.1 Chromium contamination As mentioned in the experimental section, Cr contamination is generated by FeCr-alloy compounds located upstream of the cell and exposed to the hot air flux. The gaseous partial pressure of Cr-vapors in the air flow was estimated from oxide scale growth on these high-temperature alloys as well as from the quantification of Cr accumulations in the cell [7, (ch. 6.2)]. This value is in agreement with an *in situ* measurement of Cr species [21, (ch. 7.1)], which had shown saturation of the air flux with Cr vapors in these testing conditions. A partial pressure of $9 \cdot 10^{-9}$ atm is therefore expected for CrO₂(OH)_{2(g)} species at the air entry location of the cell.

Cr accumulations are subsequently found at the electrolyte/cathode interface of sample A1 taken at the air inlet location (cf Fig. 7.11; left profile), causing cathode performance degradation by Cr-poisoning [12, (A.1)]. Further downstream along the air channel, only

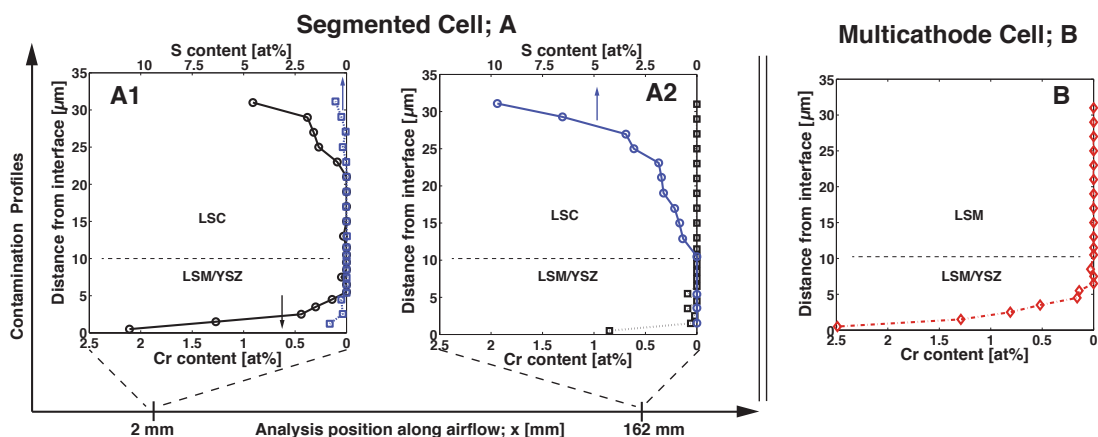


Figure 7.11: Cr and S contamination profiles for two samples of the segmented cell; samples A1 and A2 stem from air inlet and air outlet regions, respectively. The profiles are obtained by space-averaging EDS data for thin cathode slices. For comparison, a Cr profile of a sample from the multicathode cell, tested under Cr-poisoning conditions only, is shown on the right. For both sample A1 and B, Cr profiles indicates active sites near the electrolyte/cathode interface being polluted by Cr.

minor Cr amounts are found, confined to the interface (see Fig. 7.11; middle profile, sample A2). Part of the Cr contamination is trapped in the LSC CCL, mainly at the surface of this Cr getter layer. The Cr-trapping nature of LSC is underlined by increasing amounts of Cr near the CCL surface (see Fig. 7.11; left profile) that lies ca. $30\ \mu\text{m}$ distance from the interface. This finding is in agreement with previous observations of the CCL surface, where Cr was found to accumulate in the form of a SrCrO_4 -related phase [13, (ch. 7.2)], as well as with reaction schemes between LSC and acidic pollutant species like Cr described in literature [23-25]. The Cr-getter effect of LSC thus mitigated the extent of Cr-poisoning in active cathode regions of sample A1. Nevertheless, the amounts of Cr near the interface in sample A1 are found comparable with the value of Cr accumulations for cell B, without LSC CCL but exposed to lower Cr vapor concentrations (Fig. 7.10); which we believe validates their comparability in this study.

3.2 Sulfur contamination In the case of sulfur contamination (sample A), this experiment did not enable to determine the exact nature and the partial pressure of gaseous S species. The lowest prognosis can be set at the SO_2 concentration in environmental air which is around 10 ppb. Additional S contamination, originated from the insulating paste in the vicinity of the cathode segments, is poisoning the cathode (cf Fig. 7.11; S profiles) with increasing contamination load along the airflow.

Therefore, highest S-poisoning is found at cathode outlet regions, especially at the LSC CCL surface (cf. Fig. 7.11; middle profile). Near-electrolyte/cathode interface regions are free of S-poisoning in sample A2, as expected by the nature of the SrSO_4 formation reaction (as reported previously [13, (ch. 7.2)]), which is oxidative and does not take place at active sites

7.3. Combined Cr and S poisoning in solid oxide fuel cell cathodes

for oxygen reduction [9]. The effect on cathode performance of sulfur alone is thus expected to be small, and further investigations were not undertaken for sample A2.

The amounts of S measured in sample A1 are low, but are close to follow a profile corresponding to Cr accumulations; S deposits are both found on the CCL surface and near the cathode/electrolyte interface. No S is observed, and therefore not reported, for sample B, as was expected and intended. These SEM/EDS observations reported in sect. 3.1 and 3.2 (from this chapter) suggest an interaction between the two contaminant species Cr and S. This situation is aimed to be clarified at higher magnification by TEM investigations.

3.3 Combined Cr and S contamination a comparative study between contaminant accumulations in active cathode regions of samples A1 and B. In both samples A1 and B, the active cathode regions are confined to the cathode/electrolyte interface and are poisoned with similar amounts of Cr accumulations. These samples are therefore seen close enough for direct comparison of the Cr deposit's nature to investigate the effect of sulfur presence (sample A1 only) on the Cr-poisoning mechanism.

STEM-EDS observations of a near-interface region of sample A1, shown in Fig. 7.12, reveal the presence of a Sr/Cr/S-oxide grain within the LSM/YSZ composite cathode. The composition of the grain is identified by EDS as $\text{Sr}(\text{Cr}_{0.85}\text{S}_{0.15})\text{O}_4$, in agreement with observations of Sr/Cr/S-phases on the CCL surface published previously [13, (ch. 7.2)]. Indeed, always the same composition is measured on multiple analysis locations in both active cathode and CCL surface regions, whereas the impurity levels are very different above/beneath the LSC CCL (see thermodynamic analysis in section 4.2) given its trapping property. The following text reports additional proofs of the $\text{Sr}(\text{Cr}_{0.85}\text{S}_{0.15})\text{O}_4$ phase within LSM/YSZ near the cathode-electrolyte interface.

EFTEM imaging of the $\text{Sr}(\text{Cr,S})\text{O}_4$ grain confirms the homogeneous distribution of its constituting elements; the following energies were used for this analysis: Sr (1940 eV), Cr (574 eV), S (228 eV) and O (532 eV). Indexing the electronic diffraction pattern, using JEMS TEM simulation software [18], confirms the compound as monoclinic SrCrO_4 with 15 % Cr substituted by sulfur.

To further investigate the existence of this phase, a Sr/Cr/S compound was synthesized in the separate experiment by sintering a pellet pressed from the $\text{SrCO}_3/\text{Cr}_2\text{O}_3/(\text{NH}_4)_2\text{SO}_4$ -blend (see experimental section). It macroscopically shows yellow, black and green colors, indicating the presence of SrCrO_4 , $\text{Sr}_3\text{Cr}_2\text{O}_8$ and unreacted Cr_2O_3 [20]. EDS quantification reveals S to be incorporated into both the yellow (SrCrO_4), illustrated in Fig. 7.13, and the black ($\text{Sr}_3\text{Cr}_2\text{O}_8$) structure (not shown here), underlining the S-gettering nature of Sr/Cr-compounds [26].

As previously reported for SrCrO_4 compounds found on the CCL surface with identical S incorporation [13, (ch. 7.2)] - SrCrO_4 is the main reaction product in the LSC-Cr system [11]-, shifts in the XRD pattern of SrCrO_4 are expected, caused by the radii ratio S/Cr of ca. 0.6. Indeed, the XRD pattern from the synthesized $\text{Sr}(\text{Cr,S})\text{O}_4$ phase shifts from the ICDD-35743 (SrCrO_4) structure towards ICDD-730529 (SrSO_4), as reported for the conversion of celestite to Sr-chromate [27].

For sample B, with Cr contamination without the additional presence of S (cf Fig. 7.11 right

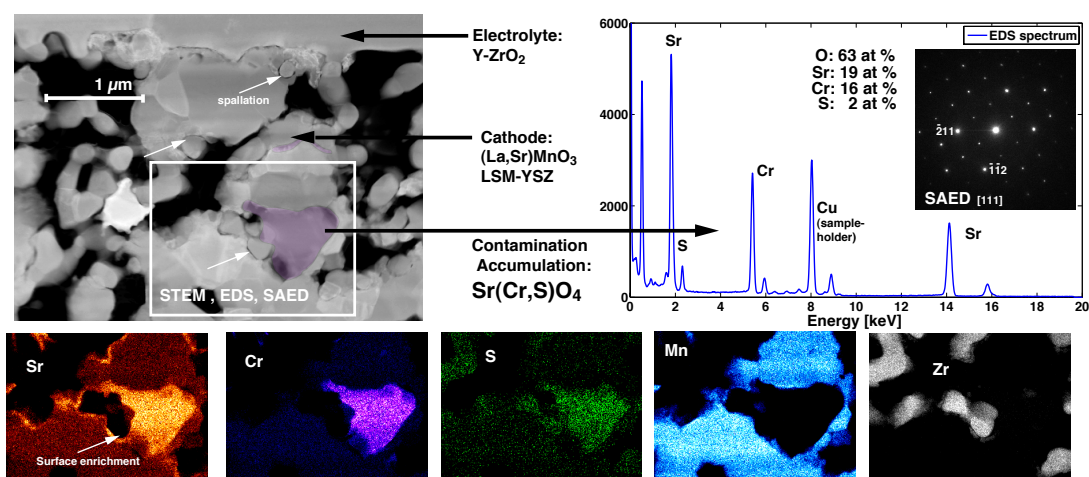


Figure 7.12: Dark-field scanning-TEM (DF-STEM) imaging of a near-electrolyte cathode region from sample A1. EDS mapping indicates S to be incorporated into the Sr-chromate grain, confirmed by quantification results of the EDS spectrum as well as by the indexation of the diffraction pattern.

profile), Cr accumulations are found in the form of Cr-Mn-spinel phases as illustrated in Fig. 7.14. Contrarily to the bulky-chromate grains found for sample A1, the observed Cr accumulations in sample B are distributed as small grains along phase-boundaries.

The observations reported here strongly suggest that the SrCrO₄ formation in LSM, although not directly expected from a thermodynamic point of view (cf. Fig. 7.15a), is enabled by the presence of sulfur dioxide in terms of formation of a solid solution between SrCrO₄ and SrSO₄ with higher stability in the air inlet location of the type A cell. This formation possibility is strengthened by the more oxidative atmosphere and lower temperature conditions, which are typically observed at the cathode air entry location (cf Fig. 7.10; sample A1). SO₂ is suggested to act as chromate formation promoter [26] and to incorporate into this phase to form a Sr(Cr,S)O₄ compound.

This hypothesis is evaluated here by means of thermodynamic analysis for the different contaminating conditions: Cr only, S only, as well as Cr and S simultaneously. As this *post-test* analysis comprise a single snapshot after SOFC operation, kinetic considerations of Cr-phase formation cannot be addressed in the present work.

4 Discussion: thermodynamic analysis

4.1: Cr-LSM reaction Additional thermodynamic analysis to that published earlier by Yokokawa *et al.* [11] is shown in Fig. 7.15, where the temperature dependence of the reaction products between LSM and Cr (0.1 mole CrO₃) at pO₂ = 1 atm indicates that SrCrO₄ formation can take place at the lower temperature region; n represents the mole number of each phase formed as a function of temperature and oxygen partial pressure.

At 1073 K, the average operating temperature of the segmented cell A, on the one hand no

7.3. Combined Cr and S poisoning in solid oxide fuel cell cathodes

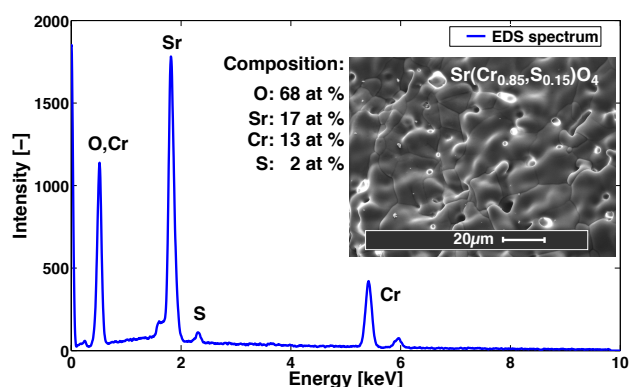


Figure 7.13: Space-averaged EDS spectrum quantification over some Sr-chromate grains, from a macroscopically yellow region of the sintered Sr/Cr/S-oxide pellet synthesized in this study, suggests the S-added Sr-chromate phase to have a composition close to the compound found in cathode sample A1.

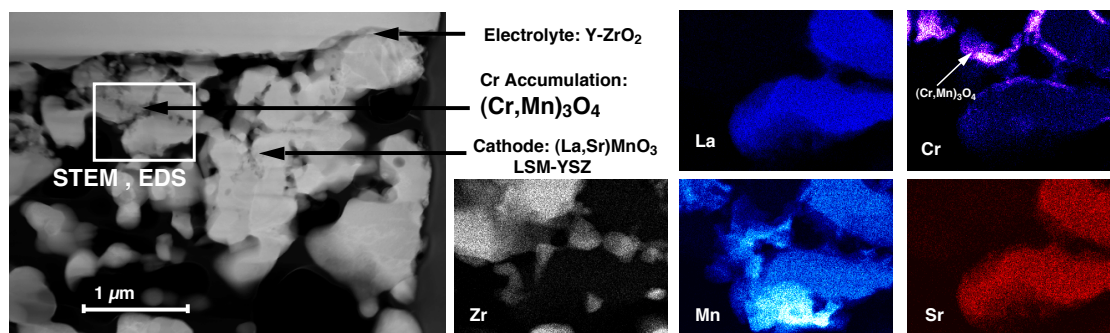


Figure 7.14: DF-STEM-EDS imaging of a near-electrolyte cathode region from sample B of the multicathode-type cell. Thin Cr accumulations are found along active phase boundaries. Point-analysis of Cr-rich phases indicates a mixed Cr,Mn-oxide composition close to $(\text{Mn,Cr})_3\text{O}_4$.

SrCrO_4 is expected; on the other hand 1073 K is close to those temperatures at which SrCrO_4 can be formed, and it must be taken into account that the inlet zone (where sample A1 was taken) will be colder than the 1073 K average (by at least 20 °C [15]).

To underline this finding, the thermodynamic activity of plausible reaction products between LSM and Cr, in particular of SrCrO_4 , is given in Figs. 7.15c (log-scale) and 7.15d (linear-scale). The thermodynamic activity, $a(\text{SrCrO}_4)$, is close to unity, i.e. SrCrO_4 is formed, in oxidative atmosphere and decreases with decreasing oxygen potential. Cr,Mn-spinel phases are on the other hand stable at the mean SOFC operating temperature of 1073 K, at low $p\text{O}_2$ (Fig. 7.15b), thus typically under conditions found at active cathode regions, near the electrolyte/cathode interface where the local overpotential is high, as observed in Fig. 7.14.

4.2 S-LSM and S-LSC reactions Besides severe sulfur-poisoning in sample A2, S contamination, although in minor extent, is also identified in sample A1 (Fig. 7.11). Therefore the effect

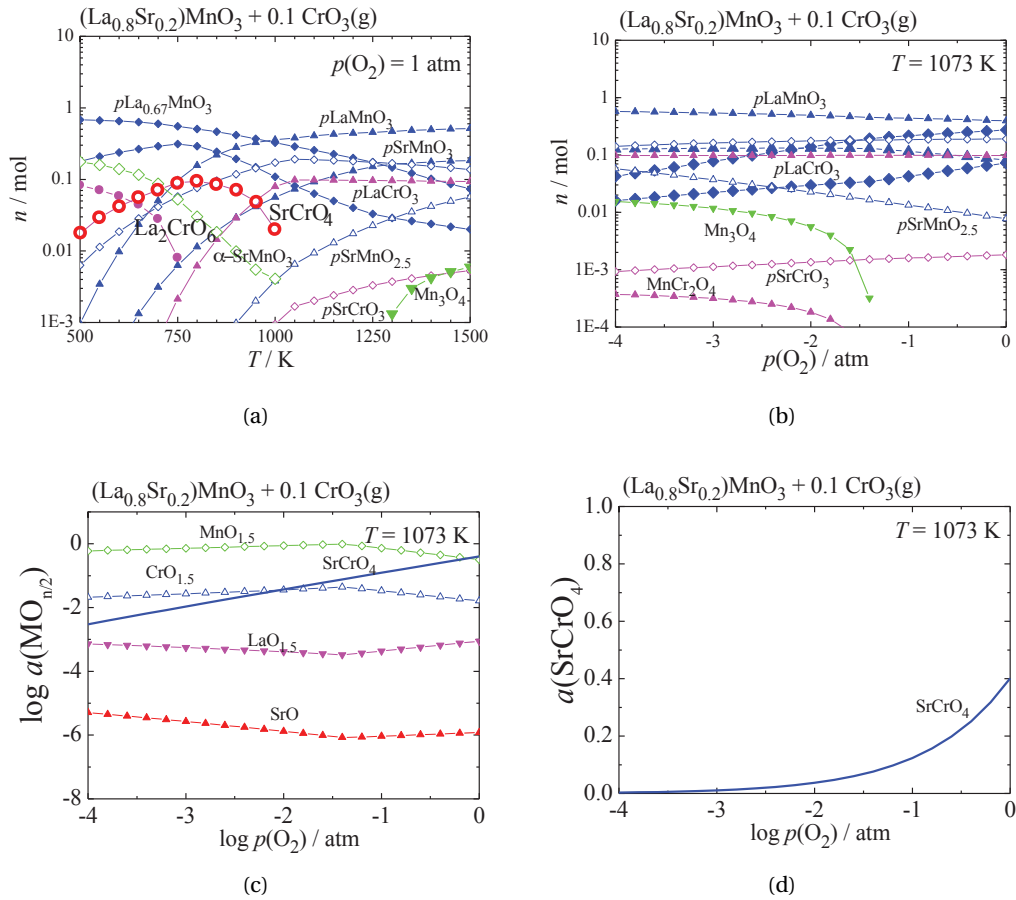
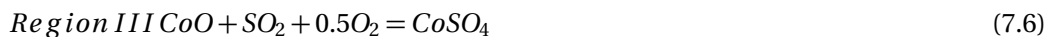
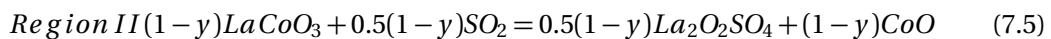
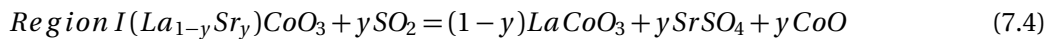


Figure 7.15: A) Temperature dependence of the reaction products between 1 mole LSM and 0.1 mole CrO₃ at pO₂ = 1 atm; SrCrO₄ formation takes place at lower temperature regions. B) pO₂ dependence of the reaction products at 1073 K; MnCr₂O₄ is formed in the low pO₂ region. C) Oxygen partial pressure dependence of the activity of the reaction products between LSM and Cr. D) In oxidative atmosphere, the activity of SrCrO₄ is close to unity.

of sulfur on LSM and LSC perovskite cathode layers is investigated to know if and how the LSC CCL traps SO₂ before this contaminant reaches the active LSM cathode. Reactions of LSC from the CCL with SO₂ can be separated into three regions (I-III) and described by the following Eqs. 7.4-7.6, as illustrated on Fig. 7.16a; the respective equilibrium partial pressures plateaus for SO₂ for the three reactions are given by Fig. 7.16b.



7.3. Combined Cr and S poisoning in solid oxide fuel cell cathodes

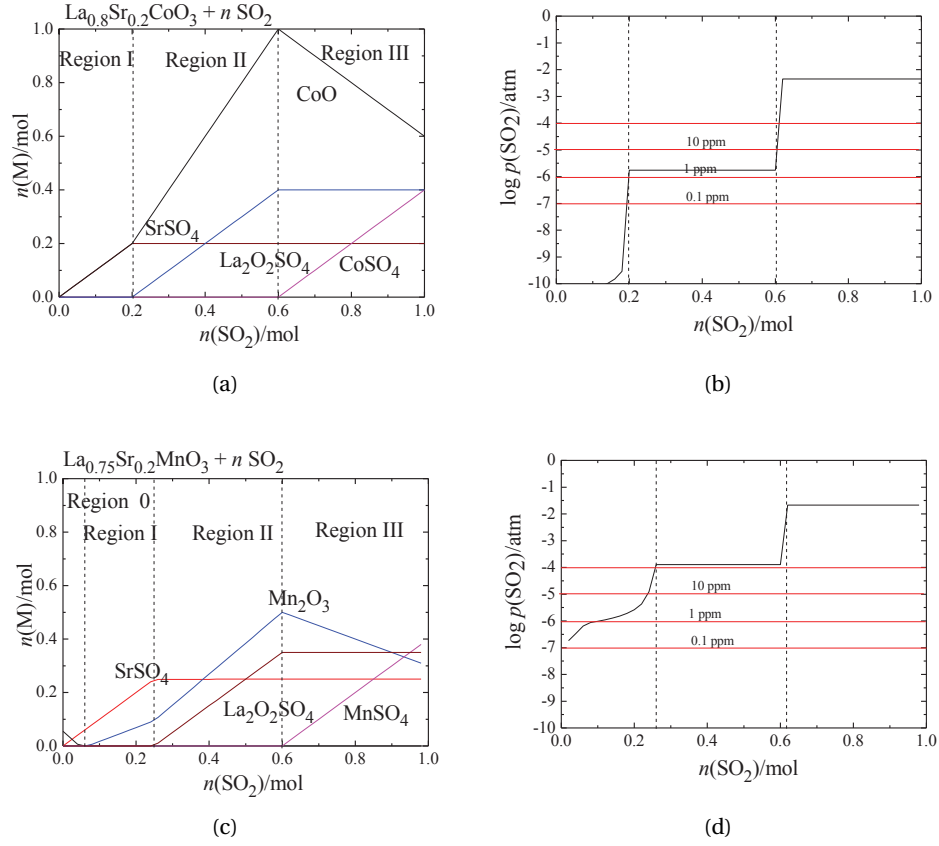
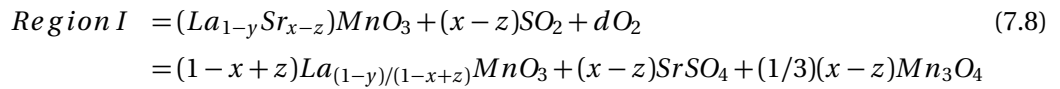
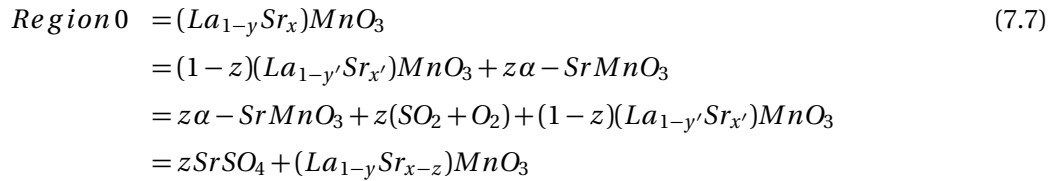
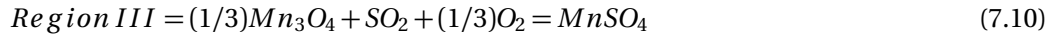
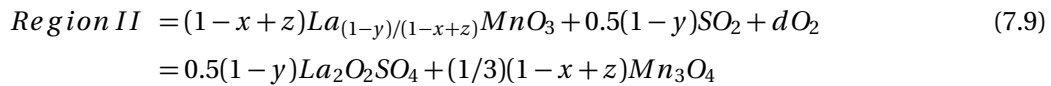


Figure 7.16: A) LSC reaction with SO_2 ; regions I, II and III correspond to equations 7.4, 7.5 and 7.6, respectively. B) The equilibrium partial pressures of SO_2 for respective reactions Eqs. 7.4-7.6. C) LSM reaction with SO_2 ; Regions 0-III correspond to Eqs. 7.7-7.10. D) Equilibrium partial pressure for SO_2 in regions I-III.

Similarly, the reactions between LSM and SO_2 are described by Eqs. 7.7-7.10, which are graphically represented on Fig. 7.16c with the corresponding partial pressure plateaus given by Fig. 7.16d.





This reaction scheme indicates the alpha-SrMnO₃ phase to be precipitated from LSM even without SO₂ gas in the air; this is due to the A-site deficiency of the LSM perovskite composition (cf. Eqn. 7.7). However, in practice, the precipitation of alpha-SrMnO₃ is not observed and the reaction of LSM with SO₂ first yields SrSO₄ alone without precipitation of manganese oxides. This precipitation is expected to be kinetically hindered, comparable to pyrochlore phase formation between LSM and YSZ that also results without the precipitation of manganese oxides. No Region O is observed for LSC in figure 7.16a, due to its stoichiometry (no A-site deficiency).

Regions I, II and III present similar reaction paths leading to SrCrO₄ formation (Region I) and other phases (Regions II,III) in LSM-SO₂ and LSC-SO₂ systems. Differences in SO₂ equilibrium pressures are found for these regions and the two perovskites; they are generally lower (i.e. more reactive) for LSC reactions compared to those for LSM, i.e. four orders of magnitude between LSM and LSC systems for the SrSO₄ formation (Regions I), below two orders of magnitude in the Regions II for the La₂O₂SO₄ formation, and below one order in Region III, for Mn- or Co-sulfate formation.

The partial pressure of SO₂ in the type A cell test being unknown, a lower and a higher level case are considered. Considering also these two materials not individually but in cell configuration with LSC on top of the LSM cathode, where the LSC CCL is thought to act as an SO₂ getter, the above findings, in particular for Fig. 7.16, indicate the following:

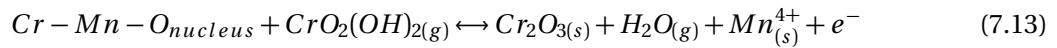
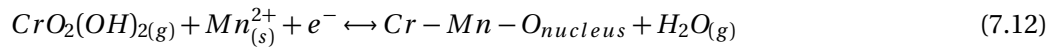
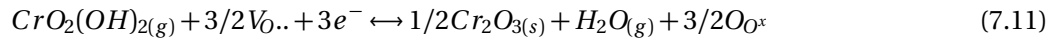
- i With a partial pressure of SO₂ lower than 1 ppm, nearly all SO₂ is captured by LSC in the CCL to form SrSO₄ (LSC-Region I, Fig. 7.16b). The remaining SO₂ passing through this trapping layer has a partial pressure of around 10⁻¹⁰ atm. The amount of sulfur reaching the cathode is therefore too low to affect LSM. The LSC protects the active cathode region unless the trapping layer becomes saturated.
- ii When the SO₂ partial pressure is between 1 and 500 ppm, LSC is decomposed into SrSO₄ and LaCoO₃ (LSC-Region II, Fig.7.16b); the trapping effect of LaCoO₃ reduces the SO₂ partial pressure to a level of 1 ppm. This remaining amount of SO₂ penetrates until the active cathode regions and reacts with LSM according to reaction equations 7.7-7.8 (LSM-Regions O and partly I, Fig.7.16d). In such cases, up to 0.1 mole of SO₂ can react with one mole of LSM to form SrSO₄.

4.3 Cr/S-LSM reactions As it was shown that up to 1 ppm SO₂ can react with active cathode regions exposed to high SO₂ contamination, the effect of Cr on LSM in simultaneous S contaminating conditions is therefore considered as follows (Fig. 7.17):

7.3. Combined Cr and S poisoning in solid oxide fuel cell cathodes

1st case: 1 mole LSM + 0.1 mole CrO₃: The reaction between LSM and CrO₃(g) favors Cr absorption into the B-site of the perovskite lattice. The A-site deficiency of LSM limits on the one hand the amount of Cr to be integrated into the perovskite lattice, but favors on the other hand the precipitation of manganese oxides. SrCrO₄ is not formed in LSM as this composition is the most stable among La,Sr-based perovskite compounds.

Chemical reactivity and electrochemical degradation are however not necessarily in relation as the chemically stable LSM suffers most from Cr-poisoning by other means than the SrCrO₄ formation, namely the preferential deposition of Cr species at active sites for oxygen reduction. Two Cr-deposition descriptions for Cr-poisoning in LSM-YSZ composite cathodes are found in literature [26,28]; by the direct electrochemical reduction of Cr^(VI) to Cr^(III) (cf. Eqn. 7.11), or via Mn^(II), generated in LSM under polarization, as nucleation sites (cf. unbalanced Eqs. 7.12-7.13).



Either way, Cr₂O₃ reacts with LSM to form the (Cr,Mn)₃O₄ spinel phase, which is the thermodynamically favored phase, at active sites for oxygen reduction where pO₂ is low (cf Fig. 7.15b and Fig. 7.17a), and which is found to be formed at the active phase boundaries, as illustrated in Fig. 7.14.

2nd case: 1mole LSM + 0.1 mole CrO₃ + 0.01 / 0.1 mole SO₂ (Fig. 7.17b, 7.17c): When sulfur contamination occurs at the same time as Cr-poisoning, SrSO₄ is formed depending on the sulfur contamination level. This SrSO₄ formation enhances the formation of a solid solution between SrCrO₄ and SrSO₄; an ideal solid solution is assumed in the thermodynamic analysis. The amount of precipitated Mn oxides also increases, due to the decrease in the A-site occupancy in the perovskite lattice (Sr-consumption by chromate and sulfate formation), leading to a decreased mole number of the perovskite lattice.

4.4 Contamination effect on cell performance Thermodynamic analysis, predicting the co-existence of SrSO₄ and SrCrO₄ phases in LSM (cf. Fig. 7.17b, 7.17c), with the assumption that these two phases form a solid-solution, is consistent with the observed formation of S-added Sr-chromate. The effect of combined Cr and S contaminating conditions in terms of cathode performance degradation is now evaluated as follows:

SrCrO₄ is (and Sr(Cr,S)O₄ is expected to be) poorly conductive and reduces the cathode porosity [11]. Impurities like S can enhance sintering leading to morphological changes [26]. Similarly, cation-depletion of LSM, after Sr consumption, favors perovskite coarsening. SrCrO₄ has a high thermal expansion coefficient (ca. 17.5·10⁻⁶ K⁻¹), and could therefore induce spallation between the different phases during thermal changes, especially in coarsened microstructures [19] as observed in Fig. 7.12. In addition, the depletion of Sr in LSM leads to a

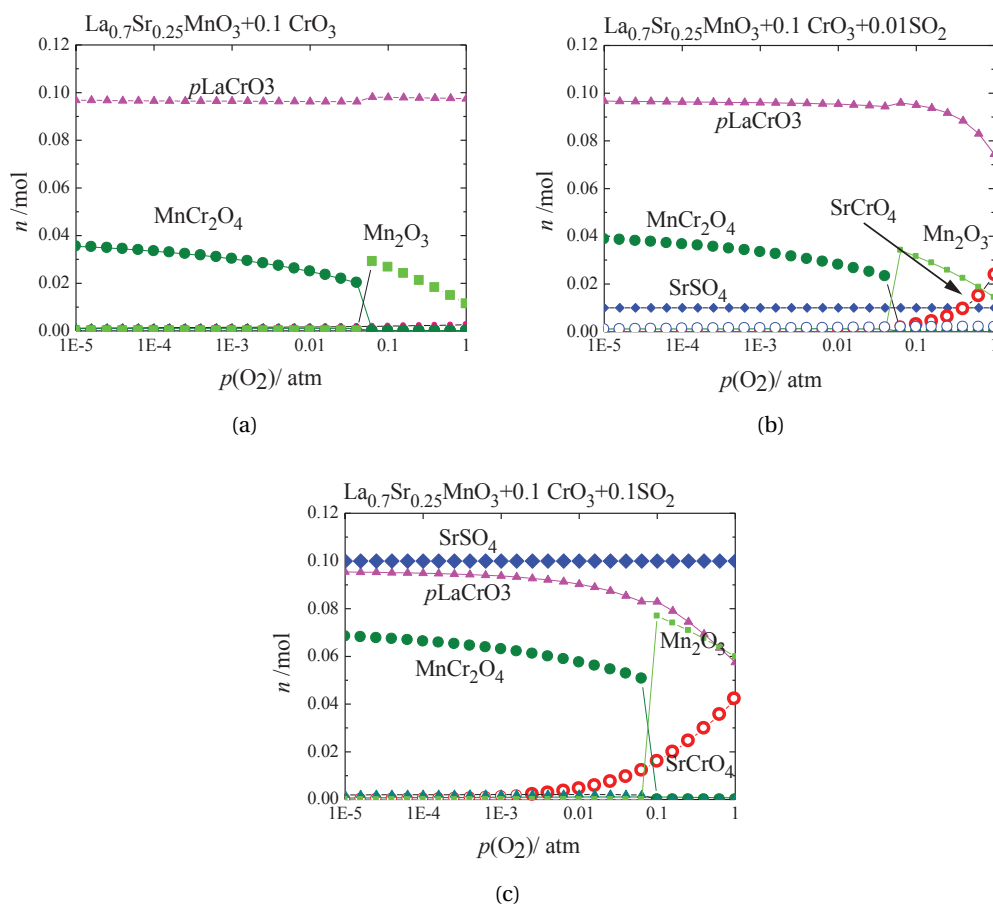


Figure 7.17: A) Reaction products between 1 mole LSM and 0.1 mole CrO_3 according to different oxygen partial pressures; Cr integration into the B-site of LSM perovskite lattice is thermodynamically favored. B) Reaction products between LSM, Cr and 0.01 mole SO_2 ; minor amounts of SrCrO_4 and SrSO_4 , compared to Cr B-site integration, are formed. C) Reaction of LSM with Cr and high S contents yields to the formation of SrCrO_4 , SrSO_4 and increased amounts of precipitated Mn-oxides.

change of the perovskite thermal expansion coefficient. In summary, $\text{Sr}(\text{Cr,S})\text{O}_4$ formation can possibly induce a delayed deleterious effect on the cathode performance, whereas the immediate effect, i.e. sparse and bulky chromate formation (cf. Fig. 7.12), is expected to be smaller compared to the formation of Cr/Mn-oxides along the triple-phase-boundaries (cf Fig. 7.14) in Cr-poisoning conditions [11].

Here, the total accumulated Cr amount for type A cell ($18 \mu\text{g}\cdot\text{cm}^{-2}$ for cathode and CLL per 1 kh operation) and the observed performance degradation (ca. $1 \%\cdot\text{kh}^{-1}$) [7, (ch. 6.2)] indicates serious cathode poisoning, comparable with findings from cell endurance testing performed elsewhere [29] ($15 \mu\text{g}\cdot\text{cm}^{-2}$ for tests with less than $1.5 \%\cdot\text{kh}^{-1}$ degradation [7, (ch. 6.2)]). The important difference between global and local degradation rates of a repeat-element suggests however that correlations can only be done between local distribution of pollutant species and

7.3. Combined Cr and S poisoning in solid oxide fuel cell cathodes

the causes of local degradation rates [12, (A.1)]; i.e. locally high performance degradation rates at the air inlet regions are consistent with the localization of high contamination accumulation, whereas the main part of the type A cell remained free of degradation-causing contamination. The actual amount of the $\text{Sr}(\text{Cr,S})\text{O}_4$ phase in the cathode, by its conductivity decrease and grain spallation contribution, cannot directly be linked to the observed decrease of local power density. The complexity of superimposed degradation effects, not limited to Cr and S (e.g. a silicon-poisoning was observed on the same cell [17, (ch. 7.1)]), precludes such direct correlations. A different situation is expected from type B cell, with only Cr accumulation near the cathode-electrolyte interface. From a multicathode-cell test [16, (ch. 4.1)] performed in identical conditions than for cell type B, we can derive that the Cr amounts observed in sample B1 should be correlated to a degradation rate of 2.5-3 %·kh⁻¹. The observed degradation was, with ca. 5% voltage decay after 700 h of testing, actually higher; the added Mn-oxide, introduced by Mn-doping of the YSZ-electrolyte, in the test of ref. [16, (ch. 4.1)], likely changed Cr-deposition mechanisms (cf. eqn. 7.12-7.13) and caused additional superimposed degradation [30].

5 Conclusions

The present study reveals SOFC cathode poisoning mechanisms in the case of chromium contaminating conditions in combination with high sulfur concentrations.

This special case of pollution, far above trace SO_2 levels in air, is not a generic situation in SOFC operation but can be representative of accelerated testing. Indeed, S-rich Sr-chromate compounds are frequently observed in LSCF-cathodes after long-term (10'000 hours) SOFC operation, where S contamination arises from environmental air. Our observations especially point out the possibility of multiple or combined poisoning phenomena, which lead to interdependent or superimposed degradation effects, hence complicating quantitative correlations between contamination amounts and degradation rates.

In many studies facing the Cr-poisoning phenomenon, different contamination levels, not limited to Cr alone, are suggested to be at least partially responsible for disagreements in the literature related to Cr accumulations. Such differences in contamination can also mitigate the severity of Cr-poisoning.

Finally, this study suggests to carefully select SOFC proximal components to limit S contamination to only the trace amounts vehicled by environmental air.

Acknowledgements

The Swiss Federal Energy Office (Contract 153569 - AccelenT), as well as the European Commission (FP6 contract SES6-019875 - Flame-SOFC) are gratefully acknowledged for financial support. Antonin Faes and Fabienne Bobard are warmly thanked for TEM-lamellae preparation; Nicola Accardo is acknowledged for the chromate synthesis.

References

- 1 D.B. Meadowcroft, *Nature* 226 (1970) 847.
- 2 W.F. Libby, *Science* 171 (1971) 499.
- 3 I. Rosso, E. Garrone, F. Geobaldo, B. Onida, G. Saracco, V. Specchia, *Appl. Catal., B* 30 (2001) 61.
- 4 H. Wang, Y. Zhu, R. Tan, W. Yao, *Catal. Lett.* 82 (2002) 199.
- 5 L. Wan in: L.G. Tejuca, J.L.G. Fierro (Eds), *Properties and Applications of Perovskite-Type Oxides*, Marcel Dekker Inc., New York 1993 pp. 145.
- 6 Y. Matsuzaki, I. Yasuda, *Solid State Ionics*, 132 (2000) 261.
- 7 J.A. Schuler, C. Gehrig, Z. Wuillemin, A.J. Schuler, J. Wochele, C. Ludwig, A. Hessler-Wyser, J. Van herle, *J. Power Sources*, 196 (2011) 7225. (ch. 6.2)
- 8 K. Yamaji, Y. Xiong, M. Yoshinaga, H. Kishimoto, M.E. Brito, T. Horita, H. Yokokawa, J. Akikusa, M. Kawano, *ECS Trans.* 25 (2009) 2853.
- 9 Y. Xiong, K. Yamaji, T. Horita, H. Yokokawa, J. Akikusa, H. Eto, T. Inagaki, *J. Electrochem. Soc.* 156 (2009) B588.
- 10 R.R. Liu, S. Taniguchi, Y. Shiratori, K. Ito, K. Sasaki, *ECS Trans.* 35 (2011) 2255
- 11 H. Yokokawa, T. Horita, N. Sakai, K. Yamaji, M.E. Brito, Y. Xiong, H. Kishimoto, *Solid State Ionics* 177 (2006) 3193.
- 12 Z. Wuillemin, A. Nakajo, A. Müller, J.A. Schuler, S. Diethelm, J. Van herle, D. Favrat, *ECS Trans.* 25 (2009) 457. (appendix 1)
- 13 J.A. Schuler, Z. Wuillemin, A. Hessler-Wyser, J. Van herle, *ECS Trans.* 25 (2009) 2845. (ch. 7.2)
- 14 A. Hessler-Wyser, Z. Wuillemin, J.A. Schuler, A. Faes, J. Van herle, *J. Mater. Sci.* 46 (2011) 4532.
- 15 Z. Wuillemin, EPFL PhD Thesis No. 4525, Lausanne Switzerland 2009.
- 16 J.A. Schuler, P. Tanasini, A. Hessler-Wyser, C. Comninellis, J. Van herle, *Electrochem. Commun.* 12 (2010) 1682. (ch. 4.1)
- 17 J.A. Schuler, Z. Wuillemin, A. Hessler-Wyser, J. Van herle, *Electrochem. Solid-State Lett.* 14 (2011) B20. (ch. 7.1)
- 18 P.A. Stadelmann, *Ultramicroscopy* 21 (1987) 131.

7.3. Combined Cr and S poisoning in solid oxide fuel cell cathodes

- 19 M. Mori, Y. Hiei, N.M. Sammes, *Solid State Ionics* 135 (2000) 743.
- 20 K.T. Jacob, K.P. Abraham, *J. Phase Equilib.* 21 (1999) 46.
- 21 T. Baikie, Z. Ahmad, M. Srinivasan, A. Maignan, S.S. Pramana, T.J. White, *J. Solid State Chem.* 180 (2007) 1538.
- 22 J.A. Schuler, A.J. Schuler, Z. Wullemin, A. Hessler-Wyser, C. Ludwig, J. Van herle, *ECS Trans.* 35 (2011) 2001. (ch. 6.1)
- 23 D. Oh, E. Armstrong, D. Jung, C. Kan, E. Wachsman, *ECS Trans.* 25 (2009) 2871.
- 24 H. Yokokawa, N. Sakai, T. Horita, K. Yamaji, M.E. Brito, H. Kishimoto, *J. Alloy Compd.* 152 (2008) 41.
- 25 C. Tofan, D. Klvana, J. Kirchnerova, *Appl. Catal., B* 36 (2002) 311.
- 26 H. Yokokawa, H. Kishimoto, K. Yamaji, T. Horita, *ECS Trans.* 25 (2009) 401.
- 27 J.C. Rendon-Angeles, Y.M. Rangel-Hernandez, J. Lopez-Cuevas, M.I. PENCH-Canul, Z. Matamoros-Veloza, K. Yanagisawa, *Proc. int. Conf. on High Press. Sci. Tech.* T13 (2005) O144.
- 28 S.P. Jiang, S. Zhang, Y.D. Zhen, *J. Electrochem. Soc.* 153 (2006) A127.
- 29 N.H. Menzler, I. Vinke, H. Lippert, *ECS Trans.* 25 (2009) 2899.
- 30 P. Tanasini, EPFL PhD Thesis No. 5004, Lausanne Switzerland (2011)

8 Long-term stack performance

Journal of Power Sources, 211 (2012) 177

8.1 Cr-poisoning in (La,Sr)(Co,Fe)O₃ cathodes after 10'000 h SOFC stack testing

J. Andreas Schuler^{a,b,c}, Zacharie Wuillmin^d, Aïcha Hessler-Wyser^b, Clément Comminges^e,
Nadia Yousfi Steiner^e, Jan Van herle^a

^a *Laboratoire d'Énergie Industrielle (LENI), École Polytechnique Fédérale de Lausanne (EPFL), 1015 Lausanne, Switzerland*

^b *Centre Interdisciplinaire de Microscopie Electronique (CIME), École Polytechnique Fédérale de Lausanne (EPFL), 1015 Lausanne, Switzerland*

^c *Laboratory for High Performance Ceramics (HPC), Swiss Federal Laboratories for Materials Science and Technology (EMPA), 8600 Dübendorf, Switzerland*

^d *HTceramix, 1400 Yverdon, Switzerland*

^e *European Institute for Energy Research (EIFER), 73131 Karlsruhe, Germany*

After 10,000 hours solid oxide fuel cell (SOFC) stack operation, the Cr-poisoning situation in (La_{0.6}Sr_{0.4})(Co_{0.2}Fe_{0.8})O₃- (LSCF)-based cathode material is depicted in this work. Systematic Cr profiling through cross-sections, by energy-dispersive X-ray spectroscopy (EDS), from post-operation samples taken at different locations within the air flow field, reveals Cr accumulation in electrochemically active cathode regions near the interface with the electrolyte, although the major amount of Cr is trapped in inactive surface-proximal cathode regions; the 20 μm thick LSCF current collector does not fully impede the Cr access to the LSCF-based functional cathode layer. The distribution of Cr within the air flow field, observed by EDS surface scans, reports on the severity of the sources and causes for Cr contamination: 1) Cr preferentially accumulates at sealing-proximal locations; this is explained by fuel-leakage through the sealing with subsequent water vapor generation in the cathode compartment, aggravating local Cr-poisoning via the Cr-oxyhydroxide vapor species; 2) high Cr amounts at air inlet regions point to system components located upstream of the cell to contribute to local Cr contamination; 3) the remaining main part of the cell experiences low Cr-poisoning; the

protective solution to prevent Cr evaporation from the metallic interconnects thus appears to be adequate. The detected low overall amounts of Cr contamination, partially correlated to the observed low performance degradation, encouragingly indicate 40,000 h operation, a prerequisite for stationary SOFC application, to be in reach for LSCF-based stacks.

1 Introduction

The market entry for solid oxide fuel cells (SOFC) as stationary application is promised for SOFC systems reaching reliably a lifespan of 40,000 h. As such a time span precludes repetitive testing in small scale SOFC development programs, 10,000 h benchmarking with low and stable degradation rates and without major incidents meets a first important step. In this context, the present work aims to depict the severity of degradation effects after such endurance testing, based on the *post-test* analysis of SOFC stack components, to forecast the device behavior at longer operating time.

The stack test dealt with in this study, a 5 cell short-stack with cell design and characteristics depicted in fig. 8.1, was operated over 9,630 h at 750°C under a constant current load of $0.5\text{ A}\cdot\text{cm}^{-2}$ (25 A for the whole stack), with simulated reformat gas at a fuel utilization of 73%. Comminges *et al.* monitored, via impedance spectroscopy, the stack performance and degradation evolution over the complete testing time [1] (cf fig. 8.2 and fig. 8.3) and recorded a stack potential decay from 3.752 V to 3.241 V, which represents 13.6% total degradation over ca. 10,000 h, caused by an area specific resistance (ASR) increase of $0.2\Omega\cdot\text{cm}^2$ that could be attributed to $0.18\Omega\cdot\text{cm}^2$ ohmic resistance increase and $0.02\Omega\cdot\text{cm}^2$ polarization resistance increase.

As only few stack tests, comprising $(\text{La}_{0.6}\text{Sr}_{0.4})(\text{Co}_{0.2}\text{Fe}_{0.8})\text{O}_3$ - (LSCF)-based cathode materials, having reached the milestone of 10,000 h lifetime, with subsequent *post-test* analysis, are reported in open literature [2], focus is brought here to the cathodic half-cell, i.e. cathode regions from the electrolyte to the current collector towards the metallic interconnector (MIC). Since the test was performed in stack configuration, the compatibility between stack/system compounds and the air electrode needs investigation. In particular, emanation of volatile $\text{Cr}_{(g)}^{(VI)}$ species from Cr-containing alloys, present in MIC and system components, such as tubing, heating and housing elements, is expected [3-5, (ch. 6.1, 6.2)]. The Cr-poisoning degradation phenomenon is therefore suspected to occur via the accumulation of reduced $\text{Cr}_{(s)}^{(III)}$ in cathode layers, blocking gaseous and electric paths necessary for the cathode oxygen reduction reaction, leading to performance degradation over time [6]. The quantity of emanated Cr species strongly depends on the partial water vapor pressure, as volatile Cr-oxyhydroxide $\text{CrO}_2(\text{OH})_{2(g)}$ generation is directly proportional to the local $p(\text{H}_2\text{O})$ [6].

Hydrogen leakage through sealing materials with subsequent water generation in the cathode compartment has been pointed out by Wuillemain *et al.* [7]. They made a model prediction of the distribution of the local water vapor pressure for the cell design dealt with in this work, depicted in fig. 8.4. Coupling thermodynamic data for Cr vapor species to the local conditions in the cathode compartment enabled to predict the local concentrations of generated Cr [8], and therefore to point out regions more or less prone to Cr-poisoning. The Cr vapor generation

8.1. Cr-poisoning in $(\text{La,Sr})(\text{Co,Fe})\text{O}_3$ cathodes after 10'000 h SOFC stack testing

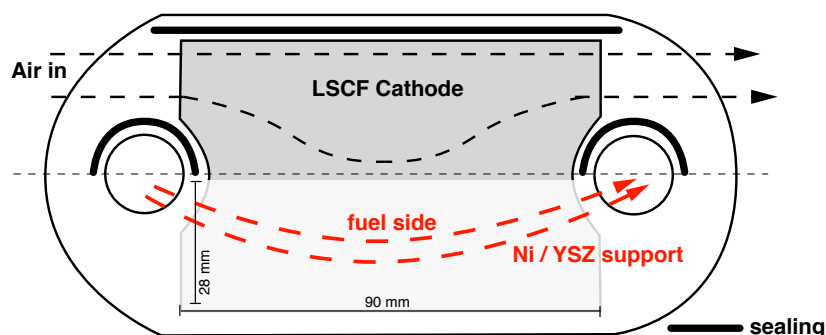


Figure 8.1: Design of the anode-supported Ni-YSZ cell with an LSCF-based cathode where the air and fuel flow field are schematically indicated.

modeling result will be illustrated in fig. 8.9b.

The combination of these modeling results, used as guidelines for sample location choice for post-operation analysis (indicating the so-called compound formation area [9] between LSCF and Cr), and the corresponding electrochemical behavior evolution is the starting point of this study.

We aim to picture the Cr-poisoning situation after 10,000 h endurance testing of a LSCF-cathode based SOFC stack. Judged on both the severity and distribution of Cr accumulations in the cathode compartment, we intend to shed light on the causes and sources of Cr-poisoning, and so to suggest solutions to mitigate Cr poisoning for the extension to 40,000 h lifetime for LSCF-based SOFC stacks.

2 Experimental

The 5 cell stack test with 50 cm^2 active area per cell as illustrated on fig. 8.1, provided by *SOFCPower/HTceramix*, comprises $(\text{ZrO}_2)_{0.92}(\text{Y}_2\text{O}_3)_{0.08}$ (YSZ) electrolyte-covered Ni-YSZ anode-supported cells with a $(\text{Ce}_{0.9}\text{Gd}_{0.1})\text{O}_{1.95}$ (CGO) barrier layer towards the $(\text{La}_{0.6}\text{Sr}_{0.4})(\text{Co}_{0.2}\text{Fe}_{0.8})\text{O}_3$ -based CGO-LSCF composite cathode, an LSCF current collector layer, a *CROFER22APU* (*ThyssenKrupp*) metallic interconnect covered with a $(\text{MnCo}_{1.9}\text{Fe}_{0.1})\text{O}_4$ protective coating and using the proprietary material *SOFCConnexTM* as gas diffusion layer (GDL).

The stack performance and degradation evolution, as previously reported [1], is summarized in tab. 8.1 and illustrated in figs 8.2-8.3.

The degradation rate during the first 5,000 h was about 1 % per 1,000 h, but increased afterwards above 1.5 % per 1,000 h due to the impact of incidents. A list of the different failures during the test is provided in tab. 8.2. Both types of incidents (fuel supply fluctuations and overloading failure of the electronic load) most probably lead to partial re-oxidation of the anode, accelerating the stack degradation towards 9,500 h.

The goal of the present work being the investigation of cathode contamination by Cr, the cell least affected by the incidents on the anode side which could have damaged the sealing also is chosen here. Cell n°5 with a voltage decay from 757 mV to 706 mV, i.e. a degradation rate

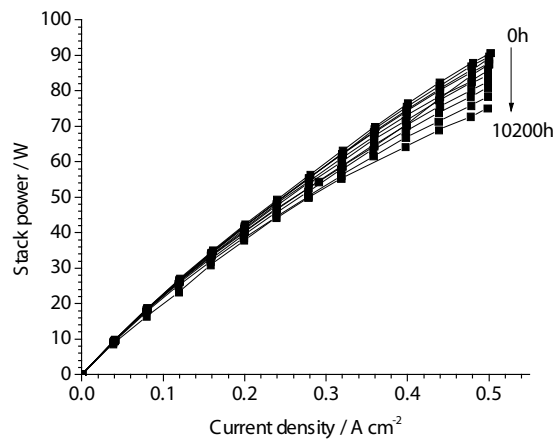


Figure 8.2: Stack output power versus time and current density; the stack power decreased from 91 W to 75 W (ca. 18 % decrease) after 10,200 h operation (Reprinted with permission from ref [1]).

below -0.7 % per 1,000 h, is therefore analyzed. Located on the top of the short-stack, this cell could also be most easily dismantled from the other stack components. The observation of all cells remaining intact after endurance testing at 73 % fuel utilization and 0.5 A/cm² positively highlights the mechanical integrity of the stack assembly. The choice of sample locations for the *post-test* analysis was done as follows.

The modeling background for p(H₂O) and Cr concentration distribution within this cell design depicted on fig. 8.4 and further on in fig. 8.9b is in-depth described elsewhere by Wullemin [8]. These modeling results suggest sealing-proximal and air in-/out-let regions to be most prone to Cr-poisoning.

The cell dissection to obtain 10 samples distributed within the air flow field followed the guidance from these p(H₂O)-/Cr-distribution modeling results; the 10 samples extracted for surface analysis, comprising 6 samples also for subsequent cross-section study (locations 1,5,7,8,9,10), were chosen along 3 air channels (named: edge, main and central, as illustrated in fig. 8.4).

Energy-dispersive X-ray spectroscopy (EDS) surface scans were performed on 1 mm² regions on the 10 samples to obtain space-averaged Cr quantification, for which the measurement device and protocol are described elsewhere [10, (ch. 7.1)].

The 6 samples dedicated for cross-section studies followed embedding in epoxy medium, cutting with a diamond wire, polishing with diamond lapping films and carbon coating steps, before EDS analysis. The acquisition parameters, previously described [11, (ch. 3.1)], were tuned towards high acceleration voltage to provoke high excitation of the Cr K-line emission needed for proper Cr quantification, and towards high count rates, enabling the collection of statistically senseful data within reasonable measurement time. The Cr-profiles depicted on fig. 8.5b and fig. 8.6 were generated by transforming qualitative 2D EDS maps into quantitative 1D elemental/phase profiles [12, (ch. 4.1)], by space-averaging EDS data over thin cathode slices.

8.1. Cr-poisoning in (La,Sr)(Co,Fe)O₃ cathodes after 10'000 h SOFC stack testing

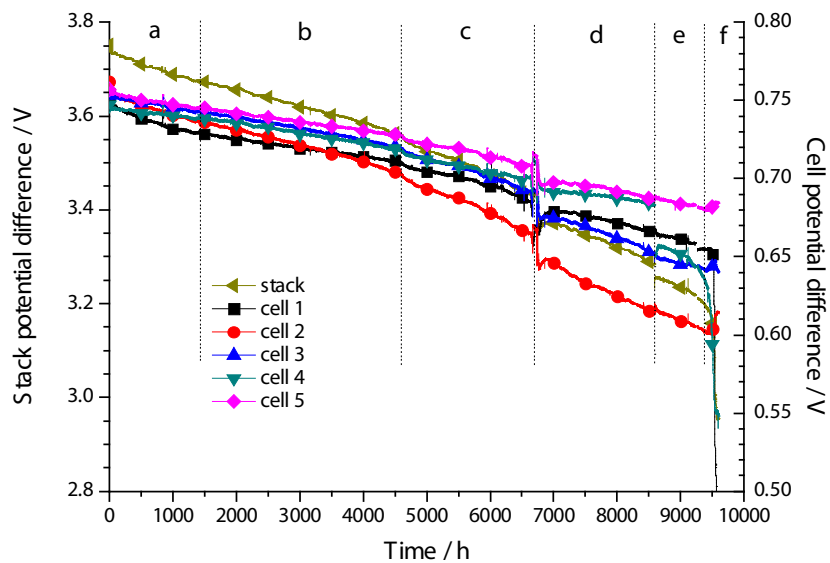


Figure 8.3: Stack and cells voltages versus time; annotations a-f correspond to 6 different degradation domains; regions a and b result from steady-state operation; domains c, d and e are accelerated domains initiated by testing setup failures reported in tab. 8.2 (Reprinted with permission from ref [1]).

3 Results and discussion

3.1 Cr profile in LSCF An objective Cr-poisoning picture independent of the investigator's eye [13] was obtained by systematically drawing elemental and phase profiles through the complete cathode thickness. Fig. 8.5a illustrates the cathode layers assembly from left to right: (i) a current collection layer (CL) made of (sub)micron LSCF grains, (ii) a functional cathode layer (FL) comprising a fraction of bulky CGO grains (light gray contrast) and (iii) a CGO buffer layer (BL). The phase profiles, with decreasing LSCF and increasing ceria contents towards the cathode/electrolyte interface, enable the CL/FL/BL assembly to be correctly identified. The LSCF and CGO phase fractions are obtained by adding to the sum of the metallic elements the corresponding oxygen amounts, i.e. $O_{LSCF} = 3/2 \sum La, Sr, Co, Fe$ and $O_{CGO} = 2 \sum Ce, Gd$ (+3 oxidation state in CGO neglected as approximation), prior to normalization.

The elemental Cr profile shown in fig. 8.5b (EDS Cr data taken from the central sample location 9) comprises two regimes of Cr accumulations in the CL and FL, respectively. A preferential distribution of Cr accumulations near the gas-CL interface, with decreasing amounts towards the FL-electrolyte interface, is observed; this was previously found by others for LSCF-based cathodes [2]. This result alone, quantified for sample location 9, only qualitatively represents the Cr-poisoning-caused contaminant distribution in a complete LSCF cathode cross-section; multiple measurements are needed to holistically depict Cr-poisoning within the cell.

Chapter 8. Long-term stack performance

Table 8.1: Summary of stack performance and degradation evolution after ca. 10,000 h operation; area specific, ohmic and polarization resistances (ASR, R_{Ohmic} and $R_{Polarization}$, respectively) are averaged values over the 5-cell stack; values for each individual cell (including the best performing cell n°5, dealt with in this study) are also given. The monitoring description, via impedance spectroscopy, is given by Comminges *et al.* in a previous work [1].

Recorded parameter	Unit	Value		Variation (%)
		0 h	9630 h	
Stack temperature	°C	756	753	-0.4
Current density	A·cm ⁻²	0.5	0.5	-
Fuel utilization	%	73	-	-
Stack voltage	V	3.752	3.241	-13.6
Stack ASR (at 0.5 A/cm ²)	Ω·cm ²	0.56	0.76	+35.7
Stack R_{Ohmic}	Ω·cm ²	0.18	0.36	+100
Stack $R_{Polarization}$	Ω·cm ²	0.38	0.4	+5.3
Cell 5 voltage	mV	757	706	-6.7
Cell 4 voltage	mV	747	646	-13.5
Cell 3 voltage	mV	753	657	-12.7
Cell 2 voltage	mV	762	624	-18.1
Cell 1 voltage	mV	754	627	-16.8

Table 8.2: Description of the failures observed during the long term test (Reprinted with permission from ref [1]).

Time (h)	Description of the incident
4533	Fluctuations of hydrogen flow rate
6535	Fluctuations of hydrogen flow rate
6660	Fluctuations of hydrogen flow rate
8587	Load failure, increase of current
9470	Cell n°1 and n°4 voltages started to decrease

3.2 Cr deposition mechanisms in LSCF-based cathodes Elemental Cr profiles for the 6 cross-section samples (locations 1,5,7,8,9,10) are presented in fig. 8.6. Differences in amounts and distributions of Cr are found for the different sample positions along the airflow and across the cell width. A characteristic Cr distribution through the LSCF cathode thickness, illustrated in fig. 8.7, is obtained by averaging the profiles of Cr amounts, normalized with respect to the most contaminated zone, i.e. the gas-CL interface.

Decreasing Cr amounts in the current collector with fairly constant values in the FL indicate a combination of Cr deposition mechanisms, suggested by other [14-15] driven both by the electrochemical activity (in cathode regions where the oxygen reduction process occurs) and the chemical reactivity (throughout the whole cathode thickness) of this mixed-conducting LSCF-based cathode. This is schematically illustrated on fig. 8.8.

On the one hand, the main part of Cr-poisoning in LSCF-cathodes is caused by the chemical

8.1. Cr-poisoning in (La,Sr)(Co,Fe)O₃ cathodes after 10'000 h SOFC stack testing

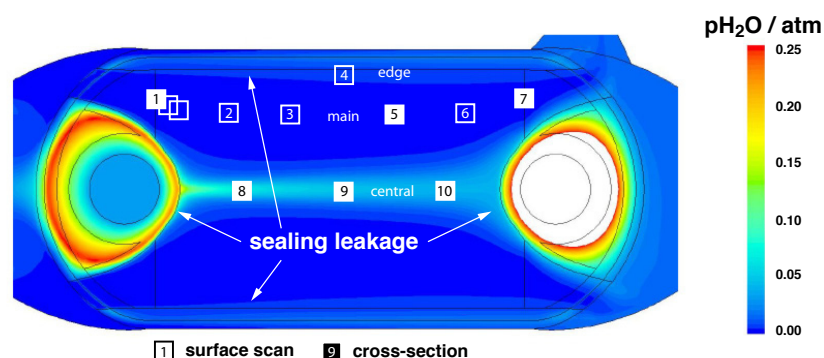


Figure 8.4: The sealing leakage-caused water generation modeling result, as previously published by Z. Wullemin [8], guides the *post-test* analyses; sample positions for surface scans are indicated by empty squares numbered 1-10; the full squares correspond to sample locations where cross-sections were investigated in addition; the larger size of *post-test* sample 1 enabled surface measurements on 3 consecutive positions along the air inlet channel (cf fig. 8.10) and the sample location is therefore indicated as tripled.

reactivity of SrO with Cr vapors to form SrCrO₄ [2], i.e. by the chemically-driven Cr deposition. Starting from the gas-CL interface, a decreasing Cr deposition rate through the whole LSCF-containing cathode thickness, caused by gas diffusion limitations, is therefore expected. On the other hand, when assuming that the electrochemically active cathode region is confined to the FL (Lu *et al.* [16] recently suggested LSCF cathodes to be active only within ca. 13 μm thickness), a polarization-driven Cr deposition rate only increasing towards the FL-electrolyte interface is expected. The electrochemically-driven Cr deposition mainly involves a reduction of Cr⁶⁺ vapor species into Cr³⁺ oxides at near-interface regions where the pO₂ is low.

Fig. 8.8 indicates schematically the combination of both decreasing (from the gas-CL interface) and increasing (towards the FL-electrolyte interface) contributions to correlate with the experimentally observed constant Cr profile within the FL. The shape of both the chemically and electrochemically driven Cr deposition profiles rely on previous experimental results [4, (ch. 6.1)].

3.3 Cr-poisoning distribution within the cell Fig. 8.9 depicts the severity of Cr-poisoning judged from surface analysis (the first microns from the LSCF surface are quantified) along three air flow channels, i.e. along the edge (location 4), within the main cell part (locations 1,2,3,5,6,7) and in the center of the cell (locations 8,9,10). As the flow field is constricted at the air in-/out-let regions (cf. fig. 8.1), these areas count as a single entry zone, split into three flow lines (main, edge and central) between inlet and outlet.

The highest Cr amounts are measured at the air inlet region (location 1), indicating the air flow feed to the cathode compartment to be loaded with Cr vapor species, hence pointing to Cr sources located upstream of the cell. The strongly decreased Cr amounts along the air channels (locations 2,3,5,6), with respect to the inlet location 1, suggest more Cr is being trapped by the LSCF CL surface than is being generated by the MIC.

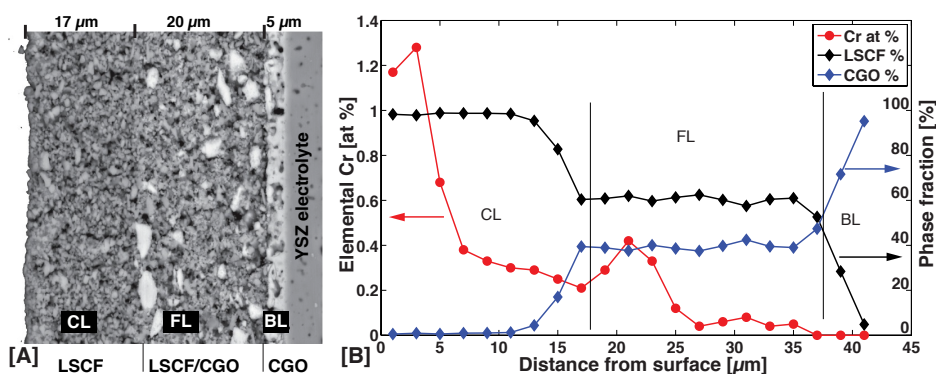


Figure 8.5: (A) SEM micrograph of SOFC cross-section showing from left to right the LSCF collector layer (CL), the LSCF-CGO functional layer (FL), a CGO buffer layer (BL), and the YSZ electrolyte; (B) LSCF and CGO phase profiles with increasing CGO-content towards the cathode/electrolyte interface; Cr-profile through the cathode thickness (location 9) reveals two trends: i) in the CL with decreasing amounts from the surface inwards ii) in the FL with again higher amounts than in the FL-proximal CL region.

The main part of the cell (locations 2,3,5,6) remains very low in Cr-poisoning, with slightly increasing amounts towards the air outlet. The protective solutions on the MIC to prevent Cr vapor emanation with an Mn/Co/Fe barrier coating in combination with the GDL thus appear to be sufficient for the time being for these operating conditions. This can in particular be brought into correlation with the measured increase in average polarization resistance of only $0.02\Omega\text{-cm}^2$ for nearly 10,000 h (cf. tab. 8.1), which translates to less than 0.4 %/1,000h ASR increase due to polarization; moreover, this ASR increase accounts for all cathode and anode contributions combined, of which the Cr contamination is only one process.

The cathode regions close/downstream the sealing locations along the cell edge flow (locations 1,4,7) and the central flow (locations 8,9,10) reveal higher Cr amounts (> 1 atomic %). These observations correlate with the model predictions for H_2O and Cr generation illustrated in fig. 8.4 and fig. 8.9b. The preferential Cr accumulation at sealing-proximal locations corroborates that H_2 fuel partly leaks through the sealing to generate steam and subsequently $\text{CrO}_2(\text{OH})_2$ vapor in the cathode compartment, to aggravate Cr-poisoning.

A direct link to cathode degradation is difficult to establish, since measurements on a greater extent of sample locations across the cell width would be needed to determine the proportion of high/low poisoned cathode regions. Moreover, to generate a link to degradation, spatially-resolved degradation data (not recorded here) would be a likewise prerequisite to locally-resolved contamination assessment, as the local degradation differs from global degradation in SOFC [17, (A.1)]. Absolute and direct correlations, such as Cr-concentration [$\text{Cr}\mu\text{g}/\text{cm}^2$] versus voltage decay [-\%/time] were reported before in button cell test investigations [12, (ch. 4.1),18], but cannot be extracted from the present work, as the test in stack configuration superimposes other degradation effects, not limited to Cr-poisoning alone.

8.1. Cr-poisoning in (La,Sr)(Co,Fe)O₃ cathodes after 10'000 h SOFC stack testing

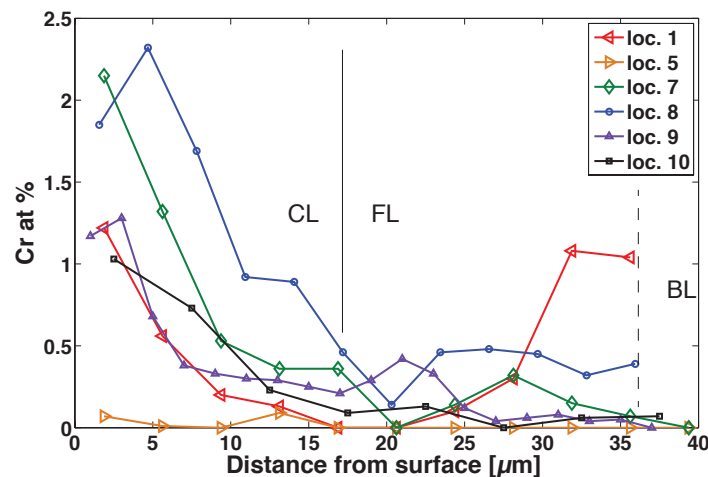


Figure 8.6: Six Cr profiles across the cathode thickness reveal differences in severity (amounts) and shape (distribution) of Cr accumulations.

3.4 Superimposed degradation Besides Cr-poisoning and other well-identified degradation phenomena such as zirconate formation [19] this work aims to shed light on the effect of the following:

- i) Fig. 8.4 having predicted differences in the local water vapor pressure according to the position within the cell, the effect of $p(\text{H}_2\text{O})$ alone on LSCF-based cathode behavior (without interference from Cr) should be discussed. Literature shows high uncertainty among different authors [20-25], reported in tab. 8.3, where statements for (La,Sr)MnO₃- (LSM)-based cathodes are included for comparison purpose. The observations in our present work do not enable, either, to give a direct correlation between water vapor and cathode degradation, other than illustrating a $p(\text{H}_2\text{O})$ -dependent aggravation of the Cr-poisoning phenomenon [6].
- ii) After 10,000 h SOFC operating time, the SO₂ content (in ppb range in environmental air fed to the cathode) is expected to lead to secondary phase formation upon reaction with LSCF-based cathode, as recently reported by Wang *et al.* [26]; i.e. SrSO₄ formation occurs when LSCF is exposed to SO₂. Indeed, also in our work fig. 8.10 identifies S contamination at the air inlet region of the cell (sample location 1), besides Cr. The EDS analysis shown in fig. 8.11 of a single grain of contamination accumulation (within the limitations of SEM-EDS analysis) suggests a combined Cr/S-strontium oxide to be formed in these combined contaminating conditions, as recently reported for LSC- and LSM-based cathodes [27-28, (ch. 7.2, 7.3)].

3.5 Solutions for Cr-poisoning mitigation: The overall air electrode pollution, in this combination of LSCF-based cathode and MnCoFe-protected MIC, remains relatively low, indicating the layer's assembly materials choice to be possible; the Cr-poisoning degradation phenomenon alone does not seem to preclude this cell to reach 40,000 h operation (when

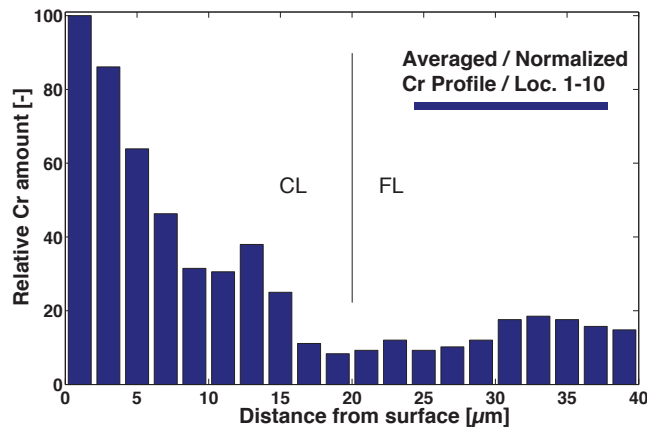


Figure 8.7: Distribution of Cr accumulation, averaged on normalized profiles for sample locations 1,5,7,8,9,10, through the cathode thickness: decreasing amounts in the CL and approximately constant severity within the FL is observed.

Table 8.3: Literature data shows an unclear effect of water vapor alone on LSCF-based cathodes; a similar picture can be drawn for (La,Sr)MnO₃, given here for comparison.

Author Ref.	Cathode Type 1	Cathode Type 2	Condition (T, p(H ₂ O))
J. Guan <i>et al.</i> [20]	LSCF:unclear	LSM/YSZ: no effect	800°C, 3%
A. Hagen <i>et al.</i> [21]	-	LSM/YSZ: partially reversible	750-850°C, 4%
X. Chen <i>et al.</i> [22]	-	LSM: no effect	900°C, 3%
R.R. Liu <i>et al.</i> [23]	LSCF: long-term decomposition	LSM: irreversible decomposition	800°C, 3-20%
J. Nielsen <i>et al.</i> [24]	LSCF/CGO: tolerance / no effect	LSM/YSZ: passivation degradation	750°C, < 13%
E. Bucher <i>et al.</i> [25]	LSCF: oxygen activity decrease		600-700°C, 30-75 RH

considering that other degradation phenomena have contributed to the overall observed -1.4 %/1,000 h stack voltage decay, predominantly by ohmic degradation). Nevertheless, since Cr contamination has been revealed after 9,630 h operation, the following points are open for possible mitigation of the extent of Cr-poisoning for future developments:

- i) Cathode material. Regarding Cr-poisoning, the LSCF cathode presents a sensefull tradeoff between cathodes prone to mainly surface reaction, as for (La,Sr)CoO₃ (LSC) [4, (ch. 6.1)], or those prone to mainly electrochemical-driven deposition like LSM [12, (ch. 4.1)]. In LSC-based cathode materials, densified and bulky SrCrO₄ grains are formed on the electrode surface, leading to conductivity and diffusion limitations as well as possible spallations of adjacent cathode layers (higher thermal expansion coefficient for SrCrO₄) [28, (ch. 7.3)], caused by the high Sr activity in LSC. LSM cathodes, although presenting the lowest Sr activity and hence the lowest reactivity with Cr vapors for La/Sr-based perovskite compositions, suffer from the most severe case of Cr-poisoning, i.e. polarization-induced MnO-driven Cr deposition on electrochemically active cathode triple-phase-boundaries, blocking the oxygen reduction reaction. Alternative Mn/Sr free cathode compositions, like (La)(Ni,Fe)O₃ (LNF) , supposedly Cr-tolerant [29-30], suffer likewise from Cr deposition mechanisms, both electrochemically- and chemically-

8.1. Cr-poisoning in (La,Sr)(Co,Fe)O₃ cathodes after 10'000 h SOFC stack testing

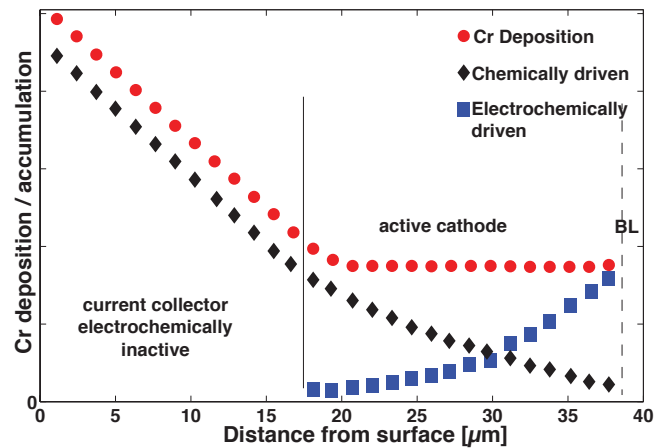


Figure 8.8: The present work suggests the observed profile (red dots - cf fig. 8.7) to result from a combination of electrochemical activity near the FL-electrolyte interface due to oxygen depletion towards this interface (blue squares), with chemical surface reactivity within the entire cathode thickness (black diamonds).

driven as demonstrated by others [31-32, (ch. 5.1)]. A choice left to mitigate the impact of Cr-poisoning might be the increase of the CL thickness to trap Cr in the current collector before reaching electrochemically active cathode regions.

- ii) MIC barrier coating. Since the main part of the cell experienced only small Cr-poisoning, and as the Cr concentration was decreasing faster by LSCF trapping in air inlet regions than the amounts generated by the cathode-proximal MIC, only limited improvement is expected with further protective solutions on the MIC.
- iii) Balance-of-plant (BoP) components. More improvement is expected by decreasing the Cr load, generated by Cr-sources located upstream the cell, of the air inlet flow. It is, however, unreasonable to protect the complete surface of complex-shaped system parts of the BoP, which represents in volume the larger part of an SOFC system. More pragmatic is the implementation of an air-filtering material, acting as chemical trap for Cr vapors generated by upstream system components [33, (ch. 9.1)].
- iv) Sealing materials. Most improvement is expected by decreasing the amount of hydrogen leakage from the anode side into the cathode compartment by perfecting the sealing. Tighter sealing would decrease the water vapor pressure over large parts of the cathode compartment, and therefore mitigate the $p(\text{H}_2\text{O})$ -dependent aggravation of Cr-poisoning.

4 Conclusion

In this work, we systematically applied an objective quantification methodology to picture the severity of Cr-poisoning in an LSCF cathode-based SOFC stack after 10,000 h operation. This approach, combined to the modeling prediction of Cr distribution given by local $p(\text{H}_2\text{O})$ -

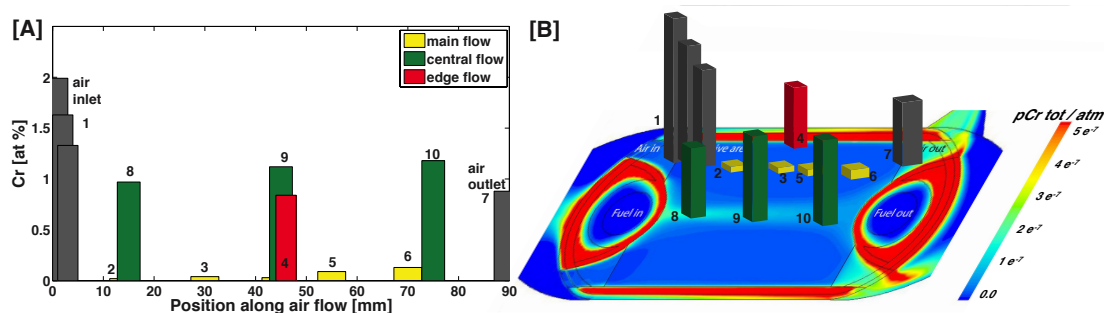


Figure 8.9: (A) Cr amounts determined by EDS scans on 1 mm^2 LSCF surface regions; (B) schematic representation of preferential Cr accumulations at the air inlet and sealing-proximal cathode locations, superimposed to a model prediction of Cr generation; predictions of fuel sealing leakage with associated steam production and subsequent Cr oxyhydroxide generation in the cathode compartment are confirmed by the locally measured Cr amounts.

dependent Cr generation and deposition, allowed the effect and causes of Cr-poisoning to be identified, leading to recommendations for Cr-poisoning mitigation and lifetime improvement.

Acknowledgements

This work was supported by the Swiss SOF-CH-ASE project, cofunded by the Swiss Federal Energy Office (BFE) and swisselectric research. Danièle Laub, Brigitte Greenwood and Nicola Accardo are warmly thanked for experimental work.

References

- 1 C. Comminges, Q. Fu, M. Zahid, N. Yousfi Steiner, O. Bucheli, *Electrochim. Acta.* 59 (2012) 367
- 2 N.H. Menzler, P. Batfalsky, S.M. Gross, V. Shemet, F. Tietz, *ECS Trans.* 35 (2011) 195
- 3 J.A. Schuler, C. Gehrig, Z. Wuillemin, A.J. Schuler, J. Wochele, C. Ludwig, A. Hessler-Wyser, J. Van herle, *J. Power Sources.* 196 (2011) 7225 (ch. 6.2)
- 4 J.A. Schuler, A.J. Schuler, Z. Wuillemin, A. Hessler-Wyser, C. Ludwig, J. Van herle, *ECS Trans.* 35 (2011) 2001 (ch. 6.1)
- 5 O. Thomann, M.H. Pihlatie, J.A. Schuler, O. Himanen, J. Kiviahho, *Electrochem. Solid-State Lett.*, 15 (2012) B35
- 6 K. Hilpert, D. Das, M. Miller, D.H. Peck, R. Weiss, *J. Electrochem. Soc.* 143 (1996) 3642
- 7 Z. Wuillemin, N. Autissier, A. Nakajo, M. Luong, J. Van herle, D. Favrat, *J. Fuel Cell. Sci. Tech.* 5 (2008) 1
- 8 Z. Wuillemin, EPFL Thesis No. 4525 (2009)
- 9 H. Yokokawa, *ECS Trans.* 35 (2011) 207

8.1. Cr-poisoning in (La,Sr)(Co,Fe)O₃ cathodes after 10'000 h SOFC stack testing

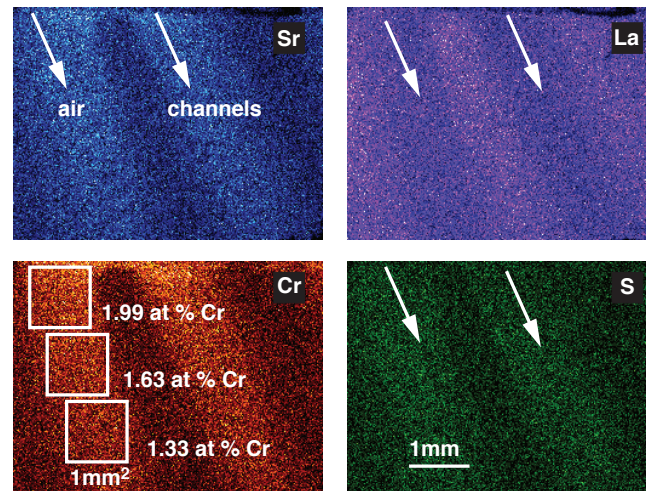


Figure 8.10: SEM-EDS elemental maps on air channels at the air inlet location, with Cr quantification on three 1 mm² regions at location 1 (cf fig. 8.4 and fig. 8.9), indicate upstream-generated Cr/S pollution to decrease along the air flow.

- 10 J.A. Schuler, Z. Wuillemin, A. Hessler-Wyser, J. Van herle, *Electrochem. Solid-State Lett.* 14 (2011) B20 (ch. 7.1)
- 11 J.A. Schuler, P. Tanasini, A. Hessler-Wyser, J. Van herle, *Scr. Mater.* 63 (2010) 895 (ch. 3.1)
- 12 J.A. Schuler, P. Tanasini, A. Hessler-Wyser, C. Comninellis, J. Van herle, *Electrochem. Commun.* 12 (2010) 1682 (ch. 4.1)
- 13 M. Ananyev, A. Gavriluk, D. Bronin, R. Steinberger-Wilckens, J. Mertens, *EFCF Proceeding B04* (2011) 21.
- 14 T. Horita, H. Kishimoto, K. Yamaji, M.E. Brito, T. Shimonosono, D. Cho, M. Izuki, F. Wang, H. Yokokawa, *ECS Trans.* 35 (2011) 511
- 15 X. Chen, L. Zhang, E. Liu, S.P. Jiang, *Int. J. Hydrogen Energ.* 36 (2011) 805
- 16 Z. Lu, J. Hardy, J. Templeton, J. Stevenson, *J. Power Sources*, 198 (2012) 90
- 17 Z. Wuillemin, A. Nakajo, A. Müller, J.A. Schuler, S. Diethelm, J. Van herle, D. Favrat, *ECS Trans.* 25 (2009) 457 (appendix 1)
- 18 M. Krumpelt, T.A. Cruse, B.J. Ingram, J.L. Routbort, S. Wang, P.A. Salvador, G. Chen, *J. Electrochem. Soc.* 157 (2010) B228
- 19 A. Hessler-Wyser, Z. Wuillemin, J.A. Schuler, A. Faes, J. Van herle, *J. Mater. Sci.* 46 (2011) 4532
- 20 J. Guan, S. Zecevic, Y. Liu, P. Lam, R. Klug, M. Alinger, S. Taylor, B. Ramamurthi, R. Sarrafi-Nour, S. Renou, *ECS Trans.* 7 (2007) 405

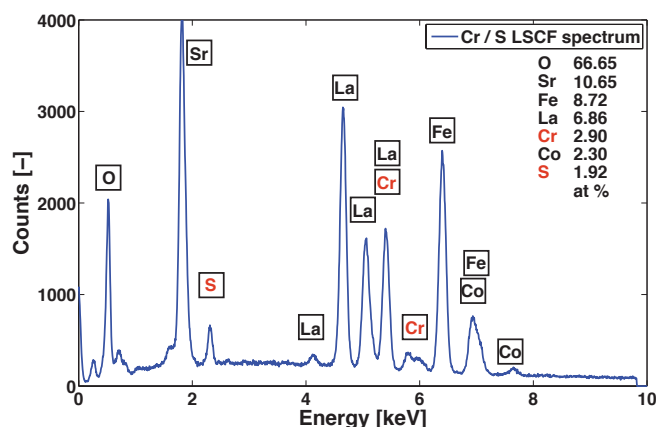


Figure 8.11: EDS spectrum of a single grain of contamination-accumulation reveals the formation of an S-added Sr-chromate phase upon combined Cr/S-poisoning of LSCF

- 21 A. Hagen, M. Chen, K. Neufeld, Y. L. Liu, ECS Trans. 25 (2009) 439
- 22 X. Chen, Y. Zhen, J. Li, S.P. Jiang, Int. J. Hydrogen Energ. 35 (2010) 2477
- 23 R.R. Liu, S.H. Kim, S. Taniguchi, T. Oshima, Y. Shiratori, K. Ito, K. Sasaki, J. Power Sources, 196 (2011) 7090
- 24 J. Nielsen, A. Hagen, Y.L. Liu, Solid State Ionics, 181 (2010) 517
- 25 E. Bucher, A. Egger, M. Yang, W. Sitte, EFCF Proceeding 0702 (2010) 1
- 26 F. Wang, K. Yamaji, D-H. Cho, T. Shimonosono, H. Kishimoto, M.E. Brito, T. Horita, H. Yokokawa, J. Electrochem. Soc. 158 (2011) B1391
- 27 J.A. Schuler, Z. Wuillemin, A. Hessler-Wyser, J. Van herle, ECS Trans. 25 (2009) 2845 (ch.7.2)
- 28 J.A. Schuler, H. Yokokawa, C.F. Calderone, Q. Jeangros, Z. Wuillemin, A. Hessler-Wyser, J. Van herle, J. Power Sources. (2012), 201 (2012) 112 (ch. 7.3)
- 29 T. Komatsu, Y. Yoshida, K. Wantanabe, R. Chiba, H. Taguchi, H. Orui, H. Arai, J. Power Sources, 195 (2010) 5601
- 30 Y. Yoshida, R. Chiba, T. Komatsu, M. Yokoo, K. Hayashi, H. Orui, H. Arai, ECS Trans. 35 (2011) 2313
- 31 M.K. Stodolny, B.A. Boukamp, F.P.F. van Berkel, ECS Trans. 35 (2011) 2035
- 32 J.A. Schuler, H. Luebbe, A. Hessler-Wyser, J. Van herle, J. Power Sources, 213 (2012) 223 (ch. 5.1)
- 33 J.A. Schuler, A.J. Schuler, D. Penner, A. Hessler-Wyser, C. Ludwig, J. Van herle, Electrochem. Solid-State Lett. 14 (2011) B132 (ch. 9.1)

9 Counteracting strategies

Electrochemical and Solid-State Letters **14** (2011) B132

9.1 Mitigating Cr contamination by hot air filtering in solid oxide fuel cells

J. Andreas Schuler^{a,b}, Albert J. Schuler^c, Dirk Penner^d, Aïcha Hessler-Wyser^b,
Christian Ludwig^{c,e}, Jan Van herle^a

^a *Laboratoire d'Énergie Industrielle (LENI), École Polytechnique Fédérale de Lausanne (EPFL), 1015 Lausanne, Switzerland*

^b *Centre Interdisciplinaire de Microscopie Electronique (CIME), École Polytechnique Fédérale de Lausanne (EPFL), 1015 Lausanne, Switzerland*

^c *Labor für Bioenergie und Katalyse (LBK), Paul Scherrer Institut (PSI), 5232 Villigen, Switzerland*

^d *Institute of Materials and Process Engineering (IMPE), Zürcher Hochschule für Angewandte Wissenschaften, 8400 Winterthur, Switzerland*

^e *Institut d'Ingénierie de l'Environnement (ENAC-IIE), École Polytechnique Fédérale de Lausanne (EPFL), 1015 Lausanne, Switzerland*

Cr contamination, generated by system components located upstream a solid oxide fuel cell (SOFC) and responsible for Cr-poisoning induced air electrode performance degradation, must be suppressed by hindering the access of Cr pollutants to the cathode compartment. For this purpose, we developed an air filter, based on a (La,Sr)CoO₃-coated ceramic foam, which was evaluated on its Cr-trapping potential within an SOFC system. An *in situ* measurement based on a novel hot air sampling technique indicated a 7-fold decrease of the Cr contaminating level after the installation of a Cr getter filter, which should significantly extend SOFC lifetime.

1 Introduction

The so-called Cr-poisoning phenomenon involves deposition of volatile Cr species at cathode regions active for oxygen reduction, with subsequent performance degradation of solid oxide fuel cells (SOFC) [1]. Taniguchi *et al.*, after their pioneering work on this degradation effect, proposed a second cathode layer of La_2O_3 to protect the electrode from Cr-vapors that emanate from SOFC-proximal Cr-containing compounds [2], where Cr vapors react to form LaCrO_3 . Despite the high electronic conductivity of ca. $0.3 \text{ S}\cdot\text{cm}^{-1}$ at $800 \text{ }^\circ\text{C}$ of this phase [3], which found application in ceramic interconnects, such a strategy shows limited feasibility due to low reactivity of La-oxide.

Contrarily, with current collection layers (CCL) based on well-conducting cobaltite perovskite compositions, the protection of active cathode regions results by the formation of the low conducting SrCrO_4 phase (ca. $0.004 \text{ S}\cdot\text{cm}^{-1}$ at $800 \text{ }^\circ\text{C}$). The formation of densified SrCrO_4 structures at CCL surfaces leads to gas diffusion limitations, especially in the case of direct contact between metallic interconnect (MIC) ribs and the perovskite phase [4, (ch. 7.2)], or in flow channels fed by air in contact with Cr emitting sources located upstream the cell [5].

Whereas protective solutions to limit Cr evaporation are extensively used inside SOFC stacks, by their application on planar MIC, it is unreasonable to build complex-shaped system parts of the balance-of-plant (BoP), which represent in volume the larger part of SOFC systems, with expensive materials showing limited Cr evaporation or to protect cheaper materials over their complete surface.

More pragmatic is to keep BoP-generated Cr distant from electrode proximity, which is the approach proposed in this work, by the implementation of an air-filtering material, acting as chemical trap for Cr vapors generated by upstream system components. MIC-induced contamination, normally suppressed by an appropriate coating, is not addressed.

The difficulties of Cr contamination level assessment under SOFC operating conditions were highlighted recently by the authors [6, (ch. 6.1)], who first proposed methods for direct quantification of Cr within SOFC systems [7, (ch. 6.2),8]. Using a hot air sampling technique for Cr analysis, this study shows *in situ* proof of the trapping efficiency of the developed hot air filter in an SOFC system environment.

2 Experimental

The filter development is based on a ceramic foam obtained by the replication of a polyurethane (PU) template using an alumina slurry prepared by ball-milling 20 g Al_2O_3 powder (Rio Tinto Alcan, Fr), 2 g AlPO_4 (FFB 705 Bundeheim, De), 0.25 g dispersant (Ce 64 Zschimmer & Schwarz, De), 0.25 g wetting agent (KM 2030 Zschimmer & Schwarz, De) and 8 g demineralized water. The PU template, with pentagone-shaped pores of ca. 2 mm^2 is shaped, taking into account the sintering shrinkage of ca. 12 %, prior to impregnation. After a drying and phosphatization step of 5 h at $200 \text{ }^\circ\text{C}$ (heating rate $50 \text{ }^\circ\text{C}/\text{h}$), giving mechanical strength to the ceramic skeleton at low temperature to prevent the structure from breaking during the polymer burnout, a second slurry coating (same as above, with only ca. 5 g Al_2O_3) is applied to strengthen the interconnectivities between the foam's cell walls. Sintering at $100 \text{ }^\circ\text{C}/\text{h}$ to $600 \text{ }^\circ\text{C}$ (polymer

9.1. Mitigating Cr contamination by hot air filtering in solid oxide fuel cells

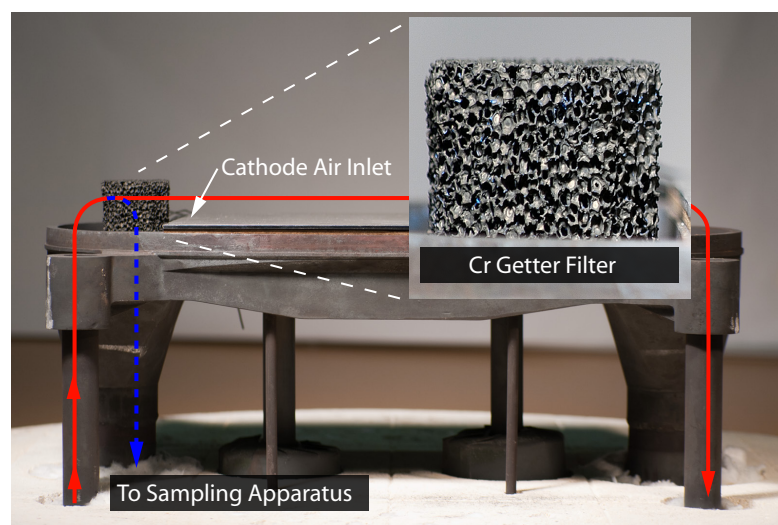


Figure 9.1: An LSC-coated Al_2O_3 -based foam, placed at the cathode air inlet location of an SOFC test bench (lower flange shown here), acts as Cr getter. Heat-exchanger, tubing and housing high-temperature alloy elements saturate the hot air flux (thick arrow) with Cr-vapors. A part of the airflow (dashed arrow) is withdrawn through the air filter and post-analyzed for residual Cr.

burnout) and then at $150\text{ }^\circ\text{C}/\text{h}$ to $1500\text{ }^\circ\text{C}$ for 2 h (alumina densification) yields a cellular ceramic with a relative density ρ_c/ρ_s of 15 % (ρ_s and ρ_c are the ceramic and foam density). The alumina foam is coated with $(\text{La}_{0.5}\text{Sr}_{0.5})\text{CoO}_3$ (LSC, Praxair, US) by applying a slurry of 4 g LSC, 3 g ethylcellulose / terpineol (proportions published elsewhere [9, (A.2)]) and 7 g isopropanol, prior to sintering at $900\text{ }^\circ\text{C}$ for 2 h.

The filter of ca. 100 cm^3 volume (30 g foam; 4 g LSC) is installed (cf. Fig. 9.1) just upstream the cathode air inlet region in an SOFC test bench [10, (A.1)], supplied with an air flux of $20\text{ L}\cdot\text{min}^{-1}$ and 5 % relative humidity at room temperature. This airflow would be needed to run a 200 cm^2 cell for which the test bench was developed. The evaluation of the filter is however done without the simultaneous testing of an SOFC, as devices for electrochemical measurements are replaced by air sampling equipment in this work. It was previously shown [7, (ch. 6.2)] that in this test bench, large surfaces (780 cm^2) of Cr-containing alloys (1.4928, 1.4849 and Incoloy 800) saturate the air fed to the cathode with Cr vapors ($9\cdot 10^{-9}\text{ atm}$).

A part of the hot air flux ($3.5\text{ L}\cdot\text{min}^{-1}$) is withdrawn through the filter, using an air sampling technique, based on a liquid quench concept [11] and described earlier [6, (ch. 6.1)]. The quench liquid is a 0.1 Mol HNO_3 solution; the base case measurement (cf Fig. 9.1) corresponds to a measurement of a previous work [6, (ch. 6.1)] done with the same acid concentration.

Quantification of Cr is done by chemical analysis, of a solution of condensed Cr species collected and digested by the quench liquid, on two inductively-coupled plasma optical emission spectrometers (ICP-OES) (PerkinElmer, model Optima3300DV, US and Shimadzu, model ICPE-9000, Jp); direct comparison of measurement results obtained on both spectrometers gives a precision of ca. $3\text{ }\mu\text{g}\cdot\text{L}^{-1}$ of this analysis.

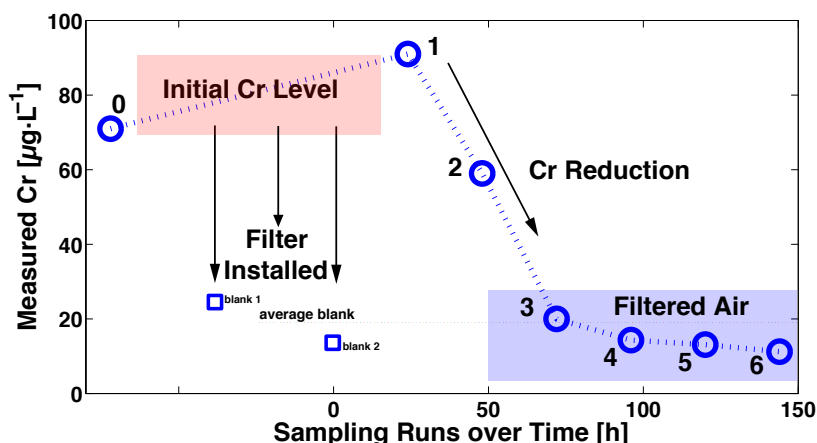


Figure 9.2: Reduction of Cr contamination by an LSC-based Cr getter. From initially high Cr amounts quantified by a hot air sampling technique (sampling run 0 prior to filter installation; runs 1 and 2 after re-mobilization of Cr residue in the sampling capillary), the measured Cr contamination levels decreased 7-fold and drop below the blank value of the measurement technique.

3 Results and discussion

Hot gas sampling results are summarized in Fig. 9.2. A base case measurement, labeled 0, performed before installing the filter, indicates the collected Cr amount from an airflow saturated with Cr vapors to be around $70 \mu\text{g}\cdot\text{L}^{-1}$.

Direct measurements of the compressed air (blank 1), as well as the air sent through the system without heating (blank 2), set an average blank value at ca. $20 \mu\text{g}\cdot\text{L}^{-1}$, and indicate the sampling device to accumulate Cr from previous runs with high Cr load that is washed out during runs with low Cr charge.

The first two measurements (labeled 1 and 2 in Fig. 9.2) performed with the filter installed were taken immediately after heating up to 800°C . Nevertheless, high Cr values were still observed at this initial stage. This is due to the re-mobilization of condensed Cr, which resulted from cleaning the sampling capillary with a concentrated HNO_3 solution after the base case measurement. As a result, Cr, accumulated during measurement 0 and earlier experiments [6, (ch. 6.1)] on the inner walls of the hot sampling capillary between the air filter and the liquid quench, was released at high temperature after the cleaning step and increased the Cr amounts in measurements 1 and 2.

The following sampling runs 3-6 drop to low Cr amounts, even below the blank value and with a tendency to decrease below $10 \mu\text{g}\cdot\text{L}^{-1}$, indicating Cr amounts passing the filter being below the quantity which is washed-out from the sampling device during the measurement. The filter therefore yields at least a 7-fold decrease in Cr contamination level.

SOFC lifetime extension is expected if the cathode flow feed is filtered using a Cr getter based on LSC, or on alkaline/rare earth oxides or carbonates [8] and if the filter porosity

9.1. Mitigating Cr contamination by hot air filtering in solid oxide fuel cells

enables to limit pressure drops. The Sr content of the LSC coating reacts with Cr vapors to form SrCrO_4 . Assuming Sr availability for reaction until its consumption and assuming that the entire air flux is filtered (complete Cr depletion), the trapping expectancy can be estimated¹. Cr quantification from a previous study [7, (ch. 6.2)], in *post-test* observations of a cell tested for 1900 h in the same test bench as described above, enabled to determine that 0.04g Cr accumulated over this time span and under the same experimental conditions. The Sr amounts used here (0.8 g Sr) should therefore ensure a filter lifetime approaching 40'000 h, which is the target lifetime needed for SOFC commercialization.

Another application potential for this Cr-getter development is in testing of protective MIC coatings. Their efficiency is generally evaluated by their impact on cell performance, i.e. on the extent of Cr-poisoning-caused cathode degradation. This response is however often hidden by superimposed degradation effects, in particular by contamination from system components. If air filtering enables to mask or reduce system contribution to degradation, MIC coatings can be more objectively evaluated.

Finally, air filtering should find application to remove additional air side contaminants like sulfur, silicon and alkali elements (Na,K) [7,12, (ch. 6.2, A.1)], promoted e.g. by the high activity of LSC to form SrSO_4 in presence of sulfur [4, (ch. 7.2)]. This will require a separate evaluation, which the presently Ti-based sampling apparatus [6, (ch. 6.1)] can suitably carry out; traditional contaminant vapor measurements rely on condensation on quartz compounds, therefore precluding Si analysis.

4 Conclusions

An *in situ* proof-of-concept for hot air filtering to decrease Cr contaminating levels is demonstrated. Application of the idea should lead to lifetime enhancement in SOFC systems by decreasing BoP-generated Cr-poisoning. The concept to use rare/alkaline earth oxides as Cr getter is simple to apply, since such compounds are known to trap Cr vapors in reactive cathode layers. The previous lack of adapted tools for Cr quantification in a hot air flux probably complicated so far the evaluation of Cr-getter developments. This study has shown a way forward to address this development.

Acknowledgements

The Swiss Federal Energy Office (contract 153569), the Competence Center Energy and Mobility (project 705028) and Swisselectric research (project TREPAS) are acknowledged for financial support. Warmly thanked are also: Andreas Mai (HEXIS Ltd) and Zacharie Wullemin (HTceramix-SOFCpower) for idea exchange on the industry needs; Jacques Castano (LC-EPFL), Jean-David Teuscher (CEAL-EPFL), Jean-Baptiste Carré (LENI-EPFL) for technical help.

¹This estimation neglects the lower reactivity of Sr-depleted LSC with Cr (lower trapping rate), or the reactivity of the decomposition products LaCoO_3 and CoO with Cr (higher trapping amount by LaCrO_3 and CoCr_2O_4 formation).

References

- 1 S. Taniguchi, M. Kadowaki, H. Kawamura, T. Yasuo, Y. Akiyama, Y. Miyake, T. Saitoh, J. Power Sources, 55 73 (1995).
- 2 S. Taniguchi, M. Kadowaki, T. Yasuo, Y. Akiyama, Y. Itoh, Y. Miyake, K.Nishio, Denki Kagaku, 64 568 (1996).
- 3 S.P. Jiang, L. Liu, K.P. Ong, P. Wu, J. Li, J. Pu, J. Power Sources, 176 82 (2008).
- 4 J.A. Schuler, Z. Wuillemin, A. Hessler-Wyser, J. Van herle, ECS Trans. 25 2845 (2009). (ch. 7.2)
- 5 N.H. Menzler, P. Batfalsky, S.M. Gross. V. Shemet, F. Tietz, ECS Trans. 35 195 (2011).
- 6 J.A. Schuler, A.J. Schuler, Z. Wuillemin, A. Hessler-Wyser, C. Ludwig, J. Van herle, ECS Trans., 35 2001 (2011). (ch. 6.1)
- 7 J.A. Schuler, C. Gehrig, Z. Wuillemin, A.J. Schuler, J. Wochele, C. Ludwig, A. Hessler-Wyser, J. Van herle, J. Power Sources, 196 7225 (2011). (ch. 6.2)
- 8 O. Thomann, M.H. Pihlatie, J.A. Schuler, O. Himanen, J. Kiviaho, ECS Trans., 35 2609 (2011).
- 9 P. Tanasini, J.A. Schuler, Z. Wuillemin, M.L. Ben Ameer, C. Comminellis, J. Van herle, J. Power Sources, 196 7097 (2011). (appendix 2)
- 10 Z. Wuillemin, A. Nakajo, A. Müller, J.A. Schuler, S. Diethelm, J. Van herle, D. Favrat, ECS Trans. 25 457 (2009). (appendix 1)
- 11 M. Koebel and M. Elsener, J. Chromatogr., A, 689 164 (1995).
- 12 J.A. Schuler, Z. Wuillemin, A. Hessler-Wyser, J. Van herle, Electrochem. Solid-State Lett. 14 B20 (2011) (ch. 7.1)

10 Synthesis

The main outcomes of this thesis are described in the three following sections on: i) measurement solutions, ii) understanding of Cr-poisoning mechanisms and iii) counteracting solutions, developed within this work at three different scales (electrode, stack and system).

10.1 Cathode material level

Overcoming measurement difficulties

The availability at EPFL-LENI of multiple samples, which have been identically exposed to SOFC operating conditions, apart from the controlled variation of a single parameter, fostered a strong backbone to start this thesis with comparative studies between Cr-poisoned cathodes. Ideal samples stemmed from the multi-cathode tests [110, 54], which ensured identical operating conditions with the added benefit of decreased total experimental time compared to repetitive button cell testing. *Post-test* analysis of such segmented single cell tests handed insights in LSM-based cathode behavior under deliberate Cr-contaminating conditions [44]. The LSM-YSZ cathode samples from the segmented repeat-unit [53, 112], for which in addition electrochemical performance and degradation was locally resolved, yielded comprehension of the cathode material within a technically relevant SOFC assembly, including LSC as a current collecting cathode material [49, 46, 50]. The LSCF-based cathode samples, finally, for the post-operation study after 10'000 h stack testing [111], provided understanding of the mixed ionic electronic conducting LSCF cathode material [51].

The measurement issues, related to quantitative and not only qualitative detection of low Cr amounts inhomogeneously distributed within the cathode (both within the thickness and gas channels), were addressed using EDS, although strong overlaps of Cr with the other cathode-constituting elements in EDS spectra are present, since this technique promised high acquisition rates needed for fast analysis purpose. The rapid Cr quantification was enabled by the use of the lanthanum peak height ratio $L_{\beta 2.15}/L_{\alpha 1}$, as previously suggested by others [113, 7, 8, 9] but translated here into a quantified empirical relation instead of only a simple Cr presence indicator [43]. The precision, accuracy and effort (time-consumption) of such an EDS measurement could be perfected, as shown by current investigations [114] briefly outlined in the outlook chapter (cf outlook section: 11.2); further EDS data treatments, such as principal component analysis [115, 116, 117], or maximum pixel spectrum techniques [118],

promise noise rejection and data quality enhancement.

The Cr profiling methodology [44] is in summary a simple EDS line scan with a line width of the mapped window (space-averaging thin cathode slices), therefore providing better statistical meaning compared to a line width given by the escape volume of the generated X-rays. Owing to its simple applicability, this technique was systematically applied on various cathode samples to objectively and quantitatively depict the Cr distribution within the cathode thickness. The $L_{\beta 2.15}/L_{\alpha 1}$ peak height ratio was used for quantified Cr profiling in LSM-YSZ composite cathodes [44], whereas standard EDS software quantification enabled the determination of Cr amounts for Mn-free perovskite/nickelate compositions (LSC, LSCF, NNO)[46, 51, 119, 45]. The profiling methodology could moreover be automatized (cf. section: 11.2) using additional software applications [114]. By yielding standardized and quantitative Cr profiles, such a methodology is seen as a promising data generation technique, needed for the experimental validation of mathematical models predicting Cr-poisoning.

Addressing Cr-poisoning mechanisms

For LSM-based SOFC cathodes, Cr deposition can be divided into two phenomena: i) chemical reaction corresponding to the incorporation of Cr into the perovskite lattice; and ii) the electrochemically enhanced deposition at active cathode sites [21].

- for case (i) thermodynamic considerations for Cr-poisoning of LSM-based cathodes include two steps. First, dissolution of Cr into the B-site of the LSM perovskite lattice. Since the LSM lattice allows A-site deficiency, such incorporation takes place without any other chemical process such as the precipitation of secondary phases. Secondly, by lowering the oxygen partial pressure, the allowance of the A-site deficiency becomes narrow so that secondary Cr_2O_3 or $(\text{Cr,Mn})_3\text{O}_4$ phases precipitate (depending on the $p\text{O}_2$) [120, 121].
- for case (ii), the actual deposition mechanism is actively debated in literature, whether Cr reacts with polarization-induced Mn^{2+} -nuclei or via a direct reductive deposition [6, 5]. The observed electrochemically-driven Cr accumulation in the Mn-free NNO cathodes, in combination with the fact that enhanced amounts of Cr are confined to electrochemically active Mn-containing cathode regions, compared to Mn-free near-interface regions in similar conditions, suggests both deposition mechanisms to be involved in Cr-poisoning of LSM.

Not fully ascertained either is the actual performance degradation cause of Cr-poisoning in LSM-YSZ composite cathodes. On the one hand, pore-LSM-YSZ TPB blockage by Cr accumulations is suggested to provoke cathode performance decay. This is currently under investigation within another collaborative work [122] that is based on the 3D reconstruction [39] of FIB-slices [123] (cf. section: 11.2). On the other hand, electrode degradation could result from LSM decomposition, mainly driven by the Mn-consumption to form Cr,Mn spinel phases [124, 16, 125].

The literature commonly only states "LSCF bulk Cr-poisoning" [126, 127], indicating that a clear picture of the Cr-poisoning effect is missing for LSCF-based cathodes. This work quantitatively demonstrated the Cr-poisoning to include both chemical (i) and electrochemically-driven deposition (ii) mechanisms, corroborating other studies [19, 128]. The main degradation contribution originates from the chemical SrCrO_4 formation with subsequent Sr-depletion of the remaining perovskite compounds. Diffusion and conductivity limitations result from the Cr-poisoned LSCF cathode surface regions. Since the nature and phase of the Cr accumulations in electrochemically active cathode parts were not confirmed within this work, the actual degradation causes of near electrolyte-cathode interface zones are not fully ascertained. In LSC cathodes, the chemical reaction of SrO with volatile Cr vapor species to form SrCrO_4 dominates. This Cr deposition is mainly confined to surface-proximal cathode regions, resulting in strong diffusion limitations besides the conductivity decrease brought by the Sr-depletion of the remaining perovskite material and the low conductivity of the chromate phase itself. In addition, SrCrO_4 has a TEC largely in mismatch with SOFC materials [129], as suggested by the delaminations within the LSM-based cathode surrounding a Sr-chromate phase [50].

The alternative cathode material $\text{Nd}_{1.95}\text{NiO}_{4+\delta}$ [130] likewise suffers from chromate formation NdCrO_4 [131]; its formation is suggested not to occur spontaneously but to be driven by the electrochemical activity. Moreover, a similar degradation effect was identified, i.e. the chromate formation-caused Nd-depletion triggers the NNO decomposition into more stable but less performing phases [119].

Solving the degradation issue

In LSM-based cathode materials, where the electrochemically-driven Cr-deposition dominates, with subsequent Cr accumulations in near electrolyte-cathode interface regions comprising the active TPB, mitigation of the Cr-caused degradation effect is predicted by the extension of the active cathode region [132]. Modeling predictions, based on percolation theory [133] with subsequent experimental verifications [110], have shown the replacement of Y by Sc-doping of zirconia in LSM-based composites cathodes to improve the effective ionic current [134]. Such cathodes, with a largely extended electrochemically active region, have yielded experimental performance stability over time-spans of about 2'000 h under deliberate Cr-poisoning conditions, with subsequent observation of an outspreaded Cr-profile in post-operation analysis.

Decreasing the cathode overpotential is likewise suggested to mitigate the Cr-poisoning in LSM-based cathodes by lowering its driving force, independently whether the Cr-deposition is considered to occur via the polarization-driven Mn^{2+} nucleus or the direct electrochemical reduction. Our findings corroborate the following statement [124]: severe cell voltage degradation due to Cr-poisoning of LSM cathodes (especially in the functional layer) can be alleviated by selecting the proper type of operating conditions, where the cathode potential is in favor of the oxygen reduction and not the spinel formation with subsequent LSM decomposition. In addition, lower current density operation was found to favor the cathode stability also independently of Cr-poisoning [135, 136].

An open question remains, concerning Mn-doping of YSZ [137] to prevent zirconate formation [138, 139], i.e. what tradeoff to expect between potentially enhanced Mn-nucleus-induced Cr deposition [140] and the zirconate formation causing performance degradation that increases the cathode overpotential. Mn-doping of YSZ is suggested to prevent Mn-dissolution into YSZ from LSM [141], thus preventing understoichiometric LSM decomposition at low pO_2 . On the one hand, Mn-doping is not expected to drastically affect the zirconia conductivity [142, 143]; on the other hand, MnO might precipitate under low pO_2 in active cathode regions.

Both the extension of electrochemically active regions and the lowering of the cathode overpotential are expected from mixed ionic electronic conducting and better performing cobaltite-based cathode materials, which should prevent Cr accumulations confined to the electrolyte-interface regions. These more reactive cathodes present however an enhanced SrO activity with subsequent $SrCrO_4$ formation, mainly confined to the surface, in particular for LSC. The LSCF cathode seems therefore to present the best tradeoff between chemical activity and electrochemical activity, with an outspreaded Cr accumulation within the cathode thickness and not with concentrated Cr amounts at the interface or surface.

Total prevention of Cr-poisoning, by the use of alternative, Sr-free MIEC, supposedly tolerant cathode compositions like LNF [18, 144, 145], was recently demonstrated to be unlikely [146, 147, 119]. Even the cathode material Nd-nickelate [148, 149, 150] failed to prove its tolerance towards Cr-poisoning [119]; owing to its high impurity loading, wide application in SOFC technology seems at present precluded for this yet immature material.

10.2 Cell and repeat-unit level

Modeling guidance

Open literature only provides few successful post-operation studies of SOFC stacks after long-term testing ($> 5'000$ h) [151, 152, 153]. The availability of an LSCF-based stack that has been monitored over about $10'000$ h [111] for *post-test* investigations offered therefore unique insights into the cell behavior under real SOFC operating conditions.

Similarly, the segmented cell that has been tested over $2'000$ h, thus cumulating a total of $36'000$ h monitoring for the 18 elements constituting the segmented cell [53, 112], also provided a unique experimental data set. New hurdles for Cr-accumulation quantification in post-operation studies resulted from the larger size with non-homogenous flow path (due to the GDL patterning) of these repeat-units, compared to button cell tests.

Only the prior knowledge of possible Cr locations, the so-called compound formation areas [154], i.e. the preferential Cr accumulation in relation to electric path and gaseous channels, enabled the success of the Cr-poisoning investigations; for both the LSCF $10'000$ h stack test and the $2'000$ h LSM-based segmented repeat-unit, modeling results from Z. Wuillemin [112] provided an ideal starting point. Since a total of 6/10 and 8/18 cross-section/surface samples were investigated for the 10 kh stack and the 2 kh segmented cell, respectively, the utility of our Cr detection methodology, with low time and cost-intensity, is seen to be strengthened.

Also for TEM investigations at higher magnification, to identify and isolate additional degradation mechanisms [155], prior knowledge of zone of interest locations facilitated the *post-test* analysis. The combination of in depth SEM analysis with the subsequent use of FIB for thin lamellae preparation, yielding TEM samples, resulted in further publications [48, 50, 119].

Link to degradation

The LSCF cell tested over 10'000 h [111] endured -1.4% voltage loss per 1000h, including all degradation phenomena, of which only $1/10^{th}$ was due to electrode polarisation increase. This result encouragingly suggests that 40'000h operation, with respect to the cathode lifetime alone against Cr-poisoning, looks well achievable for SOFC stacks, the more since additional solutions against Cr-poisoning can be implemented [51].

The high ohmic resistance increase [111] indicates MIC oxidation [156] to be one of the major contributions to the steady state degradation [70, 92, 157] on the cathodic half-cell side; for electrolyte-supported SOFC technology, the conductivity decrease of zirconia-based electrolytes [88, 89, 90, 91] can be added to the performance losses.

For the LSM-YSZ composite cathode-based segmented cell, the electrochemical degradation signatures could be correlated mainly to exogenous contaminants, similarly suggesting the repeat-unit (with adequate MIC-protection) Cr-poisoning not to be the major lifetime-limiting degradation phenomenon, although a direct correlation between Cr-amounts of the main part of the cell (the exogenous pollutants mainly contaminated the air inlet regions, whereas the main part only experienced small amounts of Cr) and the global performance decrease (about 1 % voltage decay per 1000 h) could not be established.

For button cell experiments [44], we were among the first [125] to quantitatively correlate Cr contaminant amounts to degradation rates, where others [158, 159] failed to do so, despite sharing a systematic approach but without an objective and precise Cr quantification methodology [43]. For unprotected LSM-YSZ cathodes, roughly 1 at% and 0.3 at% Cr presence in the cathode causes (total) cell voltage degradation of -2%/1000h and -1%/1000h, respectively. The comparison to protected LSCF-CGO (by LSCF) and LSM-YSZ (by LSC) confirms that those cathodes appear well armed for long durability.

Since in technically reasonable cathode assemblies the Cr-poisoning phenomenon was revealed to be rather low, acceleration of the degradation effect [128, 22], with the use of water vapor via the enhanced oxyhydroxide formation [97], was initially envisaged. The post-operation analysis of the 10'000 h test revealed a Cr-poisoning aggravation caused by sealing leaking-induced hydrogen penetration into the cathode compartment with subsequent steam formation [160]; the effect of water vapor on the cathode behavior remains however unclear [161, 162, 28, 163, 164, 165, 166, 167], precluding from rigorous accelerated testing of the Cr-poisoning effect by steam addition.

Perfecting cell assembly

Severe cell voltage degradation due to Cr-poisoning can be alleviated by selecting the proper type of chromium source, with only low resulting partial pressures of $\text{Cr}^{(VI)}$ volatile species [124], i.e. a proper MIC alloy composition with an adequate barrier coating. The low severity of Cr-poisoning in the LSCF 10'000h cell, compared to short-term LSCF investigations with

non-coated MIC [12], indicates an appropriate MIC protection with the $(\text{Mn,Co,Fe})_3\text{O}_4$ -based spinel coating [106].

MIC-cathode contact and current collector layers, capturing the $\text{Cr}^{(VI)}$ species to avoid their penetration into electrochemical active cathode regions [124], have been alleviating options since the very early investigations of Cr-poisoning [168]. Our findings showed the LSC and LSCF cathode-proximal Cr-trapping layers to offer protective properties against Cr-poisoning [46, 51].

Since hydrogen leakage through the sealing with subsequent steam generation in the cathode compartment has been shown to aggravate the extent of Cr-poisoning [51], sealing perfecting is seen as a key-issue in the search for Cr-poisoning mitigation. This finding has not been mentioned before in open literature, which mainly concentrated on MIC coating developments with the goal of the extension of Cr-poisoning-limited lifetime.

Reversed bias pulses are seen as possible regenerative acting on SOFC after the attack by Cr-poisoning species. Current interruptions [27] as well as inverse polarization [169] possibly favor the re-evaporation of accumulated Cr-oxides. The use of a gadolinium-doped ceria buffer layer promises enhanced re-evaporation by providing H^+ proton species under reversed bias (cf. section: 11.2), hence favoring the Cr evaporation in the form of Cr oxyhydroxide [169].

10.3 SOFC system level

Trace contamination analysis

Cell scale elemental EDS profiling, i.e. large dimensions for SEM analysis, by space-averaging mm^2 cathode surfaces, enabled to reveal the distribution of pollutants on the air side of an SOFC and to distinguish between endogenous and exogenous contaminants. In addition, their source location was pointed out to be located upstream of the cell for Cr, S and Si for both the segmented and the 10'000 h cells (Si not shown for the LSCF-based cell [51]).

The investigations concerning Si contamination, usually attributed to raw materials impurity [170, 14, 171, 172, 173], illustrated the need of additional chemical tricks to bypass EDS quantification difficulties, i.e. the Si overlap with Sr in the EDS spectrum was overcome by the dissolution of the perovskite content of the LSM-YSZ composite cathode [48].

Sulfur contamination, known as poisonous species for anodes [174] as well as for perovskites in other applications [175], was recently identified as SOFC cathode pollutant in button cell tests [176, 177, 163, 178, 179]. Our study revealed the formation of SrSO_4 upon reaction of cathode materials with sulfur contamination under real SOFC operating conditions [49] and not only in model experiments. The identification of sulfur poisoning in the LSCF 10'000 h test, which had been performed outside our laboratory, corroborates the importance of chapter 7, where the investigations of severe stack-component-caused sulfur contamination enables to assess long-term behavior of SOFC cathode materials with SO_2 contents vehicled by the environmental air.

Cell-proximal BoP components had already be revealed to contaminate SOFC cathodes [180]; we proposed a holistic approach for Cr contamination assessment within a complete SOFC

system [47].

With the hot air sampling technique, based on a liquid quench concept [181] and technically upgraded within this work, an *in situ* quantification of Cr vapor species was first made possible [46], hence enabling their profiling within the complete air flow path in an SOFC system, i.e. from their oxidation, evaporation, transport, deposition to their evacuation [47]. In contrast to other Cr volatilization measurements [32, 34, 95], including novel measurement methods [182, 36, 35], based on the analysis of metallic sample coupons only, our sampling techniques [183, 184, 47, 46] enabled a direct measurement within a complex-shaped BoP system or system component. In addition, contrarily to all aforementioned Cr volatilization measurement techniques, our hot air sampling device comprises a Si-free experimental assembly, which enabled the identification of air-vehicled exogenous Si contamination as well, hence corroborating our findings concerning the origin of upstream-generated cathode pollutants, other than only chromium.

Superimposed degradation effects

Contaminating species, generated upstream of the cell, additionally affect SOFC performance evolution, complicating correlations between Cr-poisoning alone and degradation rates, as outlined as follows:

Cr contaminations, generated by MIC and BoP components, although likewise affecting the cathode, impose different alleviating strategies. The removal of BoP-induced Cr pollution is a prerequisite for the objective study of MIC corrosion caused Cr-poisoning in laboratory-scale experiments.

Exogenous silicon poisoning, with the subsequent amorphous glass-formation within the cathode, not directly affects the Cr-poisoning mechanisms, but additionally blocks the oxygen incorporation into YSZ, in the case of a two-step oxygen reduction, i.e. dissociative adsorption on LSM and oxygen ion incorporation in YSZ [134]. The endogenous silicon impurity level should stay as low as possible, to avoid the formation of insulating phases, like $\text{Nd}_4\text{Si}_3\text{O}_{12}$ in the case of the NNO cathode [45].

Sulfur has been shown to affect all investigated cathode materials (LSM, LSCF, LSC and NNO) when delivered at high enough concentrations [49, 119, 51], and influences the Cr-poisoning mechanism, by favoring a solid solution between SrCrO_4 and SrSO_4 under severe combined S/Cr contaminating conditions [50].

Protecting from system components

Protective coating of complete BoP components is commonly judged unreasonable as too cost-intensive by standard techniques; Forschungszentrum Jülich therefore proposes an alternative approach to decrease Cr emanation from system parts [185] like heat-exchangers, tubing or housing elements. Such strategies do however need validation; a field where our investigation techniques [183, 184, 46] promise an objective evaluation of single or complete BoP components.

Air filtering upstream of the cell, as a cathode-remote trapping technique, is seen as an alternative protection from BoP-generated Cr contamination. The fabrication and validation of a porous ceramic LSC-based trap at the cathode air inlet of an SOFC stack as Cr-getter

allowed the measured Cr-contamination level to be decreased below detection limit [52], hence demonstrating a potential mitigation measure.

Filtering the cold air fed to the SOFC system at present not appears commercially viable (additional system costs and energy requirements), but allows at the laboratory-scale the removal of air-vehicled impurities, which possibly generate superimposed degradation effects to Cr-poisoning. Since this work pinpointed air impurities to be at least partially responsible for higher degradation rates observed for SOFC tests performed in-house (EPFL) compared to other testing locations (for instance EIFER for the 10'000 h test), the application of a commercial sub-micron air filter to the compressed air system used for the cathode air fed seems to have contributed to the lifetime extension (by the removal of S/Si-containing particulate matter) of the ongoing SOFC stack tests at LENI-EPFL.

11 Conclusion

11.1 Own contributions and achievements

The complete removal of the "Cr needle" within an "SOFC haystack" seems not to be feasible, since this would drive research towards an opposite direction of the cost-cutting strategies in SOFC development needed for their commercialization. Important steps were however achieved for the identification, understanding and alleviation of the Cr-poisoning degradation phenomenon, successfully fulfilling the thesis goals, which include the following:

goal i: Develop Cr contamination **detection** techniques in SOFC during/after operation.

- Our fast and objective Cr quantification methodology based on the EDS technique confidently enabled us to state that "Cr detection in SOFC cathodes should not longer be like searching for a needle in a haystack" [43]. The air sampling technique, henceforth adapted for trace analysis in the corrosive high temperature and oxidative atmosphere of SOFC, allowed to follow Cr within its complete path through a fuel cell system. Both techniques, built up with cost-awareness, could be readily delivered to industrial partners as "quality control" solutions regarding Cr-poisoning.

goal ii: Apply advanced investigation techniques to **understand** and predict the Cr-poisoning phenomenon and its correlation to degradation.

- Our results, besides corroborating general Cr-poisoning aspects for perovskite-based cathodes, pointed out unknown Cr-SOFC material interactions with resulting phase formation such as $\text{Sr}(\text{Cr,S})\text{O}_4$ or NdCrO_4 as well as material incompatibilities yielding, among others, $\text{NdCeO}_{3,5}$ and $\text{Nd}_4\text{Si}_3\text{O}_{12}$ phases. Since Cr-containing alloys are the major Cr contamination sources, the characterization of the oxidation behavior of different high-temperature steel compositions, is an additional step towards the prediction of the severity of the Cr-poisoning effect. Electrochemical degradation signatures of SOFC devices could qualitatively be assigned to such exogenous contamination and solid-state reaction effects; for model systems, like the multi-cathode cells, degradation rates could confidently be correlated to Cr amounts that are dependent on the initial

cathode characteristics (cathode thickness, LSM-zirconia composite composition, extent of electrochemical active region). Findings such as the sealing-leakage caused Cr-poisoning aggravation subsequently guided us towards mitigating solutions. The generation of all these results mainly relied on the application of advanced electron microscopy-based techniques; such academic key competences will find application, and are already in use for instance for Ni volatilization studies [186], in investigations of degradation phenomena other than Cr-poisoning.

goal iii: Mitigate this degradation phenomenon with guidance from the industrial needs.

- Our holistic examination of Cr-poisoning suggests the cathode assembly thickness increase to probably be the easiest implementable Cr-poisoning alleviating solution, giving protection by limiting the volatile Cr species diffusion towards the electrochemically active cathode regions; the protective effect is additionally enhanced by the reactivity of the cathode material. The use of a non-reactive and alternative cathode composition, initially thought to offer higher tolerance to Cr-poisoning, is not advised for the Nd-nickelate composition as this material is not seen mature enough for its application in SOFC systems. The Cr-poisoning effect can definitively be alleviated by perfecting the repeat-element assembly. An underestimated role plays herein the sealing material; by a decrease of hydrogen leakage from the anode side, the steam concentration is decreased in the cathode compartment, hence alleviating the Cr oxyhydroxide generation from the cell-proximal MIC. Hindering the access of contamination from Cr sources located upstream the cell was demonstrated by the use of a Cr-getter ceramic filter that could easily be installed within an SOFC system; updated versions of such a trapping solution are/will be applied within devices from our industrial partners [187].

11.2 Future work

The Cr-poisoning investigations performed on the LSM-YSZ cathode-based segmented cell test (2'000 h), the LSCF-based stack (10'000 h) as well as insights into long-term (> 10'000 h) tests from Hexis [187] give in retrospect an encouraging view on Cr-poisoning related SOFC degradation; Cr-poisoning is not seen as the major hurdle for SOFC devices to reach lifetimes over 40'000 h, the more since additional studies of Cr detection, understanding and alleviation are currently under development.

- Principal component analysis (PCA) [115, 116, 117] can be used to gather contrast information out of a noisy data set, therefore enabling to lower the EDS acquisition time while keeping the precision of the Cr quantification [114], or to enable the detection of lower Cr amounts expected in future cathode samples that have been tested with counteracting strategies.
- A model description of Cr-poisoning based on the direct reduction of six-valent Cr vapor species at electrochemically active cathode sites, to three-valent Cr-oxide, as

proposed by recent investigations from Nakajo *et al.* [136], close to the work done by others [188] but calibrated here on appropriate experimental data is currently in preparation [114]. Such modeling input is suggested to enable the implementation of lifetime predictions [110] based on electrochemical degradation models and not only on empirical relations [189].

- Stacked FIB-slices 3D data of a Cr-poisoned LSM-YSZ cathode is currently investigated to quantify the amount of TPB blocked by Cr accumulations. Since the Cr-related gray-scale strongly overlaps with other microstructural features within this data set, preventing the TPB to be easily assessed, the TPB quantification is currently under investigation [39], from 3D reconstructions based on few processed images [122] of the original slice-stack.
- Reversed bias pulses are suggested as regenerative strategies of Cr-poisoned cathode, the more if a CGO barrier layer is used between cathode and electrolyte materials [169]. Such procedures definitively need experimental validation, which is already planned at EPFL-LENI.

Bibliography

- [1] Swiss Federal Office of Energie. Energy strategie 2050. 2011.
- [2] S. Taniguchi, M. Kadowaki, H. Kawamura, T. Yasuo, Y. Akiyama, Y. Miyake, and T. Saitoh. *J. Power Sources*, 55:73, 1995.
- [3] S.P.S. Badwal, R. Deller, K. Foger, Y. Ramprakash, and J.P. Zhang. *Solid State Ionics*, 99:297, 1997.
- [4] K. Hilpert, D. Das, M. Miller, D.H. Peck, and R. Weiß. *J. Electrochem. Soc.*, 143:3642, 1996.
- [5] S.P. Jiang, J.P. Zhang, and K. Foger. *J. Electrochem. Soc.*, 147:3195, 2000.
- [6] S.P. Jiang, J.P. Zhang, L. Apateanu, and K. Foger. *J. Electrochem. Soc.*, 147:4013, 2000.
- [7] Chen X., Zhang L., and Jiang S.P. *J. Electrochem. Soc.*, 155:B1093, 2008.
- [8] M.C. Tucker, H. Kurokawa, C.P. Jacobson, L.C. De Jonghe, and S.J. Visco. *J. Power Sources*, 160:130, 2006.
- [9] G. Y. Lau, M. C. Tucker, C. P. Jacobson, S. J. Visco, S. H. Gleixner, and L. C. DeJonghe. *J. Power Sources*, 195:7540, 2010.
- [10] J.Y. Kim, V.L. Sprenkle, N.L. Canfield, K.D. Meinhardt, and L.A. Chick. *J. Electrochem. Soc.*, 153:A880, 2006.
- [11] K. Fujita, T. Hashimoto, K. Ogasawara, H. Kameda, Y. Matsuzaki, and T. Sakurai. *J. Power Sources*, 131:270, 2004.
- [12] E. Konyshva, H. Penkalla, E. Wessel, J. Mertens, U. Seeling, L. Singheiser, and K. Hilpert. *J. Electrochem. Soc.*, 153:A765, 2006.
- [13] Konyshva E., Mertens J., Penkalla H., Singheiser L., and Hilpert K. *J. Electrochem. Soc.*, 154:B1252, 2007.
- [14] Monika Backhaus-Ricoult. *Solid State Sci.*, 10:670, 2008.
- [15] V.I. Sharma and B. Yildiz. *J. Electrochem. Soc.*, 157:B441, 2010.

Bibliography

- [16] S. Wang, T.A. Cruse, M. Krumpelt, B.J. Ingram, and P.A. Salvador. *J. Electrochem. Soc.*, 158:B152, 2011.
- [17] Z. Yang, G. Xia, P.Singh, and J.W. Stevenson. *J. Power Sources*, 155:246, 2006.
- [18] T. Komatsu, R. Chiba, H. Arai, and K. Sato. *J. Power Sources*, 176:132, 2008.
- [19] X. Chen, L. Zhang, E. Liu, and S.P. Jiang. *Int. J. Hy. Energ.*, 36:805, 2011.
- [20] T. Horita, Y. Xiong, M. Yoshinaga, H. Kishimoto, K. Yamaji, M.E. Brito, and H. Yokokawa. *Electrochem. Solid-State Lett.*, 12:B146, 2009.
- [21] H. Yokokawa, H. Kishimoto, and et al. *ECS Trans.*, 35:2191, 2011.
- [22] T. Horita, Y. P. Xiong, M. Yoshinaga, H. Kishimoto, K. Yamaji, M. E. Brito, and H. Yokokawa. *ECS Trans.*, 25:2881, 2009.
- [23] H. Yokokawa, H. Kishimoto, K. Yamaji, and T. Horita. *ECS Trans.*, 25:401, 2009.
- [24] E. Bucher, M. Yang, and W. Sitte. *ECS Trans.*, 35:2019, 2011.
- [25] M. Yang, E. Bucher, and W. Sitte. *J. Power Sources*, 196:7313, 2011.
- [26] D-J. Liu, J. Almer, and T. Cruse. *J. Electrochem. Soc.*, 157:B744, 2010.
- [27] Y. Matsuzaki and I. Yasuda. *Solid State Ionics*, 132:271, 2000.
- [28] X. Chen, Y. Zhen, J. Li, and S.P. Jiang. *Int. J. Hy. Energ.*, 35:2477, 2010.
- [29] Y. Matsuzaki and I. Yasuda. *J. Electrochem. Soc.*, 148:A126, 2001.
- [30] P. Metzger, K.-A. Friedrich, H. Müller-Steinhagen, and G. Schiller. *Solid State Ionics*, 177:2045, 2006.
- [31] G. Schiller, W. Bessler, C. Willich, and K.A. Friedrich. *EFCF Proceedings*, 2010.
- [32] M. Stanislawski, U. Seeling, D.H. Peck, S.K. Woo, L. Singheiser, and K. Hilpert. *Solid State Ionics*, 176:2523, 2005.
- [33] M. Stanislawski, J. Froitzheim, L. Niewolak, W.J. Quadackers, K. Hilpert, T. Markus, and L. Singheiser. *J. Power Sources*, 164:578, 2007.
- [34] E. Konyshева, U. Seeling, A. Besmehn, L. Singheiser, and K. Hilpert. *J. Mater. Sci.*, 42:5778, 2007.
- [35] M. Casteel, P. Willson, T. Goren, P. O'Brien, and D. Lewis. *ECS Trans.*, 25:1411, 2009.
- [36] M. Casteel, D.J. Lewis, A. Renko, and P. Willette. *ECS Trans.*, 35:2601, 2011.
- [37] J. Froitzheim, E. Larsson, L. G. Johansson, and J. E. Svensson. *ECS Trans.*, 25:1423, 2009.

- [38] S. H. Hong, P. Madakashira, D-I. Kim, Y. W. Cho, S. H. Han, and H. N. Han. *ECS Trans.*, 25:1437, 2009.
- [39] M. Ananyev, A. Gavriluk, D. Bronin, R. Steinberger-Wilckens, and J. Mertents. *EFCE Proceedings*, 2011.
- [40] T. Horita, Y. Xiong, H. Kishimoto, K. Yamaji, M.E. Brito, and H. Yokokawa. *J. Electrochem. Soc.*, 157:B614, 2010.
- [41] J.A. Bearden. *Rev. Mod. Phys.*, 39:78, 1967.
- [42] M. O. Krause and J. H. Oliver. *J. Phys. Chem. Ref. Data*, 8:329, 1979.
- [43] J.A. Schuler, P.Tanasini, A. Hessler-Wyser, and J. Van herle. *Scr. Mater.*, 63:895, 2010.
- [44] J.A. Schuler, P. Tanasini, A. Hessler-Wyser, C. Comninellis, and J. Van herle. *Electrochem. Commun.*, 12:1682, 2010.
- [45] J.A. Schuler, H. Lüebbe, A. Hessler-Wyser, and J. Van herle. *J. Power Sources*, 213:223, 2012.
- [46] J.A. Schuler, A.J. Schuler, Z. Wuillemin, A. Hessler-Wyser, C. Ludwig, and J. Van herle. *ECS Trans.*, 35:2001, 2011.
- [47] J.A. Schuler, C. Gehrig, Z. Wuillemin, A.J. Schuler, J. Wochele, C. Ludwig, A. Hessler-Wyser, and J. Van herle. *J. Power Sources*, 196:7225, 2011.
- [48] J.A. Schuler, Z. Wuillemin, A. Hessler-Wyser, and J. Van herle. *Electrochem. Solid-State Lett.*, 14:B20, 2011.
- [49] J. A. Schuler, Z. Wuillemin, A. Hessler-Wyser, and J. Van herle. *ECS Trans.*, 25:2845, 2009.
- [50] J.A. Schuler, H. Yokokawa, C.F Calderone, Q. Jeangros, Z. Wuillemin, A. Hessler-Wyser, and J. Van herle. *J. Power Sources*, 201:112, 2012.
- [51] J.A. Schuler, Z. Wuillemin, A. Hessler-Wyser, C. Comminges, N. Yousfi-Steiner, and J. Van herle. *J. Power Sources*, 211:177, 2012.
- [52] J.A. Schuler, A.J. Schuler, D. Penner, A. Hessler-Wyser, C. Ludwig, and J. Van herle. *Electrochem. Solid-State Lett.*, 14:B132, 2011.
- [53] Z. Wuillemin, A. Nakajo, A. Mueller, J. A. Schuler, S. Diethelm, J. Van herle, and D. Favrat. *ECS Trans.*, 25:457, 2009.
- [54] P. Tanasini, J.A. Schuler, Z. Wuillemin, M.L. Ben Ameer, C. Comninellis, and J. Van herle. *J. Power Sources*, 196:7097, 2011.
- [55] J.W. Fergus. *J. Power Sources*, 162:30, 2006.
- [56] B. C. H. Steele. *Solid State Ionics*, 134:3, 2000.

Bibliography

- [57] S.J. Skinner. *Int. J. Inorg. Mater.*, 3:113, 2001.
- [58] A.J. McEvoy. *J. Mate. Sci.*, 36:1087, 2001.
- [59] S. P. Jiang, L. Liu, K. P. Ong, P. Wu, J. Li, and J. Pu. *J. Power Sources*, 176:82, 2008.
- [60] S. Miyoshi, S. Onuma, A. Kaimai, H. Matsumoto, K. Yashiro, Tatsuya Kawada, J. Mizusaki, and H. Yokokawa. *J. Solid State Chem.*, 177:4112, 2004.
- [61] N. Yokokawa, H. Sakai, T. Kawada, and M. Dokiya. *J. Electrochem. Soc.*, 138:1018, 1991.
- [62] P. Kofstad and R. Bredesen. *Solid State Ionics*, 52:69, 1992.
- [63] M. Stanislawski, E. Wessel, T. Markus, L. Singheiser, and W.J. Quadackers. *Solid State Ionics*, 179:2406, 2008.
- [64] K.P. Lillerud and P. Kofstad. *J. Electrochem. Soc.*, 127:2397, 1981.
- [65] K.P. Lillerud P. Kofstad. *J. Electrochem. Soc.*, 127:2410, 1981.
- [66] A. Holt and P. Kofstad. *Solid State Ionics*, 69:127, 1994.
- [67] T. Kadowaki, T. Shiomitsu, E. Matsuda, H. Nakagawa, H. Tsuneizumi, and T. Maruyama. *Solid State Ionics*, 67:65, 1993.
- [68] K. Hilpert, W.J. Quadackers, and L. Singheiser. *Handbook Fuel Cells*, 4:1037, 2003.
- [69] T. Horita, Y. Xiong, K. Yamaji, N. Sakai, and H. Yokokawa. *J. Electrochem. Soc.*, 150:A243, 2003.
- [70] J.W. Fergus. *Mater. Sci. Eng. A*, 397:271, 2005.
- [71] F. Wiener, M. Bram, H.P. Buchkremer, and D. Sebold. *J. Mater Sci.*, 42:2643, 2007.
- [72] N.H. Menzler, D. Sebold, M. Zahid, S.M. Gross, and T. Koppitz. *J. Power Sources*, 152:156, 2005.
- [73] Z. Yang, J.W. Stevenson, and K.D. Meinhardt. *Solid State Ionics*, 160:213, 2003.
- [74] T. Kawada, N. Sakai, H. Yokokawa, M. Dokiya, and I. Anzai. *Solid State Ionics*, 50:189, 1992.
- [75] Yokokawa H., Watanabe T., Ueno A., and Hoshino K. *ECS Trans.*, 7:133, 2007.
- [76] H. Yokokawa, T. Horita, K. Yamaji, H. Kishimoto, Y. P. Xiong, and M. E. Brito. *EFCF Proceedings*, 2008.
- [77] C. Levy, Y. Thong, C. Morel, and S. Marlin. *ECS Trans.*, 25:2815, 2009.
- [78] Chen A., Bourne G., Siebein K., Dehoff R., Wachsmann E., and Jones K. *J. Am. Ceram. Soc.*, 91:2670, 2008.

- [79] A. Chen, J.R. Smith, K.L. Duncan, R.T. DeHoff, K.S. Jones, and E.D. Wachsman. *J. Electrochem. Soc.*, 157:B1624, 2010.
- [80] P.S. Gentile and S. W. Sofie. *J. Power Sources*, 196:4545, 2011.
- [81] KK. Sasaki, K. Haga, D. Minematsu, T. Yoshizumi, R.R. Liu, Y. Shiratori, K. Ito and M. Koyama, and K. Yokomoto. *EFCF Proceedings*, 2010.
- [82] Hagen A., Liu Y.L., Barfod R., and Hendriksen P.V. *J. Electrochem. Soc.*, 155:B1047, 2008.
- [83] M. Mogensen, K.V. Jensen, M.J. Jorgensen, and S. Primdahl. *Solid State Ionics*, 150:123, 2002.
- [84] P. Tanasini, M. Cannarozzo, P. Costamagna, A. Faes, J. Van Herle, A. Hessler-Wyser, and C. Comninellis. *Fuel Cells*, 9:740, 2009.
- [85] M.J. Joergensen and M. Mogensen. *J. Electrochem. Soc.*, 148:A433, 2001.
- [86] H. Yokokawa, H. Tu, B. Iwanschitz, and A. Mai. *J. Power Sources*, 182:400, 2008.
- [87] F. Tietz, A. Mai, and D. Stöver. *Solid State Ionics*, 179:1509, 2008.
- [88] A.N. Vlasov and M.V. Perfiliev. *Solid State Ionics*, 25:245, 1987.
- [89] O. Yamamoto, Y. Takeda, R. Kanno, and K. Kohno. *J. Mater. Sci.*, 25:2805, 1990.
- [90] F.T. Ciacchi, S.P.S. Badwal, and J. Drennan. *J. Euro. Ceram. Soc.*, 7:185, 1991.
- [91] F.T. Ciacchi, K.M. Crane, and S.P.S. Badwal. *Solid State Ionics*, 73:49, 1994.
- [92] Z. Yang, J.S. Hardy, M.S. Walkers, G. Xia, S.P. Simmer, and J.W. Stevenson. *J. Electrochem. Soc.*, 151:A1825, 2004.
- [93] Z. Yang, M.S. Walker, P. Singh, J.W. Stevenson, and T. Norby. *J. Electrochem. Soc.*, 151:B669, 2004.
- [94] R. Bauer, M. Baccalaro, L.P.H. Jeurgens, M. Pohl, and E.J. Mittemeijer. *Oxid. Met.*, 69:265, 2008.
- [95] M. Stanislawski, E. Wessel, K. Hilpert, T. Markus, and L. Singheiser. *J. Electrochem. Soc.*, 154:A295, 2007.
- [96] B.B. Ebbinghaus. *Combu. Flam.*, 93:119, 1993.
- [97] C. Gindorf, L. Singheiser, and K. Hilpert. *J. Phys. Chem. Solids*, 66:384, 2005.
- [98] D.J. Young and B.A. Pint. *Oxid. Met.*, 66:137, 2006.
- [99] H. Asteman, J.-E. Svensson, and L.-G. Johansson. *J. Electrochem. Soc.*, 151:B141, 2004.

Bibliography

- [100] K. Ogasawara, H. Kameda, Y. Matsuzaki, T. Sakurai, T. Uehara, A. Toji, N. Sakai, K. Yamaji, T. Horita, and H. Yokokawa. *J. Electrochem. Soc.*, 154:B657, 2007.
- [101] K. Fujita, K. Ogasawara, Y. Matsuzaki, and T. Sakurai. *J. Power Sources*, 131:261, 2004.
- [102] K. Huang, P.Y. Hou, and J.B. Goodenough. *Solid State Ionics*, 129:237, 2000.
- [103] F. Tietz and D. Sebold. *Mater. Sci. Eng. B*, 150:135, 2008.
- [104] H.J. Hwang, S. Lee, E.A. Lee, J.-W. Moon, and Y. Lim. *J. Am. Ceram. Soc.*, 88:3275, 2005.
- [105] N. Sakai, T. Horita, Y.P. Xiong, K. Yamaji, H. Kishimoto, M.E. Brito, H. Yokokawa, and T. Maruyama. *Solid State Ionics*, 176:681, 2005.
- [106] M. Bertoldi, T. Zandonella, D. Montinaro, V.M. Sglavo, A. Fossati, A. Lavacchi, C. Giolli, and U. Bardi. *J. Fuel Cell Sci. Tech.*, 5:1, 2008.
- [107] C. Fu, K. Sun, X. Chen, N. Zhang, and D. Zhou. *Cor. Sci.*, 50:1926, 2008.
- [108] N. Yasuda, T. Uehara, M. Okamoto, C. Aoki, T. Ohno, and A. Toji. *ECS Trans.*, 25:1447, 2009.
- [109] Hua B., Pu J., Zhang J., Lu F., Chi B., and Jian L. *J. Electrochem. Soc.*, 156:B93, 2009.
- [110] Pietro Tanasini. *EPFL PhD Thesis*, 5004, 2011.
- [111] C. Comminges, Q.X. Fu, M. Zahid, N. Yousfi Steiner, and O. Bucheli. *Electrochim. Acta*, 59:367, 2012.
- [112] Z. Wullemmin. *EPFL PhD Thesis*, 4525, 2009.
- [113] X. Chen, B. Hua, J. Pu, J. Li, L. Zhang, and S.P. Jiang. *Int. J. Hy. Energ.*, 34:5737, 2009.
- [114] J.A. Schuler, P. Burdet, G. Lucas, M. Cantoni, A. Nakajo, P. Tanasini, and et al. *J. Power Sources, in preparation*, 2012.
- [115] M. R. Keenan and P. G. Kotula. *Surf. Interf. Anal.*, 36:203, 2004.
- [116] N. Bonnet, N. Brun, and C. Colliex. *Ultramicroscopy*, 77:97, 1999.
- [117] P. Trebbia and N. Bonnet. *Ultramicroscopy*, 34:165, 1990.
- [118] D.S. Bright and D.E. Newbury. *J. Microscopy*, 216:186, 2004.
- [119] J.A. Schuler, H. Lüebbe, A. Hessler-Wyser, and J. Van herle. *EFCE Proceedings*, 2011.
- [120] H. Yokokawa, T. Horita, N. Sakai, K. Yamaji, M.E. Brito, Y.-P. Xiong, and H. Kishimoto. *Solid State Ionics*, 177:3193, 2006.
- [121] H. Yokokawa, N. Sakai, T. Horita, K. Yamaji, M.E. Brito, and H. Kishimoto. *J. Alloys Comp.*, 452:41, 2008.

- [122] M. Ananyev, J.A. Schuler, and et al. *J.Power Sources, in preparation*, 2012.
- [123] G.J. Nelson, W.H. Harris, J.J. Lomardo, J.R. Izzo, W.K.S. Chiu, P. Tansasini, M. Cantoni, J. Van herle, C. Comninellis, J.C. Andrews, Y. Liu, P. Pianetta, and Y.S. Chu. *Electrochem. Commun.*, 13:586, 2011.
- [124] L.G.J. de Haart, A. Neumann, N.H. Menzler, and I.C. Vinke. *ECS Trans.*, 35:2027, 2011.
- [125] M. Krumpelt, T.A. Cruse, J.L. Routbort B.J. Ingram, P.A. Salvador S. Wang, and G. Chen. *J. Electrochem. Soc.*, 157:B228, 2010.
- [126] D. Oh, E. Armstrong, D. Jung, C. Kan, and E. Wachsman. *ECS Trans.*, 25:2871, 2009.
- [127] S.P. Jiang, S. Zhang, and Y.D. Zhen. *J. Electrochem. Soc.*, 153:A127, 2006.
- [128] T. Horita, H. Kishimoto, K. Yamaji, M.E. Brito, T. Shimonosono, D. Cho, M. Izuki, F. Wang, and H. Yokokawa. *ECS Trans.*, 35:511, 2011.
- [129] M. Mori, Y. Hiei, and N.M. Sammes. *Solid State Ionics*, 135:743, 2000.
- [130] H. Luebbe, J. Van herle, H. Hofmann, P. Bowen, U. Aschauer, J. A. Schuler, F. Snijkers, H.-J. Schindler, U. Vogt, and C. Lalanne. *Solid State Ionics*, 180:805, 2009.
- [131] H. Schwarz. *Z. Anorg. Allg. Chemie.*, 322:9, 1963.
- [132] S.P. Jiang, Y.D. Zhen, and S. Zhang. *J. Electrochem. Soc.*, 153:A1511, 2006.
- [133] P. Costamagna, P. Costa, and E. Arato. *Electrochim. Acta*, 43:967, 1998.
- [134] S.B. Adler. *Chem. Rev.*, 104:4791, 2004.
- [135] A. Hagen, R. Barfod, P.V. Hendriksen, Y-L Liu, and S. Ramousse. *J. Electrochem. Soc.*, 153:A1165, 2006.
- [136] A. Nakajo, P. Tanasini, S. Diethelm, J. Van herle, and D. Favrat. *J. Electrochem. Soc.*, 158:B1102, 2011.
- [137] J. Van Herle, A. J. McEvoy, and K. Ravindranathan Thampi. *Electrochim. Acta*, 41:1447, 1996.
- [138] A. Mitterdorfer and L. J. Gauckler. *Solid State Ionics*, 111:185, 1998.
- [139] D. Kuscer, J. Holc, M. Hrovat, S. Bernik, Z. Samardzija, and D. Kolar. *Solid State Ionics*, 78:79, 1995.
- [140] S.P. Jiang. *J. Mater. Sci.*, 43:6799, 2008.
- [141] H. Yokokawa. *Annu. Rev. Mater. Res.*, 33:581, 2003.
- [142] J. Van Herle and R. Vasquez. *J. Euro. Ceram. Soc.*, 24:1177, 2004.

Bibliography

- [143] T. Kawada, N. Sakai, H. Yokokawa, and M. Dokiya. *Solid State Ionics*, 50:418, 1992.
- [144] Y. Yoshida, R. Chiba, T. Komatsu, M. Yokoo, K. Hayashi, H. Orui, and H. Arai. *ECS Trans.*, 35:2313, 2011.
- [145] T. Komatsu, H. Arai, R. Chiba, K. Nozawa, M. Arakawa, and K. Sato. *Electrochem. Solid-State Lett.*, 9:A9, 2006.
- [146] M.K. Stodolny, B.A. Boukamp, and F.P.F. van Berkel. *ECS Trans.*, 35:2035, 2011.
- [147] T. Komatsu, Y. Yoshida, K. Wantanabe, R. Chiba, H. Taguchi, H. Orui, and H. Arai. *J. Power Sources*, 195:5601, 2010.
- [148] E. Boehm, J.-M. Bassat, P. Dordor, F. Mauvy, J.-C. Grenier, and Ph. Stevens. *Solid State Ionics*, 176:2717, 2005.
- [149] F. Mauvy, C. Lalanne, J.M. Bassat, J.C. Grenier, H. Zhao, L. Huo, and P. Stevens. *J. Electrochem. Soc.*, 153:A1547, 2006.
- [150] A. Egger, E. Bucher, W. Sitte, C. Lalanne, and J. M. Bassat. *ECS Trans.*, 25:2547, 2009.
- [151] N.H. Menzler, P. Batfalsky, L. Blum, B. Bram, S.M. Gross, V.A.C. Haanappel, J. Malzbender, V. Shemet, R.W. Steinbrech, and I. Vinke. *Fuel Cells*, 5:356, 2007.
- [152] R. Steinberger-Wilckens, H-P. Buchkremer, J. Malzbender, L. Blum, L.G.J (Bert) de Haart, and M. Pap. *EFCE Proceedings*, 2010.
- [153] N.H. Menzler, P. Batfalsky, S.M. Gross, V. Shemet, and F. Tietz. *ECS Trans.*, 35:195, 2011.
- [154] H. Yokokawa. *ECS Trans.*, 35:207, 2011.
- [155] A. Hessler-Wyser, Z. Wuillemin, J.A. Schuler, A. Faes, and J. Van herle. *J. Mater. Sci.*, 46:4532, 2011.
- [156] C.S. Tedmon. *J. Electrochem. Soc.*, 113:766, 1966.
- [157] Z. Yang, K.S. Weil, D.M. Paxton, and J.W. Stevenson. *J. Electrochem. Soc.*, 150:A1188, 2003.
- [158] A. Neumann, N. H. Menzler, I. Vinke, and H. Lippert. *ECS Trans.*, 25:2889, 2009.
- [159] N. H. Menzler, I. Vinke, and H. Lippert. *ECS Trans.*, 25:2899, 2009.
- [160] Z. Wuillemin, N. Autissier, A Nakajo, M. Luong, J. Van Herle, and D. Favrat. *J. Fuel Cell Sci. Tech.*, 5:1, 2008.
- [161] J. Guan, S. Zecevic, Y. Liu, P. Lam, R. Klug, M. Alinger, S. Taylor, B. Ramamurthi, R. Sarraf-Nour, and S. Renou. *ECS Trans.*, 25:405, 2007.
- [162] A. Hagen, M. Chen, K. Neufeld, and Y. L. Liu. *ECS Trans.*, 25:439, 2009.

- [163] R.R. Liu, S.H. Kim, S. Taniguchi, T. Oshima, Y. Shiratori, K. Ito, and K. Sasaki. *J. Power Sources*, 196:7090, 2011.
- [164] J. Nielsen, A. Hagen, and Y.L. Liu. *Solid State Ionics*, 181:517, 2010.
- [165] E. Bucher, A. Egger, M. Yang, and W. Sitte. *EFCF Proceedings*, 2010.
- [166] A. Egger, W. Sitte, F. Klauser, and E. Bertel. *J. Electrochem. Soc.*, 157:B1537, 2010.
- [167] C. Knöfel, M. Chen, and M. Mogensen. *Fuel Cells*, 11:669, 2011.
- [168] S. Taniguchi, M. Kadowaki, T. Yasuo, Y. Akiyama, Y. Itoh, Y. Miyake, and K. Nishio. *Denki Kagaku*, 64:568, 1996.
- [169] T. Horita et al. *2nd Int. Workshop on Degradation Issues of Fuel Cells*, 2011.
- [170] M. de Ridder, A. G. J. Vervoort, R. G. van Welzenis, and H. H. Brongersma. *Solid State Ionics*, 156:255, 2003.
- [171] J.M. Bae and B. C. H. Steele. *Solid State Ionics*, 106:247, 1998.
- [172] J.L. Hertz, A. Rothschild, and H.L. Tuller. *J. Electroceram.*, 22:428, 2009.
- [173] M. de Ridder, R.G. van Welzenis, A.W. Denier van der Gon, H.H. Brongersma, S. Wulff, W.-F. Chu, and W. Weppner. *J. Appl. Phys.*, 92:3056, 2002.
- [174] Y. Matsuzaki and I. Yasuda. *Solid State Ionics*, 132:261, 2000.
- [175] L. Wan, L.G. Tejuca, and J.L.G. Fierro. *Prop. Appl. Perovskite-Type Oxides*, New York, 1993.
- [176] K. Yamaji, Y. Xiong, M. Yoshinaga, H. Kishimoto, M. E. Brito, T. Horita, H. Yokokawa, J. Akikusa, and M. Kawano. *ECS Trans.*, 25:2853, 2009.
- [177] Y. Xiong, K. Yamaji, T. Horita, H. Yokokawa, J. Akikusa, H. Eto, and T. Inagaki. *J. Electrochem. Soc.*, 156:B588, 2009.
- [178] R. R. Liu, S. H. Kim, Y. Shiratori, T. Oshima, K. Ito, and K. Sasaki. *ECS Trans.*, 25:2859, 2009.
- [179] F. Wang, K. Yamaji, D-H. Cho, T. Shimonosono, H. Kihimoto, M. E. Brito, T. Horita, and H. Yokokawa. *J. Electrochem. Soc.*, 158:B1391, 2011.
- [180] K. Gerdes and C. Johnson. *J. Fuel Cell Sci. Tech.*, 6:1, 2009.
- [181] M. Koebel and M. Elsener. *J. Chromato. A*, 689:164, 1995.
- [182] J. Froitzheim, H. Ravash, L.G. Johansson, and J.E. Svensson. *EFCF Proceedings*, 2010.
- [183] O. Thomann, M. Pihlatie, J.A. Schuler, O. Himanen, and J. Kiviaho. *ECS Trans.*, 35:2609, 2011.

Bibliography

- [184] O. Thomann, M. Pihlatie, J.A. Schuler, O. Himanen, and J. Kiviaho. *Electrochem. Solid-State Lett.*, 15:B35, 2012.
- [185] M. Stanislawski, K. Hilpert, and U. Hilpert. *Patent*, 20090317679, 2010.
- [186] J.A. Schuler, B. Iwanschitz, L. Holzer, M. Cantoni, and T. Graule. *EFCF Proceedings*, 2012.
- [187] J.A. Schuler. *Privat Communications with HTceramix and Hexis*, 2009-2012.
- [188] A.A. Kulikovsky. *J. Electrochem. Soc.*, 158:B253, 2011.
- [189] G. DiGiuseppe and L. Sun. *ECS Trans.*, 25:801, 2009.

A Appendix

ECS Transactions 25 (2009) 457

A.1 Locally-resolved study of degradation in a SOFC repeat-element

Zacharie Wuilemin, Arata Nakajo, Andres Müller, J. Andreas Schuler, Stefan Diethelm, Jan Van herle and Daniel Favrat

Experimental

The stack developed for the FlameSOFC project consists of planar anode-supported cells with an active area of 200 cm^2 , supplied with air and fuel by external manifolds in a co-flow configuration (Figure A.1). The gas diffusion layers (GDL) are made of SOFCConnexTM provided by HTceramix-SOFCpower.

The local characterization is performed by separating the active area of the cell in electrically independent areas called segments (Figure A.1 and A.2), in a similar manner as presented by Ravussin *et al.* (Europ. Ceram. Soc., 27 (2007) 1035) and Metzger *et al.* (Solid State Ionics, 177 (2006) 2045). The polarization of each single segment is controlled externally for electrochemical characterization. In addition, impedance spectroscopy measurements are performed locally. Finally, each segment is equipped with a K-type thermocouple to monitor the local temperature.

A total number of 18 segments of 1.7 cm^2 active area each were distributed on the surface, in ad-

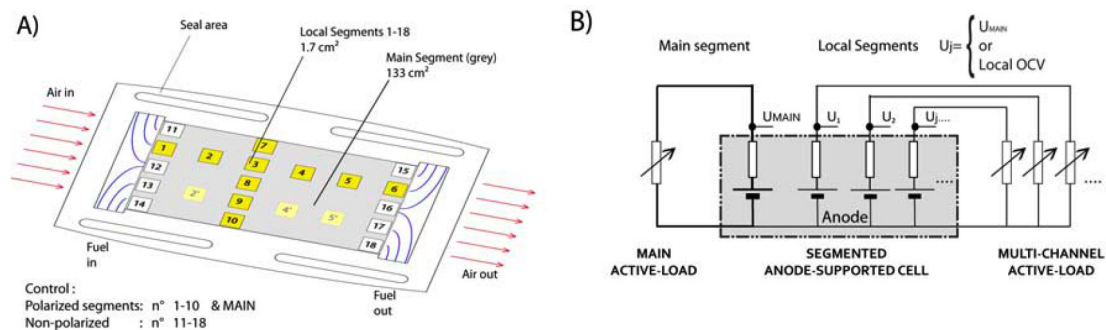


Figure A.1: Distribution of the segments and connection to the active loads.

Appendix A. Appendix

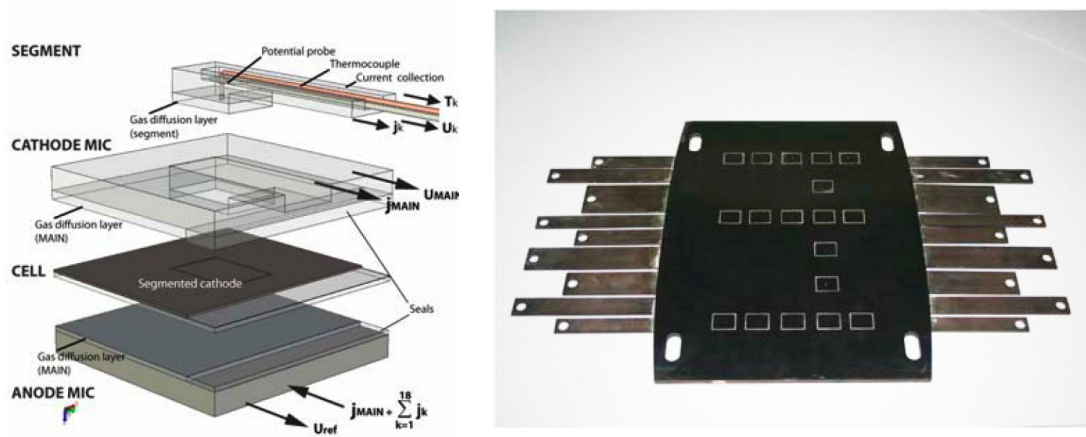


Figure A.2: Segmentation of the cathode MIC and instrumentation.

dition to a large main segment of 133 cm^2 . The segments were organized as one 6-segment line along the flow, and three 5-segment columns perpendicular to the flow path (see Figure A.1). For the present experiment, an anode-supported cell provided by HTceramix-SOFCpower was used, on which a segmented $(\text{La,Sr})\text{MnO}_3$ / yttria-stabilized zirconia (LSM/YSZ) composite cathode and segmented $(\text{La,Sr})\text{CoO}_3$ (LSC) current-collection layer were screen-printed. Metallic interconnects (MICs) were used, made of F18TNb alloy. The 18 small segments are connected to two different multichannel active loads built in house, in order to obtain an equipotential in the cathode MIC similarly to the situation in a repeat-element. This active polarization control of each segment allows avoiding the limitations encountered by Ravussin and Metzger in similar experiments, where the cell potentials of all segments differed due to potential losses in the current collection lines. In addition, the polarization of each segment can be stopped individually to measure the local open circuit voltage (OCV) as a measurement of the local Nernst potential. One of the active multi-channel active loads became instable at the beginning of operation due to insufficient signal filtering, and was disabled. For this reason, the segments 11 to 18 remained unpolarized during the whole test, giving the possibility to study the effect of polarization on local degradation.

A.2 Segmented cell testing for cathode parameter investigation

Pietro Tanasini, J. Andreas Schuler, Zacharie Wuillemin, Myriam L. Ben Ameer, Christos Comninellis and Jan Van herle

Experimental

Cell preparation Two types of supports have been used: electrolyte-covered anode supports (AS) and electrolyte supports (ES) (figure A.3). The 250 μm thick anode supported half cells were manufactured by tape casting (HTceramix SA, Switzerland) using 55 wt% NiO and 45 wt% yttria-stabilized zirconia and cosintering with a 5 μm thick 8% yttria-stabilized zirconia (8YSZ) electrolyte. The anode supports were then laser-cut to the shape of 60 mm discs; this allowed avoiding curved edges. The electrolyte supports were made of 3% yttria-stabilized zirconia (3YSZ) (Kerafol, Germany) as 82 mm-sided squares with a thickness of 115 μm .

All the other cell active layers were deposited by screen-printing and were made of lanthanum-strontium manganite (LSM) of different composition and 8YSZ with a volume ratio of 50/50. The composite powder was prepared mixing the as-received LSM and YSZ with ethanol in a ball-mill for 24h in presence of zirconia spheres. Inks were printed layer by layer through stainless steel mesh on the anode supported half cells. The inks were obtained mixing the powders on an alumina triple-roll mill with 3.2% ethylcellulose in terpineol as a binder (ratio powder/binder around 1.36).

Three experiments done on anode supports and one on electrolyte support will be illustrated in this publication.

The test on anode support A (AS-A) aimed to investigate the effect of the current density on the cell operation; therefore four identical cathodes were deposited on the anode support. The materials used for the cathode inks were as received LSM ($\text{La}_{0.75}\text{Sr}_{0.25}\text{MnO}_{3\pm\delta}$) from Praxair, USA (LSM25) and 8YSZ (Tosoh Corp., Japan) both with a nominal average particle diameter of 0.5 μm . The cell was then sintered at 1100°C for 1 hour. The cathodes, covered

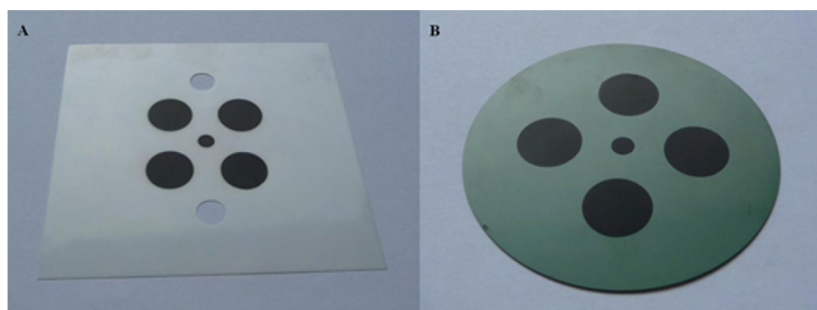


Figure A.3: (A) LSM-YSZ electrodes symmetrically deposited on both sides of 3YSZ electrolyte support.(B) LSM-YSZ cathodes deposited on a Ni-YSZ anode support.

with a LSM25 current collection layer, were contacted with platinum meshes.

The test on anode support B (AS-B) aimed to investigate the effect of cathode thickness on cell operation; therefore four cathodes of identical composition were deposited on the anode support by screen-printing successively a different numbers of layers. Each layer consisted of approximately 5 μm of cathode material. The composition of the as received cathode material (Fuel Cells Materials, USA) was $(\text{La}_{0.70}\text{Sr}_{0.30})_{0.90}\text{MnO}_{3\pm\delta}$ (LSM30) with an average particle diameter equal to 0.3 μm and grinded 8YSZ (Tosoh Corp., Japan). Grinding was necessary in order to bring the average YSZ particle diameter down from 0.5 μm to 0.3 μm , so as to have the ratio between the particle diameters of the two phases close to the unity, which is a key parameter for percolation [P. Costamagna, et al. *Electrochim. Acta*, 43 (1998) 375]. All particle size distributions and average particle diameters (d_{50}) have been measured by laser diffraction on a Mastersizer (Malvern Instrument, UK). The cell was then sintered at 1050°C for 1 hour. The cathodes, covered with a $(\text{La}_{0.65}\text{Sr}_{0.35})_{0.95}\text{MnO}_{3\pm\delta}$ (LSM35, Fuel Cells Materials, USA) current collection layer, were contacted with platinum meshes.

The test on anode support C (AS-C) aimed to investigate the effect of Mn doping of the YSZ phase in the composite cathode on the cell operation; therefore four cathodes made of LSM30 and Mn-enriched 8YSZ were deposited. The dissolution of Mn oxide into the 8YSZ powder was carried out heating for 100 hours a mixture of 8YSZ powder and Mn-acetate at different temperatures (900°C, 1000°C and 1100°C). The heat treatment temperature controlled the theoretical amount of Mn oxide dissolved into the 8YSZ phase; the expected concentrations have been calculated by extrapolating literature data [T. Kawada, et al. *Solid State Ionics*, 53 (1992) 418] and were expected to be 2.5%, 4.5% and 6.5% moles of Mn oxide per mole of YSZ for 900°C, 1000°C and 1100°C, respectively. The Mn-enriched powders, as well as the as-received 8YSZ powder, were grinded mechanically in order to decrease the average particle size and were then mixed with LSM30 to prepare the cathode pastes deposited on the anode support. The 2.5% Mn-enriched YSZ was overgrinded to a d_{50} of 0.2 μm while the other YSZ powders, including the as-received 8YSZ, to 0.3 μm ; the as-received LSM30 had a d_{50} of 0.3 μm . The cell was then sintered at 1050°C for 1 hour; the cathodes, covered with a LSM35 current collection layer, were contacted with gold meshes. Electrical contacting for all anodes supports was achieved with a unique Ni mesh, covering the whole anode area opposite to the four cathodes for current collection.

The test on electrolyte support (ES-A) aimed to investigate the effect of Cr poisoning in a three-electrode configuration; therefore a metallic interconnect (MIC) sheet (Fe-26Cr stainless steel from Plansee) was placed as a source of Cr in proximity of working cathode electrodes. The electrode inks were prepared identically to test AS-B and deposited symmetrically on both sides of the electrolyte support, before sintering for 1 hour at 1100°C and contacting gold meshes to LSM30 current collection layers painted on the electrodes.

Anode support testing Cell operation was carried out in a Rohde oven with a Bentrup TC 505 temperature controller. The cells were placed between two alumina felts and inserted between two metallic flasks (figure A.4); the test rig was then compressed with calibrated springs in order to maintain the metallic meshes under constant pressure on the electrodes.

A.2. Segmented cell testing for cathode parameter investigation

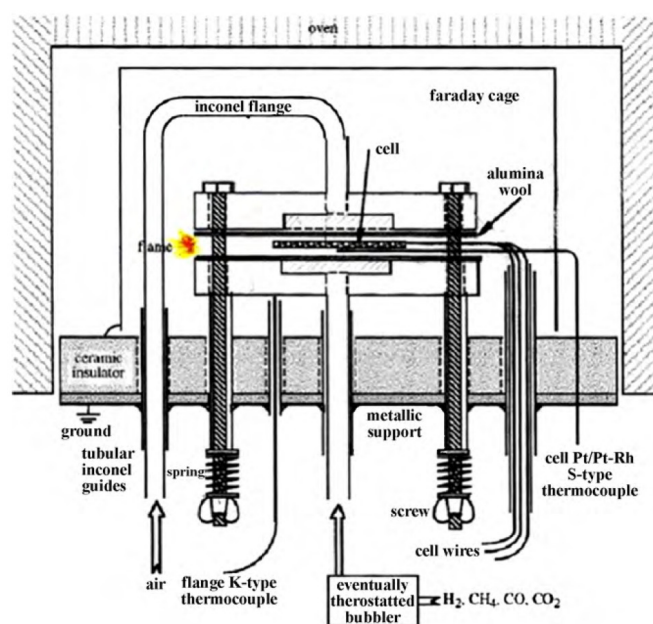


Figure A.4: Test rig used for electrochemical testing. The cells are sandwiched between two alumina felts and placed in the middle of gas feeding flanges. Since no sealing is present, post combustion of fuel gases takes place around the cell. Local measurement of the temperature is performed by a thermocouple in contact with the cell.

The flasks had central gas inlets in order to feed air to the cathode side and humidified H_2 to the anode side.

There was no sealing between the two compartments so that, during the fuel cell testing, excess H_2 was post-combusted around the cell. Gas flow was adjusted in order to maintain the flame front far from the electrochemical reaction and to minimize H_2O diffusion toward the centre of the support. Typical values for air and H_2 flow were 600 ml/min and 250 ml/min respectively. Local temperature measurement was done through a thermocouple placed near the centre of the support, placed on the air side.

Reduction of the anode supports was conducted at 850°C while feeding air to the cathode side and H_2 diluted in Ar to the anode side. The reduction of the NiO took place by a stepwise replacement of argon by hydrogen (H_2 flow varied from 10% to 100%). The polarization of the cell was done in galvanostatic mode with a fourchannel active load built in-house. Measurements were performed in a four-wire configuration. Potential difference, current and temperature data were acquired and stored in a computer through a multichannel online acquisition device. Electrochemical impedance spectroscopy measurements (EIS) and current-voltage curves were taken with an Eco Chemie Autolab.

Electrolyte support testing Cell operation was performed similarly to anode supported cells; although only air was fed to both sides of the electrolyte, with a flow rate of 250ml/min, and the system temperature was kept at 800°C by the furnace.

A.3 Coached student projects

Nickel coated metallic interconnects for solid oxide fuel cells - influence of high fuel utilization and thermal cycling, L. Arietano, Semester (Bachelor) Project, 2010

Etude électrochimique du comportement de cathodes de piles à combustible à oxyde solide, M. Ben Ameer, Diploma Thesis, 2010

Contributions des grains et joints de grains sur la diminution de la conductivité de la zircone stabilisée au cours du temps, J. Newton, Semester (Bachelor) Project, 2010

Localisation et quantification des polluants d'un test d'une pile à combustible à oxyde solide SOFC, C. Gehrig, Diploma Thesis, 2009

Caractérisation de la dégradation de piles à combustibles à oxydes solides (SOFC) grâce à l'étude microstructurale des cathodes et électrolytes par microscopie électronique à transmission (TEM), C. Calderone, Diploma Thesis, 2009

Spectroscopie d'impédance sur les électrolytes à base de zircone pour une application dans les piles à combustibles à oxyde solide, J. Roch, Semester (Bachelor) Project, 2009

Empoisonnement au chrome de la cathode des piles à combustible à oxyde solide, N. Leresche, Semester (Master) Project, 2009

Protection d'alliages par galvanodéposition, C. Augsburger, Semester (Master) Project, 2008

A.4 Publications

Cr-poisoning in (La,Sr)(Co,Fe)O₃ Cathodes after 10'000 h SOFC Stack Testing, J.A. Schuler, Z. Wuillemin, A. Hessler-Wyser, C. Comminges, N. Yousfi Steiner, J. Van herle, *Journal of Power Sources* 211 (2012) 177

Nd-Nickelate Solid Oxide Fuel Cell Cathode Sensitivity to Cr and Si Contamination, J.A. Schuler, H. Luebbe, A. Hessler-Wyser, J. Van herle, *Journal of Power Sources* 213 (2012) 223

Combined Cr and S Poisoning in Solid Oxide Fuel Cell Cathodes, J.A. Schuler, H. Yokokawa, C.F. Calderone, Q. Jeangros, Z. Wuillemin, A. Hessler-Wyser J. Van herle, *Journal of Power Sources* 201 (2012) 112

Method to Quantify Chromium Evaporation from Balance of Plant Components, O. Thomann, M.H. Pihlatie, J.A. Schuler, O. Himanen, J. Kiviao, *Electrochemical and Solid State Letters* 15 (2012) B35

Mitigating Cr Contamination by Hot Air Filtering in Solid Oxide Fuel Cells, J.A. Schuler, A.J. Schuler, D. Penner, A. Hessler-Wyser, C. Ludwig, J. Van herle, *Electrochemical and Solid State Letters* 14 (2011) B132

Glass-Forming Exogenous Silicon Contamination in Solid Oxide Fuel Cell Cathodes, J.A. Schuler, Z. Wuillemin, A. Hessler-Wyser, J. Van herle, *Electrochemical and Solid State Letters* 14 (2011) B20

Cathode Thickness-Dependent Tolerance to Cr-Poisoning in Solid Oxide Fuel Cells, J.A. Schuler, P. Tanasini, A. Hessler-Wyser, C. Comminellis, J. Van herle, *Electrochemistry Communications* 12 (2010) 1682

TEM Investigation on Zirconate Formation and Chromium Poisoning in LSM/YSZ Cathode, A. Hessler-Wyser, Z. Wuillemin, J.A. Schuler, A. Faes, J. Van herle, *Journal of Materials Science* 46 (2011) 4532

Rapid Cr Quantification in Solid Oxide Fuel Cell Cathodes, J. A. Schuler, P. Tanasini, A. Hessler-Wyser, J. Van herle, *Scripta Materialia* 63 (2010) 895

Air Side Contamination in SOFC Stack Testing, J. A. Schuler, C. Gehrig, Z. Wuillemin, A.J. Schuler, J. Wochele, C. Ludwig, A. Hessler-Wyser, J. Van herle, *Journal of Power Sources* 196 (2011) 7225

Segmented Cell Testing for Cathode Parameter Investigation, P. Tanasini, J.A. Schuler, M. Ben Ameer, C. Comminellis, J. Van herle, *Journal of Power Sources* 196 (2011) 7097

Cathode-Supported Micro-Tubular SOFCs based on $\text{Nd}_{1.95}\text{NiO}_{4+\delta}$: Fabrication and Characterisation of Dip-Coated Electrolyte Layers, H. Luebbe, J. Van herle, H. Hofmann, P. Bowen, U. Aschauer, J.A. Schuler, F. Snijkers, H-J. Schindler. U. Vogt, C. Lalanne, *Solid State Ionics* 180 (2009) 805

Conference papers

Stroboscopic Ni Growth/Volatilization Picture, J. A. Schuler, B. Iwanschitz, L. Holzer, M. Cantoni, T. Graule, *Proceedings of the European Fuel Cell Forum* B0501 (2012) 1

Multi-Scale Assessment of Cr-Contamination Levels in SOFC Cathode Environment, J. A. Schuler, A.J. Schuler, Z. Wuillemin, A. Hessler-Wyser, C. Ludwig, J. Van herle, *ECS Transactions* 35 (2011) 2001

Method to Quantify Chromium Evaporation from Balance of Plant Components, O. Thomann, M.H. Pihlatie, J.A. Schuler, O. Himanen, J. Kiviao, *ECS Transactions* 35 (2011) 2609

Nd-Nickelate Based Solid Oxide Fuel Cell Cathodes Sensitivity to Cr-, Si-Contamination, J. A. Schuler, H. Luebbe, A. Hessler-Wyser, J. Van herle, *Proceedings of the European Fuel Cell Forum* B0503 (2011) 19

Air Side Contamination in SOFC Stack Testing, J. A. Schuler, C. Gehrig, Z. Wuillemin, A.J. Schuler, J. Wochele, C. Ludwig, A. Hessler-Wyser, J. Van herle, *Proceedings of the European Fuel Cell Forum* 0715 (2010) 7

Segmented Cell Testing for Cathode Parameter Investigation, P. Tanasini, J.A. Schuler, M. Ben Ameer, C. Comninellis, J. Van herle, *Proceedings of the European Fuel Cell Forum* 1504 (2010) 15

Sulfur as Pollutant Species on the Air Side of a SOFC System, J. A. Schuler, Z. Wuillemin, A. Hessler-Wyser, J. Van herle, *ECS Transactions* 25 (2009) 2845

Locally-Resolved Study of Degradation in a SOFC Repeat-Element, Z. Wuillemin, A. Nakajo, A. Mueller, J.A. Schuler, S. Diethelm, J. Van herle, D. Favrat, *ECS Transactions* 25 (2009) 457

Talks and posters

Stroboscopic Ni Growth/Volatilization Picture, Presentation: *European Fuel Cell Forum* Luzern Switzerland June 2012

Cr-Poisoning in Button/Stacked SOFC, Presentation: *International Workshop on Degradation Issues in Fuel Cells* Thessaloniki Greece September 2011

Nd-Nickelate Based Solid Oxide Fuel Cell Cathodes Sensitivity to Cr-, Si-Contamination, Presentation: *European Fuel Cell Forum* Luzern Switzerland June 2011

Multi-Scale Assessment of Cr-Contamination Levels in SOFC Cathode Environment, Presentation: *218th ECS meeting* Montreal Canada Mai 2011

Air Side Contamination in SOFC Stack Testing, Poster: *European Fuel Cell Forum* Luzern Switzerland June 2010

Sulfur as Pollutant Species on the Air Side of a SOFC System, Poster: *216th ECS meeting* Vienna Austria October 2009

Sulfur as Pollutant Species on the Air Side of a SOFC System, Poster: *Microscopy Conference* Graz Austria September 2009



ing. sc. mat. dipl. EPF

J. Andreas Schuler

06.11.1983 Swiss; Single
756.3599.4333.74 Origin: Sattel SZ
+41 (0)79 254 12 33 j.andreas.schuler@gmail.com

Domicile: ZH(1983) → SG → VD → SWE → VD → ZH(2012)

Performance

- Christian F. Schönbein Contribution to Science Medal 2011
- Prix 2009 des Sports Universitaires
- Student Yachting World Champion 2007

Team-player

- Friendship Award: Tokyo-Tech - EPFL workshop
- Milizfeuerwehr KP Sihltal
- Nautical Society Rolle (SNR)

Leadership

- Boat Captain EPFL Sailing Team
- J&S: Jeunesse et Sports Instructor

Ambition

- Longest and most Extreme Orienteering Sailing Race: ArchipelagoRaid 2009
- Construction of a Carbon lightweight Boat.

Equilibrium

- Gardening, Reading, Tango, Cross-country, Snow-shoes, DIY
- Hiking, Climbing and Observation of Bearded Vultures

Languages

- (Swiss)German
- French
- English
- Swedish

Informatics

- Microsoft Office
- Illustrator
- Photoshop, C++
- Fiji, Aviso
- Latex, Matlab

Education

- expect. 2012 *Doctor sc. mat.* EPFL
- june 2008 *Master sc. mat.* EPFL
- 2006 - 2007 *Erasmus Stockholm* KTH
- 2002 - 2006 *Bachelor sc. mat.* EPFL

Scientist 2011 → present

- SOFC Research / EMPA Dübendorf
- RD on Ni/alternative Fuel Electrodes by X-ray Spectroscopy and Image Processing.
- Planning and Management of SOFC and Nanocomposite related Work Packages.
- Project Proposals and External Funding Applications Composition.
- Technology Transfer, PR Work, Publication of Scientific Results.

PhD Thesis 2009 → present

- Chromium Contamination Management in Solid Oxide Fuel Cell Systems / EPFL Lausanne
- Electron Microscopy Investigations of Cr-Poisoning -caused Performance Degradation Phenomena to set Counteracting Strategies at the System Level and increase the SOFC Device Lifetime.
- Outcome: 20(13 first Author) Publications
- Teaching: 3 Diploma / 5 Semester Project Supervision; Assistant: Electron Microscopy

Internships

- Calcite precipitation: EPFL LTP q3-q4 2007 for Sika AG, Switzerland
- Tribocorrosion of austenitic steels: EPFL LMCH q3 2007 for Outokumpu Stainless AB, Sweden